

ADVECTION AT A FOREST SITE – AN UPDATED APPROACH

A dissertation submitted to the

FACULTY OF BIOLOGY, CHEMISTRY AND GEOSCIENCES
AT THE UNIVERSITY OF BAYREUTH, GERMANY

to attain the academic degree of

DR. RER. NAT.

presented by

LUKAS SIEBICKE

Diplom Geoökologe

born 28 October, 1979
in Lübeck, Germany

Bayreuth, September 2010

ADVECTION AT A FOREST SITE
– AN UPDATED APPROACH

Supervisor Prof. Dr. Thomas Foken

Die vorliegende Arbeit wurde in der Zeit von März 2007 bis September 2010 an der Universität Bayreuth, in der Abteilung Mikrometeorologie, unter Betreuung von Prof. Dr. Thomas Foken angefertigt.

Vollständiger Abdruck der von der Fakultät für Biologie, Chemie und Geowissenschaften der Universität Bayreuth genehmigten Dissertation zur Erlangung des akademischen Grades eines Doktor der Naturwissenschaften (Dr. rer. nat.).

Promotionsgesuch eingereicht am: 28. September 2010

Wissenschaftliches Kolloquium am: 19. Januar 2011

Prüfungsausschuss:

Prof. Dr. Th. Foken (Erstgutachter)

Prof. Dr. A. Held (Zweitgutachter)

Prof. Dr. Th. Nauß (Vorsitzender)

Prof. Dr. B. Huwe

Prof. Dr. J. Tenhunen

Dekan: Prof. Dr. Stephan Clemens

Contents

List of Manuscripts	iv
Acknowledgements	vi
Summary	vii
Zusammenfassung	viii
1 Introduction	1
1.1 Scope of the research topic	1
1.2 Objectives of the thesis	9
2 Experiments	11
2.1 Site	11
2.2 Footprint analysis	11
2.3 The EGER experiment	12
2.4 Design of a multi-analyzer system	14
2.4.1 The sampling system	14
2.4.2 Post-processing of multi-analyzer data	20
2.5 Vertical wind velocity	23
3 Results	24
4 Conclusions	31
References	35
List of Appendices	48
A Individual contributions to the joint publications	49
B CO₂-gradient measurements using a parallel multi-analyzer setup	52
C Linking CO₂-advection estimates to vegetation structure at a forest site	68
D Some aspects of CO₂-advection measurements in discussion	92
Erklärung	113

List of Manuscripts

The dissertation is presented in cumulative form. It consists of three individual manuscripts. One manuscript has been published by the peer-reviewed journal *Atmospheric Measurement Techniques Discussions*. A second manuscript is going to be re-submitted in a revised version to the peer-reviewed journal *Agricultural and Forest Meteorology*. The third manuscript has been submitted for publication to the peer-reviewed journal *Theoretical and Applied Climatology*.

Manuscript published

Siebicke, L., Steinfeld, G., Foken, T., 2010. CO₂-gradient measurements using a parallel multi-analyzer setup. *Atmospheric Measurement Techniques Discussions* 3, 4383–4421.

Manuscript to be re-submitted in revised version

Siebicke, L., Serafimovich, A., Foken, T., 2011. Linking CO₂-advection estimates to vegetation structure at a forest site. *Agric. For. Meteorol.* (to be re-submitted in revised version).

Manuscript submitted

Siebicke, L., Hunner, M., Foken, T., 2010. Some aspects of CO₂-advection measurements in discussion. *Theoretical and Applied Climatology* (submitted).

Peer-reviewed publications not included in this thesis

Göckede, M., Foken, T., Aubinet, M., Aurela, M., Banza, J., Bernhofer, C., Carrara, J.-M. B. Y. B. A., Clement, R., Dellwik, E., Elbers, J., Eugster, W., Fuhrer, J., Granier, A., Grünwald, T., Heinesch, B., Janssens,

-
- I., Knohl, A., Kooble, R., Laurila, T., Longdoz, B., Manca, G., Marekand, M., Markkanen, T., Mateus, J., Matteucci, G., Mauder, M., Migliavacca, M., Minerbi, S., Moncrieff, J., Montagnani, L., Moors, E., Ourcival, J.-M., Papale, D., Pereira, J., Pilegaard, K., Pita, G., Rambal, S., Rebmann, C., Rodrigues, A., Rotenberg, E., Sanz, M., Sedlak, P., Seufert, G., Siebicke, L., Soussana, J., Valentini, R., Vesala, T., Verbeeck, H., Yakir, D., 2008. Quality control of CarboEurope flux data – Part 1: Coupling footprint analyses with flux data quality assessment to evaluate sites in forest ecosystems. *Biogeosciences* 5, 433–450, "CarboEurope-IP Best Paper Award 2008".
- Hussain, M., Otieno, D., Mirzaee, H., Li, Y.-L., Schmidt, M. W., Siebicke, L., Foken, T., Ribeiro, N., Pereira, J., Tenhunen, J., 2009. CO₂ exchange and biomass development of the herbaceous vegetation in the Portuguese montado ecosystem during spring. *Agriculture, Ecosystems & Environment* 132, 143–152.
- Li, Y.-L., Tenhunen, J., Mirzaei, H., Hussain, M., Siebicke, L., Foken, T., Otieno, D., Schmidt, M., Ribeiro, N., Aires, L., Pio, C., Banza, J., Pereira, J., 2008. Assessment and up-scaling of CO₂ exchange by patches of the herbaceous vegetation mosaic in a Portuguese cork oak woodland. *Agric. For. Meteorol.* 148, 1318–1331.
- Staudt, K., Serafimovich, A., Siebicke, L., Pyles, R. D., Falge, E., 2010. Vertical structure of evapotranspiration at a forest site (a case study). *Agric. For. Meteorol.* doi: 10.1016/j.agrformet.2010.10.009.

Acknowledgements

I wish to acknowledge the help of all people contributing to this thesis. Among those are my colleagues at the Department of Micrometeorology, particularly Andrei Serafimovich, with whom I shared important parts of experimental work and who was also helpful during the analysis, Katharina Staudt for several discussions during the analysis and Martina Hunner, who has jointly tackled the advection topic during her Diploma thesis and thus provided valuable input both to experimental work and to data analysis. I would further like to acknowledge the LES related work of my coauthor Gerald Steinfeld. I also thank the people from the group of the Max Planck Institute for Chemistry in Mainz for the joint experiment EGER, further the technicians from the Department of Micrometeorology and the Bayreuth Centre for Ecology and Environmental Research (BayCEER) as well as several students for their support during field work. Last but not least I thank my Supervisor Prof. Thomas Foken for providing guidance through this thesis from the perspective of his long-term experience on micrometeorological flux measurements. The work was funded by the German Science Foundation (FO 226/16-1, ME2100/4-1, ZE 792/4-1).

Summary

The exchange of carbon dioxide (CO_2) across the vegetation-atmosphere interface of a spruce forest was investigated. Horizontal and vertical advection are recognized as important terms of the Net Ecosystem Exchange (NEE) budget in addition to the commonly measured turbulent flux and storage flux. Direct advection measurements are challenging because of the instrumental accuracy required to observe small concentration gradients and small wind velocities and because of the spatio-temporal measurement resolution required to observe complex 3-D flow phenomena. This work presents an experimental multi-analyzer setup for the observation of horizontal CO_2 concentration gradients with high temporal resolution and good spatial resolution with no tradeoff between the two. A statistical approach was developed to correct for inter-instrument bias by applying a conditional time dependent bias correction. This approach relies on properties of probability density distributions of concentration differences between one sample point and the spatial average of the sample point field. Sub-canopy CO_2 concentration gradients observed with the above presented system showed a high spatial variability which was dependent on vegetation structure. Local concentration perturbations correlated with statistical properties of coherent structures and were explained by vertical exchange between CO_2 enriched sub-canopy air and low concentration above-canopy air. The small-scale variability of CO_2 concentration gradients brings into question the representativity of horizontal advection measurements for the control volume if observed with a low spatial resolution. Vertical advection estimates rely on accurate measurements of vertical wind velocity (w). Different procedures were applied during coordinate rotation to align the coordinate system of the sonic anemometer with the long-term stream lines. Spatial variability of the wind field was addressed by a sector-wise coordinate rotation. An investigation of temporal aspects of vertical wind velocity showed significant contributions from low frequencies in the spectrum of w . The impact of the data set length used for coordinate rotation on w and on vertical advection was investigated and observed to be large. A sequential coordinate rotation with controlled window length was proposed. Advection contributed significantly to NEE during the night and during transition periods at the Waldstein-Weidenbrunnen (DE-Bay) FLUXNET site. Daily NEE budgets were more realistic, compared to NEE from turbulent flux and storage change alone, if direct advection measurements from continuous and bias corrected gradient sampling were included, reducing the estimated daily carbon sequestration of the forest by almost 50 %.

Zusammenfassung

Der Austausch von Kohlendioxid (CO_2) zwischen der Vegetation eines Fichtenwaldes und der Atmosphäre ist Gegenstand dieser Studie. Horizontale und vertikale Advektion sind wichtige Terme des Netto-Ökosystem-Austauschs (NEE), zusätzlich zum typischerweise gemessenen turbulenten Fluss und Speicherterm. Kleine Konzentrationsgradienten und Windgeschwindigkeiten sowie die notwendige räumlich-zeitliche Messauflösung zur Beobachtung des 3-D Strömungsfeldes stellen große Anforderungen an die Genauigkeit der Instrumente bei der experimentellen Erfassung der Advektion. Ein experimenteller Aufbau zur Messung horizontaler CO_2 -Konzentrationsgradienten wird vorgestellt, der sich durch eine hohe zeitliche und gute räumliche Auflösung auszeichnet, ohne dass sich die beiden gegenseitig einschränken. Ein statistisches Verfahren wurde entwickelt, um relative Fehler zwischen den Geräten mit einer konditionalen, zeitabhängigen Korrektur zu beseitigen. Dazu werden Eigenschaften von Wahrscheinlichkeitsdichtefunktionen von Konzentrationsunterschieden zwischen einem einzelnen Messpunkt und dem räumlichen Durchschnitt aller Punkte verwendet. Derart beobachtete Konzentrationsgradienten waren räumlich variabel und abhängig von der Vegetationsstruktur. Die lokalen Konzentrationsabweichungen korrelierten mit statistischen Eigenschaften kohärenter Strukturen und wurden teilweise als Ursache von vertikalem Austausch zwischen der CO_2 reichen bodennahen Luft und der abgereicherten Luft oberhalb der Krone erklärt. Die Bestimmung der vertikalen Advektion erfordert genaue Messungen des Vertikalwinds (w). Unterschiedliche Ansätze wurden bei der Rotation des Ultraschallanemometer-Koordinatensystems entsprechend dem Langzeit-Strömungsfeld verwendet. Die räumliche Variabilität des Windfeldes konnte durch sektorweise Koordinatenrotation berücksichtigt werden. Eine Untersuchung zeitlicher Aspekte zeigte einen bedeutenden niederfrequenten Anteil des Vertikalwindpektrums. Die zur Koordinatenrotation verwendete Datensatzlänge hatte großen Einfluss auf den rotierten Vertikalwind und damit auf die vertikale Advektion. Daher wurde eine sequentielle Rotation mit bewusst gewählter Fensterlänge vorgeschlagen. Advektion an der Waldstein-Weidenbrunnen (DE-Bay) FLUXNET Messstelle zeigte einen bedeutenden Anteil am NEE während der Nacht und während Übergangszeiten. Tagessummen des NEE waren realistischer wenn direkte Advektionsmessungen unter Verwendung kontinuierlicher und statistisch korrigierter Gradientenmessungen berücksichtigt wurden im Vergleich zu NEE , welcher nur aus turbulentem Fluss und Speicherterm bestimmt wurde, und verursachten eine Verringerung der geschätzten täglichen Kohlenstoffaufnahme des Waldes um nahezu 50 %.

1 Introduction

1.1 Scope of the research topic

In a nutshell, this work aims at improving the quality of trace gas flux measurements at the vegetation-atmosphere interface with a particular focus on the advective component of Net Ecosystem Exchange of carbon dioxide (CO_2).

In recent years, many ecologists and micrometeorologists have studied the exchange of CO_2 between the vegetation and the atmosphere in order not only to understand the processes involved but also to quantify the source and sink strength of various ecosystems and to establish long-term carbon balances. Today, there are several hundreds of stations worldwide observing Net Ecosystem Exchange on a long-term basis, which are organized as the FLUXNET (Baldocchi et al., 2001). The eddy-covariance (EC) technique (Moncrieff et al., 1997; Aubinet et al., 2000; Baldocchi et al., 2001; Baldocchi, 2003) is the most widely used method to quantify the turbulent exchange of momentum, sensible and latent heat as well as trace gases, in particular CO_2 , at the vegetation-atmosphere interface.

The exchange of CO_2 between the ecosystem (control volume) and the atmosphere, the Net Ecosystem Exchange (NEE), which is largely controlled by the net effect of assimilation and respiration, can be expressed by the mass conservation equation of CO_2 (Finnigan, 1999; Finnigan et al., 2003; Aubinet et al., 2003; Feigenwinter et al., 2004, and others):

$$\begin{aligned}
 NEE = & \frac{1}{V_m} \int_0^h \left(\frac{\partial \bar{c}}{\partial t} \right) dz + \frac{1}{V_m} (\overline{w'c'})_h + \frac{1}{V_m} \int_0^h \left(\bar{w}(z) \frac{\partial \bar{c}}{\partial z} + \bar{c}(z) \frac{\partial \bar{w}}{\partial z} \right) dz \\
 & + \frac{1}{V_m} \int_0^h \left(\bar{u}(z) \frac{\partial \bar{c}}{\partial x} + \bar{v}(z) \frac{\partial \bar{c}}{\partial y} \right) dz \quad (1)
 \end{aligned}$$

with the molar volume of dry air V_m , CO_2 concentration c , horizontal distances x and y , vertical distance above ground z , height of the control volume h , horizontal wind velocity u along the x -direction, horizontal wind velocity v along the y -direction and vertical wind velocity w along the z -direction. Overbars denote temporal means and primes denote the temporal fluctuations relative to the temporal mean. The terms on the right hand side of Eq. 1 are the change of storage (term I), the vertical turbulent flux (term II), vertical advection (term IIIa), vertical mass flow from the surface e.g. due to evaporation (term IIIb) according to Webb et al. (1980), and horizontal advection (term IV). The form of NEE presented in Eq. 1 excludes

the horizontal variation of the vertical turbulent flux and the horizontal variation of vertical advection. Eq. 1 further neglects the flux divergence term:

$$\frac{1}{V_m} \int_0^h \left(\frac{\partial(\overline{w'c'})}{\partial x} + \frac{\partial(\overline{v'c'})}{\partial y} \right) dz.$$

It should be noted that Kramm et al. (2008) argued that the type of mass balance equation presented in Eq. 1 and previously used by the above cited authors and many others (Kramm et al. (2008) call it “alternative mass balance equation”) were non self-consistent and physically incorrect and the terms were afflicted with different physical units. Even if this was true it does not become clear from their study (which for unknown reasons has received very few citations) what the quantitative error of NEE and its terms might be. This would be an analysis in itself and is outside the scope of the current study. However, we still assume that the principal findings presented in this work hold true even though an “alternative mass balance equation” is used.

Most often, NEE is described as the sum of the change of storage (term I of Eq. 1) and the turbulent flux (term II of Eq. 1) observed at a single tower. During daytime when turbulence is well developed the turbulent flux is the dominating term in the NEE budget allowing other terms of the equation to be neglected while retaining acceptable error limits. The turbulent flux term is generally obtained from a single above canopy measurement using the EC technique, the application of which has become relatively standardized today. The turbulent flux of CO_2 is obtained from measurements of the covariance of the wind vector measured by a 3-D sonic anemometer and the scalar CO_2 concentration measured by an infrared gas analyzer. Raw covariances are post-processed using filters, conversions and flux corrections typically including spike detection (Vickers and Mahrt, 1997), determination of the time delay between sonic anemometer and gas analyzer using cross-correlation analysis, cross-wind correction of sonic temperature (Liu et al., 2001), planar fit coordinate transformation (Wilczak et al., 2001), high frequency spectral correction (Moore, 1986), conversion of sonic temperature fluctuations into actual temperature fluctuations (Schotanus et al., 1983), density correction for scalar fluxes of H_2O and CO_2 and correction for mean vertical mass flow (Webb et al., 1980) as well as quality control (Foken and Wichura, 1996; Vickers and Mahrt, 1997; Foken et al., 2004).

The change of storage of CO_2 in the control volume can be deduced from measurements of the vertical CO_2 distribution. In the absence of vertical profile measurements it can be calculated using concentration measurements from a single above canopy measurement following an approach by Hollinger et al. (1994), which assumes the same mean CO_2 density $\overline{\rho_c}$ for the entire air

column below measurement height h . The storage flux $F_{S(i)}$ is then written:

$$F_{S(i)} = \frac{\overline{\rho_{c(i+1)}} - \overline{\rho_{c(i-1)}}}{t(i+1) - t(i-1)} h \quad (2)$$

with time t and measurement interval i . However, this simplified estimate can underestimate the storage term under certain conditions (Finnigan, 2006).

Fundamental requirements for the application of the EC technique are stationarity and horizontal homogeneity. Those are often not fulfilled in complex terrain (Foken and Wichura, 1996; Massman and Lee, 2002; Finnigan, 2004; Katul et al., 2006; Beyrich et al., 2006; Oncley et al., 2007; Sun et al., 2007; Belcher et al., 2008; Aubinet, 2008; Rebmann et al., 2010, and many others). Furthermore the EC technique fails in the absence of turbulence or under conditions characterized by low turbulence intensity, notably at night. Stable atmospheric stratification and consequently the lack of turbulence in the nocturnal boundary-layer leads to an underestimation of fluxes measured by EC (Goulden et al., 1996; Lee, 1998; Acevedo et al., 2007; Gorsel, van et al., 2007; Aubinet, 2008; Finnigan, 2008). This is known as night-flux error. More specifically, Goulden et al. (1996) found that the nocturnal flux (ecosystem respiration) measured by EC was systematically lower than flux estimates extrapolated from chamber measurements and that the EC flux was dependent on friction velocity (u_*) although there was no biological reason for respiration to depend on u_* . Similar findings were reported later for many sites (Aubinet et al., 2000; Gu et al., 2005). Underestimating the nocturnal flux of CO_2 leads to a selective systematic error in long-term budgets of CO_2 because assimilation (daytime measurements) is better represented in the budget than respiration (night-time measurements) which leads to an overestimation of carbon sequestration.

A widely applied means to deal with the night flux problem of the EC technique is to filter fluxes according to turbulence intensity, i.e. friction velocity (u_*), retaining fluxes recorded under sufficiently turbulent conditions and discarding fluxes under conditions of low turbulence when u_* is below a certain threshold. This is known as “ u_* -filtering” (Goulden et al., 1996). When aiming at long-term CO_2 budgets, data gaps including gaps created by the u_* -filtering have to be filled with modelled data (Falge et al., 2001; Ruppert et al., 2006). This introduces additional uncertainty in the long-term balance, the latter being the relatively small net effect of fluxes with opposing sign (assimilation and respiration). The benefit of the u_* -filter approach is that it can be applied to a large number of sites without the need for additional instrumentation. Among its drawbacks are the non-physical nature of the correction (Aubinet, 2008) as well as the often subjective identification of a site-dependent u_* -threshold, although attempts were made to

find more objective threshold values using automated methods (Gu et al., 2005). Furthermore, for some sites, including the Waldstein-Weidenbrunnen (DE-Bay) site, no clear u_* -threshold was found for which alternative gap filling techniques (Ruppert et al., 2006) would be required.

There are two aspects to nocturnal flux measurements which make them problematic. One is the limited ability of the eddy-covariance technique to measure fluxes under conditions of low turbulence and the challenge of accurate measurements of the storage change. The reasons include instrument related measurement errors, and more importantly, meteorological conditions invalidating the assumptions of the EC technique. The other aspect is the representativeness of fluxes measured in the stable boundary-layer, because the observed fluxes need not be representative of their local source and sink term. This means that nocturnal fluxes are difficult to interpret as they are difficult to relate to their source, which is commonly achieved by modeling the footprint of the eddy covariance measurement (Schmid, 2002; Leclerc et al., 2003; Göckede et al., 2004; Sogachev et al., 2005; Klaassen and Sogachev, 2006; Vesala et al., 2008). Instrument related issues regarding the determination of the turbulent flux term and the change of storage flux were reviewed in Massman and Lee (2002) and shall not be detailed here. However, meteorological conditions affecting the measurement and interpretation of night-time fluxes will be discussed in the following.

Meteorological phenomena observed during nocturnal conditions include turbulent ramps, gravity waves, small-scale turbulence, intermittent turbulence, land, sea and lake breezes and drainage flows as listed in an analysis of nocturnal EC measurements by Aubinet (2008). All of those phenomena can compromise the quality of turbulent flux measurements by the EC technique because they can generate a thin sublayer close to the ground causing a decoupling of the EC measurement height from sources at or close to ground, typically under but not limited to the presence of a forest canopy. The extension of the footprint is generally much larger under stable conditions, which makes it more difficult to relate the flux to its sources (Foken and Leclerc, 2004) and means that changing sources contribute to the flux over the course of the day. Above-mentioned meteorological phenomena can further cause instationarity, invalidating assumptions of the EC technique. Also, similarity needs not be fulfilled, causing related problems with quality tests and footprint evaluation. Most importantly, those phenomena can generate conditions where the remaining terms of the NEE budget (Eq. 1) other than turbulent flux and change of storage can become dominant, most notably horizontal and vertical advection.

Turbulent ramps (Shaw et al., 1989; Paw U et al., 1992; Lee et al., 1997; Thomas and Foken, 2007a,b) are observed during periods of well developed

turbulence and are therefore less problematic for flux measurements by EC. Gravity waves, which can be generated by stably stratified flow over irregular surfaces (Lee et al., 1997), cause little net contribution to the flux of CO₂ as they mainly cause oscillating movement of an air parcel around a buoyancy-determined equilibrium position. Small-scale turbulence under conditions with low turbulence intensity is not well accounted for by the standard EC technique (Mahrt and Vickers, 2006). The contribution to *NEE*, however, is very small. Intermittent turbulence (Mahrt, 1999), i.e. brief periods of well developed turbulence separated by calm periods during stable stratification, can cause significant flux error, affecting both the turbulent and the storage flux measurements, either because of measurement problems, which are related to instationarity and spatial and temporal sampling resolution (Heinesch et al., 2007), or because turbulent fluxes need not be representative of the local source. The CO₂ emitted during an intermittent turbulent event, even if it was registered by an above-canopy EC measurement, need not represent the true accumulation of CO₂ from local sources since the last emission; it could also have a foreign source and could have been advected into the control volume. This would cause an overestimation of the flux determined with EC from intermittent turbulent events. Similarly, accumulated CO₂ could also be advected out of the control volume, causing an underestimation of the flux determined with EC under conditions of intermittent turbulence. Advection and intermittent turbulence are thus related processes. Among the causes for intermittent turbulence is sheer generated turbulence in the presence of nocturnal low-level jets Mahrt (1999).

Breezes and drainage flows are the major causes of advection. Breezes are related to areas with different surface properties, e.g. different radiation and thermal properties of forest versus clearings or low vegetation, dry versus wet land or open water bodies. Breezes can cause significant advection of CO₂ (Sun et al., 1998). Drainage flows are characterized by katabatic drainage, i.e. the downslope movement of cold air due to its high density (Stull, 1988). They develop in the stable nocturnal boundary layer close to the ground with a typical thickness of the drainage layer of only a few meters to tens of meters. Drainage follows depressions in the terrain and is affected by surface roughness elements. Forest canopies can modify the dimensions of katabatic flows, with the drainage sublayer often being restricted to the trunk-space (Aubinet et al., 2003), causing a decoupling of the atmosphere above and below the canopy roughness elements. Drainage flows, which have been analyzed by several authors (Mahrt, 1999; Mahrt et al., 2001; Soler et al., 2002; Komatsu et al., 2003; Yi et al., 2005; Froelich and Schmid, 2006; Goulden et al., 2006; Pypker et al., 2007), occur even at gentle slopes of about 1°. Nocturnal sub-canopy drainage flows, which are decoupled from the above-

canopy level, invalidate above-canopy EC measurements as an estimate of the local ground source of CO₂ because they are not linked to the EC footprint and are likely to transport CO₂ of non-local origin by advection.

Advection can contribute significantly to *NEE* and even become the dominating term in the budget in the presence of above mentioned meteorological phenomena in the nocturnal boundary layer. The direct measurement of advective flux terms is an alternative to the u_* -filter and gap filling approach. It is attractive because it is physically based but it is experimentally very challenging. Therefore, direct advection measurements shall be discussed in the following.

Lee (1998); Finnigan (1999); Lee (1999) and later Baldocchi et al. (2000); Paw U et al. (2000); Lee and Hu (2002) suggested the inclusion of a vertical advection term in the *NEE* equation. See Paw U et al. (2000) for a comparison of the two approaches to the mean vertical flux by Lee (1998), addressing term IIIa of Eq. 1, and by Webb et al. (1980), addressing term IIIb of Eq. 1. The approach by Lee (1998), which assumed incompressible flow and included only a vertical component of advection, was criticized by Finnigan (1999) and Paw U et al. (2000) as neglecting the horizontal component of advection as well as horizontal derivatives of turbulent fluxes, thus oversimplifying the budget calculation to one dimension. Based on a simple model study which showed that horizontal and vertical advection could be of similar magnitude but with opposing sign, Finnigan (1999) also pointed to the risk of degrading the quality of the budget by including vertical advection alone. To address the 3-dimensional nature of the flux, it was proposed that not only vertical advection but also horizontal advection be included in the *NEE* equation (Finnigan, 1999; Paw U et al., 2000; Baldocchi et al., 2000; Aubinet et al., 2003; Staebler and Fitzjarrald, 2004). Many studies have attempted to measure the full *NEE* budget including advection (Baldocchi et al., 2000; Aubinet et al., 2003; Staebler and Fitzjarrald, 2004; Feigenwinter et al., 2004; Paw U et al., 2004; Aubinet et al., 2005; Wang et al., 2005; Marcolla et al., 2005; Sun et al., 2007; Zeri, 2007; Heinesch et al., 2007, 2008; Mammarella et al., 2007; Leuning et al., 2008; Kutsch et al., 2008; Yi et al., 2008; de Araujo et al., 2008; Oncley et al., 2008; Tóta et al., 2008; Feigenwinter et al., 2010b,a; Zeri et al., 2010; Etzold et al., 2010) including the ADVEX campaign (Feigenwinter et al., 2008; Montagnani et al., 2010), which intended to apply a uniform methodology at sites in Italy (Renon), Germany (Wetzstein) and Sweden (Norunda).

Despite the effort of the above cited experiments, direct advection measurements have not been adopted as a mainstream solution to the nightflux problem. Among the reasons are large scatter and uncertainty of the advection measurements, the high resource requirements for advection experi-

ments, as well as the site dependent behavior of advective flux contribution. However, several authors claimed the observation of consistent patterns of advective fluxes at their site. Observed advection did account for the missing flux at night at some sites and could be related to meaningful physical drivers such as katabatic drainage. Aubinet (2008) presented a site classification with respect to advection, which highlights common advection patterns at different sites and can be used as a tool for inter-site comparisons. Aubinet et al. (2003); Sun et al. (2007); Yi et al. (2008) and others found that advective flux terms can be of considerable magnitude at night, although vertical and horizontal advection partly cancelled each other. Sun et al. (2007); Rebmann et al. (2010) and others reported large uncertainty which they related to the above-mentioned partial cancellation of vertical and horizontal advection. Aubinet et al. (2010) concluded from the ADVEX campaign that direct advection measurements do not help to solve the night-time CO₂ closure problem. One reason for the inability of advection measurements to close the *NEE* balance is the mismatch of the spatial representativeness of different terms of the *NEE* equation. The footprint of the turbulent flux measurements above the canopy need not match the footprint of advective flux measurements inside the canopy for reasons stated above. Another reason is the uncertainty of advection estimates.

Major challenges for accurate advection measurements are the measurement of horizontal concentration gradients which are often small relative to the instrument accuracy and the measurement of vertical wind velocity w (Heinesch et al., 2007). When using the commonly applied sequential sampling of several measurement points, the synchronous observation of horizontal gradients is not possible. Therefore averaging is needed which results in a low temporal resolution of horizontal gradient measurements. Furthermore, owing to the limited spatial resolution of observations, the 3-dimensional wind and concentration field is generally undersampled (Aubinet et al., 2010). Heinesch et al. (2007) investigated the influence of the sampling resolution on a CO₂ concentration time series recorded at a single point and estimated related uncertainties concerning the calculation of storage change and advection. Their results confirm that increasing the temporal resolution of concentration sampling reduces the uncertainty. However, the ability to increase the number of samples per half hour is limited in a sequential system by the tradeoff between temporal resolution and spatial resolution (number of sample locations). Leuning et al. (2008) addressed the issue of spatial resolution by line integrated concentration measurements using perforated tubing at several levels as opposed to the more common point measurement setup. Spatially representative measurements of horizontal wind velocity as well as accurate vertical velocity measurements remained challenging.

Vertical wind velocity measurements are essential for the computation of vertical advection but they are difficult to obtain with sufficient accuracy. Heinesch et al. (2007) estimated an uncertainty of w of 0.042 ms^{-1} which was on the order of the vertical velocity itself. Accurate measurements of vertical wind velocity are not only limited by the instrument's specifications but also by the ability to define a suitable coordinate reference. It is common practice to perform a coordinate rotation to minimize flow distortion effects and to align the sonic coordinate system with the stream lines (McMillen, 1988; Wilczak et al., 2001; Paw U et al., 2000; Geissbühler et al., 2000; Finnigan et al., 2003; Finnigan, 2004; Froelich et al., 2005; Vickers and Mahrt, 2006; Sun, 2007; Dellwik et al., 2010). The rotation is performed in order to obtain a zero mean vertical wind velocity $\bar{w} = 0$ either on a short term basis (McMillen, 1988), for the averaging interval of the flux, e.g. 30-min interval (e.g. Lee et al., 2004a, and others) or for a longer period which is the case for the planar fit technique (Wilczak et al., 2001). Whereas the choice of coordinate rotation procedure or sonic orientation (see e.g. Geissbühler et al. (2000) for surface normal versus vertical orientation) is comparatively less critical for turbulent flux measurements, they can have a large impact on the estimate of vertical advection at night when vertical concentration gradients are large. For a given tilt correction approach the choice of time scale for averaging the wind components is critical (Finnigan et al., 2003; Vickers and Mahrt, 2006). Furthermore, regardless of the coordinate rotation chosen, a single above-canopy point measurement can only determine the local vector basis at that point but not the streamlines for the complete surface of the volume under consideration (Lee et al., 2004a; Sun, 2007; Mahrt, 2010). However, by choosing a suitable coordinate rotation the information from a point measurement can be optimized in terms of its representativity for the surface of the control volume (Finnigan, 2004).

Limitations of single point measurements of vertical wind velocity have stimulated modeling studies as an alternative. Finnigan and Belcher (2004); Harman and Finnigan (2007) described flow over hills and Lee et al. (2004b); Yi et al. (2005); Sun et al. (2006a,b); Sogachev et al. (2008) modelled advection inside canopies. As an alternative to direct point measurements of vertical wind velocity and modeling, w can be inferred from a mass balance approach using observations of horizontal wind velocity. This was proposed by Aubinet et al. (2005) and applied by Vickers and Mahrt (2006); Heinesch et al. (2007); Montagnani et al. (2010). Canepa et al. (2010) used the mass balance approach in combination with modeling. Mahrt (2010) further proposed multi-tower measurements of w , possibly in combination with aircraft observations. However, the resources required limit those methods to highly specialized campaigns.

1.2 Objectives of the thesis

The current study investigates the advective contribution to NEE as observed by the most common experimental setup with a turbulent flux measurement at a single high tower. The tower measurements were complemented by observations of sub-canopy advection using an array of CO_2 concentration and wind measurements. The study aims at improving the temporal and spatial measurement resolution of horizontal concentration gradients. It further aims at optimizing information about w obtained from single tower measurements because most sites and long-term measurements rely on incomplete observations of the 3-dimensional flow field. Both spatial and temporal effects of coordinate rotation will be addressed. Thus, two of the main issues concerning the accuracy of advection estimates which have evolved during previous studies are considered in the current work with the aim of improving estimates of NEE . Furthermore, footprint analysis is performed in order to interpret the spatial representativeness of turbulent and advective flux terms. The focus of the individual contributions to this work is given in the following.

The first manuscript has the objective of

- presenting an experimental multi-analyzer setup for CO_2 concentration gradient measurements with high temporal and yet good spatial resolution,
- presenting a method to deal with inter-instrument bias which is a well known challenge in multi-analyzer setups.

The second manuscript has the objective of

- investigating the interaction of the flow field with the forest canopy structure and identifying corresponding impacts on the in-canopy CO_2 concentration field,
- highlighting the link between coherent motion in the canopy (sweeps and ejections) and sub-canopy CO_2 concentration gradients which are used for the computation of advection,
- analyzing spatial and temporal scales of coherent structures and the CO_2 concentration field in an attempt to evaluate and improve the existing spatio-temporal measurement resolution of advection measurements.

The third manuscript has the objective of

- presenting the regime of CO₂ advection and Net Ecosystem Exchange at the FLUXNET site Waldstein-Weidenbrunnen (DE-Bay),
- investigating the differences between continuous high frequency measurements of horizontal concentration gradients designed for improved horizontal advection estimates and the common discontinuous sampling approach,
- investigating different approaches to how to apply the planar fit coordinate rotation aiming at an optimized representativity of vertical wind velocity at the control volume scale in order to improve vertical advection estimates (and turbulent flux estimates) given one above-canopy point measurement of 3-D wind velocity, and quantify the impact on vertical advection,
- evaluating the effect of the above mentioned alternative approaches to advection observation on the *NEE* budget.

2 Experiments

2.1 Site

Experimental field work was conducted at the Waldstein-Weidenbrunnen (DE-Bay) FLUXNET site (Fig. 1), $50^{\circ} 08' 31''$ N, $11^{\circ} 52' 01''$ E, located in the Fichtelgebirge Mountains in Southern Germany. The 25 m high Norway spruce (*Picea abies*) stand is about 55 years old and is situated in complex terrain on the upper section of a hill 775 m ASL, with a 3° slope facing south-west. The flow regime at the site is characterized by prevailing winds from west-south-west approaching the north-west facing slope of the Waldstein massif, further by anabatic winds which originate from the Lehstenbach valley and approach the site from south-east and further by katabatic drainage following the slope from north-east to south-west. The site is described in detail in Gerstberger et al. (2004) and a summary of background data can be found in Staudt and Foken (2007). The forest in the vicinity of the site is heterogeneous. Tree density, age and species composition varies and a storm in Spring 2007 has created additional clearings. Such heterogeneity challenges the representativity of turbulent flux measurements and generates advective flux components in the *NEE* of CO_2 . It also requires footprint evaluation.

2.2 Footprint analysis

Footprint analysis was performed to relate observed fluxes to forest and clearings respectively. The footprint synthesis presented in Sec. 3 (Fig. 6) follows a site evaluation methodology using a combination of quality criteria of flux data and footprint analysis presented in Göckede et al. (2004); Rebmann et al. (2005); Göckede et al. (2006) and used in the context of the quality assessment of FLUXNET sites within the framework of CarboEurope, as described in Göckede et al. (2008).

The footprint model itself uses a stochastic forward Lagrangian algorithm (Thomson, 1987) of Langevin type (Wilson and Sawford, 1996) in the implementation by Rannik et al. (2003). The model accounts for fluxes within the canopy and three-dimensional turbulent diffusion. However, it is subject to the limitations of the “inverted plume assumption” (Schmid, 2002), i.e. it is limited to horizontally homogeneous conditions.

Meteorological input data for the footprint calculation were prepared using the TK2 software (Mauder and Foken, 2004). Roughness length z_0 information as input for the footprint model was prepared using the “microscale aggregation model” from Hasager and Jensen (1999) with $z_0 = 1.8$ m for



Figure 1: Aerial view of study site showing Norway spruce forest, clearings, sparser forest upslope, and towers. “M5” to “M14” indicate approx. positions of sub-canopy CO₂ concentration and wind measurements during EGER IOP2. See Fig. 2 for a closeup. High towers are marked with “MT” for “main tower” and “TT” for “turbulence tower”. Photograph taken by Th. Foken on March 15, 2007.

“coniferous forest”, $z_0 = 0.6$ m for “clearing, 2003” and $z_0 = 0.3$ m for “clearing, 2007”, with land use classes according to Fig. 6. The synthesis of the footprint climatology was performed using the program “TERRAFEX” (Göckede et al., 2004). Relative flux contribution from specific land use classes were computed using the program “EXASITE” (Göckede et al., 2006).

2.3 The EGER experiment

This work is part of the EGER (“ExchanGE processes in mountainous Regions”) experiment (Foken et al., 2011), which comprised two intensive observation periods (IOP). The first intensive observation period was conducted from 06th of September to 7th of October 2007 (IOP1) and the second intensive observation period from 1st of June to 15th of July 2008 (IOP2). The EGER experiment is a biogeochemical project combining chemical mea-

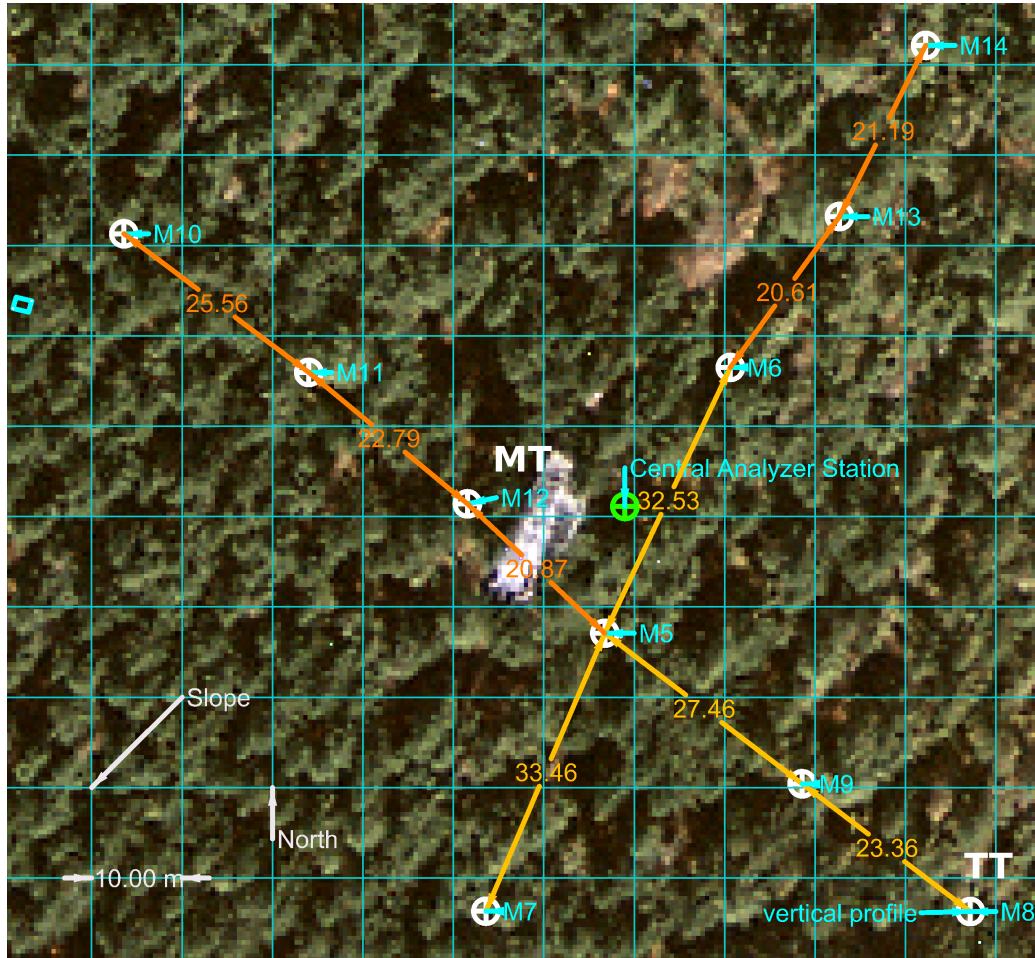


Figure 2: Setup of sub-canopy CO_2 advection measurements at a 2.25 m height. White circles indicate mast locations with line intakes for CO_2 samples at M5 to M14 and wind velocity measurements at M5 to M10. High towers are marked with “MT” for “main tower” and “TT” for “turbulence tower”. Distances between sample points are given in meters. Grid spacing: 10 m. Photo courtesy of Landesamt für Vermessung und Geoinformation, München, Germany.

measurements of reactive and non-reactive trace gases with micrometeorological investigations of fluxes. Methods of flux observation applied by the combined research group included chamber and cuvette measurements, gradient based flux measurements, eddy-covariance, direct advection measurements and remote sensing with SODAR/RASS. Field observations were combined with flux modeling using the multi-layer model ACASA, i.e. Advanced Canopy-Atmosphere-Soil Algorithm, (Pyles et al., 2000).

A detailed documentation of the micrometeorological instrumentation in-

stalled during the EGER experiment is given in Serafimovich et al. (2008b) for IOP1 and in Serafimovich et al. (2008a) for IOP2, including instrument settings and calibrations. Sonic anemometers were evaluated in a wind tunnel experiment prior to field operation (Siebicke and Serafimovich, 2007).

The instrumental setup of direct measurements of vertical advection was based on vertical profiles of CO₂ concentration and wind velocity from the forest floor to the above-canopy eddy-covariance measurement height of 36 m. The location of the high towers is given in Fig. 1 and 2.

Direct measurements of horizontal advection were based on a sub-canopy array of wind velocity and CO₂ concentration measurements at a 2.25 m height and auxiliary measurements at a 1 m height. The spatial layout of the sub-canopy array, which was arranged in one transect parallel to the terrain slope and one perpendicular to the slope, is shown in Fig. 2. A summary of all instruments used for advection measurements, their location, assignment to measurement height and observation period is given in Table 1 in Appendix D.

During the first intensive observation period (IOP1) sub-canopy CO₂ concentration gradients were sampled with a multiplexer system based on a single LI-820 (LI-COR, Inc.) analyzer, which was available from previous work by Ruppert (2005). Due to the limited performance of the system for horizontal gradient measurements a new CO₂ sampling system was developed within the scope of this thesis for the observation of the sub-canopy concentration field during the second intensive observation period (IOP2). This included the planning, design, manufacturing of parts, assembly, set-up and operation of a sampling system with ten closed-path infrared gas analyzers and an automatic calibration and remote control system. The new system is characterized by improved temporal and spatial measurement resolution and uses analyzers with higher accuracy and less noise. Measurement principles and further characteristics of the system are described in Appendix B. The following section provides additional details on the technical realization and performance of the system, some of which are not covered by the publication in Appendix B.

2.4 Design of a multi-analyzer system

2.4.1 The sampling system

A sampling system was designed for the synchronous observation of the CO₂ concentration and the wind field at multiple locations in the sub-canopy. Ten sample inlets for CO₂ were mounted at the top of individual small towers M5, M6, M7, M8, M9, M10, M11, M12, M13, M14 (see Fig. 2) at a height of 2 m.

Towers M5, M6, M7, M8, M9, M10 were equipped with sonic anemometers at a 2.25 m height (USA-1, Metek GmbH at M5, M6, M7, M9, M10, CSAT3, Campbell Scientific, Inc. at M8). Each point was continuously sampled by an individual closed-path infrared gas analyzer. Instruments used were five LI-6262 (LI-COR Biosciences Inc.) at mast locations M5, M6, M7, M8, M10, respectively, one LI-6251 (LI-COR Biosciences Inc.) at mast M14, four BINOS (Leybold Heraeus GmbH) at masts M9, M11, M12, M13. Analyzers names “A01” to “A10” refer to analyzers located at masts M5, M6, M7, M8, M10, M9, M11, M12, M13, M14, respectively. CO₂ concentration measurements were recorded at a 1 Hz frequency at each sample point, sonic data were recorded at a 20 Hz frequency. Refer to Table 1 for individual response times of the different analyzer models.

To reduce the risk of systematic concentration differences between individual closed-path gas analyzers the system was carefully designed to avoid any possible bias of the concentration measurement from differences in pressure or temperature (sample air temperature, ambient analyzer temperature, radiation). All CO₂ closed-path gas analyzers shared a common housing in a central position with controlled conditions resulting in a constant common temperature and common pressure regime. A schematic drawing of hydraulic system components is given in Fig. 3.

Individual technical measures taken to avoid systematic inter-instrument bias included the following:

- The length of tubing connecting each sample point with the corresponding gas analyzer was exactly 75 m for every point. Sample tubes used were of polyethylene-aluminum composite structure, model DEKABON 1300-M060X (Serto AG, Fulda, Germany) with an inner diameter of 4 mm.
- Large diameter line intake air filters were checked regularly and replaced synchronously at all points, if necessary.
- Common ambient temperature and pressure for all gas analyzers and calibration unit, including radiation protection, active automatic temperature control by heating and cooling as well as carefully designed ambient air circulation.
- Quality control of performance of automatic temperature control system, making sure that ambient air temperatures measured at several points surrounding the gas analyzers remain within acceptable range.
- Temperature adaptation for sample lines, to allow the temperature of

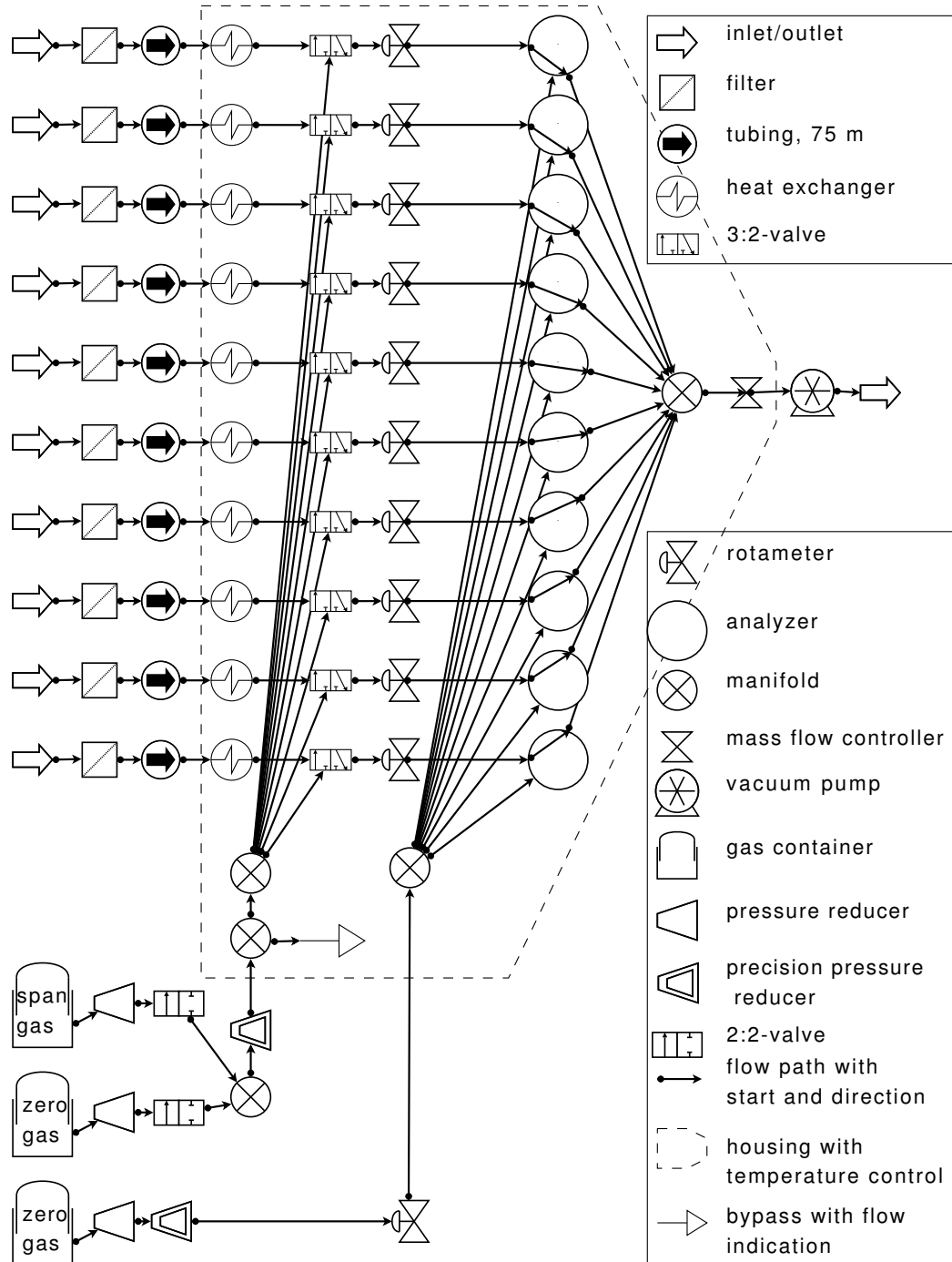


Figure 3: Schematic drawing of multi-analyzer system with automatic calibration unit. Hydraulic components only. Electrical and software components not shown.

sample air in all sample lines to equilibrate to a common temperature prior to entering the analyzer.

- Common temperature and radiation shielding for all reference gases.
- Minimization of dead volumes in calibration and valve system to ensure turbulent flow conditions and avoid contamination by previous samples.
- Flow rate of 2 L min^{-1} (Reynolds number $Re = 2520$) above critical flow rate of 1.8 L min^{-1} at critical Reynolds number ($Re_{crit} = 2320$) to ensure turbulent flow conditions in all tubes, at the same time keeping the flow rate as low as possible to minimize pressure drop across the system.
- Regular flow rate check and adjustment for all sample lines.
- Bypass system to avoid back pressure effects during calibration, featuring a low pressure drop bypass flow rate control device to ensure minimum necessary bypass flow and avoid possible reverse flow and sample contamination by ambient air.
- One common pump downstream of the analyzers to reduce effects of the pump on the concentration signals and to guarantee common pressure for all analyzers, assuming equal pipe geometry of all sample lines.
- Automatic control of constant overall system flow rate by mass flow controller.
- Passive system to allow for pressure equilibration between sample cells of individual gas analyzers by connecting all analyzer outlets to a manifold with a sufficiently large diameter and keeping the tubing between analyzer outlet and manifold as short as possible to minimize pressure drop.
- Pre-assembly measurement and evaluation of the pressure drop caused by individual system components to ensure that associated errors of the CO_2 concentration measurements are below accepted threshold.
- Vacuum and over pressure assisted leak check for the complete system to rule out sample contamination by ambient air.

All analyzers shared a common tailor-made automatic calibration system, using high precision reference gases (accuracy $0.1 \mu\text{mol mol}^{-1}$). The calibration routine included an automatic calibration every 4 hours using

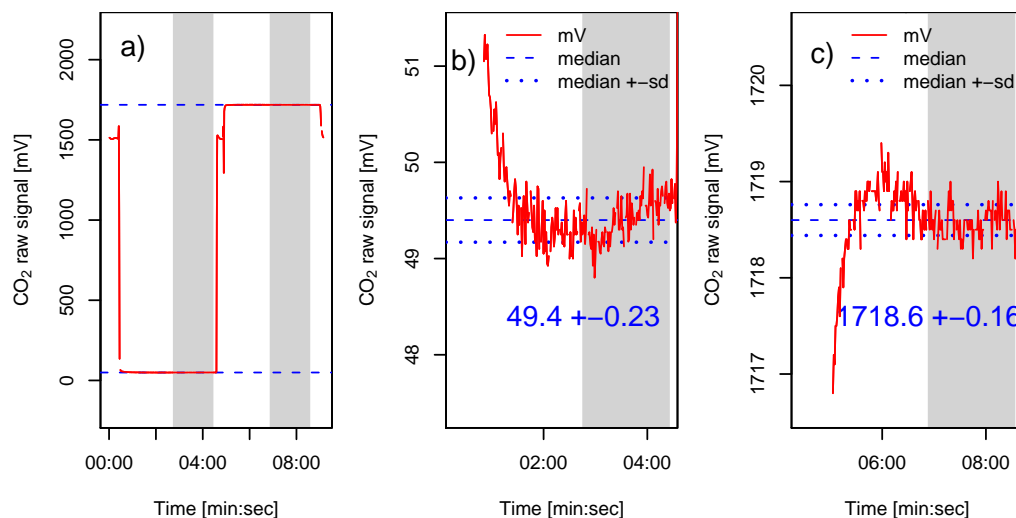


Figure 4: Raw CO_2 concentration signal (mV) during zero and span gas measurement. a) shows both zero and span gas measurement, b) is a closeup of the zero and c) a closeup of the span gas measurement, showing the adaptation of the signal to the reference concentration as well as the noise of the signal. Grey shaded areas mark data selected for zero and span calibration. Median and standard deviation (sd) also refer to the grey shaded areas. Start of measurement: June 30, 2008, 16:00:00. Location: M5. Values given in b) in units of mV correspond to $0 \pm 0.12 \mu\text{mol mol}^{-1}$ and values in c) correspond to $387.60 \pm 0.05 \mu\text{mol mol}^{-1}$.

two reference concentrations. Zero and span gas was applied for a duration of 240 s each, the last 40 % of which, i.e. 96 s, being used for zero and span calibration during data post-processing and the first 144 s allowing solely for adjustment of the signal to a stable reading (an initial small overshoot of the signal being common). The repeatability of the zero and span concentration reading was good (deviations of fractions of a $\mu\text{mol mol}^{-1}$ only) and readings had low noise levels during zero and span calibration. Fig. 4 shows the performance of the system during a selected zero and span measurement. The median standard deviations (complete IOP2 data set) of the concentration reading during individual applications of zero gas were 0.06, 0.06, 0.08, 0.17, 0.06, 0.08, 0.34, 0.11, 0.35, 0.06 $\mu\text{mol mol}^{-1}$, and standard deviation during the application of span gas were 0.07, 0.06, 0.08, 0.16, 0.06, 0.10, 0.38, 0.14, 0.52, 0.05 $\mu\text{mol mol}^{-1}$, for analyzers A01 through A10, respectively. After an initial zero and span calibration any further calibrations were performed by post-processing in software using zero and span measurements rather than making adjustments to the instrument's hardware. Analyzing the zero drift between individual calibration events yielded an inter-quartile range of 0.11,

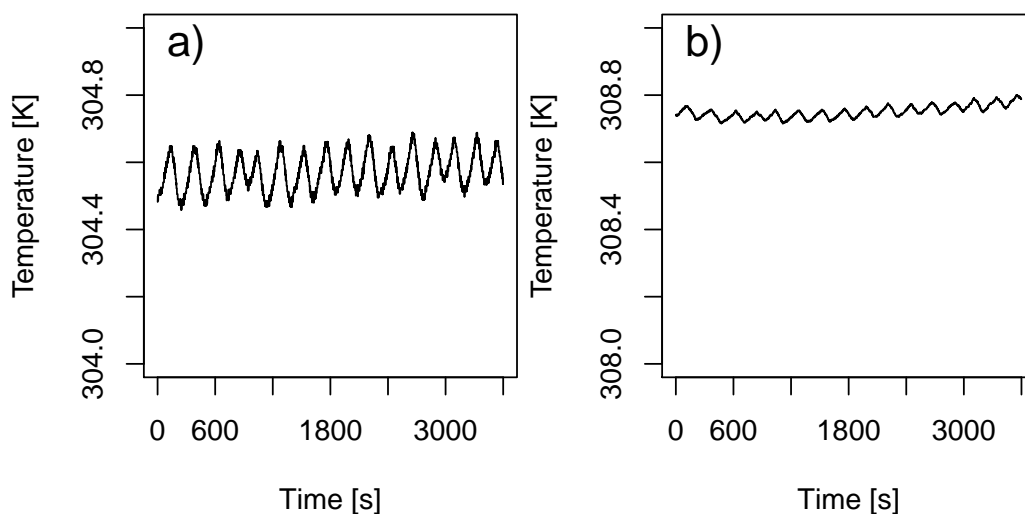


Figure 5: Performance of the automatic active temperature control system. a) Air temperature inside insulated housing. b) Cell temperature inside infrared gas analyzer. y-axis range is 1 K. 60 min data set starting at June 30, 2008, 21:00.

0.11, 0.25, 0.43, 0.12, 0.24, 0.23, 0.12, 0.16, $0.60 \mu\text{mol mol}^{-1}$, for analyzers A01 through A10, respectively. The same analysis for the span drift gave 0.97, 1.06, 1.24, 1.06, 0.97, 0.92, 0.82, 0.87, 0.73, $1.26 \mu\text{mol mol}^{-1}$.

In addition to factory calibration, each instrument's polynomial calibration function was established on site, using multiple standards. The polynomial was checked before and during the experiment. The carefully established polynomial functions were used for conversion of the recorded raw voltage signals to CO_2 concentrations in units of $\mu\text{mol mol}^{-1}$ during data post-processing. The advantage of the determination of calibration polynomials in the field is due to the combined real influences to the instruments in the field being reflected in the on-site established polynomials. A tight match could be achieved between fitted polynomials and measured reference concentrations, with maximum deviations between the two being 0.43, 0.49, 0.58, 0.55, 0.23, 1.38, 0.47, 0.28, 0.35, $0.40 \mu\text{mol mol}^{-1}$, for analyzers A01 through A10, respectively.

Heating and cooling devices were installed inside the insulated housing containing all analyzers in order to establish a common constant temperature environment. Temperature was controlled by an automatic controller set to a fixed temperature of 303 K. Figure 5 illustrates the performance of the temperature control system. The range of air temperature inside the insulated housing for the 60-min example given in Fig. 5 is only 0.23 K due to active control. The range of the cell temperature inside the infrared gas analyzer

is as small as 0.09 K owing to thermal inertia of the analyzer. Several fans were installed inside the housing for proper air circulation to ensure an even temperature distribution.

Concerning the accuracy of the analyzers, a selection of rated performance data is compiled in Table 1. The table suggests that the new system designed for and used during IOP2 should have superior performance to the system used during IOP1 due to the limited accuracy of the LI-820 analyzer. Results from the two observation periods presented in Appendix D confirm this. We therefore advise against further use of the LI-820 system for the measurement of horizontal gradients. Regarding the performance of the LI-6262 compared to its contemporary equivalent LI-7000 the reader is referred to LI-COR, Inc. (2005) for a comparison. On the basis of the published technical data of the two instruments it can be concluded that the relevant values concerning the accuracy which can be expected during horizontal gradient measurements are not very different if certain precautions are taken when working with the LI-6262, although the LI-7000 is more user-friendly and frees the user from controlling certain parameters. Among those are equilibration of sample temperature to external temperature and the choice of a sufficiently low flow rate to avoid pressure drop problems when using the LI-6262 (smaller line diameter). However, some published data are even superior for the LI-6262 compared to the LI-7000. Among those are a smaller zero drift of CO₂ and H₂O and the instrument's temperature equilibration time.

2.4.2 Post-processing of multi-analyzer data

Great care was taken to minimize inter-instrument bias in the CO₂ sampling system described above by appropriate system design and frequent control measurements of known standards. However, even after calibration to the standards, inter-instrument bias was too large to be acceptable for the strict requirements of horizontal gradient measurements. The remaining bias can be explained by instrument-specific differences of conditions (pressure) during regular measurements versus conditions during the measurement of reference gases.

Therefore a post-processing approach has been developed which performs a bias correction. The proposed concentration adjustment of a time series from a single analyzer is based on mutual information obtained from concentration time series from all analyzers. The basic assumption of the correction approach is that for spatially sufficiently close sample points during well mixed turbulent atmospheric conditions, the difference most likely to be observed between the concentration $c_i(t)$ at sample point i at time t and the average field concentration $\tilde{c}(t)$ is close to zero. The statistical measure de-

Table 1: Infrared gas analyzer accuracy and precision comparison. The values given refer to conditions at $350 \mu\text{mol mol}^{-1}$ and 298.15 K according to manufacturer's specification and converted to comparable units and standard conditions where necessary. Maximum values are given in parenthesis, typical values without.

	LI-6262	LI-6251	BINOS 4b2/4a2T	LI-840	LI-820
Range [$\mu\text{mol mol}^{-1}$]	0 to 3000	0 to 3000	Na	0 to 3000	0 to 1000
Accuracy [$\mu\text{mol mol}^{-1}$]	± 1 (<3)	± 1 (<3)	<1	5.3	14 ± 10
Zero drift [$\mu\text{mol mol}^{-1}$]	< 1 h^{-1}	< 1 h^{-1} , < 2 d^{-1}	<1	Na	< 1 d^{-1}
Zero drift with temp. [$\mu\text{mol mol}^{-1} \text{ K}^{-1}$]	0.12 (<0.45)	0.12 (<0.45)	Na	<0.15	Na
Span drift [$\mu\text{mol mol}^{-1}$]	< 1 d^{-1}	< 1 d^{-1}	<0.15	< 0.11 K^{-1}	< 1 d^{-1}
Total drift [$\mu\text{mol mol}^{-1}$]	Na	Na	Na	< 0.39 K^{-1}	Na
Linearity deviation [$\mu\text{mol mol}^{-1}$]	Na	Na	<0.5	Na	Na
Signal noise (pk-pk)	0.2 (<0.4) @1 s, 0.6 (<1) @0.1 s	0.2 @1 s, 0.1 @4 s	<0.25 @1.8 s	<1 @1 s	3.0 @1 s, 1.0 @20 s
Short term re- peatability [$\mu\text{mol mol}^{-1}$]	± 0.2	± 0.2	Na	Na	Na
ADC conversion	16-bits	–	–	14-bits	13-bits
Flow rate [L min^{-1}]	≤ 10	Na	0.5 to 2.5	≤ 1	≤ 1
Response time [s]	0.2	1	1.8	0.5 ?	0.5 ?

describing the concentration difference most likely to be observed is the mode of the probability density distribution (pdf) of the concentration differences $c_i(t) - \tilde{c}(t)$. A time dependent correction was performed for each sample point. Analyzer-specific values of instrument bias Δc_i were calculated for every 60 minute interval T_F of the concentration time series $c_i(t)$ by estimating the mode ($\max(\text{density})$) of the probability density distribution (pdf) of the instantaneous concentration differences $c_i(t) - \tilde{c}(t)$ according to

$$\Delta c_i = \max(\text{pdf}(c_i(t) - \tilde{c}(t))) \quad (3)$$

with the total number of analyzers $n = 10$ and the median field concentration $\tilde{c}(t)$ defined as

$$\tilde{c} = \begin{cases} c_{\frac{k+1}{2}} & k \text{ odd} \\ \frac{1}{2} (c_{\frac{k}{2}} + c_{\frac{k}{2}+1}) & k \text{ even} \end{cases} \quad (4)$$

with $k = 1 \dots n$ observations (c_1, c_2, \dots, c_k) being the concentration measurements ($c_1(t), c_2(t), \dots, c_n(t)$) at n locations sorted in ascending order.

The fulfillment of the above-stated requirement for well mixed conditions was monitored by the use of a mixing index, which was proposed as a measure of the degree of mixing and is based on cross-correlation between time series from individual sample points. The bias correction was only trained during periods when the mixing index was above a certain threshold. However, the complete time series were bias corrected by subtracting the bias from the time series in the specific 60-min interval. Periods for which no bias value could be determined due to insufficient mixing were corrected using the last valid bias value. Note that distributions with a mode equal to zero can have a mean value different from zero due to skewness. This is important for the computation of advection which relies on mean concentrations.

A detailed description of the bias correction approach is given in the publication in Appendix B. This includes a validity test of the above-stated basic assumption using Large Eddy Simulation (LES) modeling, the definition of the mixing index, methods for mode estimation, the detailed procedure of the correction approach, performance data and an error evaluation.

It could be shown that the bias correction approach proposed in the publication in Appendix B could be successfully applied to the observation of horizontal concentration gradients and advection as presented in the publication in Appendix D. The results presented therein suggest that advection estimates using data from the bias correction approach are more realistic than those obtained during IOP1 using the single analyzer system based on the LI-820.

2.5 Vertical wind velocity

The study of vertical wind velocity w which is needed for the computation of vertical advection was centered around the question of how to best apply coordinate rotation. Both spatial and temporal aspects of w were analyzed. As there were indications of significant contributions of long wavelengths in the signal of vertical wind velocity, a long-term data set of w was analyzed. More than ten years of turbulence data from the main tower at a 32 m height were processed and analyzed, starting from the raw data as they were recorded in the field.

Using a selected three-year subset of the long-term data set an analysis was performed on the impact of the length of the data set used during coordinate rotation by the planar fit method. Spectral analysis was applied to identify relevant frequencies and period lengths. Significant contributions from long wavelengths to the signal of w lead to the proposal of a sequential application of the coordinate rotation. Rotation coefficients are then determined for a sequence of windows with equal length, where the length no longer depends on the total length of the data set which is used during flux processing but can be specified by the user and adjusted to spectral characteristics of w at a given site. This has the potential to have a sufficiently large input for coordinate rotation procedures such as planar fit, at the same avoiding adverse effects of long-term trends of w .

The same long-term data set was used to study spatial characteristics of the wind field. The planar fit technique was applied on a sector-wise basis. This could eliminate directional dependencies of vertical wind velocity and achieve a mean vertical wind velocity close to zero ($\bar{w} = 0$) which is required by the eddy-covariance technique. Several filters on input data for the determination of rotation coefficients according to work from Hunner (2009) were tested using the long-term data set.

Details about the coordinate rotation procedure, data filters, the sequential rotation approach and the impact of the window length of the sequential coordinate rotation on vertical advection are given in the publication in Appendix D.

3 Results

The results presented in this section are derived from measurements over heterogeneous surface cover in complex terrain. The introduction to flux measurements in heterogeneous terrain in Sec. 1 already pointed to the importance and difficulties of relating the measured fluxes to their sources and sinks. A footprint based method has been indicated in Sec. 2, which was used to assess the footprint of the turbulent flux measurements for various conditions of atmospheric stratification. The following results show the relevance of the measured turbulent fluxes for the target land use at the site Waldstein-Weidenbrunnen (DE-Bay). The footprint climatology of the site is presented in Fig. 6 for flux measurements at a 36 m height at the turbulence tower during IOP1. Similar results were obtained during IOP2. One key finding here is that during daytime with unstable and neutral atmospheric stratification most of the footprint is located on Norway Spruce forest, which is the target land use of the site. Forest clearings are located in a marginal position relative to the footprint. With advection being relatively small during the day, the dominant part of daytime *NEE* of the spruce forest can be adequately described by the turbulent flux measured by eddy-covariance. However, during stable stratification of the nocturnal boundary-layer, the footprint is large and covers not only forest but also clearings, including a large clearing due to the storm “Kyrill” on January 18, 2007 (see “clearing 2007”, Fig. 6). This implies that turbulent flux measurements during stable stratification relate to mixed surface cover. A mixture of clearings and forest with different thermal and roughness properties can furthermore cause advective flux. Clearings also resemble preferred drainage paths into or out of the otherwise closed forest. This is important for katabatic drainage flows and CO₂ advection. The argument about footprint and katabatic drainage remains qualitative because the footprint model applies to the turbulent flux rather than drainage flows.

Forest areas which appear as a closed forest canopy on a larger scale, i.e. hundreds of meters (Fig. 6) were found to be heterogeneous on scales of meters to tens of meters as indicated by the spatial distribution of Plant Area Index (*PAI*) in Fig. 7. Gaps in the canopy provide less resistance to vertical exchange than dense canopy regions. The spatial heterogeneity of vertical exchange pathways has implications for horizontal concentration gradients inside the canopy, which will be presented below.

A complex wind regime was observed at the site. Whereas typical daytime conditions were characterized by prevailing winds from south-west and anabatic flow above and below the canopy, decoupling of conditions above

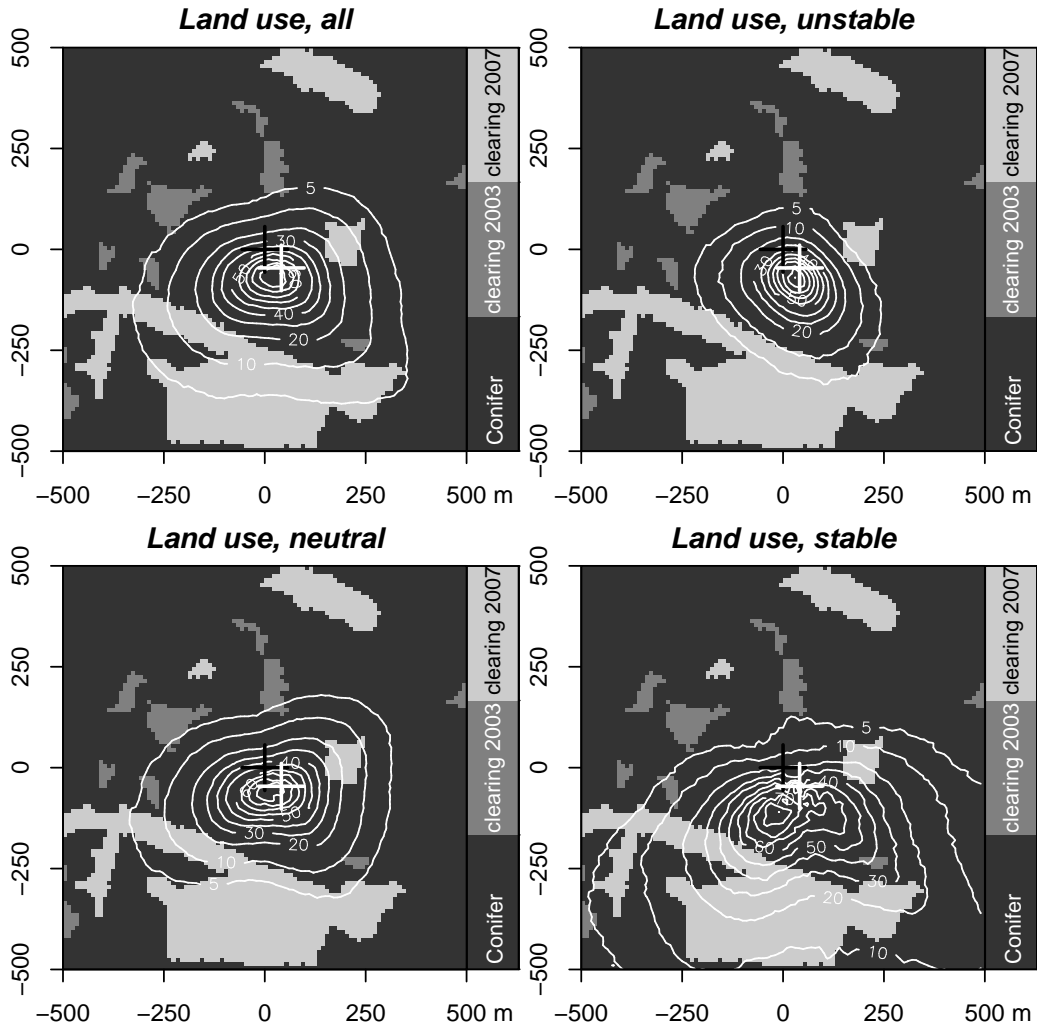


Figure 6: Footprint climatology over land use map, EGER IOP1, turbulence tower, for four classes of atmospheric stratification. White isolines show the relative flux contribution of the corresponding footprint area in 10 % intervals. The outermost isoline indicates the area from where 95 % of the flux originates. The black cross indicates the position of the main tower, the white cross the position of the turbulence tower. The plot is a map projection. X- and y-axis show distances in meters.

and below the canopy was frequently observed during the night with above-canopy wind direction either south-westerly (synoptic) or south-easterly due to channeled flow from the Lehstenbach valley in the South-East and sub-canopy katabatic drainage from North-East. This implies different footprints for above-canopy (turbulent flux) and below-canopy (horizontal advection)

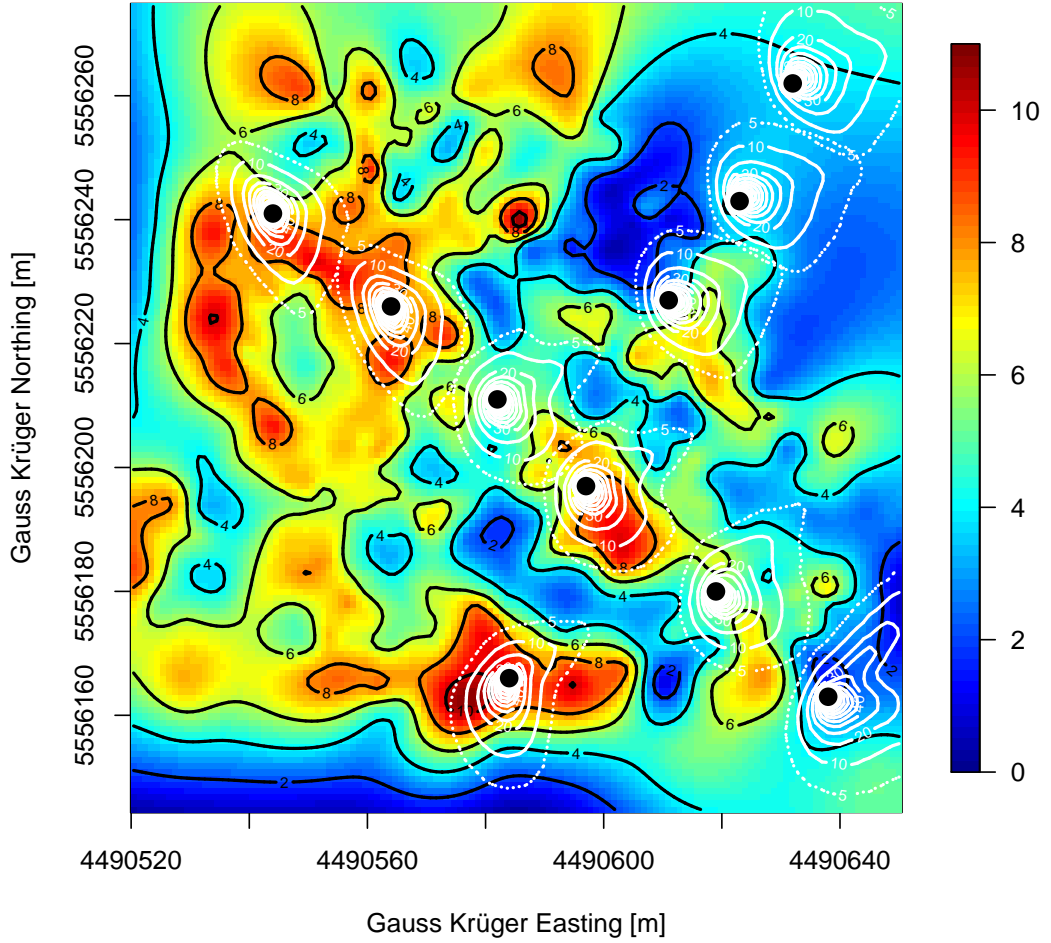


Figure 7: Map of Plant Area Index given as colors and black contour lines. Black points show the positions of the towers for sub-canopy measurements. X- and y-axis are distances in meters in the Gauss-Krüger coordinate system. White isolines show the relative flux contribution of the corresponding footprint area in 10 % intervals for stable cases only (IOP2). The outermost, dashed isoline indicates the area from where 95 % of the flux originates. Raw data of *PAI* were provided by E. Falge. Figure from Siebicke et al. (2011).

measurements during stable stratification.

Figure 8 shows the effect of sampling frequency of sub-canopy CO_2 concentration on 30-minute mean values of $c_i(t) - \tilde{c}(t)$. Large differences are observed between 30-min mean values from discontinuous sampling (simulating a single-analyzer which sequentially samples multiple points) and from continuous sampling (representing the newly developed multi-analyzer system). The scatter of their regression (Fig. 8a) is high (typical deviation of $5 \mu\text{mol mol}^{-1}$ as estimated from the cross-sectional width of the point cloud),

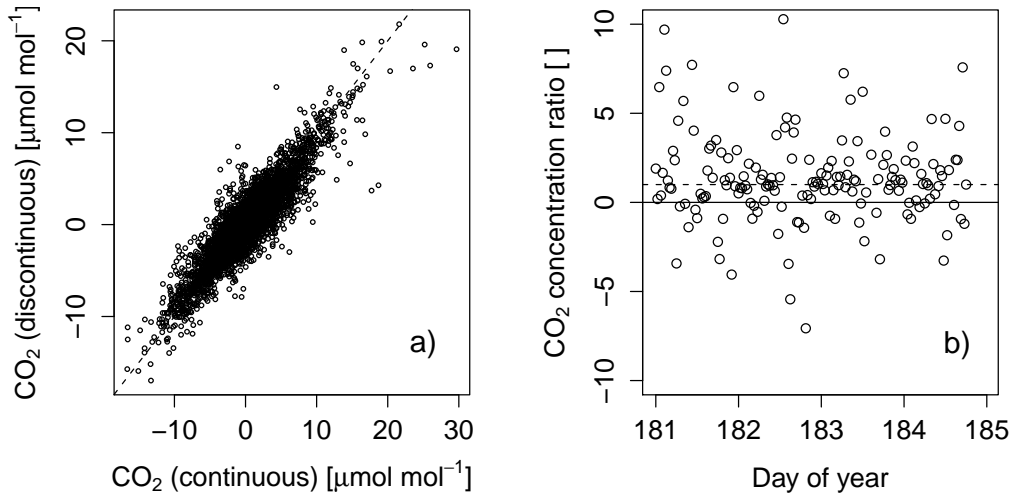


Figure 8: a) Regression of 30-minute mean CO₂ concentration differences during IOP2 from the discontinuous sampling approach versus CO₂ concentration differences from the continuous sampling approach. Concentration differences $c_i(t) - \tilde{c}(t)$ for $i \in (1, 10)$ are calculated as the local concentration minus the instantaneous median field concentration. b) Ratio of 30-minute mean CO₂ concentration differences from the discontinuous sampling approach to values from the continuous sampling approach for a selected four day period (“golden days”: DOY 181 to 184, 2008). Dashed line marks a ratio equal to one. Figure from Siebicke et al. (2010a).

and their fraction is often far from unity (Figure 8b). This implies that the often employed discontinuous sampling causes significant concentration errors which subsequently affect estimates of horizontal advection.

The analysis of sub-canopy CO₂ concentration and vegetation structure showed that local perturbations from the average concentration, $c_i(t) - \tilde{c}(t)$, were correlated with *PAI*, a measure of canopy density, as shown in Fig. 9. This was interpreted as the exposure of sub-canopy sample points to low concentration air entrainment from above the canopy and/or venting of CO₂ enriched sub-canopy air being affected by canopy density, i.e. a lower canopy density causes more vertical exchange and therefore a lower sub-canopy concentration due to mixing with above canopy air. This interpretation is supported by characteristics of coherent structures analyzed for the different sub-canopy locations. Local concentration perturbations during stable stratification were positively correlated with the number of coherent structures and negatively correlated with duration and amplitude of the latter (see example in Fig. 9b), all showing high correlation coefficients. This means that a low canopy density favors few but long lived structures with large impact on the sub-canopy concentration and vice versa. Combining this information

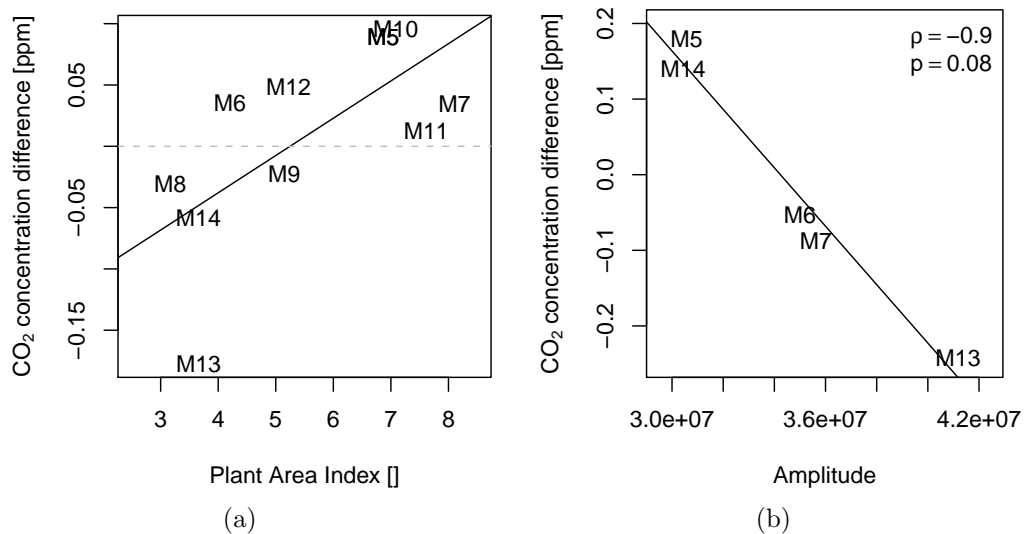


Figure 9: a) Mean local CO₂ concentration perturbations $c_i(t) - \tilde{c}(t)$ versus Plant Area Index, neutral stratification, all sample locations. b) Mean local CO₂ concentration perturbations (downslope transect) versus amplitude of wavelet variance of coherent structures per 30 minute interval (stable stratification). Linear regressions shown as solid line. Number of values: 307 from 11th of June to 13th of July, 2008. Sample locations according to Fig. 2. Figure from Siebicke et al. (2011).

with the small scale variability of PAI implies that sub-canopy concentration measurements need not be representative of the average gradients throughout the control volume but are affected by local concentration perturbations. Deduced horizontal advection estimates are therefore not necessarily representative for the control volume.

Coordinate rotation analysis indicated a significant impact of the planar fit window length on the amplitude of vertical wind velocity during the mean daily cycle (Fig. 10a). A planar fit window length of 400 days causes a 50 % increase in vertical advection compared to a 2.5 days window length (Fig. 10b). An intentional choice of a suitable window length is therefore essential for meaningful estimates of vertical advection and NEE .

Figure 11 summarizes the impact of advection on NEE during IOP1 (Fig. 11a) and IOP2 (Fig. 11b). The average daily cycle of NEE is shown on the one hand without advection (as the sum of turbulent flux and change of storage) and on the other hand including horizontal and vertical advection. Storage change and advection are also shown separately. While storage is the smallest term of the NEE budget advection is significant during the night and during transition periods, particularly in the evening. Major differences

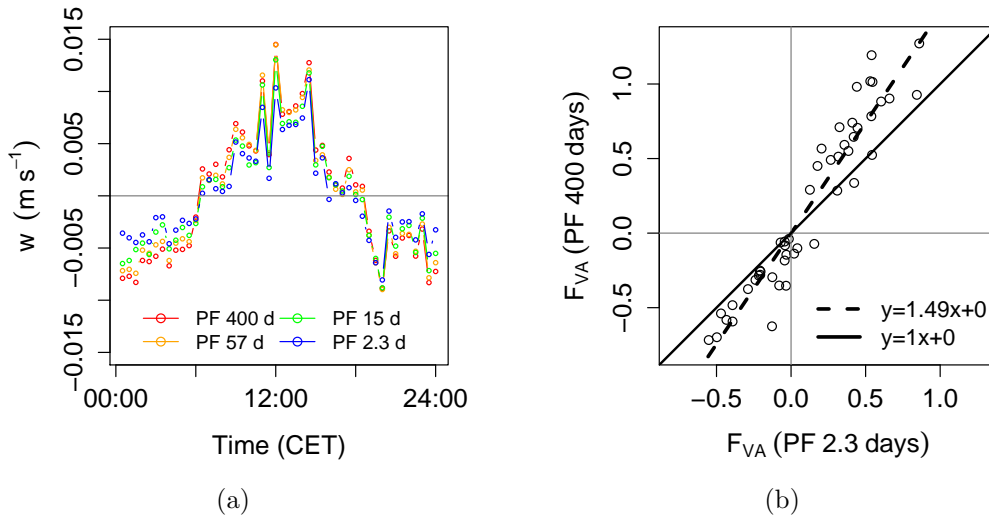


Figure 10: a) Mean daily cycle (30-min resolution) of vertical wind velocity on top of the main tower (long-term data set) for planar fit window lengths from 2.3 to 400 days. b) regression of vertical advection (as in Subfig. c) with a planar fit window length of 400 days versus vertical advection with a planar fit window length of 2.3 days and linear model fit (dashed line). Siebicke et al. (2010a).

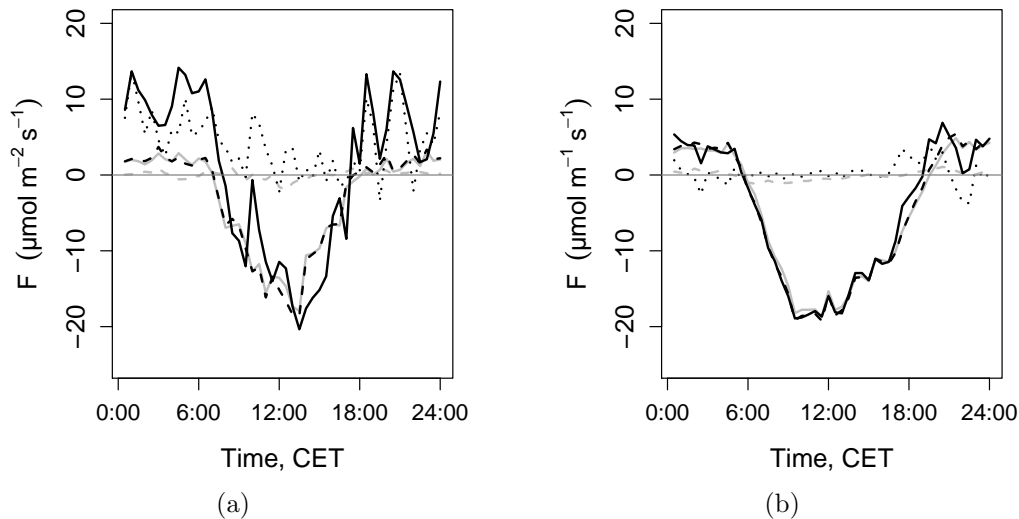


Figure 11: Median daily cycle of NEE with a 30-min resolution for IOP1 a), and IOP2 b), without advection (black dashed line), calculated as the sum of turbulent flux (grey solid line) and storage flux (grey dashed line) in comparison with NEE including advection (black solid line), calculated as the sum of turbulent flux, storage flux and the sum of vertical and horizontal advection (dotted line). Figure from Siebicke et al. (2010a).

were observed when comparing total advection from IOP1 and IOP2. Large values and rapid changes during IOP1 are mainly related to horizontal advection estimates. Despite different seasons, differences between horizontal advection observed during IOP1 and IOP2 were interpreted mainly as a consequence of the different sampling scheme, the analyzers used and the bias correction applied to sub-canopy CO₂ concentration measurements. Daily sums of *NEE* of carbon during IOP2 including advection were less negative ($-2.6 \text{ g C m}^{-2} \text{ d}^{-1}$) than *NEE* without advection ($-5.0 \text{ g C m}^{-2} \text{ d}^{-1}$). This was interpreted as an effect of the night flux error of the EC measurements, i.e. an overestimation of carbon sequestration due to missing flux at night in the case without advection and a better representation of the true flux when including advection. This interpretation was supported by soil chamber measurements. However, daily sums of *NEE* during IOP1 were overcorrected when including advection from discontinuous sampling (changing the carbon flux from -6.0 to $1.3 \text{ g C m}^{-2} \text{ d}^{-1}$).

4 Conclusions

Observations during the two field campaigns IOP1 and IOP2 of the EGER experiment showed that horizontal and vertical advection contributed significantly to the Net Ecosystem Exchange of carbon dioxide at the Waldstein-Weidenbrunnen (DE-Bay) FLUXNET site. This study addressed two of the major experimental challenges for direct advection measurements. These are the observation of horizontal CO₂ concentration gradients and the observation of vertical wind velocity. Measurements need to be accurate enough to observe small concentration differences and small wind velocities, and they need to have a high spatio-temporal resolution to give representative estimates of the 3-dimensional structure of the concentration and wind field in the control volume.

Regarding direct measurements of horizontal advection, which rely on measurements of horizontal CO₂ concentration gradients, the following is concluded with respect to the measurement system:

- the novel CO₂ sampling system which was developed allows for the synchronous observation of multiple sampling positions (ten in this case),
- the temporal sampling resolution of each point could be improved from several minutes (typically 30 min mean values of gradients in a conventional system) to 1 s,
- the new system is free of the tradeoff between temporal and spatial resolution of conventional single-analyzer systems, because it utilizes an individual analyzer for each sampling point,
- the novel statistical correction method which was developed and successfully applied accounts for inter-instrument bias, which used to be a major drawback of multi-analyzer systems.

Concerning the spatio-temporal representativity of (nocturnal) sub-canopy CO₂ concentration gradients for the control volume it can be concluded that

- the sub-canopy concentration field is not only controlled by large scale katabatic drainage and the distribution of sources and sinks in the canopy and in the soil, but it is also affected by vertical exchange across large vertical concentration gradients, with CO₂ enriched air close to the ground and low concentration air above the canopy.

- While the entrainment of above-canopy air and mixing with the sub-canopy drainage layer had been previously suggested by Aubinet et al. (2003), with the high frequency measurement setup of the current study it was possible to show the effect of vertical mixing on sub-canopy CO₂ concentration by actual measurements, and furthermore, to show that this vertical exchange was related to coherent structures, and to show how vertical exchange was dependent on atmospheric stratification and the coupling of different layers of the canopy.
- The observation of short lived phenomena such as coherent structures was only possible due to the high temporal sampling resolution of the new system.
- The sampling frequency had a large impact on local 30-min mean concentration values, suggesting that mean values obtained with a low sampling frequency could be affected by a significant error.
- Local sub-canopy CO₂ concentration characteristics correlated with vegetation structure. Observed concentration gradients were thus not consistent throughout the control volume but varied locally with a length scale on the order of the size of vegetation elements (single trees or small groups of trees).
- Most current advection measurement designs are unable to capture the small scale variability of the in-canopy concentration variation.

Therefore, the design of further advection experiments should take into account both the characteristics of katabatic drainage flows as well as the effect of vertical mixing on in-canopy concentration, with significant vertical exchange not being limited to day time conditions. The combination of multi-sensor setups with the presented statistical correction approach provides the chance in future experiments of closing the gap between the spatial resolution of existing measurement designs and the characteristic length scale of variations of the concentration field if enough sensors can be deployed.

The statistical bias correction approach need not be limited to the application of concentration measurements. It should be tested whether a dense network of simple sensors measuring a scalar quantity and combined with statistical bias correction can be used to infer the 3-D flow field in the control volume by statistical means. Hopefully, such a dense sensor network setup will yield estimates of the wind field which satisfy mass continuity better than existing designs with sparse observation points, and therefore

resolve the problem of the often limited representativity of current advection estimates for the control volume.

Regarding vertical advection estimates, which rely on the measurement of vertical wind velocity, it can be concluded that

- coordinate rotation is a crucial post-processing step for vertical advection estimates,
- the data set length used for coordinate rotation had large impact on vertical advection, resulting in 50 % larger vertical advection estimates when using window lengths of 400 d versus window lengths of 2.3 d, due to the low frequency component in the spectrum of vertical wind velocity,
- therefore, a sequential coordinate rotation was proposed to account for this effect, which allows to choose an appropriate window length,
- sector-wise coordinate rotation clearly performed better than the original planar fit in producing a mean vertical wind velocity close to zero without directional dependencies,
- sequential and sector-wise coordinate rotation improve the representativity of the vertical wind velocity measurement but cannot overcome the limitations of a single point measurement,
- if the above-mentioned dense sensor network approach proves to be successful it might be used to infer vertical wind velocity by means of a mass continuity approach.

With respect to the contribution of combined advection to Net Ecosystem Exchange at the Waldstein-Weidenbrunnen (DE-Bay) site we conclude that

- advection contributed significantly to NEE during the night and during transition periods,
- horizontal advection estimates from continuous gradient sampling during IOP2 were of realistic magnitude and could be related to meteorological drivers, while horizontal advection estimates from discontinuous gradient sampling during IOP1 were unrealistically large and noisy,
- NEE budgets during IOP2 were improved if direct advection measurements were included compared to NEE from turbulent flux and storage change alone, reducing the estimated daily carbon sequestration of the forest by almost 50 %.

Given their large contribution to budgets of Net Ecosystem Exchange mentioned above, the advective flux components need to be accounted for in long-term carbon budget assessments. However, due to their extensive resource requirements, advection measurements are still limited to specialized campaigns without an obvious solution for an advection measurement setup simple enough to accompany routine measurements of the turbulent flux and storage flux at many of the existing sites. Alternative measurement approaches presented in the current work can already be used to improve the spatio-temporal representativity of advection estimates, and further directions were indicated which will hopefully improve spatio-temporal representativity even further. It remains to be shown by experiments to come whether a cost effective sensor network solution can be found to measure advection at a large number of sites or whether advection needs to be parametrized or modelled.

References

- Acevedo, O., Moraes, O., Fitzjarrald, D., Sakai, R., Mahrt, L., 2007. Turbulent carbon exchange in very stable conditions. *Boundary-Layer Meteorol.* 125, 49–61.
- Aubinet, M., 2008. Eddy covariance CO₂ flux measurements in nocturnal conditions: an analysis of the problem. *Ecological Applications* 18, 1368–1378.
- Aubinet, M., Berbigier, P., Bernhofer, C., Cescatti, A., Feigenwinter, C., Graniers, A., Grunwald, T., Havrankova, K., Heinesch, B., Longdoz, B., Marcolla, B., Montagnani, L., Sedlak, P., 2005. Comparing CO₂ storage and advection conditions at night at different CARBOEUROFLUX sites. *Boundary-Layer Meteorol.* 116, 63–94.
- Aubinet, M., Feigenwinter, C., Heinesch, B., Bernhofer, C., Canepa, E., Lindroth, A., Montagnani, L., Rebmann, C., Sedlak, P., Gorsel, E. V., 2010. Direct advection measurements do not help to solve the night-time CO₂ closure problem: Evidence from three different forests. *Agric. For. Meteorol.* 150, 655–664.
- Aubinet, M., Grelle, A., Ibrom, A., Rannik, Ü., Moncrieff, J. B., Foken, T., Kowalski, A. S., Martin, P., Berbigier, P., Bernhofer, C., Clement, R., Elbers, J. A., Granier, A., Grünwald, T., Morgenstern, K., Pilegaard, K., Rebmann, C., Snijders, W., Valentini, R., Vesala, T., 2000. Estimates of the annual net carbon and water exchange of European forests: the EUROFLUX methodology. *Advances in Ecological Research* 30, 113–175.
- Aubinet, M., Heinesch, B., Yernaux, M., 2003. Horizontal and vertical CO₂ advection in a sloping forest. *Boundary-Layer Meteorol.* 108, 397–417.
- Baldocchi, D., Finnigan, J. J., Wilson, K., Paw U, K. T., Falge, E., 2000. On measuring net ecosystem carbon exchange over tall vegetation on complex terrain. *Boundary-Layer Meteorol.* 96, 257–291.
- Baldocchi, D. D., 2003. Assessing the eddy covariance technique for evaluating carbon dioxide exchange rates of ecosystems: past, present and future. *Global Change Biology* 9 (4), 479–492.
- Baldocchi, D. D., Falge, E., Gu, L., Olson, R., Hollinger, D., Running, S., Anthoni, P., Bernhofer, C., Davis, K., Evans, R., Fuentes, J., Goldstein, A., Katul, G., Law, B., Lee, X., Malhi, Y., Meyers, T., Munger, W., Oechel,

- W., Paw, K. T., Pilegaard, K., Schmid, H. P., Valentini, R., Verma, S., Vesala, T., Wilson, K., Wofsy, S., 2001. Fluxnet: A new tool to study the temporal and spatial variability of ecosystem-scale carbon dioxide, water vapor, and energy flux densities. *Bulletin of the American Meteorological Society* 82 (11), 2415–2434.
- Belcher, S. E., Finnigan, J. J., Harman, I. N., 2008. Flows through forest canopies in complex terrain. *Ecological Applications* 18, 1436–1453.
- Beyrich, F., Leps, J.-P., Mauder, M., Bange, J., Foken, T., Huneke, S., Lohse, H., Lüdi, A., Meijninger, W., Mironov, D., Weisensee, U., Zittel, P., 2006. Area-averaged surface fluxes over the Litfass region based on eddy-covariance measurements. *Boundary-Layer Meteorol.* 121, 33–65.
- Canepa, E., Georgieva, E., Manca, G., Feigenwinter, C., 2010. Application of a mass consistent flow model to study the CO₂ mass balance of forests. *Agric. For. Meteorol.* 150, 712–723.
- de Araujo, A. C., Kruijt, B., Nobre, A. D., Dolman, A. J., Waterloo, M. J., Moors, E. J., de Souza, J. S., 2008. Nocturnal accumulation of CO₂ underneath a tropical forest canopy along a topographical gradient. *Ecological Applications* 18, 1406–1419.
- Dellwik, E., Mann, J., Larsen, K. S., 2010. Flow tilt angles near forest edges – Part 1: Sonic anemometry. *Biogeosciences* 7, 1745–1757.
- Etzold, S., Buchmann, N., Eugster, W., 2010. Contribution of advection to the carbon budget measured by eddy covariance at a steep mountain slope forest in Switzerland. *Biogeosciences* 7, 2461–2475.
- Falge, E., Baldocchi, D., Olson, R., Anthoni, P., Aubinet, M., Bernhofer, C., Burba, G., Ceulemans, R., Clement, R., Dolman, H., Granier, A., Gross, P., Grünwald, T., Hollinger, D., Jensen, N.-O., Katul, G., Keronen, P., Kowalski, A., Laim, C. T., Law, B. E., Meyers, T., Moncrieff, J., Moors, E., Munger, J. W., Pilegaard, K., Rannik, Ü., Rebmann, C., Suyker, A., Tenhunen, J., Tu, K., Verma, S., Vesala, T., Wilson, K., Wofsy, S., 2001. Gap filling strategies for defensible annual sums of net ecosystem exchange. *Agric. For. Meteorol.* 107, 43–69.
- Feigenwinter, C., Bernhofer, C., Eichelmann, U., Heinesch, B., Hertel, M., Janous, D., Kolle, O., Lagergren, F., Lindroth, A., Minerbi, S., Moderow, U., Molder, M., Montagnani, L., Queck, R., Rebmann, C., Vestin, P., Yernaux, M., Zeri, M., Ziegler, W., Aubinet, M., 2008. Comparison of

- horizontal and vertical advective CO₂ fluxes at three forest sites. *Agric. For. Meteorol.* 148, 12–24.
- Feigenwinter, C., Bernhofer, C., Vogt, R., 2004. The influence of advection on the short term CO₂-budget in and above a forest canopy. *Boundary-Layer Meteorol.* 113, 201–224.
- Feigenwinter, C., Montagnani, L., Aubinet, M., 2010a. Plot-scale vertical and horizontal transport of CO₂ modified by a persistent slope wind system in and above an alpine forest. *Agric. For. Meteorol.* 150 (5), 665 – 673.
- Feigenwinter, C., Mölder, M., Lindroth, A., Aubinet, M., 2010b. Spatiotemporal evolution of CO₂ concentration, temperature, and wind field during stable nights at the Norunda forest site. *Agric. For. Meteorol.* 150 (5), 692 – 701.
- Finnigan, J., 1999. A comment on the paper by Lee (1998): "on micrometeorological observations of surface–air surface exchange over tall vegetation". *Agric. For. Meteorol.* 97, 55–67.
- Finnigan, J., 2006. The storage term in eddy flux calculations. *Agric. For. Meteorol.* 136 (3-4), 108 – 113.
- Finnigan, J., 2008. An introduction to flux measurements in difficult conditions. *Ecological Applications* 18, 1340–1350.
- Finnigan, J. J., 2004. A Re-Evaluation of Long-Term Flux Measurement Techniques Part II: Coordinate Systems. *Boundary-Layer Meteorol.* 113, 1–41.
- Finnigan, J. J., Belcher, S. E., 2004. Flow over a hill covered with a plant canopy. *Quarterly Journal of the Royal Meteorological Society* 130, 1–29.
- Finnigan, J. J., Clement, R., Malhi, Y., Leuning, R., Cleugh, H., 2003. A Re-Evaluation of Long-Term Flux Measurement Techniques Part I: Averaging and Coordinate Rotation. *Boundary-Layer Meteorol.* 107, 1–48.
- Foken, T., Göckede, M., Mauder, M., Mahrt, L., Amiro, B. D., Munger, J. W., 2004. Post-field data quality control. In: *Handbook of Micrometeorology: A Guide for Surface Flux Measurements*. Kluwer Academic Publishers, Dordrecht, pp. 181–208.
- Foken, T., Leclerc, M. Y., 2004. Methods and limitations in validation of footprint models. *Agric. For. Meteorol.* 127, 223–234.

- Foken, T., Meixner, F. X., Falge, E., Zetzsch, C., Serafimovich, A., Bargsten, A., Behrendt, T., Biermann, T., Breuninger, C., Gerken, T., Hunner, M., Lehmann-Pape, L., Hens, K., Jocher, G., Kesselmeier, J., Lüers, J., Mayer, J.-C., Moravek, A., Plake, D., Riederer, M., Rütz, F., Schier, S., Siebicke, L., Sörgel, M., Staudt, K., Trebs, I., Tsokankunku, A., Wolff, V., Zhu, Z., 2011. Atmospheric transport and chemistry in forest ecosystems – overview of the EGER-project. *Agric. For. Meteorol.* (to be submitted).
- Foken, T., Wichura, B., 1996. Tools for quality assessment of surface-based flux measurements. *Agric. For. Meteorol.* 78, 83–105.
- Froelich, N. J., Schmid, H. P., 2006. Flow divergence and density flows above and below a deciduous forest Part II. Below-canopy thermotopographic flows. *Agric. For. Meteorol.* 138, 29–43.
- Froelich, N. J., Schmid, H. P., Grimmond, C. S. B., Su, H.-B., Oliphant, A. J., 2005. Flow divergence and density flows above and below a deciduous forest: Part I. Non-zero mean vertical wind above canopy. *Agric. For. Meteorol.* 133 (1-4), 140 – 152.
- Geissbühler, P., Siegwolf, R., Eugster, W., 2000. Eddy covariance measurements on mountain slopes: the advantage of surface-normal sensor orientation over a vertical set-up. *Boundary-Layer Meteorol.* 96, 371–392.
- Gerstberger, P., Foken, T., Kalbitz, K., 2004. The Lehstenbach and Steinkreuz Catchments in NE Bavaria, Germany. In: Matzner, E. (Ed.), *Biogeochemistry of Forested Catchments in a Changing Environment: A German Case Study*. Vol. 172. Springer, Heidelberg, pp. 15–41.
- Gorsel, van, E., Ev, A., Leuning, R., Cleugh, H. A., Keith, H., Suni, T., 2007. Nocturnal carbon efflux: reconciliation of eddy covariance and chamber measurements using an alternative to the u_* -threshold filtering technique. *Tellus B* 59, 397–403.
- Goulden, M. L., Miller, S. D., Humberto, da Rocha, R., 2006. Nocturnal cold air drainage and pooling in a tropical forest. *Journal of Geophysical Research* 111, D08S04.
- Goulden, M. L., Munger, J. W., Fan, S.-M., Daube, B. C., Wofsy, S. C., 1996. Measurements of carbon sequestration by long-term eddy covariance: methods and a critical evaluation of accuracy. *Global Change Biology* 2 (3), 169–182.

- Gu, L., Falge, E. M., Boden, T., Baldocchi, D. D., Black, T., Saleska, S. R., Suni, T., Verma, S. B., Vesala, T., Wofsy, S. C., Xu, L., 2005. Objective threshold determination for nighttime eddy flux filtering. *Agric. For. Meteorol.* 128, 179–197.
- Göckede, M., Foken, T., Aubinet, M., Aurela, M., Banza, J., Bernhofer, C., Carrara, J.-M. B. Y. B. A., Clement, R., Dellwik, E., Elbers, J., Eugster, W., Fuhrer, J., Granier, A., Grünwald, T., Heinesch, B., Janssens, I., Knohl, A., Koeble, R., Laurila, T., Longdoz, B., Manca, G., Marekand, M., Markkanen, T., Mateus, J., Matteucci, G., Mauder, M., Migliavacca, M., Minerbi, S., Moncrieff, J., Montagnani, L., Moors, E., Ourcival, J.-M., Papale, D., Pereira, J., Pilegaard, K., Pita, G., Rambal, S., Rebmann, C., Rodrigues, A., Rotenberg, E., Sanz, M., Sedlak, P., Seufert, G., Siebicke, L., Soussana, J., Valentini, R., Vesala, T., Verbeeck, H., Yakir, D., 2008. Quality control of CarboEurope flux data – Part 1: Coupling footprint analyses with flux data quality assessment to evaluate sites in forest ecosystems. *Biogeosciences* 5, 433–450, "CarboEurope-IP Best Paper Award 2008".
- Göckede, M., Markkanen, T., Hasager, C. B., Foken, T., 2006. Update of a footprint-based approach for the characterisation of complex measurement sites. *Boundary-Layer Meteorol.* 118, 635–655.
- Göckede, M., Rebmann, C., Foken, T., 2004. A combination of quality assessment tools for eddy covariance measurements with footprint modelling for the characterisation of complex sites. *Agric. For. Meteorol.* 127, 175–188.
- Harman, I. N., Finnigan, J. J., 2007. A simple unified theory for flow in the canopy and roughness sublayer. *Boundary-Layer Meteorol.* 123, 339–363.
- Hasager, C. B., Jensen, N. O., 1999. Surface-flux aggregation in heterogeneous terrain. *Quarterly Journal of the Royal Meteorological Society* 125, 2075–2102.
- Heinesch, B., Yernaux, M., Aubinet, M., 2008. Dependence of CO₂ advection patterns on wind direction on a gentle forested slope. *Biogeosciences* 5, 657–668.
- Heinesch, B., Yernaux, M., Aubinet, M., 2007. Some methodological questions concerning advection measurements: a case study. *Boundary-Layer Meteorol.* 122, 457–478.

- Hollinger, D. Y., Kelliher, F. M., Byers, J. N., Hunt, J. E., McSeveny, T. M., Weir, P. L., 1994. Carbon dioxide exchange between an undisturbed old-growth temperate forest and the atmosphere. *Ecology* 75, 134–150.
- Hunner, M., April 2009. Investigation of advection and the wind field in a spruce forest. Master's thesis, Department of Micrometeorology, University of Bayreuth, Germany, 90 pp.
- Katul, G., Finnigan, J., Poggi, D., Leuning, R., Belcher, S., 2006. The influence of hilly terrain on canopy-atmosphere carbon dioxide exchange. *Boundary-Layer Meteorol.* 118, 189–216.
- Klaassen, W., Sogachev, A., 2006. Flux footprint simulation downwind of a forest edge. *Boundary-Layer Meteorol.* 121, 459–473.
- Komatsu, H., Yoshida, N., Takizawa, H., Kosaka, I., Tantasirin, C., Suzuki, M., 2003. Seasonal trend in the occurrence of nocturnal drainage flow on a forested slope under a tropical monsoon climate. *Boundary-Layer Meteorol.* 106, 573–592.
- Kramm, G., Dlugi, R., Zelger, M., 2008. On the recognition of fundamental physical principles in recent atmospheric-environmental studies. *Journal of the Calcutta Mathematical Society* 4, 31–56.
- Kutsch, W. L., Kolle, O., Rebmann, C., Knohl, A., Ziegler, W., Schulze, E.-D., 2008. Advection and resulting CO₂ exchange uncertainty in a tall forest in central Germany. *Ecological Applications* 18, 1391–1405.
- Leclerc, M. Y., Karipot, A., Prabha, T., Allwine, G., Lamb, B., Gholz, H. L., 2003. Impact of non-local advection on flux footprints over a tall forest canopy: a tracer flux experiment. *Agric. For. Meteorol.* 115 (1-2), 19 – 30.
- Lee, X., 1998. On micrometeorological observations of surface–air surface exchange over tall vegetation. *Agric. For. Meteorol.* 91, 39–49.
- Lee, X., 1999. Reply to comment by Finnigan on “On micrometeorological observations of surface-air exchange over tall vegetation”. *Agric. For. Meteorol.* 97 (1), 65 – 67.
- Lee, X., Finnigan, J., Paw U, K., 2004a. Handbook of Micrometeorology—A Guide for Surface Flux Measurement and Analysis. Kluwer Academic Publishers, Ch. Coordinate systems and flux bias error, p. 33–54.

- Lee, X., Hu, X., 2002. Forest-air fluxes of carbon, water and energy over non-flat terrain. *Boundary-Layer Meteorol.* 103, 277–301.
- Lee, X., Neumann, H., Hartog, G., Mickle, R., Fuentes, J., Black, T., Yang, P., Blanken, P., 1997. Observation of gravity waves in a boreal forest. *Boundary-Layer Meteorol.* 84, 383–398.
- Lee, X., Yu, Q., Sun, X., Liu, J., Min, Q., Liu, Y., Zhang, X., 2004b. Micrometeorological fluxes under the influence of regional and local advection: a revisit. *Agric. For. Meteorol.* 122 (1-2), 111 – 124.
- Leuning, R., Zegelin, S. J., Jones, K., Keith, H., Hughes, D., 2008. Measurement of horizontal and vertical advection of CO₂ within a forest canopy. *Agric. For. Meteorol.* 148, 1777–1797.
- LI-COR, Inc., 10 2005. Why the LI-7000? A Comparison Between LI-7000 and LI-6262. http://www.licor.com/env/2010/pdf/gas_analyzers/7000/7000_6262-3.7b.pdf, pN980-06623 Rev. 1.
- Liu, H., Peters, G., Foken, T., 2001. New equations for sonic temperature variance and buoyancy heat flux with an omnidirectional sonic anemometer. *Boundary-Layer Meteorol.* 100, 459–468.
- Mahrt, L., 1999. Stratified atmospheric boundary layers. *Boundary-Layer Meteorol.* 90, 375–396.
- Mahrt, L., 2010. Computing turbulent fluxes near the surface: Needed improvements. *Agric. For. Meteorol.* 150 (4), 501 – 509.
- Mahrt, L., Vickers, D., 2006. Extremely weak mixing in stable conditions. *Boundary-Layer Meteorol.* 119, 19–39.
- Mahrt, L., Vickers, D., Nakamura, R., Soler, M. R., Sun, J., Burns, S., Lenchow, D., 2001. Shallow drainage flows. *Boundary-Layer Meteorol.* 101, 243–260.
- Mammarella, I. ., Kolar, P., Rinne, J. ., Keronen, P., Pumpanen, J. ., Vesala, T., 2007. Determining the contribution of vertical advection to the net ecosystem exchange at Hyytiälä forest, Finland. *Tellus* 59B, 900–909.
- Marcolla, B., Cescatti, A., Montagnani, L., Manca, G., Kerschbaumer, G., Minerbi, S., 2005. Importance of advection in the atmospheric CO₂ exchanges of an alpine forest. *Agric. For. Meteorol.* 130, 193–206.

- Massman, W. J., Lee, X., 2002. Eddy covariance flux corrections and uncertainties in long-term studies of carbon and energy exchanges. *Agric. For. Meteorol.* 113 (1-4), 121 – 144.
- Mauder, M., Foken, T., 2004. Documentation and instruction manual of the eddy covariance software package TK2. *Arbeitsergebnisse* 26, University of Bayreuth, Department of Micrometeorology, ISSN 1614-8916, 45 pp.
- McMillen, R. T., 1988. An eddy correlation technique with extended applicability to non-simple terrain. *Boundary-Layer Meteorol.* 43, 231–245.
- Moncrieff, J. B., Massheder, J. M., de Bruin, H., Elbers, J., Friborg, T., Heusinkveld, B., Kabat, P., Scott, S., Soegaard, H., Verhoef, A., 1997. A system to measure surface fluxes of momentum, sensible heat, water vapour and carbon dioxide. *Journal of Hydrology* 188–189, 589–611.
- Montagnani, L., Manca, G., Canepa, E., Georgieva, E., 2010. Assessing the method-specific differences in quantification of CO₂ advection at three forest sites during the ADVEX campaign. *Agric. For. Meteorol.* 150, 702–711.
- Moore, C. J., 1986. Frequency response corrections for eddy correlation systems. *Boundary-Layer Meteorol.* 37, 17–35.
- Oncley, S., Foken, T., Vogt, R., Kohsiek, W., DeBruin, H., Bernhofer, C., Christen, A., Gorsel, E., Grantz, D., Feigenwinter, C., Lehner, I., Liebethal, C., Liu, H., Mauder, M., Pitacco, A., Ribeiro, L., Weidinger, T., 2007. The Energy Balance Experiment EBEX-2000. Part I: overview and energy balance. *Boundary-Layer Meteorol.* 123, 1–28.
- Oncley, S. P., Schwenz, K., Sun, J., Burns, S. P., Monson, R. K., 2008. Measuring in-canopy advection of carbon dioxide using a new transect measurement system (TRAM). In: 28th Conference on Agricultural and Forest Meteorology, American Meteorological Society, 28 April–2 May 2008.
- Paw U, K. T., Baldocchi, D. D., Meyers, T. P., Wilson, K. B., 2000. Correction of eddy-covariance measurements incorporating both advective effects and density fluxes. *Boundary-Layer Meteorol.* 97, 487–511.
- Paw U, K. T., Brunet, Y., Collineau, S., Shaw, R. H., Maitani, T., Qiu, J., Hipps, L., 1992. On coherent structures in turbulence above and within agricultural plant canopies. *Agric. For. Meteorol.* 61, 55–68.
- Paw U, K. T., Falk, M., Suchanek, T. H., Ustin, S. L., Chen, J., Park, Y.-S., Winner, W. E., Thomas, S. C., Hsiao, T. C., Shaw, R. H., King,

- T. S., Pyles, R. D., Schroeder, M., Matista, A. A., 2004. Carbon dioxide exchange between an old-growth forest and the atmosphere. *Ecosystems* 7, 513–524.
- Pyles, R. D., Weare, B. C., Paw U, K. T., 2000. The UCD Advanced Canopy-Atmosphere-Soil Algorithm: comparisons with observations from different climate and vegetation regimes. *Quarterly Journal of the Royal Meteorological Society* 126, 2951–2980.
- Pypker, T., Unsworth, M., Lamb, B., Allwine, E., Edburg, S., Sulzman, E., Mix, A., Bond, B., 2007. Cold air drainage in a forested valley: Investigating the feasibility of monitoring ecosystem metabolism. *Agric. For. Meteorol.* 145 (3-4), 149 – 166.
- Rannik, Ü., Markkanen, T., Raittila, J., Hari, P., Vesala, T., 2003. Turbulence statistics inside and over forest: Influence on footprint prediction. *Boundary-Layer Meteorol.* 109, 163–189.
- Rebmann, C., Göckede, M., Foken, T., Aubinet, M., Aurela, M., Berbigier, P., Bernhofer, C., Buchmann, N., Carrara, A., Cescatti, A., Ceulemans, R., Clement, R., Elbers, J. A., Granier, A., Grunwald, T., Guyon, D., Havrankova, K., Heinesch, B., Knohl, A., Laurila, T., Longdoz, B., Marcolla, B., Markkanen, T., Miglietta, F., Moncrieff, J., Montagnani, L., Moors, E., Nardino, M., Ourcival, J. M., Rambal, S., Rannik, U., Rotenberg, E., Sedlak, P., Unterhuber, G., Vesala, T., Yakir, D., 2005. Quality analysis applied on eddy covariance measurements at complex forest sites using footprint modelling. *Theoretical and Applied Climatology* 80, 121–141.
- Rebmann, C., Zeri, M., Lasslop, G., Mund, M., Kolle, O., Schulze, E.-D., Feigenwinter, C., 2010. Treatment and assessment of the CO₂-exchange at a complex forest site in Thuringia, Germany. *Agric. For. Meteorol.* 150, 684–691.
- Ruppert, J., 2005. ATEM software for atmospheric turbulent exchange measurements using eddy covariance and relaxed eddy accumulation systems and Bayreuth whole-air REA system setup. *Arbeitsergebnisse*, 28, University of Bayreuth, Department of Micrometeorology, ISSN 1614-8916, 29 pp.
- Ruppert, J., Mauder, M., Thomas, C., Lüers, J., 2006. Innovative gap-filling strategy for annual sums of CO₂ net ecosystem exchange. *Agric. For. Meteorol.* 138, 5–18.

- Schmid, H. P., 2002. Footprint modeling for vegetation atmosphere exchange studies: a review and perspective. *Agric. For. Meteorol.* 113, 159–183.
- Schotanus, P., Nieuwstadt, F. T. M., Bruin, H. A. R. D., 1983. Temperature measurement with a sonic anemometer and its application to heat and moisture fluxes. *Boundary-Layer Meteorol.* 26 (1), 81–93.
- Serafimovich, A., Siebicke, L., Staudt, K., Lüers, J., Hunner, M., Gerken, T., Schier, S., Biermann, T., Rütz, F., von Buttler, J., Riederer, M., Falge, E., Mayer, J.-C., Foken, T., 2008a. Exchange processes in mountainous regions (EGER) - documentation of the intensive observation period (IOP2) June, 1st to July, 15th 2008. *Arbeitsergebnisse*, 37, University of Bayreuth, Department of Micrometeorology, ISSN 1614-8916, 180 pp.
- Serafimovich, A., Siebicke, L., Staudt, K., Lüers, J., Biermann, T., Schier, S., Mayer, J.-C., Foken, T., 2008b. Exchange processes in mountainous regions (EGER) - documentation of the intensive observation period (IOP1) September, 6th to October, 7th 2007. *Arbeitsergebnisse*, 36, University of Bayreuth, Department of Micrometeorology, ISSN 1614-8916, 147 pp.
- Shaw, R. H., Paw U, K. T., Gao, W., 1989. Detection of temperature ramps and flow structures at a deciduous forest site. *Agric. For. Meteorol.* 47, 123–138.
- Siebicke, L., Hunner, M., Foken, T., 2010a. Some aspects of CO₂-advection measurements in discussion. *Theoretical and Applied Climatology* (submitted).
- Siebicke, L., Serafimovich, A., April 2007. Ultraschallanemometer-Überprüfung im Windkanal der TU Dresden 2007. *Arbeitsergebnisse* 30, University of Bayreuth, Department of Micrometeorology, ISSN 1614-8916, 12 pp.
- Siebicke, L., Serafimovich, A., Foken, T., 2011. Linking CO₂-advection estimates to vegetation structure at a forest site. *Agric. For. Meteorol.* (to be re-submitted in revised version).
- Siebicke, L., Steinfeld, G., Foken, T., 2010b. CO₂-gradient measurements using a parallel multi-analyzer setup. *Atmospheric Measurement Techniques Discussions* 3, 4383–4421.
- Sogachev, A., Leclerc, M. Y., Zhang, G., Rannik, U., Vesala, T., 2008. CO₂ fluxes near a forest edge: a numerical study. *Ecological Applications* 18, 1454–1469.

- Sogachev, A., Panferov, O., Gravenhorst, G., Vesala, T., 2005. Numerical analysis for flux footprints for different landscapes. *Theoretical and Applied Climatology* 80, 169–185.
- Soler, M., Infante, C., Buenestado, P., Mahrt, L., 2002. Observations of nocturnal drainage flow in a shallow gully. *Boundary-Layer Meteorol.* 105, 253–273.
- Staebler, R., Fitzjarrald, D., 2004. Observing subcanopy CO₂ advection. *Agric. For. Meteorol.* 122, 139–156.
- Staudt, K., Foken, T., 2007. Documentation of reference data for the experimental areas of the Bayreuth Centre for Ecology and Environmental Research (BayCEER) at the Waldstein site. *Arbeitsergebnisse* 35, University of Bayreuth, Department of Micrometeorology, ISSN 1614-8916, 37 pp.
- Stull, R. B., 1988. *An Introduction to Boundary Layer Meteorology*. Kluwer Academic Publishers, Dordrecht, The Netherlands, 666 pp.
- Sun, H., Clark, T. L., Stull, R. B., Black, T. A., 2006a. Two-dimensional simulation of airflow and carbon dioxide transport over a forested mountain: Part I: Interactions between thermally-forced circulations. *Agric. For. Meteorol.* 140 (1-4), 338 – 351.
- Sun, H., Clark, T. L., Stull, R. B., Black, T. A., 2006b. Two-dimensional simulation of airflow and carbon dioxide transport over a forested mountain: Part II. Carbon dioxide budget analysis and advection effects. *Agric. For. Meteorol.* 140 (1-4), 352 – 364.
- Sun, J., 2007. Tilt corrections over complex terrain and their implication for CO₂ transport. *Boundary-Layer Meteorol.* 124, 143–159.
- Sun, J., Burns, S. P., Delany, A. C., Oncley, S. P., Turnipseed, A. A., Stephens, B. B., Lenschow, D. H., LeMone, M. A., Monson, R. K., Anderson, D. E., 2007. CO₂ transport over complex terrain. *Agric. For. Meteorol.* 145 (1-2), 1 – 21.
- Sun, J., Desjardins, R., Mahrt, L., MacPherson, I., 1998. Transport of carbon dioxide, water vapor, and ozone by turbulence and local circulations. *Journal of Geophysical Research* 103, 25873–25885.
- Thomas, C., Foken, T., 2007a. Flux contribution of coherent structures and its implications for the exchange of energy and matter in a tall spruce canopy. *Boundary-Layer Meteorol.* 123, 317–337.

- Thomas, C., Foken, T., 2007b. Organised motion in a tall spruce canopy: temporal scales, structure spacing and terrain effects. *Boundary-Layer Meteorol.* 122, 123–147.
- Thomson, D. J., 1987. Criteria for the selection of stochastic models of particle trajectories in turbulent flows. *Journal of Fluid Mechanics* 189, 529–552.
- Tóta, J., Fitzjarrald, D. R., Staebler, R. M., Sakai, R. K., Moraes, O. M. M., Acevedo, O. C., Wofsy, S. C., Manzi, A. O., 2008. Amazon rain forest sub-canopy flow and the carbon budget: Santarém LBA-ECO site. *J. Geophys. Res.* 113.
- Vesala, T., Kljun, N., Rannik, Ü., Rinne, J., Sogachev, A., Markkanen, T., Sabelfeld, K., Foken, T., Leclerc, M., 2008. Flux and concentration footprint modelling: State of the art. *Environmental Pollution* 152 (3), 653 – 666.
- Vickers, D., Mahrt, L., 1997. Quality control and flux sampling problems for tower and aircraft data. *Journal of Atmospheric and Oceanic Technology* 14 (3), 512–526.
- Vickers, D., Mahrt, L., 2006. Contrasting mean vertical motion from tilt correction methods and mass continuity. *Agric. For. Meteorol.* 138 (1-4), 93 – 103.
- Wang, W., Davis, K. J., Cook, B. D., Bakwin, P. S., Yi, C., Butler, M. P., Ricciuto, D. M., 2005. Surface layer CO₂ budget and advective contributions to measurements of net ecosystem-atmosphere exchange of CO₂. *Agric. For. Meteorol.* 135 (1-4), 202 – 214.
- Webb, E. K., Pearman, G. I., Leuning, R., 1980. Correction of the flux measurements for density effects due to heat and water vapour transfer. *Q. J. R. Meteorol. Soc.* 106, 85–100.
- Wilczak, J. M., Oncley, S. P., Stage, S. A., 2001. Sonic anemometer tilt correction algorithms. *Boundary-Layer Meteorol.* 99, 127–150.
- Wilson, J. D., Sawford, B. L., 1996. Review of lagrangian stochastic models for trajectories in the turbulent atmosphere. *Boundary-Layer Meteorol.* 78, 191–210.
- Yi, C., Anderson, D. E., Turnipseed, A. A., Burns, S. P., Sparks, J. P., Stannard, D. I., Monson, R. K., 2008. The contribution of advective fluxes to net ecosystem exchange in a high-elevation, subalpine forest. *Ecological Applications* 18, 1379–1390.

-
- Yi, C., Monson, R. K., Zhai, Z., Anderson, D. E., Lamb, B., Allwine, G., Turnipseed, A. A., Burns, S. P., 2005. Modeling and measuring the nocturnal drainage flow in a high-elevation, subalpine forest with complex terrain. *Journal of Geophysical Research* 110, D22303.
- Zeri, M., 2007. Investigation of high nighttime CO₂-fluxes at the Wetstein spruce forest site in Thuringia, Germany. Ph.D. thesis, University of Bayreuth, Germany, 102 pp.
- Zeri, M., Rebmann, C., Feigenwinter, C., Sedlak, P., 2010. Analysis of periods with strong and coherent CO₂ advection over a forested hill. *Agric. For. Meteorol.* 150 (5), 674 – 683.

List of Appendices

List of Appendices	48
Appendix A: Individual contributions to the joint publications	49
Appendix B: CO ₂ -gradient measurements using a parallel multi-analyzer setup	52
Appendix C: Linking CO ₂ -advection estimates to vegetation structure at a forest site	68
Appendix D: Some aspects of CO ₂ -advection measurements in discussion	92

A Individual contributions to the joint publications

The publications of which this cumulative thesis consists were composed in cooperation with other researchers. Hence, other authors also contributed to the publications listed in appendices B to D in different ways. This section is to specify my own contributions to the individual manuscripts.

Appendix B

Siebicke, L., Steinfeld, G., Foken, T., 2010. CO₂-gradient measurements using a parallel multi-analyzer setup. *Atmospheric Measurement Techniques Discussions* 3, 4383–4421.

I was fully responsible for the planning, design, assembly, set-up and operation of the sub-canopy CO₂ gradient and wind velocity sampling array. This included a novel design of a multi-analyzer CO₂ concentration sampling system with an automatic calibration and remote control system. The instrument set-up in the field involved many people of the Department of Micrometeorology of the University of Bayreuth. After operation in the field, I performed the post-processing of the data from the sub-canopy array and I myself developed the new statistical calibration approach presented in the manuscript. Gerald Steinfeld performed the LES simulation which was included in the verification procedure of the latter approach. He also provided text for the manuscript in the section describing the LES setup. Apart from that the entire publication was conceptualized and written by myself. Th. Foken, as my supervisor, contributed to this publication through fruitful discussions.

Appendix C

Siebicke, L., Serafimovich, A., Foken, T., 2011. Linking CO₂-advection estimates to vegetation structure at a forest site. *Agric. For. Meteorol.* (to be re-submitted in revised version).

This publication is based on measurements from the sub-canopy CO₂ concentration sampling array with my leading contribution to it already described for the publication above. The work further relies on data from a vertical profile of turbulence measurements which was within the responsibility of Andrei Serafimovich. Together with him, I was actively involved in the calibration, installation, supervision and data acquisition of the turbulence measurements. Andrei Serafimovich performed the data analysis concerning the coherent structures with data from the sub-canopy array. He also provided the text related to the analysis of coherent structures (Section 2.4.7) and was helpful in many discussions about the manuscript. I performed the entire analysis concerning horizontal gradients, the combined analysis of sub-canopy CO₂ concentration and coherent structures, the dependend analysis of CO₂ concentration gradients and vegetation structure and the analysis of the vertical profiles. I myself suggested and analyzed the link between vegetation structure and the sub-canopy CO₂ concentration field. The data about vegetation structure (Plant Area Index) and the understorey vegetation map were provided by the group of the Max Planck Institute for Chemistry in Mainz. The entire publication was written by myself, except for above mentioned section. Th. Foken, as my supervisor, encouraged the structure of this publication, particularly because he suggested to investigate the link between coherent structures and advection and he contributed to it in several discussions.

Appendix D

Siebicke, L., Hunner, M., Foken, T., 2010. Some aspects of CO₂-advection measurements in discussion. Theoretical and Applied Climatology (submitted).

This publication uses data from the sub-canopy sampling array with my contributions already described above for the first publication. It further uses turbulence measurements. My contribution to the installation and operation of those measurements was already described for the second publication. I myself performed the post-processing of the turbulence data and calculation of eddy covariance fluxes for this publication as well as for the entire research project EGER for Intensive Observatoin Periods IOP1 and IOP2 using the TK2 software. I calculated all components of Net Ecosystem Exchange (NEE) presented in the manuscript and conceptualized and wrote the entire manuscript. I partly advised the Diploma thesis of Martina Hunner who computed vertical advection (IOP1 and IOP2), horizontal advection

(IOP1) and NEE, investigated the different filter approaches in the application of the planar fit coordinate rotation and found a time dependence of the rotation from the data set length. The results of Martina Hunner's thesis were very helpful for writing this publication and are partly presented herein (vertical advection and horizontal advection of IOP1). I myself suggested the sequential planar fit approach and performed all the relevant data analysis using the long-term data set. The chamber measurement flux data as well as data from vertical profiles of CO₂ concentration and wind velocity were measured by the group of the Max Planck Institute for Chemistry in Mainz. Th. Foken, as my supervisor, encouraged me during this publication and contributed to it in discussions.

B Siebicke et al. (2010b)

Siebicke, L., Steinfeld, G., Foken, T., 2010. CO₂-gradient measurements using a parallel multi-analyzer setup. *Atmospheric Measurement Techniques Discussions* 3, 4383–4421.

Manuscript prepared for Atmos. Meas. Tech.
with version 3.2 of the L^AT_EX class copernicus.cls.
Date: 20 January 2011

CO₂-gradient measurements using a parallel multi-analyzer setup

Lukas Siebicke¹, Gerald Steinfeld², and Thomas Foken¹

¹Department of Micrometeorology, University of Bayreuth, Germany

²Institute of Physics, ForWind, Center for Wind Energy Research, Carl von Ossietzky University of Oldenburg, Germany

Abstract. Accurate CO₂ concentration gradient measurements are needed for the computation of advective flux terms, which are part of the full Net Ecosystem Exchange (*NEE*) budget equation. A typical draw back of current gradient measurement designs in advection research is the inadequate sampling of complex flow phenomena using too few observation points in space and time. To overcome this draw back, a new measurement design is presented which allows the parallel measurement of several sampling points at a high frequency. Due to the multi-analyzer nature of the design, inter-instrument bias becomes more of a concern compared to conventional setups. Therefore a statistical approach is presented which allows for accurate observations of concentration gradients, which are typically small in relation to analyzer accuracy, to be obtained. This bias correction approach applies a conditional, time dependent signal correction. The correction depends on a mixing index based on cross correlation analysis, which characterizes the degree of mixing of the atmosphere between individual sample points. The approach assumes statistical properties of probability density functions (pdf) of concentration differences between a sample point and the field average which are common to the pdf's from several sample points. The applicability of the assumptions made was tested by Large Eddy Simulation (LES) using the model PALM and could be verified for a test case of well mixed conditions. The study presents concentration time series before and after correction, measured at a 2 m height in the sub-canopy at the FLUXNET spruce forest site Waldstein-Weidenbrunnen (DE-Bay), analyzes the dependence of statistical parameters of pdf's from atmospheric parameters such as stratification, quantifies the errors and evaluates the performance of the bias correction approach. The improvements that are achieved by applying the bias correction approach are one order of magnitude larger than

possible errors associated with it, which is a strong incentive to use the correction approach. In conclusion, the presented bias correction approach is well suited for – but not limited to – horizontal gradient measurements in a multi-analyzer setup, which would not have been reliable without this approach. Finally, possible future improvements of the bias correction approach are outlined and further fields of application indicated.

1 Introduction

Advection is a part of Net Ecosystem Exchange (*NEE*) of carbon dioxide, the determination of the latter being a primary focus of a world wide network of vegetation-atmosphere exchange measuring stations, the FLUXNET (Baldocchi et al., 2001). Not only are reliable measurements of advection lacking for most FLUXNET sites, but they continue to be a challenge even for specialized advection research experiments (e.g. Aubinet et al., 2003; Staebler and Fitzjarrald, 2004; Feigenwinter et al., 2008; Aubinet et al., 2010). Advection remains further to be a major reason for the night flux problem (Finnigan, 2008). Mathematically, scalar advection is the product of the mean spatial gradient of a scalar – CO₂ in the case of the current study – and the mean wind velocity, i.e. scalar transport with the mean flow. Advection is typically addressed as vertical advection (Lee, 1998; Baldocchi et al., 2000) and horizontal advection (Baldocchi et al., 2000; Aubinet et al., 2003).

There are two main conceptually different reasons why valid and representative advection measurements are difficult to obtain. One is the instrument related accuracy, with which scalar gradients and wind vectors of the mean flow can be measured. The other reason being undersampling of complex flow phenomena due to limited resources of real world experiments, thus yielding measurements which are not rep-

Correspondence to: Lukas Siebicke
(Lukas.Siebicke@uni-bayreuth.de)

2

L. Siebicke, G. Steinfeld and T. Foken: CO₂ gradient measurements using a parallel multi-analyzer setup

representative for a spatial (volume) and temporal (time period) mean but for a point only.

Vertical and horizontal advection pose different measurement challenges. With regards to vertical advection, reliable vertical CO₂ concentration gradients can be obtained due to vertical concentration gradients which are relatively large compared to sampling uncertainties. Measurements of vertical wind velocity are difficult to obtain, both for reasons of accuracy, precision, and resolution of sonic anemometers and particularly for reasons of the limited spatial representativity of a point measurement. Spatially representative measurements of vertical wind speed can never be obtained from a single point measurement in complex flow, due to theoretical reasons; therefore multi-tower measurements – possibly in combination with airborne measurements – are being suggested to improve spatial representativity of vertical wind measurements (e.g. Mahrt, 2010). Alternatively, the vertical wind velocity measurement problem is avoided by using a mass continuity approach, i.e. inferring vertical motion from horizontal divergence (e.g. Vickers and Mahrt, 2006; Montagnani et al., 2010) or a combination of the mass continuity approach and modeling (Canepa et al., 2010). Regarding horizontal advection, measurements of horizontal wind speed can be obtained with sufficiently high accuracy with sonic anemometers, even though they are often not spatially representative. In contrast, horizontal gradients are very difficult to measure with the required accuracy, because mean gradients are small in relation to instrument related uncertainty and difficult to measure at a large enough number of locations with a sufficiently high temporal resolution.

It is the main aim of this study to provide improvements for the measurement of horizontal CO₂ concentration gradients by means of a better temporal and potentially better spatial resolution. An improved resolution is needed for advection measurements in heterogeneous forests as could be shown by analyzing the effects of spatial heterogeneity and short lived phenomena on mean horizontal CO₂ concentration gradients at the site under study.

The most commonly used setup for horizontal gradient measurements is based on a switching valve system (e.g. Burns et al., 2009), which uses a single closed-path infrared gas analyzer to sample several points one after the other (“sequential approach”), returning to the same sample point once every few minutes. There is an inherent tradeoff between achievable spatial and temporal resolution. The main benefit of this setup is a common analyzer for a number of sample locations, reducing the risk of bias between those points. The current study utilizes a multi-analyzer setup, featuring an individual closed-path infrared gas analyzer for every measurement point, enabling simultaneous measurements of all points (“parallel approach”) with a high frequency. Temporal resolution is no longer parasitic to spatial resolution, the latter depending on available resources only. With ten individual analyzers used, the spatial resolution is on the order of a sequential system. Thus the system described is capa-

ble of making measurements which are representative in the temporal domain since it can observe all relevant temporal scales of the CO₂ concentration signal.

Valid concentration measurements need to be both precise and accurate. Precision of the parallel approach used in this study is higher compared to the conventional sequential approach because there are potentially much more values available in one averaging interval, thus reducing random error. The advance in the number of values is proportional to the number of sample locations per analyzer for the sequential approach. Lower accuracy of a multi-analyzer setup compared to a single analyzer setup due to inter-instrument bias is the major drawback of the parallel approach, in addition to higher resource requirements. Bias can be reduced by careful system design and frequent calibration against accurate, known standards. Section 2.2 lists technical measures that have been taken to that end for the presented system. How to deal with the remaining bias will be the topic of the rest of the paper. The basic assumption regarding concentration differences originating from natural gradients stated in Sect. 2.4.2, which is the justification of the proposed bias correction approach, has been implicitly used by Aubinet et al. (2003) and applied for time series correction in a simple, time independent manner whereas the current study applies a conditional, time dependent signal correction. Previous studies using more than one closed path gas analyzer in a multiplexer system with multiple sampling inlets have often used co-located inlets to deal with time dependent inter-instrument bias (e.g. Sun et al., 2007), and the same procedure was applied to vertical profile measurements at the site of the current study. However, due to the characteristics of the multi-analyzer system presented in this study with only one inlet per analyzer, co-located inlets cannot be used in the same way and a new approach is needed. A number of options for inter-instrument comparison using direct measurements, which combine the setup described in the present study with the concept of co-located inlets are discussed in Siebicke (2011) in order to aid independent evaluation of the statistical calibration method presented here.

It should be noted that the term “CO₂ concentration” is used throughout this paper to describe basic principles in a consistent way. It specifically refers to “molar fraction” in units of mol mol⁻¹ or μmol mol⁻¹, which were used for all measured values presented herein, whereas it refers to “CO₂ density” in units of kg m⁻³ for modelled values from the Large Eddy Simulation study (Sect. 2.5 and Sect. 3). However, further applications of the ideas about bias correction presented in this paper may prefer to describe CO₂ in terms of “mixing ratio” in units of kg kg⁻¹ (Kowalski and Serrano-Ortiz, 2007).

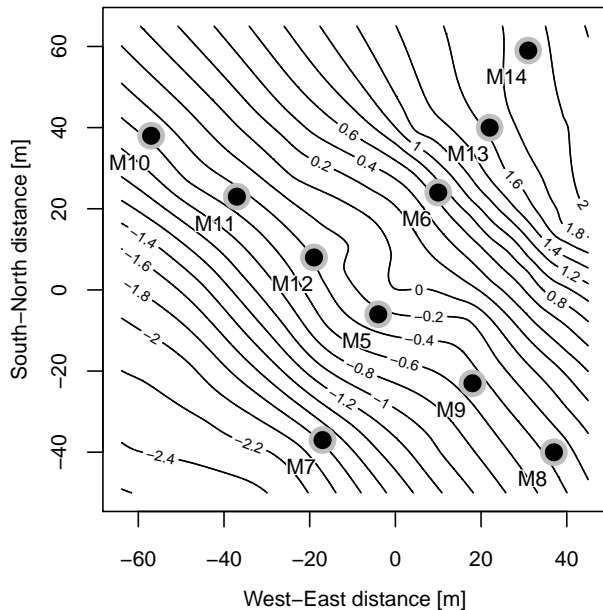


Fig. 1. Sampling locations for sub-canopy CO₂ concentration at a 2.25 m height. M-numbers are used for reference in the text. Topography is shown by isolines with an equidistance of 0.2 m relative to 750 m ASL.

2 Material and methods

2.1 Site

Measurements were carried out at the FLUXNET site Waldstein-Weidenbrunnen (DE-Bay), 50° 08' 31"N, 11° 52' 01"E, a hill site in the Fichtelgebirge Mountains in Southern Germany. The Norway spruce (*Picea abies*) stand is on the upper section of a forested hill, 775 m ASL, with a 3° slope facing south-west. The tree height within the footprint of the measurements is 25 m. The site is described in detail in Gerstberger et al. (2004) and a summary of background data can be found in Staudt and Foken (2007).

2.2 Instrumental setup

Wind vector and CO₂ concentration time series were recorded along horizontal transects at a 2.25 m height in the sub-canopy space. The spatial setup of sub-canopy sample locations is shown in Fig. 1. Ten CO₂ concentration sample points were distributed between an along slope transect from north-east to south-west (5 sample points) and an across slope transect from north-west to south-east (6 sample points), including one common point. Each point was sampled by an individual closed-path infrared gas analyzer. Instruments used were five LI-6262, one LI-6251 (LI-COR Biosciences Inc.), four BINOS (Leybold Heraeus GmbH). In addition to CO₂ concentration measurements at a 2.25 m height, sample locations M5, M6, M7, M8, M9, M10

(see Fig. 1) were equipped with sonic anemometers (USA-1, METEK GmbH) to measure wind speed, wind direction and sonic temperature at the same height. CO₂ concentration measurements are available with a frequency of 1 Hz at each sample point, sonic data were recorded at a 20 Hz frequency. To reduce the risk of systematic differences between individual closed-path gas analyzers the system was carefully designed to avoid any possible bias of the concentration measurement from differences in pressure or temperature (sample air temperature, ambient analyzer temperature, radiation). All CO₂ closed-path gas analyzers shared a common housing in a central position with controlled conditions resulting in a constant common temperature and common pressure regime. Moreover, all analyzers shared a common tailor-made automatic calibration system, using high precision reference gases (accuracy 0.1 μmol mol⁻¹). The calibration routine included an automatic calibration every 4 hours using two reference concentrations, which were sampled by all ten analyzers at the same time. In addition to factory calibration, each instrument's polynomial calibration function was established on site, using multiple standards. The polynomial was checked before and during the experiment.

Individual technical measures taken to avoid systematic inter-instrument bias include the following:

- The length of tubing connecting each sample point with the corresponding gas analyzer was exactly 75 m for every point. Sample tubes used were of polyethylene-aluminum composite structure, model DEKABON 1300-M060X (Serto AG, Fuldabrück, Germany) with an inner diameter of 4 mm.
- Large diameter line intake air filters were checked regularly and replaced synchronously at all points, if necessary.
- Common ambient temperature and pressure for all gas analyzers and calibration unit, including radiation protection, active automatic temperature control by heating and cooling as well as carefully designed ambient air circulation.
- Quality control of performance of automatic temperature control system, making sure that ambient air temperatures measured at several points surrounding the gas analyzers remain within acceptable range.
- Temperature adaptation for sample lines, to allow the temperature of sample air in all sample lines to equilibrate to a common temperature prior to entering the analyzer.
- Common temperature and radiation shielding for reference gases.

4

L. Siebicke, G. Steinfeld and T. Foken: CO₂ gradient measurements using a parallel multi-analyzer setup

- Minimization of dead volumes in calibration and valve system to ensure turbulent flow conditions and avoid contamination by previous samples.
- Flow rate of 2 L min⁻¹ (Reynolds number $Re = 2520$) above critical flow rate of 1.8 L min⁻¹ at critical Reynolds number ($Re_{crit} = 2320$) to ensure turbulent flow conditions in all tubes, at the same time keeping the flow rate as low as possible to minimize pressure drop across the system.
- Regular flow rate check and adjustment for all sample lines.
- Bypass system to avoid back pressure effects during calibration, featuring a low pressure drop bypass flow rate control device to ensure minimum necessary bypass flow and avoid possible reverse flow and sample contamination by ambient air.
- One common pump downstream of the analyzers to reduce effects of the pump on the concentration signals and to guarantee common pressure for all analyzers, assuming equal pipe geometry of all sample lines.
- Automatic control of constant overall system flow rate by mass flow controller.
- Passive system to allow for pressure equilibration between sample cells of individual gas analyzers by connecting all analyzer outlets to a manifold with a sufficiently large diameter.
- Pre-assembly measurement and evaluation of the pressure drop caused by individual system components to ensure that associated errors of the CO₂ concentration measurements are below accepted threshold.
- Vacuum and over pressure assisted leak check for the complete system to rule out sample contamination by ambient air.

2.3 Data set

The data set was collected during the second intensive observation period (IOP2), 1st of June to 15th of July 2008 of the EGER (“ExchanGE processes in mountainous Regions”) experiment (Serafimovich et al., 2008). 24.6 days worth of data were used for the analysis, i.e. 1181 half hourly values taken from a window of 32.0 days (11th of June to 13th of July). Periods were excluded from the analysis when instruments were powered off or obviously malfunctioning.

2.4 Theoretical considerations regarding concentration differences

2.4.1 Bias

An observed concentration difference between two spatially separated sample points is the sum of a concentration difference originating from a natural atmospheric concentration gradient and the inter instrument bias, the latter being determined by systematic (bias) and random error of the individual instruments. We will refer to this composite concentration difference also as a concentration offset, Δc . While random error of the instruments is a minor concern in the current study due to sufficiently long averaging period, instrument bias can be reduced by calibration against known standards. The calibration procedure used in this study was outlined in Sect. 2.2. The remaining bias is the sum of the error of the calibration plus the instrument drift between two consecutive calibration events. This remaining bias cannot be removed by calibration since it is intrinsic to the calibration procedure itself. However, a statistical approach detailed in Sect. 2.7 can help to distinguish between remaining bias and concentration differences originating from natural gradients based on the observed signal.

2.4.2 Natural concentration differences

To separate concentration differences originating from natural gradients between two spatially disjunct (i.e. up to a few tens of meters) sample points from instrument bias the following assumption is made and is the basis for bias correction used in the current study: for certain meteorological conditions the concentration time series observed simultaneously at the two locations can be statistically linked to a reference concentration which is common to both sample locations. To be more precise, under the condition of well mixed, i.e. sufficiently turbulent atmospheric conditions (hereafter “mixed” conditions) the concentration difference between the two locations which is most likely to be observed is zero. If this statement is true for the concentration difference between any two points, it can also be applied to the difference between the concentration at one sample location c_i , and the spatial average concentration of the sample point field $\tilde{c}(t)$ at a given time t . $\tilde{c}(t)$, which serves as a reference concentration, describes the background concentration of the sample point field at time t using the median field concentration according to Eq. (1)

$$\tilde{c} = \begin{cases} c_{\frac{k+1}{2}} & k \text{ odd} \\ \frac{1}{2} (c_{\frac{k}{2}} + c_{\frac{k}{2}+1}) & k \text{ even} \end{cases} \quad (1)$$

with $k = 1 \dots n$ observations (c_1, c_2, \dots, c_k) being the concentration measurements ($c_1(t), c_2(t), \dots, c_n(t)$) at n locations sorted in ascending order. The statistical measure describing the concentration difference most likely to be observed

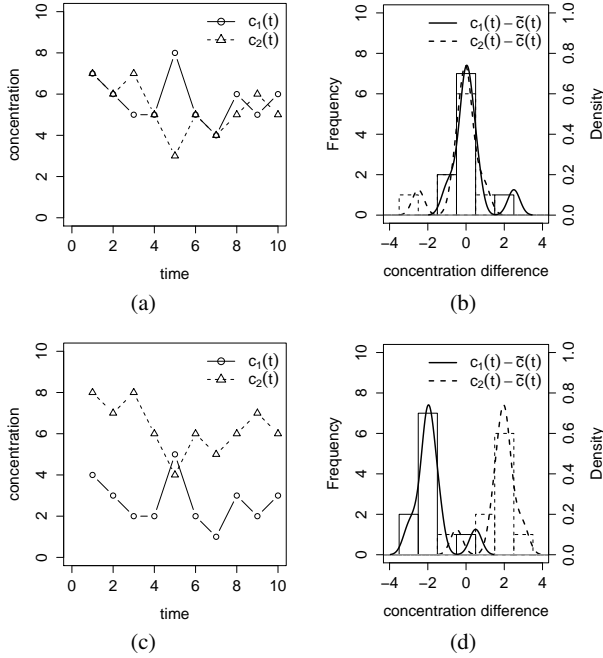


Fig. 2. Hypothetical concentration time series $c_1(t)$ and $c_2(t)$ with time $t \in [1, 10]$ (a,c), and corresponding frequency and density distributions of concentration differences $c_i(t) - \tilde{c}(t)$ (b,d) for mixed conditions (a,b) and for non mixed conditions (c,d). Regarding the density distributions in Subfig. (b) and (d), the histogram bars indicate the frequency for binwidths of 1.0, the solid line is a kernel density estimation generated with the same tools which were used for density estimation of measured concentration data as described in Sect. 2.7.

is the mode of the probability density distribution (pdf) of the concentration differences $c_i(t) - \tilde{c}(t)$, which is assumed to be close to zero under the condition of well mixed i.e. sufficiently turbulent atmospheric conditions.

This is illustrated in Fig.2(b) for two hypothetical time series $c_1(t) = 7, 6, 5, 5, 8, 5, 4, 6, 5, 6$ and $c_2(t) = 7, 6, 7, 5, 3, 5, 4, 5, 6, 5$, displayed in Fig. 2(a). The characteristics of turbulence justify the assumed mode of the pdf to be close to zero, i.e. turbulence consists of temporal perturbations of a mean state which are stochastic and relatively short in duration compared to the observation period. The mode is zero even though the time series $c_1(t)$ and $c_2(t)$ given in Fig. 2(a) have a different mean (temporal mean indicated by overline): $\overline{c_1(t)} = 5.7$ and $\overline{c_2(t)} = 5.3$, and even though the mean of the concentration difference $c_i(t) - \tilde{c}(t)$ is different from zero: $\overline{c_1(t) - \tilde{c}(t)} = 0.2$ and $\overline{c_2(t) - \tilde{c}(t)} = -0.2$.

For atmospheric conditions without turbulent mixing (hereafter “non mixed” conditions) above stated assumption does not need to be fulfilled. Since there is no effective mechanism of mixing, two sample locations can be continuously exposed to air masses with different concentrations – see concentration time series $c_1(t) = 4, 3, 2, 2, 5, 2, 1, 3, 2, 3$

and $c_2(t) = 8, 7, 8, 6, 4, 6, 5, 6, 7, 6$ in Fig. 2(c) – i.e. there is a persistent natural gradient and no common background concentration is observed at both sample points. Thus, the two points will most frequently sample a concentration difference which represents this gradient, and the mode of the probability density distribution is non zero, Fig. 2(d).

All combinations of the well mixed and non mixed case are possible. It depends on turbulence statistics and the length of the time series incorporated in the probability density distribution whether mixing is sufficient to produce a mode of the pdf close to zero or not. A method to quantify the degree of mixing will be presented in Sect. 2.6.

2.5 Large Eddy Simulation

An idealized Large Eddy Simulation (LES) case study was performed in order to check whether the assumption made in Sec. 2.4.2 is true, i.e. whether the mode of the probability density function of the difference $c_i(t) - \tilde{c}(t)$ between the scalar concentration at one sample location $c_i(t)$ and the scalar concentration averaged over all sample points $\tilde{c}(t)$ is close to zero for well mixed conditions, even in the case that the distribution of sources and sinks of the scalar is not homogeneous and a mean spatial concentration gradient $\frac{\partial \bar{c}}{\partial y}$ with concentration c and horizontal distance y exists. Large Eddy Simulation is a tool that is used to study turbulence related processes in the atmospheric boundary layer. It can therefore be used to extract statistical properties of turbulence for the well mixed case. The simulation does not intend to perfectly mimic subcanopy conditions but to test general statistical properties of turbulent mixing, i.e. whether strong turbulent mixing is able to allow the average field background concentration $\tilde{c}(t)$ to emerge as the dominant mode of the probability density function rather than local sources or sinks producing the dominant mode.

The LES model used in this study is the Parallelised LES Model (PALM) that has been developed at the Institute of Meteorology and Climatology at the Leibniz University in Hannover, Germany. Detailed information on the LES approach, model equations and numerical schemes applied in PALM are given in Raasch and Schröter (2001) or – continuously updated – on-line on the homepage of the PALM group (Raasch, 2010). In our applications of PALM presented here an additional prognostic equation for a scalar quantity was solved so that the temporal development of a scalar concentration field with distributed sources and sinks could be simulated.

Two simulations with different setups were carried out for this study. In our first simulation (“case A”) a horizontally homogeneous distribution of scalar sources and sinks was prescribed. However, the scalar concentration field was initialized with a horizontal concentration gradient. This setup resulted in a temporally decaying horizontal concentration gradient due to turbulent mixing.

6

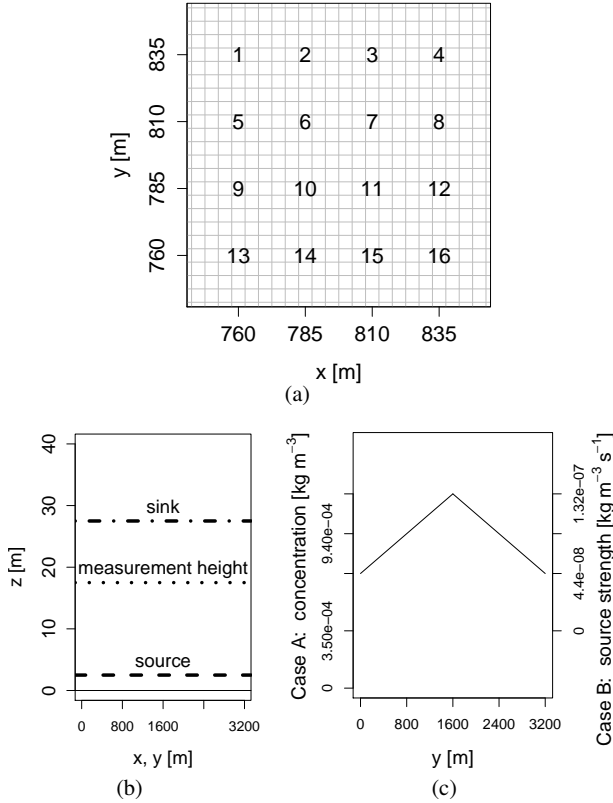
L. Siebicke, G. Steinfeld and T. Foken: CO₂ gradient measurements using a parallel multi-analyzer setup

Fig. 3. Setup of Large Eddy Simulation study. Virtual sensor locations (a), Source-sink distribution (b) and background concentration gradient (c). Grid spacing: 5 m.

In the second simulation (“case B”) the initial field of scalar concentration and the sinks of scalar concentration were prescribed to be horizontally homogeneous. However, the sources of scalar concentration were horizontally heterogeneously distributed. This setup resulted in a temporally evolving concentration gradient.

In the following paragraphs the setup of the two simulation runs will be described in detail. First of all those settings common to both simulations will be reported before pointing out details regarding the scalar concentration field which are specific to each setup.

In both simulations the model domain consisted of $640 \times 640 \times 256$ grid points and a basic grid spacing of 5 m was used. Above a height of 1000 m the grid was stretched vertically until a maximum grid size of 20 m was reached. The total extension of the model domain was $3.2 \times 3.2 \times 2$ km.

Both LES simulations were initialized with wind profiles that were obtained from a one-dimensional prerun in order to accelerate the transition to a stationary state in the three-dimensional main run. The geostrophic wind (u_g, v_g) was prescribed as ($3 \text{ m s}^{-1}, 0 \text{ m s}^{-1}$) while u and v correspond to the x - and y -direction, respectively. The roughness length

was 0.1 m. At the bottom boundary of the model domain a near-surface heat flux of 0.01 K m s^{-1} was prescribed, so that a convective boundary layer with a Monin-Obukhov-length in the range between -40 and -50 m developed with time. The Coriolis parameter corresponded to a geographical latitude of 55° .

Sources and sinks of the scalar were switched on as soon as the simulation had reached a quasi-stationary state, i.e. after a spin-up time of 2 hours. The sources of the scalar were situated at a height of 2.5 m and distributed homogeneously over the total horizontal extension of the model domain. The sinks of the scalar were also distributed over the total horizontal extension of the model domain but situated at a height of 27.5 m.

In both simulations time series of scalar concentration were recorded at 16 observation points within the xy -cross section of the model domain at a height of 17.5 m beginning from the first release of scalar quantity until the end of the LES 7200 s later. Data from these time series could be used in order to calculate the differences between the concentration at a single sample point and the concentration averaged over all sample points as required in order to check the validity of the assumption made in Sec. 2.4.2. Figure 3 shows the locations of these observation points of the two LES. The coordinates of the 16 observation points were composed out of the x -coordinates (760 m, 785 m, 810 m, 835 m) and y -coordinates (760 m, 785 m, 810 m, 835 m). Thus, the distance between two adjacent observation points along the x - or y -direction was 25 m.

In case A the initial scalar concentration field showed a gradient along the y -direction. The initial concentration increased by $3.038 \times 10^{-7} \text{ kg m}^{-4}$ from $y = 0$ to $y = \frac{L_y}{2}$, while it decreased by $3.038 \times 10^{-7} \text{ kg m}^{-4}$ from $y = \frac{L_y}{2}$ to $y = L_y$ (L_y is the length of the model domain along the y -direction). It is worth mentioning that the prescribed gradients are equivalent to $\pm 0.16 \mu\text{mol mol}^{-1} \text{ m}^{-1}$ which deliberately has been chosen to represent the maximum of gradients observed in the field at the site under study and published for other sites (Aubinet et al., 2003; Heinesch et al., 2007) during stable stratification, even though gradients are smaller during neutral and unstable stratification, i.e. the stratification regime present in the LES. In that sense, the LES with strong gradients tests a worst case scenario.

As in case B the initial mean scalar concentration prior to imposing the additional spatial gradients in case A was $6.997 \times 10^{-4} \text{ kg m}^{-3}$. Note that this is equivalent to $378 \mu\text{mol mol}^{-1} \text{ CO}_2$, which was the background concentration observed at the experimental test site described in Sec. 2.1. The resulting initial concentration field is shown in Fig. 3c). The source strength was set to $8.8 \times 10^{-8} \text{ kg m}^{-3} \text{ s}^{-1}$, while the sink had a strength of $-8.8 \times 10^{-8} \text{ kg m}^{-3} \text{ s}^{-1}$. It was chosen to correspond to a typical maximum daytime Net Ecosystem Exchange of $-20 \mu\text{mol m}^{-2} \text{ s}^{-1}$ observed at the measurement site.

In case B (horizontally homogeneous initial concentration field) a basic source strength of $4.4 \times 10^{-8} \text{ kg m}^{-3} \text{ s}^{-1}$ was prescribed at $y=0$ and $y=L_y$. Between $y=0$ and $y=\frac{L_y}{2}$ the gradient of the source strength, $\frac{\partial s}{\partial y}$, was $5.5 \times 10^{-11} \text{ kg m}^{-4} \text{ s}^{-1}$ for $y < \frac{L_y}{2}$, while it was $-5.5 \times 10^{-11} \text{ kg m}^{-4} \text{ s}^{-1}$ between $y=\frac{L_y}{2}$ and $y=L_y$. Thus, the mean horizontal source strength was exactly the same as in case A. The sink strength was prescribed as in case A (and thus again approx. equivalent to a typical maximum daytime Net Ecosystem Exchange of $-20 \mu\text{mol m}^{-2} \text{ s}^{-1}$ observed at the site).

It is obvious that the Large Eddy Simulations presented here are an idealization and do not account for the complexity of the given forest site, particularly because they do not fully account for the forest canopy. However, we would like to stress that the purpose of the simulation is to test the idealized case of turbulent mixing given realistic physical values of scalar concentration gradients and a vertical source and sink distribution that does mimic sources at the forest floor and sinks in the forest canopy with respect to their vertical distribution and their intensity. Verifying and accepting the assumption made in Sec. 2.4.2 first for an idealized case is necessary before addressing measurements from the more complex forest setting. Whether conditions in the forest at any given time show sufficient mixing is not evaluated by LES but by the application of an empirical mixing index (see Sec. 2.6) which is based on measured data.

2.6 Mixing index

A ‘‘mixing index’’ MI was formulated to quantify the degree of mixing between the real world sample points given in Fig. 1. A threshold value MI_c was then used to separate conditions which satisfy the assumption from those violating it. The mixing index MI is based on the cross correlation $R_{c_1 c_2}(\tau)$ of the simultaneous concentration time series $c_1(t)$ and $c_2(t)$ of spatially separated sample locations normalized by their mean variance σ^2 . The cross correlation function is given as

$$R_{c_1 c_2}(\tau) = \frac{1}{T_F} \int_{-T_F/2}^{T_F/2} c_1(t) \cdot c_2(t+\tau) dt \quad (2)$$

with time lag τ between concentration time series $c_1(t)$ and $c_2(t)$, T_F being the length of the time window of $c_1(t)$ and $c_2(t)$ and $\tau \in [-T_F, T_F]$. MI then writes:

$$MI = \max(|R_{c_1 c_2}(\tau)|) \cdot \left(\frac{\sigma_{c_1}^2 + \sigma_{c_2}^2}{2} \right)^{-1}. \quad (3)$$

More specifically, MI was calculated using the mean cross correlation of CO₂ concentration time series c_5 and c_6 recorded at a sample point pair oriented along the terrain slope (locations M5, M6) and c_5 and c_8 recorded at a sample point pair oriented across the slope (M5, M8) divided

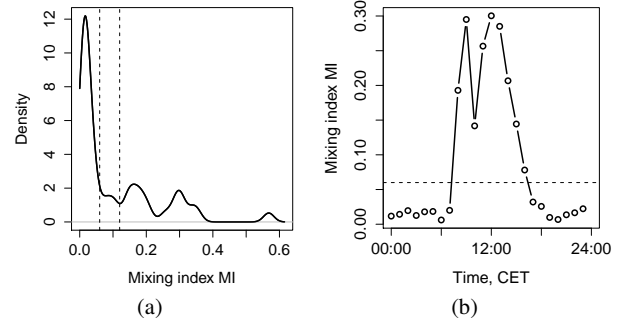


Fig. 4. Density distribution of mixing index MI (solid line). Dashed lines at $MI=0.06$ and $MI=0.12$ enclose range for sensible choices of a critical mixing index MI_c , (a). Diurnal course of mixing index on 29 June 2008 (solid line) and MI_c (dashed line), (b). MI is representative for the whole sample point field (see Sect. 2.6 for details of the calculation).

by the mean field variance of all concentration time series c_5, c_6, \dots, c_{14} at sample locations M5, M6, ..., M14 using a window length of $T_F = 60$ min. The critical mixing index MI_c was empirically inferred from the density distribution of MI given in Fig. 4(a). Sensible values were found to be in the range $MI_c \in [0.06, 0.12]$, corresponding to a sharp bend in the density distribution separating MI 's representative of well mixed daytime conditions (distribution tail to the right of MI_c in Fig. 4a) from low MI 's representative of night time conditions with little mixing (distribution peak to the left of MI_c in Fig. 4a). Figure 4b presents a typical diurnal cycle of the mixing index which is clearly separated into mixed and non mixed conditions by MI_c .

2.7 Bias correction

Instrument related bias of the CO₂ concentration signal was observed to vary over time. It is therefore appropriate to apply a bias correction that is time dependent, too. Analyzer specific values of instrument bias Δc_i were computed for every 60-minute interval T_F of the concentration time series $c_i(t)$ by finding the mode ($\max(\text{density})$) of the probability density distribution (pdf) of the instantaneous concentration differences of an individual analyzer $c_i(t)$ relative to the field average concentration $\tilde{c}(t)$ according to

$$\Delta c_i = \max(\text{pdf}(c_i(t) - \tilde{c}(t))) \quad (4)$$

with $\tilde{c}(t)$ defined in Eq. (1) and the total number of analyzers $n = 10$. Identifying the mode of the pdf requires a robust estimate of the distribution. A comparison of histogram based and kernel-density-estimator based approaches showed that the latter are superior in terms of robustness relative to scatter in the distribution, which is a valuable feature particularly for limited sample sizes. Density estimates were generated using a moving window Gaussian kernel for smoothing (Wand and

Jones, 1995). The optimal width of the window was adaptively and automatically found using pilot-density-estimates according to Sheather and Jones (1991), implemented in the `dpik` function of the `KernSmooth` library (Ripley, 2009) provided with R (R Development Core Team, 2009), also providing the `bkde` function which was used to estimate the density. Having found an individual bias value for every analyzer, the mixing index was checked to decide whether concentration time series correction was applicable. For well mixed conditions, i.e. $MI \geq MI_c$, the observed 60-minute concentration time series $c_i(t)$ of every analyzer was shifted by the analyzer specific bias value Δc_i found for the given 60-minute interval, yielding the bias corrected concentration time series $c_{i,corr}(t)$ according to Eq. (5).

$$c_{i,corr}(t) = c_i(t) - \Delta c_i \quad \text{for } MI \geq MI_c \quad (5)$$

For $MI < MI_c$ the correction was applied using the last valid bias value satisfying $MI \geq MI_c$.

In order to verify that concentration offsets Δc_i found are related to slow drift of the analyzers (instrument bias) rather than driven by meteorological forcing of natural concentration gradients, a regression analysis was performed studying the correlation of Δc_i versus ambient air temperature, pressure and atmospheric stability ζ , respectively. The stability parameter ζ is defined as $\zeta = (z - d)L^{-1}$ with measurement height z , displacement height d and Obukhov-length L . No significant correlation was found between the concentration offset and the three meteorological parameters, which is an indication that the calculated offset Δc_i is dominated by instrument bias and should therefore be removed with the proposed conditional bias correction approach, respecting $MI \geq MI_c$.

Because, even under mixed conditions, natural concentration differences could account for a (very small) part of the observed concentration offsets Δc_i , an error analysis was performed. The aim was to quantify the benefit of the application of the bias correction approach in a hypothetical “worst case” scenario, i.e. assuming that observed concentration offsets Δc_i are solely determined by natural concentration differences rather than instrument bias. A relative error is defined in Eq. (6), describing the ratio of the error possibly attributed to the bias correction approach to the improvement achieved by the correction, which can be expressed as the span of the range of instrument bias (“drift span”). This relative error writes

$$error_{rel} = \frac{Q_1(\Delta of f_i) - Q_4(\Delta of f_i)}{\max(of f_i) - \min(of f_i)} \quad (6)$$

with the change of the concentration offset Δc_i between two consecutive 60-minute intervals $\Delta of f_i = \Delta c_i(t) - \Delta c_i(t - 60 \text{ min})$ and with Q_1 and Q_4 being the 25 % and 75 % quartiles of the density distribution, respectively, which reflect a typical range of $\Delta of f_i$.

2.8 Net Ecosystem Exchange and horizontal advection

This section indicates the relevance of measurements of CO₂ concentration gradients for the quantification of the exchange of CO₂ across the vegetation-atmosphere interface, i.e. the Net Ecosystem Exchange of CO₂ (NEE). NEE can be calculated according to the following formula (Aubinet et al., 2003; Feigenwinter et al., 2004, and others):

$$\begin{aligned} NEE = & \frac{1}{V_m} \int_0^h \left(\frac{\partial \bar{c}}{\partial t} \right) dz + \frac{1}{V_m} (\overline{w'c'})_h \\ & + \frac{1}{V_m} \int_0^h \left(\bar{w}(z) \frac{\partial \bar{c}}{\partial z} + \bar{c}(z) \frac{\partial \bar{w}}{\partial z} \right) dz \\ & + \frac{1}{V_m} \int_0^h \left(\bar{u}(z) \frac{\partial \bar{c}}{\partial x} + \bar{v}(z) \frac{\partial \bar{c}}{\partial y} \right) dz \end{aligned} \quad (7)$$

with the molar volume of dry air V_m , CO₂ concentration c , time t , horizontal distances x and y , vertical distance above ground z , height of the control volume h , horizontal wind velocity u along the x -direction, horizontal wind velocity v along the y -direction and vertical wind velocity w along the z -direction. Over-bars denote temporal means and primes denote the temporal fluctuations relative to the temporal mean. The terms on the right hand side of Eq. (7) are the change of storage (term I), the vertical turbulent flux (term II), vertical advection (term IIIa), vertical mass flow from the surface e.g. due to evaporation (term IIIb) according to Webb et al. (1980), and horizontal advection (term IV). The form of NEE presented in Eq. (7) excludes the horizontal variation of the vertical turbulent flux and the horizontal variation of vertical advection. Eq. (7) further neglects the flux divergence term: $\frac{1}{V_m} \int_0^h \left(\frac{\partial (\overline{u'c'})}{\partial x} + \frac{\partial (\overline{v'c'})}{\partial y} \right) dz$. Term II and sometimes terms I and III on the right hand side of Eq. (7) are central components of routine flux measurements at many sites and will not be discussed here. In contrast, term IV, the observation of which is challenging and has only been realized in a limited number of experiments, shall be addressed here. Accurate observations of horizontal concentration gradients of CO₂ are important for the determination of horizontal advection F_{HA} , because F_{HA} is the product of the horizontal wind velocity and the horizontal concentration gradient of the scalar CO₂ according to Eq. (8):

$$F_{HA} = \frac{1}{V_m} \int_0^h \left(\bar{u}(z) \frac{\partial \bar{c}}{\partial x} + \bar{v}(z) \frac{\partial \bar{c}}{\partial y} \right) dz. \quad (8)$$

The fact that density distributions of concentration differences can have a mode of zero and a non zero mean, as seen in Fig. 5(b), is a crucial feature for the computation of

horizontal advection, because only a non zero mean gradient $\frac{\partial \bar{c}}{\partial x} \neq 0$ and/or $\frac{\partial \bar{c}}{\partial y} \neq 0$ can generate a non zero horizontal advection term F_{HA} .

3 Results

After presenting results of the LES study, which contribute to the acceptance of the assumptions stated in Sect. 2.4.2, this section subsequently presents results of measured CO₂ concentration time series and gradients before and after applying the conditional bias correction as well as statistics about the improvement which can be achieved by the correction. Furthermore, observed concentration differences are put in the context of atmospheric stratification.

The results of the LES study demonstrate that for the given simulation the assumption stated in Sect. 2.4.2 is valid, i.e. the mode of the density distribution of the concentration difference between any sample point and the sample point field average is essentially zero, Fig. 5(a). Since both case A and case B lead to the same conclusion, only data of case A are shown in Fig. 5. Observed deviations of the density distribution mode from zero are insignificant, with the maximum deviation, considering all instrument's distributions, divided by the mean distance of the sample point from the sample point field center, accounting for a 2.0% fraction only of the prescribed concentration gradient in the LES (case A). For case B the maximum deviations of the mode from zero were +0.015 and -0.025 $\mu\text{mol mol}^{-1}$. Dividing this range of distribution modes by the range of the distributions means yields a fraction of 0.15. Considering the small gradients under well mixed conditions, this is a very small error. Conditions with large gradients are not an issue because they are excluded by the mixing index filter and are not used to determine concentration offsets when applying the bias correction approach.

The given deviations of the pdf's modes translate to an error attributed to estimates of the horizontal advective flux component, if estimates are based on concentration measurements corrected using the bias correction approach and thus removing the small deviation of the mode from zero. This potential error in the advection estimate is small compared to other uncertainties typically associated with advection estimates, e.g. due to an insufficient number of sampling points in space such as the often limited number of observation height levels of horizontal gradients.

An important feature of the density distributions shown is their skewness, separating mode and mean of a given distribution as illustrated in Fig. 5(b) for two selected sample points. The difference in the mean values of the density distributions is due to the concentration gradient and source-sink distribution prescribed in the LES. It thus demonstrates that it is possible to compute advective flux terms even from distributions with mode equal to zero, since the mean gradient, which is necessary to compute F_{HA} according to Eq. (8),

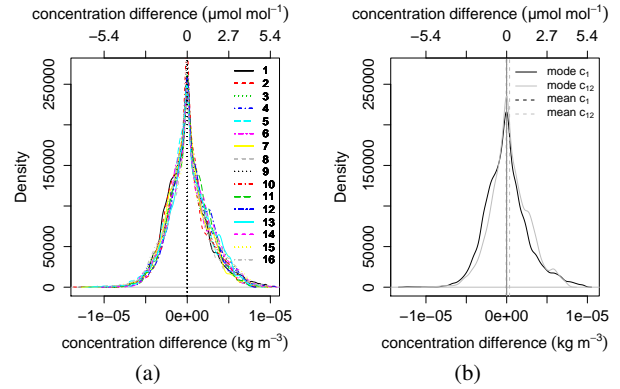


Fig. 5. Density distribution of LES modelled concentration differences $c_i(t) - \bar{c}(t)$ of a point measurement $c_i(t)$ relative to the field average concentration $\bar{c}(t)$ for concentration time series $c_1(t), c_2(t), \dots, c_{16}(t)$ and $n = 16$ sensor locations 1, 2, ..., 16 (a), and for $c_1(t)$ and $c_{12}(t)$ at sensor locations 1 and 12 (b). Note that the density distributions of $c_1(t) - \bar{c}(t)$ and $c_{12}(t) - \bar{c}(t)$ have a common mode but different mean.

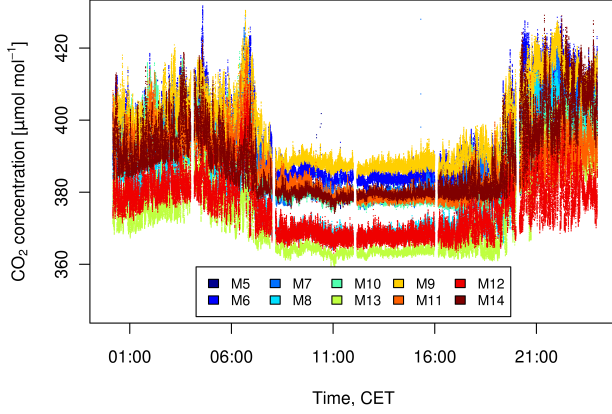
is expressed in the mean which does not need to be zero even though the mode is essentially zero.

In order to evaluate the performance of the bias correction, Fig. 6(a) shows the CO₂ concentration evolution during one day measured at ten locations in the sub-canopy on 29 June 2008 without bias correction but including calibration using known reference gas standards. Figure 6(b) presents the same data after applying the bias correction. The comparison of the two figures clearly demonstrates that the bias correction is able to remove systematic concentration offsets between different analyzers in the uncorrected measurements (Fig. 6a). The offsets are most obvious during well mixed daytime conditions – when natural concentration differences are relatively small – and could be eliminated successfully in the bias corrected time series at all times of the day (Fig. 6b).

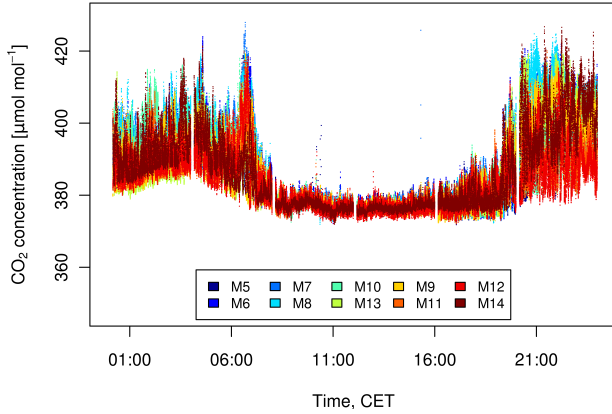
Inter-instrument bias leads to relatively constant offsets between individual concentration measurements $c_i(t)$ during daytime conditions (Fig. 6a), exactly matching the period of a high mixing index (Fig. 4b). The minor importance of concentration differences due to natural gradients during well mixed conditions is the reason why inter-instrument bias becomes the prominent component of observed inter-instrument concentration differences (compare also Fig. 9 and Fig. 10). Well mixed conditions with $MI \geq MI_c$ and $MI_c = 0.13$ were observed every day during the experiment, accounting for 30% of the entire data set. There are a few cases where mixed conditions are present for short isolated periods (e.g. one or two 60-minute MI values) at transition times in the early morning or sometimes in the early evening.

While Fig. 6(a) and 6(b) presented CO₂ concentration time series before and after bias correction on 29 June 2008, Fig. 7

10

L. Siebicke, G. Steinfeld and T. Foken: CO₂ gradient measurements using a parallel multi-analyzer setup

(a)

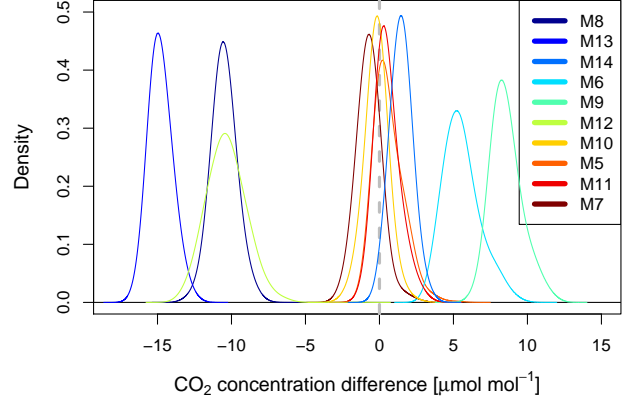


(b)

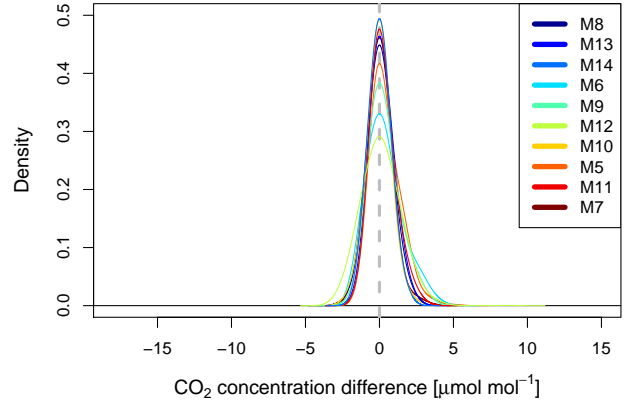
Fig. 6. Calibrated CO₂ concentration time series, *before* bias correction (a), and *after* bias correction with $MI_c = 0.12$ (b), measured at ten sub-canopy locations M5, M6, ..., M14 at a 2.25 m height with a 1 Hz resolution on 29 June 2008.

displays an example of corresponding density distributions of concentration differences during a well mixed 60-minute period at midday of the same day, which were used during bias correction. Probability density distributions with analyzer specific non-zero distribution modes in the uncorrected data of Fig. 7(a) have been shifted by their mode so that the new mode of the distributions is equal to zero after bias correction (Fig. 7b). Figure 7(b) also emphasizes sample location specific differences of the distribution shape, such as different skewness and kurtosis, which is an effect of natural concentration gradients being unique for every sample location.

Having discussed probability density distributions above for an ideal case with mixed conditions, Fig. 8 demonstrates the effect of atmospheric stratification (ζ) and the degree of mixing (MI) on the shape of selected 60-minute probability density distributions of concentration differences, which mark typical conditions during the course of a fair weather day, 29 June, 2008. Distributions of the well mixed case in Subfig. 8c are unimodal and show high kurtosis. This is ben-



(a)



(b)

Fig. 7. Density distribution of concentration differences $c_i(t) - \bar{c}(t)$ using measured 60-minute concentration timeseries $c_i(t)$ *before* bias correction (a) and *after* bias correction (b). Number of sample locations $n = 10$ (M5, M6, ..., M14), sampling resolution 1 Hz, on 29 June 2008, 12:00-13:00. Legend indicates measurement locations according to Fig. 1.

eficial for the reliable estimation of the mode, which is necessary for bias correction. High kurtosis is a consequence of small natural horizontal and vertical gradients during well mixed conditions in the middle of the day. Subfigures 8b and 8d represent transition periods between night and day and between day and night, respectively, while Subfig. 8a and 8e are examples of night time conditions, with Subfig. 8e being a representative example for conditions with katabatic sub-canopy drainage flow under very stable conditions. The kurtosis of the distributions correlates with ζ (indicator for atmospheric stratification) as well as with MI (indicator for turbulent mixing), the result being that kurtosis decreases and skewness often increases with increasing stability parameter ζ and decreasing mixing index MI . This is due to large horizontal and vertical scalar concentration gradients during such conditions, also potentially causing multimodal distributions (Subfig. 8b and 8d), which can lead to disambiguities con-

L. Siebicke, G. Steinfeld and T. Foken: CO₂ gradient measurements using a parallel multi-analyzer setup

11

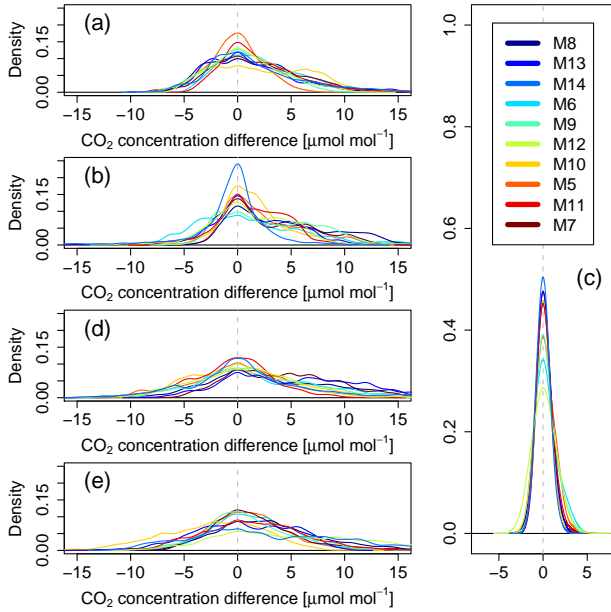


Fig. 8. Density distribution of concentration differences $c_i(t) - \bar{c}(t)$ using bias corrected measured 60-minute concentration timeseries $c_i(t)$, number of sample locations $n = 10$, for five typical cases over the course of the day on 29 June 2008 with varying stability parameter ζ (measured at a 36 m height) and mixing index MI (according to Eq. 3), night time, 01:00-02:00, $\zeta = -0.16$, $MI = 0.015$ (a), night-day transition, 07:00-08:00, $\zeta = 0.65$, $MI = 0.020$ (b), daytime, 12:00-13:00, $\zeta = -0.27$, $MI = 0.218$ (c), day-night transition, 19:00-20:00, $\zeta = 0.06$, $MI = 0.010$ (d) and nighttime with katabatic drainage flow, 22:00-23:00, $\zeta = 19.50$, $MI = 0.016$ (e). Legend indicates measurement locations according to Fig. 1.

cerning the relevant mode if they were to be used for bias correction, which they are not due to the mixing index condition. However, the effect of atmospheric stability ζ is not uniform, meaning that multiple modes and skewed distributions (Subfig. 8b) and low kurtosis (Subfig. 8d) are more pronounced during transition periods with moderate vertical exchange, whereas the night time cases such as Subfig. 8e with the highest stability parameter ζ and least vertical exchange are less skewed and more homogeneous with respect to different sample locations. The absence of vertical exchange results in horizontally relatively homogeneous sub-canopy scalar concentrations even though there are large vertical gradients.

Figures 9 and 10 demonstrate that observed concentration offsets Δc_i can be separated into offsets which are mainly determined by instrument bias alone and into offsets which are determined by instrument bias as well as significant natural concentration differences. Figure 9(a) shows offset time series over two days with a succession of mixed daytime conditions (approx. 8 h to 16 h) with little scatter in the offset time series when natural gradients are small and offsets are mainly controlled by low frequency instrument bias and

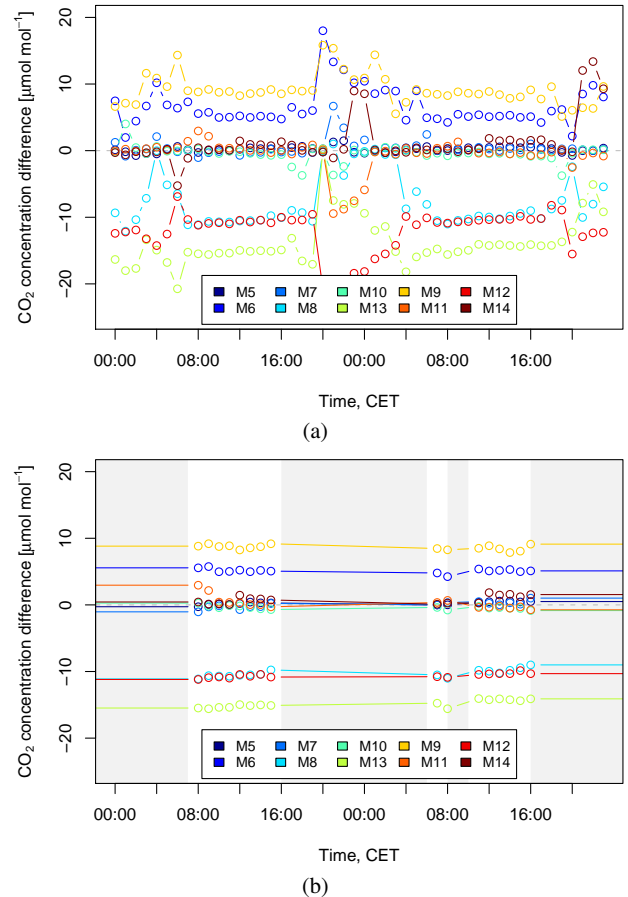


Fig. 9. Time series of the modes of density distributions of concentration differences $c_i(t) - \bar{c}(t)$ (see Fig. 7(a) for example distributions for one 60-minute time step) for 10 sampling locations on 29 June and 30 June 2008, *before* filtering with mixing index (a), and *after* filtering with mixing index $MI_c = 0.13$ (b). Modes from periods which satisfy $MI < MI_c$ are not used during bias correction (grey mask). The last mode at a time with $MI \geq MI_c$ is used instead (solid lines).

night time conditions with high scatter and large absolute values in the offsets time series when natural gradients are the predominant cause. After applying the mixing index to filter the offset time series, those periods with predominant natural gradients were effectively excluded (Fig. 9b). The remaining offsets are controlled by instrument bias and can therefore be used in the bias correction approach.

The different offset characteristics during daytime and nighttime described above are due to the dependence of natural concentration differences on the mixing index and atmospheric stability, both of which have a distinct daily cycle. Figure 10 illustrates the dependence of concentration offsets on the mixing index MI . For low values of MI , natural horizontal gradients are large, as a result of horizontal source heterogeneities and potential mixing of a vertical concentration

12

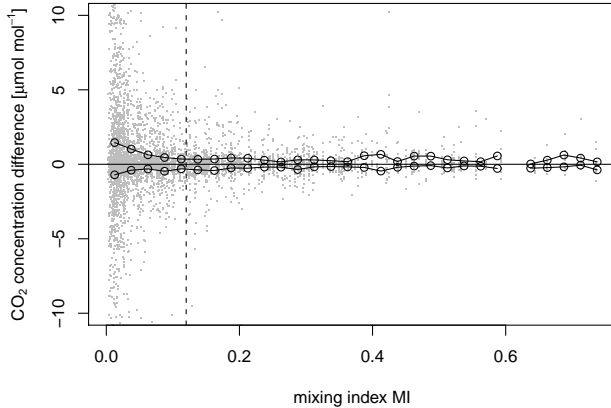
L. Siebicke, G. Steinfeld and T. Foken: CO₂ gradient measurements using a parallel multi-analyzer setup

Fig. 10. Modes of 60-minute density distributions of concentration differences $c_i(t) - \bar{c}$ minus analyzer drift (mode of 24 hour pdf of 60-minute modes subtracted daily) versus mixing index MI . Grey points indicate measurements, the solid line marks the 25 % and 75 % quantiles for mixing index binwidths of 0.025 with the circles centered at each bin. Dashed line at $MI = 0.12$ indicates a sensible choice for the critical mixing index MI_c .

profile with large vertical gradients. For larger values of MI , particularly for $MI > MI_c$, offsets are relatively small. Figure 10 displays the dependence of only natural concentration differences on MI . The graph shows offsets with instrument bias removed by subtracting a low frequency component (see figure caption for details). The fact that this technique does not perfectly separate natural concentration differences from instrument bias explains the scatter and outliers in Fig. 10 which are present even at higher values of MI . The majority of data points (indicated by solid lines for the 25 % and 75 % quantiles) in Fig. 10 is quite close to zero concentration difference for higher values of MI ($MI > MI_c$). That indicates that there are no major natural concentration differences under those conditions which could unintentionally be removed by the bias correction approach.

To compare the benefits of the bias correction approach with potential errors, Tab. 1 displays results of an error analysis, listing the potential for improvement by using the bias correction approach (drift span), an estimate of the potential absolute error ($Q_4(\Delta off_i) - Q_1(\Delta off_i)$) and the relative error ($error_{rel}$) for ten sampling locations. Values of the relative error are on the order of 10 %, which is a satisfying result, keeping in mind that those are “worst case” values pretending that offsets during mixed conditions, i.e. when the bias correction is applied, were purely caused by natural gradients, which they are not in reality. Therefore the true relative error will be even smaller than values given in Tab. 1 for $error_{rel}$.

Table 1. Offset statistics and error analysis for ten sample points, i.e. ten analyzers, demonstrating the correction potential of the bias correction approach (“drift span”), typical values for the maximum error possibly attributed to the bias correction approach for a “worst case” scenario (from quartile $Q_1(\Delta off_i)$ to quartile $Q_4(\Delta off_i)$) and their ratio, i.e. the relative error $error_{rel}$ according to Eq. (6). See Sect. 2.7 for definition of the terms.

Sample point	drift span [$\mu\text{mol mol}^{-1}$]	$Q_1(\Delta off_i)$ [$\mu\text{mol mol}^{-1}$]	$Q_4(\Delta off_i)$ [$\mu\text{mol mol}^{-1}$]	$error_{rel}$ [%]
M5	9.4	-0.46	0.41	0.09
M6	10.4	-0.86	0.72	0.15
M7	8.1	-0.53	0.47	0.12
M8	7.2	-0.7	0.49	0.16
M9	6.1	-0.36	0.41	0.13
M10	23.1	-1.11	0.93	0.09
M11	9.2	-0.89	0.66	0.17
M12	23	-0.43	0.45	0.04
M13	14.3	-0.55	0.54	0.08
M14	12.4	-0.58	0.56	0.09

4 Discussion

There are three issues connected to the quality of the bias correction approach which shall be discussed in this section: potential underestimation of natural concentration differences (signal loss), tradeoff between limiting instrument drift and limiting signal loss, and finding the appropriate window length when applying the bias correction. Finally, this section discusses possibilities for an independent evaluation of the statistical calibration method presented.

The previous section has shown that the improvements that were achieved by applying the bias correction approach are one order of magnitude larger than possible errors associated with it, which is a strong incentive to use the correction approach. However, there is potential for losing part of the natural concentration gradients when applying the correction, due to possibly imperfect separation of instrument bias and concentration differences originating from a natural gradient, even during mixed conditions. A quantification of this phenomenon was given in Tab. 1. The acceptance of this relatively small potential error when applying the bias correction approach needs to be compared to errors which are likely to be attributed to the gradient measurements with no correction applied. It is known from various advection experiments that instrument related bias between sampling points can be on the order of the natural horizontal concentration gradients, particularly at relatively homogeneous sites. This in turn can lead to considerable overestimation of the absolute value of horizontal advection, which is one of the reasons why including the horizontal advection flux term in the Net Ecosystem Exchange (NEE) budget equation often leads to increased scatter of NEE and does not necessarily produce reliable NEE estimates. As a consequence, NEE is often

computed using the turbulent and storage fluxes only. We suggest that rather than including a noisy and potentially too large advection estimate in the NEE equation, it is better to include a bias corrected estimate of horizontal advection. Doing so and at the same time accounting for vertical advection – the same arguments apply here as to avoid overestimation and noise – should give more realistic NEE estimates than those obtained from turbulent and storage flux alone.

When applying the bias correction, a balance should be found between limiting the effect of instrument drift on the gradient measurements and signal loss by potential underestimation of natural gradients. This balance can be tuned by the choice of the value for the critical mixing index MI_c . A high value of MI_c better preserves natural gradients because bias correction values are only determined from data during well mixed conditions and therefore can not eliminate natural gradients during other conditions, particularly at night when natural gradients are typically large. A low value of MI_c removes instrument drift more thoroughly since bias correction values can be found more often, i.e. from well mixed as well as partly mixed conditions. Therefore, we recommend to choose a higher MI_c the more stable the analyzer is and just low enough to allow the instrument to “survive” periods during which no bias correction values can be found (i.e. nighttime) using previously established correction values (inherited from daytime) without facing prohibitive instrument drift during those periods.

The third issue is finding the appropriate window length T_F when applying the bias correction. This is the length of the time series used to compute density distributions of concentration differences (pdf) to find their mode as outlined in Sect. 2.7. For this study the window length was chosen to be $T_F = 60$ minutes. The higher the instrument drift is, the shorter this window has to be in order to find a mode which is representative for the instrument bias during that time window and not affected by a significant trend of the bias. On the other hand, choosing the window as long as possible helps to preserve natural gradients which are persistent for longer periods, since persistent natural gradients with periods longer than the window length and present during non mixed conditions, and therefore affecting the mode of the pdf, are removed by the bias correction for $MI > MI_c$. However, we can conclude from the data that it is not satisfactory to choose an infinite window length (such as the time constant bias correction applied by Aubinet et al. (2003)) in order to preserve natural gradients because observed instrument bias is subject to drift over time. Given the window length of 60-minutes used in the current study, the concentration difference error due to signal loss of natural concentration differences during the day has been shown to be smaller than the error of the concentration offset which would be caused by the drift of the instrument bias if the latter was corrected by a time constant bias value. Future studies should test window lengths larger than 60-minutes, particularly when using more stable analyzers.

Future work on the improvement of the bias correction approach should include a refined condition to test which data should be used when determining the pdf and the bias. Rather than using fixed 60-minute intervals to determine MI and accepting all data in a 60-minute interval satisfying $MI \geq MI_c$, a more fine grained selection of data entering the pdf can be used to select only those parts of the time series which have common properties at more than one sample point for a time period on the order of the duration of coherent structures, i.e. seconds to minutes. Among the tools which can be used to find common properties within the time series are cross correlation analysis and pattern recognition. Thereby only data with similar concentration at several sample points will enter the pdf. This helps to exclude the influence of natural gradients on the mode of the pdf, which will then be determined by instrument bias alone. Such short term correlation of time series at several sample points by tracking individual structures in the time series should be done for sample point pairs rather than using properties of the complete sample point field. These pair wise correlations then need to be linked together by choosing different configurations of sample point pairs and combining their information.

Future work can also test the applicability of the bias correction approach to sensor networks with a possibly large number of sampling points. The approach can be used when working with sensors which have a relatively high resolution but suffer from low accuracy. Whereas those sensors will deliver the fine structure (high frequency part) of the time series, the bias correction approach corrects constant and drifting instrument bias (low frequency part) and thus ensures the accuracy of the measurements.

5 Conclusions

This paper has presented a measurement design capable of addressing the issue of inadequate sampling of natural concentration gradients in the temporal domain – a common characteristic of many advection measurement setups – by increasing the temporal resolution of the gradient measurements. Observing gradients with a sufficiently high temporal resolution and therefore capturing as much information as possible over a large range of temporal scales is crucial for reliable advection estimates computed from concentration gradients. In order to produce accurate gradient measurements in a multi-analyzer setup, an approach was presented which adequately addresses the problem of inter-instrument bias. It was shown that the uncertainties associated with this approach are one order of magnitude smaller compared to the benefit achieved for the given setup. For completeness it should be stated that it is always advisable to avoid instrument bias as far as possible by appropriate technical measures, e.g. sampling system design and calibration against known reference gas standards (conventional calibration). However, presented statistical calibration method is

independent of conventional calibration in the sense that it solely deals with the remaining bias after conventional calibration and that the functioning of the statistical calibration is to the largest extent independent of the magnitude of this remaining bias. The proposed bias correction approach is therefore a suitable tool at least for multi-analyzer setups measuring horizontal gradients at one height, given a certain proximity of individual sampling locations. There might also be benefits from applying the bias correction approach to sequentially measured data from switching valve systems in a single-analyzer setup. It should be tested in the future whether the bias correction approach can be transferred to measurements of vertical gradients, although care has to be taken due to strong systematic vertical gradients particularly at night in the case of CO₂ concentration. The concept outlined in the current paper should not be limited to measurements of CO₂ concentration but be useful for the accurate observation of gradients of other scalars, too. Furthermore, it need not be limited to gradient measurements for the computation of advective flux components but is worth considering for any gradient based flux measurement application. Finally, the bias correction approach might be useful for the relative adjustment of signal levels between individual sensors in any kind of sensor network that samples phenomena which – at least part of the time – lead to common characteristics of the observed signal at several locations in the network. We therefore propose to test presented method at other experimental sites measuring CO₂ concentration gradients and to explore above mentioned additional applications.

Acknowledgements. The authors wish to acknowledge the help and technical support performed by the staff of the Bayreuth Center for Ecology and Environmental Research (BayCEER) of the University of Bayreuth. The experiment was funded by the German Science Foundation (FO 226/16-1, ME2100/4-1, ZE 792/4-1). We would further like to acknowledge S. Raasch and his group for developing and providing the LES tool PALM. The LES runs were carried out on the HLRN-II-system of the HLRN (North German Alliance for Supercomputing).

References

- Aubinet, M., Heinesch, B., and Yernaux, M.: Horizontal and vertical CO₂ advection in a sloping forest, *Boundary-Layer Meteorol.*, 108, 397–417, 2003.
- Aubinet, M., Feigenwinter, C., Heinesch, B., Bernhofer, C., Canepa, E., Lindroth, A., Montagnani, L., Rebmann, C., Sedlak, P., and Gorsel, E. V.: Direct advection measurements do not help to solve the night-time CO₂ closure problem: Evidence from three different forests, *Agric. For. Meteorol.*, 150, 655–664, 2010.
- Baldocchi, D., Finnigan, J. J., Wilson, K., Paw U, K. T., and Falge, E.: On measuring net ecosystem carbon exchange over tall vegetation on complex terrain, *Boundary-Layer Meteorol.*, 96, 257–291, 2000.
- Baldocchi, D. D., Falge, E., Gu, L., Olson, R., Hollinger, D., Running, S., Anthoni, P., Bernhofer, C., Davis, K., Evans, R., Fuentes, J., Goldstein, A., Katul, G., Law, B., Lee, X., Malhi, Y., Meyers, T., Munger, W., Oechel, W., Paw, K. T., Pilegaard, K., Schmid, H. P., Valentini, R., Verma, S., Vesala, T., Wilson, K., and Wofsy, S.: FLUXNET: A New Tool to Study the Temporal and Spatial Variability of Ecosystem-Scale Carbon Dioxide, Water Vapor, and Energy Flux Densities, *Bulletin of the American Meteorological Society*, 82, 2415–2434, 2001.
- Burns, S. P., Delany, A. C., Sun, J., Stephens, B. B., Oncley, S. P., Maclean, G. D., Semmer, S. R., Schröter, J., and Ruppert, J.: A Programmable Portable Trace-Gas Measuring System and an Evaluation of Calibration Techniques for In-Situ Carbon Dioxide Measurements, *Journal of Atmospheric and Oceanic Technology*, 26, 291–316, 2009.
- Canepa, E., Georgieva, E., Manca, G., and Feigenwinter, C.: Application of a mass consistent flow model to study the CO₂ mass balance of forests, *Agric. For. Meteorol.*, 150, 712–723, 2010.
- Feigenwinter, C., Bernhofer, C., and Vogt, R.: The influence of advection on the short term CO₂-budget in and above a forest canopy, *Boundary-Layer Meteorol.*, 113, 201–224, 2004.
- Feigenwinter, C., Bernhofer, C., Eichelmann, U., Heinesch, B., Hertel, M., Janous, D., Kolle, O., Lagergren, F., Lindroth, A., Minerbi, S., Moderow, U., Molder, M., Montagnani, L., Queck, R., Rebmann, C., Vestin, P., Yernaux, M., Zeri, M., Ziegler, W., and Aubinet, M.: Comparison of horizontal and vertical advective CO₂ fluxes at three forest sites, *Agric. For. Meteorol.*, 148, 12–24, 2008.
- Finnigan, J.: An introduction to flux measurements in difficult conditions, *Ecological Applications*, 18, 1340–1350, 2008.
- Gerstberger, P., Foken, T., and Kalbitz, K.: The Lehstenbach and Steinkreuz Catchments in NE Bavaria, Germany, in: *Biogeochemistry of Forested Catchments in a Changing Environment: A German Case Study*, edited by Matzner, E., vol. 172, pp. 15–41, Springer, Heidelberg, 2004.
- Heinesch, B., Yernaux, M., and Aubinet, M.: Some methodological questions concerning advection measurements: a case study, *Boundary-Layer Meteorol.*, 122, 457–478, 2007.
- Kowalski, A. and Serrano-Ortiz, P.: On the relationship between the eddy covariance, the turbulent flux, and surface exchange for a trace gas such as CO₂, *Boundary-Layer Meteorol.*, 124, 129–141, 2007.
- Lee, X.: On micrometeorological observations of surface–air surface exchange over tall vegetation, *Agric. For. Meteorol.*, 91, 39–49, 1998.
- Mahrt, L.: Computing turbulent fluxes near the surface: Needed improvements, *Agric. For. Meteorol.*, 150, 501 – 509, 2010.
- Montagnani, L., Manca, G., Canepa, E., and Georgieva, E.: Assessing the method-specific differences in quantification of CO₂ advection at three forest sites during the ADVEX campaign, *Agric. For. Meteorol.*, 150, 702–711, 2010.
- R Development Core Team: R: A Language and Environment for Statistical Computing, R Foundation for Statistical Computing, Vienna, Austria, <http://www.R-project.org>, ISBN 3-900051-07-0, 2009.
- Raasch, S.: PALM group available online under, <http://palm.muk.uni-hannover.de>, 2010.
- Raasch, S. and Schröter, M.: PALM – A large-eddy simulation model performing on massively parallel computers, *Meteorologische Zeitschrift*, 10, 363–372, 2001.
- Ripley, B.: KernSmooth: Functions for kernel smoothing for

L. Siebicke, G. Steinfeld and T. Foken: CO₂ gradient measurements using a parallel multi-analyzer setup

15

- Wand & Jones (1995), <http://CRAN.R-project.org/package=KernSmooth>, S original by Matt Wand. R port by Brian Ripley. R package version 2.23-3, 2009.
- Serafimovich, A., Siebicke, L., Staudt, K., Lüers, J., Hunner, M., Gerken, T., Schier, S., Biermann, T., Rütz, F., von Buttlar, J., Riederer, M., Falge, E., Mayer, J.-C., and Foken, T.: ExchanGE processes in mountainous Regions (EGER) - Documentation of the Intensive Observation Period (IOP2) June, 1st to July, 15th 2008, Arbeitsergebnisse, 37, University of Bayreuth, Department of Micrometeorology, ISSN 1614-8916, 180 pp., 2008.
- Sheather, S. J. and Jones, M. C.: A reliable data-based bandwidth selection method for kernel density estimation, *Journal of the Royal Statistical Society, Series B*, 53, 683–690, 1991.
- Siebicke, L.: Interactive comment on "CO₂ gradient measurements using a parallel multi-analyzer setup" by L. Siebicke et al., *Atmospheric Measurement Techniques Discussions*, 3, C2390–2406, 2011.
- Staebler, R. and Fitzjarrald, D.: Observing subcanopy CO₂ advection, *Agric. For. Meteorol.*, 122, 139–156, 2004.
- Staudt, K. and Foken, T.: Documentation of reference data for the experimental areas of the Bayreuth Centre for Ecology and Environmental Research (BayCEER) at the Waldstein site, Arbeitsergebnisse 35, University of Bayreuth, Department of Micrometeorology, ISSN 1614-8916, 37 pp., 2007.
- Sun, J., Burns, S. P., Delany, A. C., Oncley, S. P., Turnipseed, A. A., Stephens, B. B., Lenschow, D. H., LeMone, M. A., Monson, R. K., and Anderson, D. E.: CO₂ transport over complex terrain, *Agric. For. Meteorol.*, 145, 1 – 21, 2007.
- Vickers, D. and Mahrt, L.: Contrasting mean vertical motion from tilt correction methods and mass continuity, *Agric. For. Meteorol.*, 138, 93 – 103, 2006.
- Wand, M. P. and Jones, M. C.: *Kernel Smoothing*, Chapman and Hall, London, 1995.
- Webb, E. K., Pearman, G. I., and Leuning, R.: Correction of the flux measurements for density effects due to heat and water vapour transfer, *Q. J. R. Meteorol. Soc.*, 106, 85–100, 1980.

C Siebicke et al. (2011)

Siebicke, L., Serafimovich, A., Foken, T., 2011. Linking CO₂-advection estimates to vegetation structure at a forest site. *Agric. For. Meteorol.* (to be re-submitted in revised version).

Linking CO₂-advection estimates to vegetation structure at a forest site

Lukas Siebicke^{a,*} Andrei Serafimovich^a Thomas Foken^a

^aDept. of Micrometeorology, University of Bayreuth, Universitätsstr. 30, 95440 Bayreuth, Germany

Abstract

Surface exchange flux measurements of Net Ecosystem Exchange *NEE* are incomplete if only the turbulent flux is considered and advection neglected. However, including advective terms in the budget has not proven to be a robust alternative since the uncertainties inherent in advection estimates are large and thus increase the uncertainty and scatter of *NEE* estimates. The current study investigates some of the processes generating measured horizontal CO₂ concentration gradients, which are generally used to compute horizontal advective flux terms. In contrast to standard methodology, where gradients are computed over 30-minute time frames and a spatial extent on the order of tens to hundreds of meters, the focus of this study is on short and small events such as coherent structures. Moreover, the effect of vegetation structure on concentration gradients is considered. The results suggest that coherent structures act as a mechanism relating vegetation structure such as Plant Area Index *PAI* and sub-canopy CO₂ concentration. Very local mixing by coherent structures of a CO₂ concentration distribution with strong vertical gradients is an alternative explanation for horizontal variability of sub-canopy CO₂ concentration as opposed to consistent larger scale motion representative for the whole area under study, which is an often made assumption. The small scale variability of vegetation structure leads to high local variability of the concentration field. Gradients are thus not representative for the scale they need to be to complement above-canopy turbulent flux measurements with advective flux terms. The findings do not directly improve the *NEE* budget but help to understand the mechanisms generating observed CO₂ concentration signals.

Key words: CO₂ advection measurements, CO₂-flux, vegetation structure, coherent structures, concentration gradients

1. Introduction

Flux measurements have become an important tool over the past years for ecosystem research. However, the night-flux error, related to the eddy covariance method, remains one of the most essential problems for reliable CO₂-flux measurements (see review by Finnigan, 2008). Measurements at a variety of sites have contributed to a better understanding of advection, spanning a wide range of locations from the temperate forests of Europe (e.g. Aubinet et al. (2003) in Belgium, Kutsch et al. (2008) in Germany, six CARBOEUROPE-sites, reviewed by Aubinet et al. (2005), three ADVEX-sites reviewed by Feigenwinter et al. (2008) in Italy, Germany, Sweden to montane (Staebler and Fitzjarrald, 2004; Etzold et al., 2010) and subalpine forests (Yi et al., 2008) in Northern America, in an Australian Eucalyptus stand (Leuning et al., 2008), to

tropical forest (de Araujo et al., 2008; Tóta et al., 2008) in Brazil). However, even after many years of advection research, no generally satisfying solution could be found for the night flux problem in terms of accounting for advective terms in the Net Ecosystem Exchange *NEE* budget equation. This failure is partly related to non matching scales of the terms involved in the equation. Moreover, there is increasing awareness of the limitations of currently applied advection measurement approaches and of the inability to reliably close the night time carbon budget by including advection, as expressed in Aubinet et al. (2010) on the basis of the ADVEX experiment. When estimating advective flux terms most studies rely on the existence of CO₂-gradients which are persistent over some longer time and some larger spatial extent. This is the underlying assumption in a number of studies summarized by Aubinet (2008), who developed a scheme to classify the advective regime of a given site in relation to source intensity distribution and mass flow characteristics. In a spatial context this means gradients are taken to be representative along one axis of an assumed control volume, potentially comprising several sampling points. In the temporal context it has

* Corresponding author: Lukas Siebicke, Dept. of Micrometeorology, University of Bayreuth, Universitätsstr. 30, 95440 Bayreuth, Germany, Tel.: 0049-921-552176.

Email address: lukas.siebicke@uni-bayreuth.de (Lukas Siebicke).

to be assumed that gradients are persistent for a minimum time frame equal or longer to the time it takes to sample all points along the gradient transect. Given the most commonly used switching valve system, e.g. Burns et al. (2009), which samples several points one after the other (“sequential approach”), this sampling time is in the order of minutes. Therefore the process scales which can be explained by the observations are limited by the measurement setup, although higher resolution time series obtained separately from the measurements used for advection computation are taken to study short lived phenomena by Heinesch et al. (2007), who looked at short concentration deviations in the time series from a sampling error perspective. The current study, which is part of the multidisciplinary micrometeorological and chemical EGER (“ExchanGE processes in mountainous Regions”) project (Foken et al., 2011), investigates some of the more small scale phenomena, looking at gradient variability within one transect comprising several sampling points, and secondly exploring phenomena with timescales potentially much shorter than the conventional design-limited averaging period of several minutes, i.e. the order of seconds. This was made possible by the development and application of a new measurement design with reasonable spatial resolution and an excellent temporal resolution of one second using multiple gas analyzers (“parallel approach”). Specific processes under study are the effect of small scale variability in vegetation structure on gradient measurements by means of coherent structures under various exchange regimes (Thomas and Foken, 2007a). Small scale vegetation heterogeneity and coherent structures influence the concentration field close to the ground, in addition to previously described drivers such as soil respiration rates, depending on soil composition, temperature and moisture (Staebler and Fitzjarrald, 2004).

The turbulence within and immediately above the canopy is dominated by coherent structures. “Coherent structures, in contrast to stochastically distributed turbulence eddies, are well organized, relatively stable long-living eddy structures, which occur mostly with regularity in either time or space” Holmes et al. (1996). These structures contribute significantly to the exchange processes between the atmosphere and the forest canopy. Gao et al. (1989) demonstrated that the coherent structures are repeated and well-organized cycles of ejection-like upwelling flow and the subsequent sweep-like descending motions generated in the proximity of plant canopies by a wind shear effect. The organized ejections and sweeps can produce more efficient transport of momentum, heat, water vapor, and trace gases than local turbulence. Garratt (1978) and Raupach (1979) showed that the turbulent transport above the canopy is by a factor of two larger than predicted by the flux gradient relations. The experimental evidence for the coherent structures was found from observations in cereal canopies (Finnigan, 1979a,b), wind tunnel simulations (Raupach and Thom, 1981), plant canopies in the field (Shaw et al., 1983). Coherent structures have become a key point of many studies in

turbulence research of flow dynamics in laboratory flows and the atmospheric boundary layer (Raupach and Thom, 1981; Bergström and Högström, 1989; Shaw et al., 1989; Paw U et al., 1992; Katul et al., 1997; Finnigan, 2000). According to the mixing layer theory (Raupach et al., 1989, 1996) under near-neutral conditions coherent structures originate from Kelvin-Helmholtz instabilities. Brunet and Irvine (2000) then extended the mixing layer analogy for different plant canopies and range of atmospheric stabilities. Later studies of coherent exchange using automated detection algorithms such as wavelet transform (Collineau and Brunet, 1993; Thomas and Foken, 2005) allowed the investigation of the characteristics of coherent structures at the Waldstein-Weidenbrunnen site, their contribution to the turbulent flux transport (Thomas and Foken, 2007a) and the implication for the exchange regimes (Thomas and Foken, 2007b). Furthermore, Serafimovich et al. (2010) investigated sweep and ejection motions of coherent structures and showed that their contribution is essential to the exchange processes in all canopy regions and applies not only to the transport of momentum and sensible heat, but is valid for gaseous scalar transport as well.

Coherent structures might be viewed as a time-dependent mechanism relating time “constant” vegetation structure to observed gradients. Transport by coherent structures is of an intermittent nature and thus links two important components of the night flux problem: intermittency and advection (Aubinet, 2008). The main aim of the current study is to explain the variability of those CO₂-gradients which cannot be described as large scale phenomena (i.e. larger than the control volume and typical averaging time) such as gravity flows and external source heterogeneity, thereby shedding light on why accounting for advective terms was often not able to reliably improve *NEE* estimates for forested settings and will be unable to do so in the future as long as the scales of observation of the different terms of the *NEE* budget cannot be matched.

2. Material and Methods

2.1. Site

Measurements were carried out at the FLUXNET site Waldstein-Weidenbrunnen (DE-Bay), 50° 08' 31" N, 11° 52' 01" E, a hill site in the Fichtelgebirge Mountains in Southern Germany. The 25 m high spruce stand is on the upper section of a hill, 775 m ASL, with a 3° slope facing southwest. The site is described in detail in Gerstberger et al. (2004) and a summary of background data can be found in Staudt and Foken (2007). Fig. 1 shows the understorey vegetation at the site together with the sub-canopy CO₂ sampling setup. The upslope region of the plot is characterized by lush green, photosynthetically active understorey vegetation dominated by blueberries and young growth trees, whereas the downslope area mostly shows moss and litter.

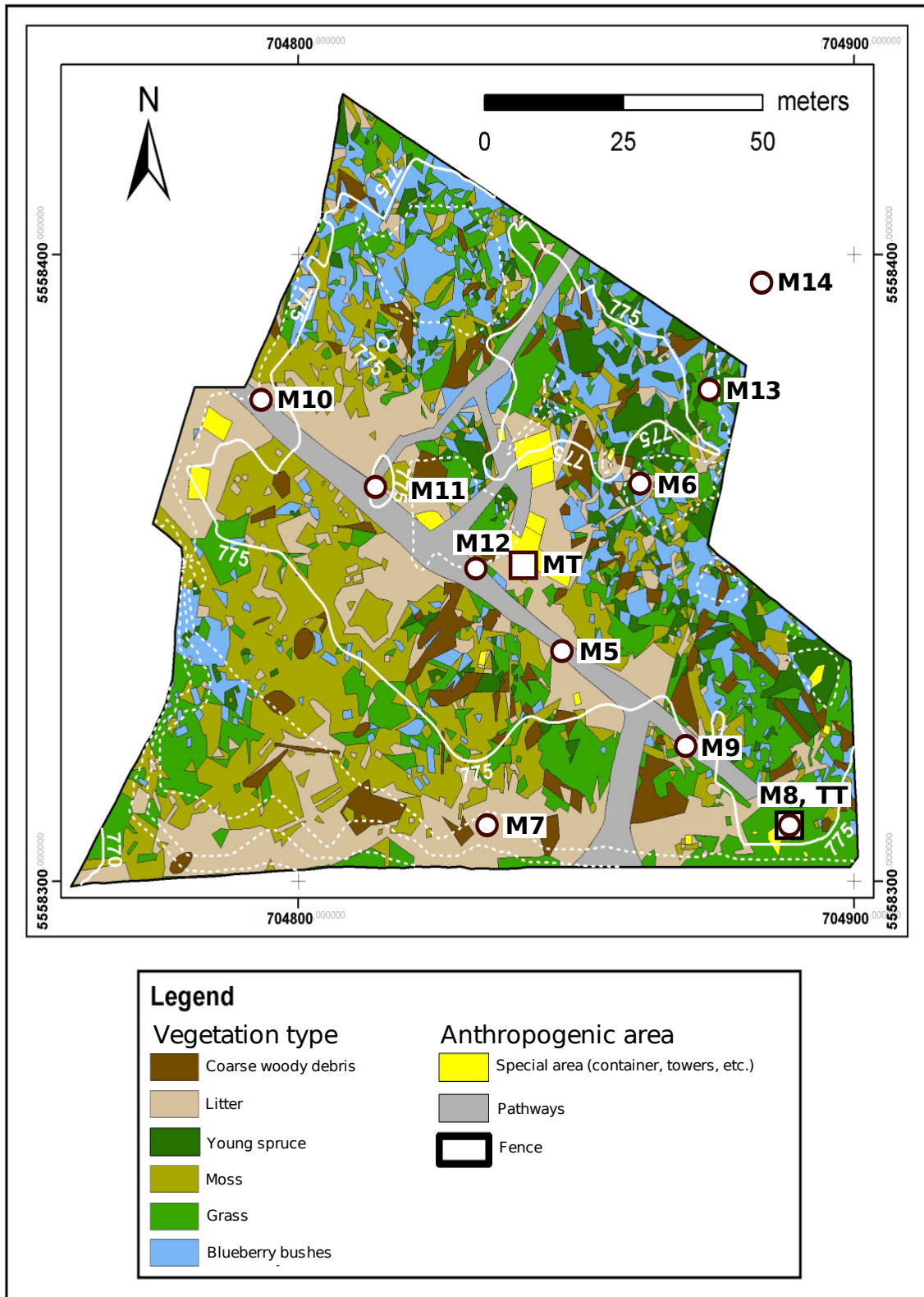


Fig. 1. Mast locations, understory vegetation and topography (shown as white isolines). Equidistance of dashed lines: 1 m. Coordinate system: Universal Transverse Mercator (UTM), zone 32U. Circles indicate position of 2 m masts with line intakes for CO₂ samples and wind measurements, squares indicate position of tall towers: “main tower” (MT) and “turbulence tower” (TT), see Section 2.2. “M-numbers” are used throughout the text for mast identification. Understorey vegetation data and graphics produced by Behrendt (2010).

2.2. Instrumental setup

Wind vector and CO₂ concentration time series were recorded along horizontal transects at a 2.25 m height in the sub-canopy space as well as along two vertical profiles reaching from groundlevel to above-canopy level. Regarding the sub-canopy measurements the spatial setup of sample locations is shown in Fig. 1. Ten CO₂ concentration sample points were distributed between an along slope transect from north-east to south-west (5 sample points) and an across slope transect from north-west to south-east (6 sample points), including one common point. Each point was sampled by an individual closed-path infrared gas analyzer. Instruments used were 5 LI-6262, 1 LI-6251 (LI-COR Biosciences Inc.), 4 BINOS (Leybold Heraeus GmbH). All CO₂ closed-path gas analyzers shared a common housing in a central position, with controlled conditions resulting in a constant common temperature and common pressure regime as well as radiation protection. Moreover, all analyzers shared a common tailor made automatic calibration system, using high precision reference gases (accuracy 0.1 μmol mol⁻¹). The calibration routine included an automatic calibration every 4 hours using 2 reference concentrations. In addition to factory calibration, each instrument's polynomial calibration function was established on site, using multiple standards. The polynomial was checked before and during the experiment. CO₂ concentration measurements are available with a frequency of 1 Hz at each sample point. In addition to CO₂ concentration measurements at a 2.25 m height, sample locations M5, M6, M7, M8, M9, M10 (see Fig. 1) were equipped with sonic anemometers (USA-1, METEK GmbH) to measure wind speed, wind direction and sonic temperature at the same height as well as cup anemometers for wind speed and dry and wet bulb thermometers for temperature and humidity measurements at a 1 m height. Sonic data were recorded at a 20 Hz frequency, cup anemometers and psychrometers every minute.

Two vertical profiles of wind speed and direction as well as CO₂ and water vapor concentration were measured. One was installed on a 32 m high tower, hereafter referred to as “main tower”, MT, (location between M5 and M12, see Fig. 1) using a combination of two closed-path infrared gas analyzers (LI-7000 and LI-820, LI-COR Biosciences Inc.), sequentially sampling 11 inlets at heights of 0.005, 0.03, 0.1, 0.3, 0.9, 3, 10, 16.5, 20.5, 25 and 31.5 m (Plake, 2009) and one closed-path infrared gas analyzers (LI-7000) for continuously sampling at a 32 m height. Wind speed and direction were measured at the same tower using sonic anemometers at heights of 0.03 m, 0.3 m, 1 m, 2 m (Wind Sensor WS425, Vaisala), 16 m, 25 m (Solent R2, Gill Instruments Ltd.) and 32 m (USA-1, METEK GmbH). The profile was additionally equipped with cup anemometers at heights of 2, 4.6, 7.6, 10, 13.3, 16.5, 18, 19.8, 21, 24.3, 25, 26.3, 31 and 31.2 m and psychrometers at heights of 0.05, 2, 4.9, 5, 9.9, 13, 15.9, 19.5, 21, 24.4, 26.6, 30.9 and 31 m. The other vertical profile was installed on a 36 m high slim tower, hereafter re-

ferred to as “turbulence tower”, TT, (Fig. 1). Six levels were equipped with sonic anemometers and open-path infrared gas analyzers at heights of 2.25, 5.5, 13, 23 m (CSAT3, Campbell Scientific Inc. and LI-7500, LI-COR Biosciences Inc.), 18 m (Solent R3-50, Gill instruments Ltd. and LI-7500, LI-COR Biosciences Inc.) and 36 m (USA-1, METEK GmbH and LI-7500, LI-COR Biosciences Inc.). More detail and additional instrumentation is given in Serafimovich et al. (2008).

2.3. Data sets

The data set was collected during the second intensive observation period (IOP2), 1st of June to 15th of July 2008 (Foken et al., 2011) of the EGER (“Exchange processes in mountainous Regions”) experiment. 24.6 days worth of data were used for the analysis, i.e. 1181 half hourly values taken from a window of 32.0 days (11th of June to 13th). Data meeting the following criteria were excluded: instruments powered off or malfunctioning, or atmospheric stratification outside of specified range (see section 1 for definition and ranges of stability criterion).

2.4. Data analysis

2.4.1. Stratification

Atmospheric stratification was used as a primary means of differential analysis and grouping of data for the results presented. In the following, atmospheric stratification is expressed in terms of the stability parameter ζ , measured at a 2.25 m height. ζ is defined as $\zeta = (z - d)L^{-1}$ with measurement height z , displacement height d and Obukhov-length L . Results were distinguished with respect to different classes of atmospheric stratification, using the criteria given in Equation (1) according to Foken et al. (1991):

$$\zeta = \begin{cases} \text{free convection} & \text{for } \zeta < -1 \\ \text{unstable} & \text{for } -1 < \zeta < -0,0625 \\ \text{neutral} & \text{for } -0,0625 < \zeta < 0,125 \\ \text{stable} & \text{for } +0,125 < \zeta < 1 \\ \text{extremely stable} & \text{for } \zeta > 1 \end{cases} \quad (1)$$

The following classes are used during the analysis: “unstable”, “neutral”, “stable” and “all”, where “all” refers to the sum of unstable, neutral and stable.

2.4.2. Gradients

In the context of this work the term “local concentration perturbation” is used for the difference between the concentration at one sample location c_i , and the spatial average concentration of the sample point field $\bar{c}(t)$ at a given time t . Increments of t are equal to the temporal resolution of the concentration time series of 1 Hz. $\bar{c}(t)$, which serves as a reference concentration, describes the background concen-

tration of the sample point field at time t using the median field concentration according to Eq. 2

$$\tilde{c} = \begin{cases} c_{\frac{k+1}{2}} & k \text{ odd} \\ \frac{1}{2} \left(c_{\frac{k}{2}} + c_{\frac{k}{2}+1} \right) & k \text{ even} \end{cases} \quad (2)$$

with $k = 1 \dots n$ observations (c_1, c_2, \dots, c_k) being the concentration measurements ($c_1(t), c_2(t), \dots, c_n(t)$) at n locations sorted in ascending order.

In order to investigate the effect of atmospheric stratification on CO₂ concentration gradients, mean gradients were computed for four classes of atmospheric stratification using the whole data set. Mean gradients shown in this analysis are derived from the 1 Hz concentration time series.

In addition to statistical analysis of gradients based on the whole data set, characteristics of limited snapshots of the time series were investigated to see whether results derived from mean values can be explained by short lived events, such as coherent structures, i.e. an atmospheric condition with respect to wind direction, wind speed and CO₂ concentration, which is persistent for a short amount of time on the order of seconds to minutes.

Prior to any gradient analysis each individual concentration time series was corrected to account for concentration offsets characteristic of any multi-analyzer setup. A new approach, tailored to the given setup, was developed within the EGER project and was based on conditional signal shifting, using statistical properties of distributions of concentration differences between sample points and the sample point field median. It accounts for characteristics of the atmospheric mixing between sample points based on cross correlation. A detailed description of the bias correction approach is given in Siebicke et al. (2010).

2.4.3. Horizontal advection

Horizontal advection F_{HA} was estimated based on both CO₂ concentration gradients and sonic wind measurements, both at a 2.25 m height as one term of the *NEE* budget equation in the form given in Aubinet et al. (2003). Horizontal advection terms were computed for the along slope transect, i.e. x -direction, for the across slope transect, i.e. y -direction, and for a combination of all sampling points, with a 30-minute time resolution according to Equation (3). The x -axis of the coordinate system was defined parallel to the up-slope direction running from south-west (218.71°) to north-east (38.71°). The y -axis was defined perpendicular to the slope running from north-west (308.71°) to south-east (128.71°), which corresponds to the line of sight between M10 and M8 (Fig. 1). The z -axis was defined in the vertical starting at the forest floor with a positive sign upwards.

$$F_{HA} = \frac{1}{V_m} \int_0^h \left(\bar{u}(z) \frac{\partial \bar{c}}{\partial x} + \bar{v}(z) \frac{\partial \bar{c}}{\partial y} \right) dz \quad (3)$$

with the molar volume of dry air V_m , CO₂ concentration c (overbars denote temporal means), horizontal distances

x and y , vertical distance above ground z , horizontal wind velocity u along the x -direction, horizontal wind velocity v along the y -direction and integration height $h = 14$ m, equal to the height of the maximum of the vertical *PAI* profile (see reasoning below). Horizontal CO₂ concentration gradients were measured at a height of $z_1 = 2.25$ m. Since it is practically infeasible to measure horizontal gradients with high spatial resolution at a large number of heights, which is a common limitation of previously published advection research, assumptions have to be made in order to be able to vertically integrate horizontal advection. The current study follows an approach published by Aubinet et al. (2003) and Staebler and Fitzjarrald (2004), which is based on the assumption of similarity between horizontal gradients and the vertical profile, assuming that a single vertical profile of CO₂ concentration and wind speed, measured at a central location, translates with spatial similarity to all sub-canopy sampling points (“similarity approach”). Staebler and Fitzjarrald (2004) substitute absolute CO₂ concentration c by a concentration $c^* = c - c_0$ relative to a baseline level c_0 , the latter having no effect on budget calculations, chosen to be $c_0 = c(h)$, i.e. equal to above-canopy concentration. Using the above-stated assumptions, vertical integration of horizontal advection was performed according to Equation (4)

$$F_{HA} = \frac{1}{V_m} \left(u(x, z_1) \frac{\partial c^*(x, z_1)}{\partial x} \right) \int_0^h f(z)g(z) dz + \frac{1}{V_m} \left(v(y, z_1) \frac{\partial c^*(y, z_1)}{\partial y} \right) \int_0^h f(z)g(z) dz \quad (4)$$

with $f(z)$ and $g(z)$ being profile functions of the vertical profile of CO₂ concentration c^* and the vertical profile of the horizontal wind velocity component respectively, normalized by their value at z_1 . To obtain $\int_0^h f(z)g(z) dz$, measurements of CO₂ concentration (closed-path infrared gas analyzer system) and wind speed (sonic anemometers) along a vertical profile at the main tower, discrete measurement heights, detailed in Section 2.2, were used to fit continuous Akima interpolation functions (Akima, 1970), which were then numerically integrated.

Concerning the validity of horizontal advection estimates generated on the basis of the vertical integration approach cited above, the assumption of spatial similarity of vertical profiles can only be partially valid, given the heterogeneous canopy structure, presented in Section 3.3. Therefore, general applicability of Staebler and Fitzjarrald (2004)’s approach is questionable. Aubinet et al. (2003) limit the validity to the trunk-space and to stable stratification. Yi et al. (2008) question the similarity approach by Staebler and Fitzjarrald (2004) and Aubinet et al. (2003) since estimates of F_{HA} obtained using the similarity approach did not agree with estimates computed from gradient measurements at several heights at the Niwot Ridge site, with dis-

crepancies increasing with height. Due to the decoupling effect of the canopy, separating above and below canopy conditions, gradients measured in the trunk-space need not be representative for above-canopy conditions. Therefore, we restricted vertical integration of $f(z)$ and $g(z)$ to the trunk-space and the lower canopy ($h = 14\text{m}$), which yields more realistic estimates of F_{HA} at our site compared to using Staebler and Fitzjarrald (2004)'s original approach with an integration height $h = 32\text{m}$ equal to the top measurement level. Our calculation scheme therefore considers the above-mentioned constraints of the similarity approach noted by Aubinet et al. (2003) and Yi et al. (2008). The current study uses the similarity approach to present estimates of F_{HA} comparable to previously published advection fluxes at other sites, and as a consequence of the common limitation of gradient measurement levels, which makes some assumptions inevitable if fluxes are to be computed for a volume. Increasing the vertical resolution of horizontal gradient measurements on expense of a high horizontal resolution would be no alternative since it does not guarantee reliable horizontal gradients either and requires the assumption of horizontal gradients being consistent along one horizontal transect throughout the control volume. As the current study particularly investigates the within-transect variability of the sub-canopy CO_2 concentration field, the latter being the basis for estimates of F_{HA} , it is justified to concentrate the observation focus and the vertical integration of F_{HA} to the sub-canopy and the lower canopy. Even though the similarity assumption of Aubinet et al. (2003) and Staebler and Fitzjarrald (2004) can not be strictly valid at any site with horizontal heterogeneity, it does serve as an objective and reproducible basis for vertically integrating horizontal advection.

2.4.4. Plant Area Index

Plant Area Index (PAI) is a measure similar to the often used Leaf Area Index (LAI), which is the ratio of projected leaf area per unit ground area. PAI relates total projected plant area, including the woody parts of the trees, to ground area. In this work, PAI is used to characterize vegetation structure since it gives an indication of vegetation density, which in turn can be seen as a resistance possibly acting to damp or reduce air movement and exchange processes by coherent structures. PAI was estimated using an indirect optical method and the LAI-2000 Plant Canopy Analyzer from LI-COR Biosciences Inc.. The LAI-2000 calculates PAI from radiation measurements made with a "fish eye" optical sensor. Measurements made at a 32 m height above the canopy and below the canopy are used to determine canopy light interception at five angles, from which PAI is computed using a model of radiative transfer for vegetative canopies. Data from the two most vertical angles were used. 532 sample points were spatially interpolated, fitting a thin plate spline surface to irregularly spaced data using the "Tps" function (Furrer et al., 2008) provided with R (R Development Core Team, 2009).

2.4.5. Footprint

In order to characterize individual sub-canopy measurement points according to their representative vegetation structure, i.e. PAI , footprint modeling was used to define a relevant area influencing the signal of a single measurement position, which was then used to weigh the PAI distribution. The program TERRAFEX (Göckede et al., 2006) was used for footprint calculations. The footprint model uses a stochastic forward Lagrangian algorithm (Thomson, 1987) of Langevin type (Wilson and Sawford, 1996) in the implementation by Rannik et al. (2003). The model accounts for fluxes within the canopy and three-dimensional turbulent diffusion. However, it is subject to the limitations of the "inverted plume assumption" (Schmid, 2002), i.e. it is limited to horizontally homogeneous conditions. The effect of atmospheric stratification as well as wind direction is, however, represented. The approach used can therefore serve as an approximation of the area of interest when defining the representative PAI for every sample position. The main goal is to define the footprint for each sample position according to the same methodology to allow comparative analysis. Sub-canopy sample locations without turbulence measurements use the footprint estimate of the closest available measurement, i.e. mast M11 shares M10 data, M12 shares M5 data and M13 and M14 share M6 data.

2.4.6. Exchange regimes

In addition to atmospheric stratification, "exchange regimes" (Table 1) were used for grouping data during the analysis, to identify how the effect of coherent structures on CO_2 concentration gradients varies under different atmospheric conditions. Exchange regimes indicate which parts of the canopy are coupled and controlled by coherent exchange. The coupling situation was computed for each 30-minute interval, using sensible heat flux measurements along a vertical profile at the turbulence tower according to Thomas and Foken (2007a).

2.4.7. Coherent structures

Two approaches were followed in the analysis of coherent structures. One is the automated analysis of the statistical properties of a large number of coherent structures identified with the wavelet transform technique. The other is the inspection of individual coherent structures after manual identification.

Following the first approach, a spectral analysis technique based on the wavelet transform has been used to detect coherent structures in turbulent time series and define their statistical properties. First, outliers were removed using a despiking test (Vickers and Mahrt, 1997). Wind components were then corrected on a sector-wise basis using the planar fit method (Wilczak et al., 2001). Next, each 30-minute scalar time series was corrected for time lags. After averaging to a 2 Hz time resolution all data were passed through a low-pass wavelet filter. Finally, for every 30-minute time interval a continuous wavelet transform was

Table 1
Definition of exchange regimes according to Thomas and Foken (2007a).

Regime code	Regime description
Wave motion Wa	Wave motion is detected.
Decoupled canopy Dc	Air layer above the canopy is coupled, but decoupled with the canopy.
Decoupled sub-canopy Ds	Air layer above the canopy is coupled with the canopy but not with the sub-canopy.
Coupled sub-canopy by sweeps Cs	Air layer above the canopy is coupled with the canopy, but with the sub-canopy only by strong sweeps.
Fully coupled canopy C	Air layer above the canopy, canopy and sub-canopy layers are fully coupled.

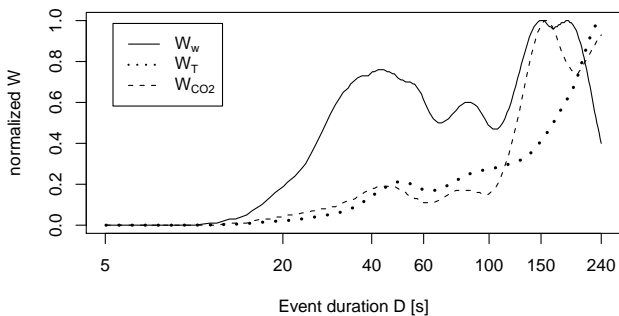


Fig. 2. Normalized wavelet variance of vertical wind velocity W_w , sonic temperature W_T and CO_2 concentration W_{CO_2} , measured at a 2 m height at M13 on June 29, 2008, for the 30-min interval from 19:00 to 19:30.

performed and a wavelet variance spectrum was derived. The Morlet function has been used as the mother wavelet because it is best suited for the current analysis according to tests of several mother wavelets, including the Morlet and the Haar wavelet, which were performed by Thomas and Foken (2005) for the site under study. Fig. 2 presents an example of a normalized wavelet variance spectrum for a selected 30-minute interval at location M13. Normalized wavelet variance of vertical wind velocity w , sonic temperature T and CO_2 concentration is plotted versus event duration D on a log scale. Local maxima of the wavelet variance spectrum mark characteristic event durations. For the example given in Fig. 2, three local maxima are observed for W_w , i.e. at event durations of 43 s, 85 s and 151 s. For W_T only the first maximum is found at 50 s. For W_{CO_2} the local maxima are at 45 s, 82 s and 156 s, closely matching characteristic event durations stated for W_w . Locating the first local maximum of the wavelet variance spectrum, the characteristic duration of coherent structures for each 30-minute time interval was obtained and used for further analysis. Amplitudes of the detected maxima give us the information about the relative strength of coherent structures. More detail about the methods described above can be found in Thomas and Foken (2005). Applying conditional sampling analysis described by Antonia (1981), all time series were sampled according to derived characteristic event duration, and total number of detected coherent structures was estimated.

In the second approach, individual coherent structures were analyzed in a graphical representation of the wind and the CO_2 concentration field in a height versus time

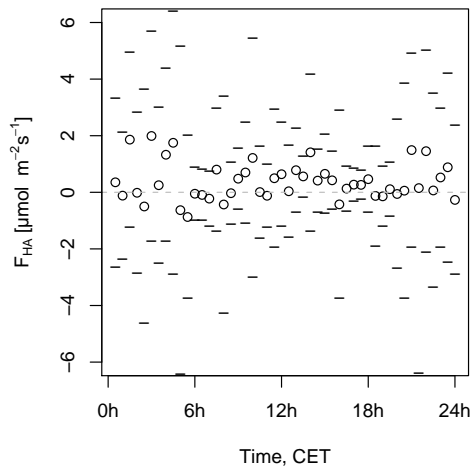
plot (Sec. 3.6). High frequency turbulent time series of wind and CO_2 concentration at six measurement heights from the turbulence tower were averaged to obtain a 30 second resolution. Considering that the mean event duration of coherent structures deduced from the first local maximum of the normalized wavelet variance spectrum at the different sub-canopy sample locations is in the range of 51 to 60 s (see also Fig. 10b) a 30 s averaging time of the graphics allows for approximately two data points per coherent structure if the latter is defined by the first maximum of the wavelet variance spectrum. The graphs allow investigation of coupling of different vertical heights under various exchange regimes on a visual basis. Thereby individual structures and sequences of structures, penetrating from above the canopy to the trunk-space, and their impact on CO_2 concentration measurements at a 2 m height, can be identified. The second local maximum of W_w and W_{CO_2} shown in Fig. 2 is a typical duration of sweep and ejection events shown in Fig. 13 to 17. These events can be composed of a series of shorter events. This is a direct consequence of multi-modal wavelet variance spectra such as the example spectra given in Fig. 2.

3. Results and Discussion

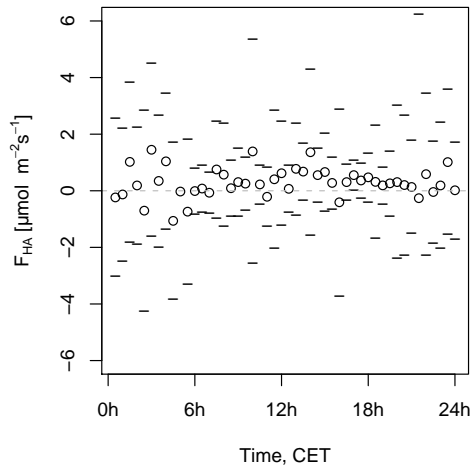
This section deals with estimates of the horizontal advection term of the NEE budget equation and subsequently presents processes which possibly generate patterns observed in the advection estimate. The analysis will focus on horizontal gradients rather than wind speed, despite the fact that both are needed to compute horizontal advection. Furthermore, it is not intended to present terms of the NEE budget – other than horizontal advection F_{HA} – but to concentrate on details of horizontal gradients. Note that units of ppm are used instead of the SI unit $\mu\text{mol mol}^{-1}$ at some figures for the sake of brevity.

3.1. Mean horizontal advection

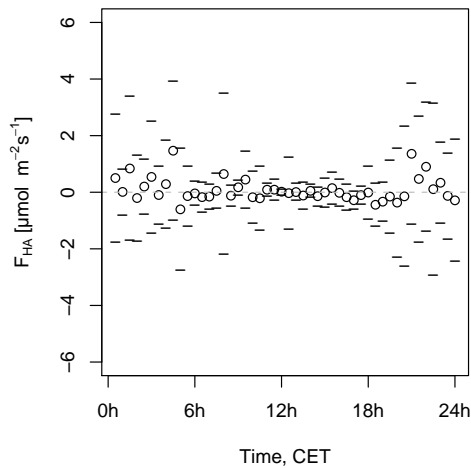
The mean daily cycle of horizontal advection F_{HA} (Fig. 3) is moderately positive during the day and positive at night, with some negative values during transition times, e.g. at around 05:00 CET (Fig. 3a). The scatter of the mean and the standard deviation are larger at night than during the day. Differentiating F_{HA} relative to sample



(a)

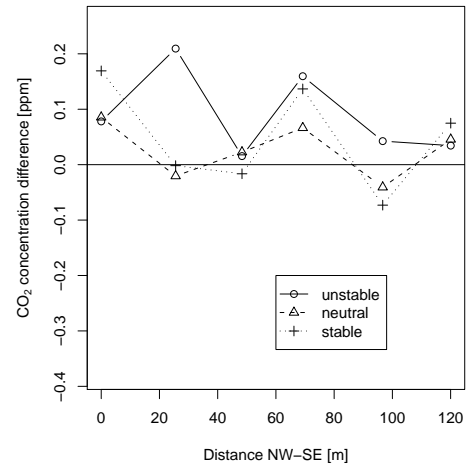


(b)

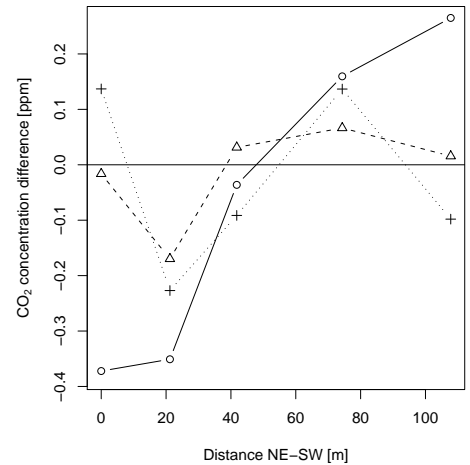


(c)

Fig. 3. Mean daily cycle of horizontal advection F_{HA} with a 30-minute time resolution for all sample locations (a), for the across slope transect (b) and the along slope transect (c). Circles show the mean, dashes the standard deviation for 30-minute intervals. Number of values: 1181 from 11th of June to 13th of July 2008.



(a)



(b)

Fig. 4. Mean CO_2 -gradients for three classes of atmospheric stratification: unstable, neutral, stable. Across slope sample points (a), along slope sample points (b). Note that (a) and (b) have one sample point in common (fourth point from left to right).

transect orientation versus slope orientation, the variation of F_{HA} is smaller for the along slope direction (Fig. 3c) as compared to the across slope direction (Fig. 3b), with a minimum before noon and in the afternoon.

3.2. Gradients versus stratification

The effect of atmospheric stratification and terrain slope on CO_2 concentration gradients is displayed in Fig. 4. In the along slope case (Fig. 4b) there is consistent behavior of as a function of stratification: the gradient increases downslope with increasing stability parameter ζ , i.e. the downslope gradient is positive for unstable, near zero for neutral and negative for stable stratification. The stability effect accounts for about half of the variance of the data shown. Other drivers possibly explaining some of the remaining variance are related to vegetation structure and will be presented in section 3.4 and 3.5. Regarding the across slope

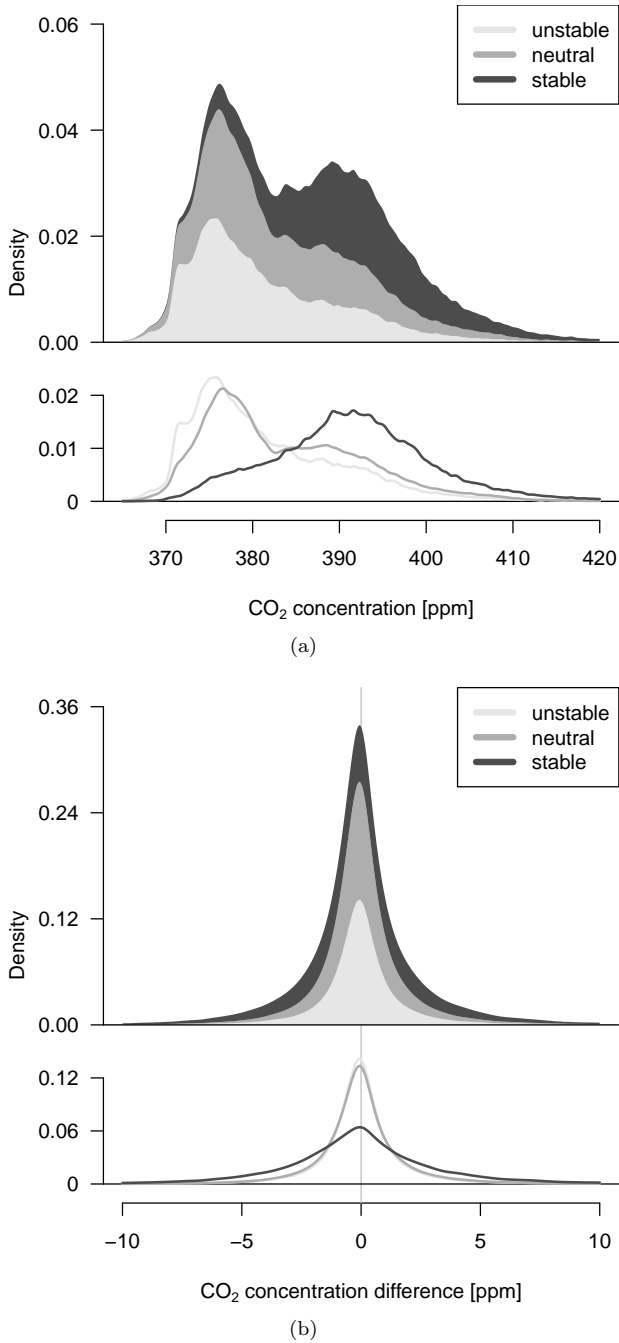


Fig. 5. Density distribution of CO₂ concentration (a) and of local perturbations from the average field CO₂ concentration (b) for unstable, neutral and stable stratification. The upper panel is a cumulative representation of the density of stratification classes, the lower panel shows stability classes separately.

case there is little dependence of CO₂ concentration gradients on stratification, in that case leaving most of the variance to be explained by other factors. Thus slope enhances the effect of stratification on gradients. This is in line with other studies and can be explained by the downslope orientation of drainage flows during stable stratification which were found for the site, characterized by a sec-

ondary wind maximum in the trunk-space and a dominant downslope wind direction during stable stratification (not shown), combined with accumulation of high CO₂ concentrations close to the ground.

Regarding trunk-space CO₂ concentration, there is a distinct relationship to atmospheric stratification (Fig. 5). For unstable and neutral cases, the density distribution of the CO₂ concentration (Fig. 5a) is clearly right-skewed with a pronounced peak at around 375 $\mu\text{mol mol}^{-1}$. The lower end of the distribution is limited by the background concentration above the canopy, as opposed to high concentration sources close to the ground, which explain the long tail of the distribution towards higher values. During stable stratification, the mode of the more symmetric distribution is shifted towards higher values. Note that the combined density distribution (Fig. 5a, top panel) is bimodal, indicating a rapid change between unstable/neutral and stable stratification. This is consistent with the uneven distribution of exchange regimes presented in Sec. 3.6. In contrast to concentration distributions, the density distributions of local concentration perturbations are quasi symmetric with high kurtosis, which is largest for unstable and neutral conditions (Fig. 5b). The latter can be attributed to frequent vertical coupling, tying sub-canopy measurements to more constant above-canopy concentrations. This is not the case for stable stratification, where sub-canopy measurements are exposed to accumulation of high CO₂ concentrations close to the ground. Strong vertical gradients at night combined with occasional mixing explain the long tails of the distribution at both sides.

3.3. Plant Area Index and footprint

As Plant Area Index is possibly a factor explaining local differences of sub-canopy CO₂ concentration, its spatial distribution was investigated. The distribution of *PAI* (Fig. 6) is characterized by a large amplitude with minimum *PAI* of less than two and maximum *PAI* of eleven. Since *PAI* variability is high, maximum and minimum *PAI* values can be found very close together, even within the footprint of one sub-canopy measurement point, e.g. M7. Regarding the along slope transect there is an increase of *PAI* in the downslope direction, which is interrupted by canopy gaps with low *PAI*. For the across slope transect *PAI* increases from south-east to north-west, again with areas of lower *PAI*. Note that for the downslope transect most sample positions have an adjacent area of low *PAI* in the upslope direction. This is important to remember when looking at local concentration perturbations during stable stratification presented in the following discussion, since those situations are often characterized by katabatic flow. Canopy gaps increase the chance of air entrainment from above-canopy height which generally has lower CO₂ concentration at night compared to conditions close to the ground (Sec. 3.6) and might thus affect sub-canopy concentration locally.

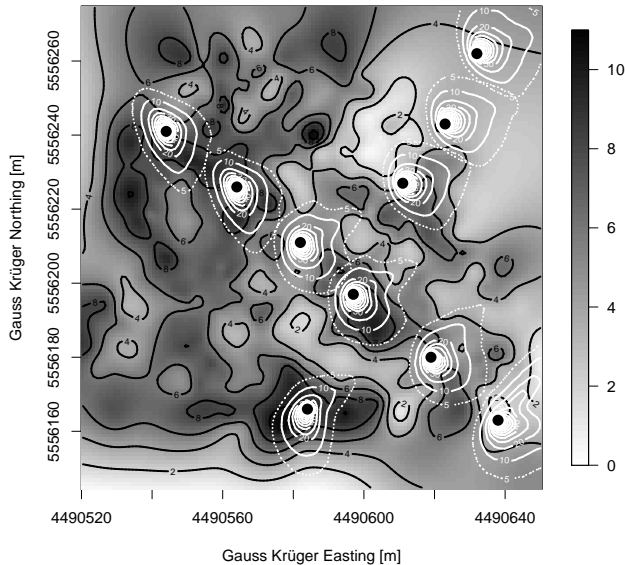
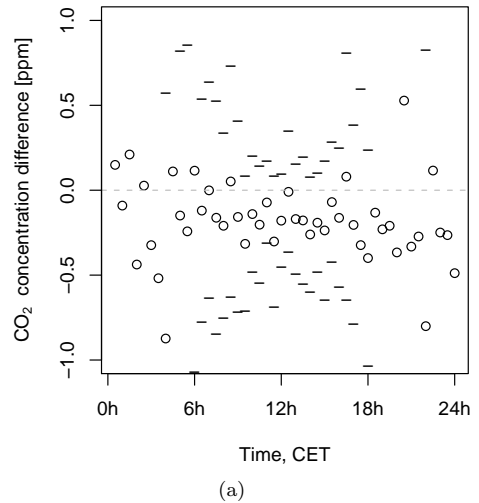


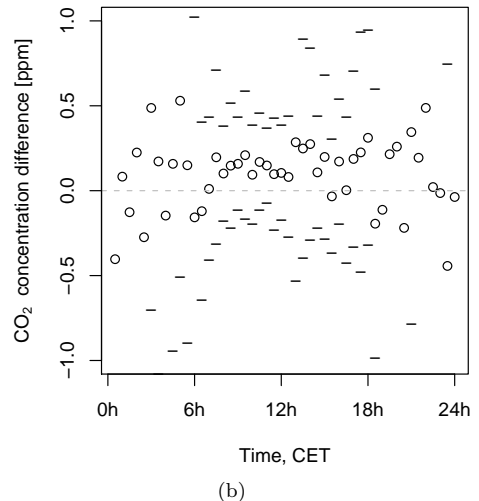
Fig. 6. Map of Plant Area Index given as gray scale and black contour lines. Black points show the positions of the towers for sub-canopy measurements. X- and y-axis are distances in meters in the Gauss-Krüger coordinate system. White isolines show the relative flux contribution of the corresponding footprint area in 10 % intervals for stable cases only. The outermost, dashed isoline indicates the area from where 95 % of the flux originates. Raw data of *PAI* were provided by E. Falge.

In addition to the horizontal *PAI* distribution, vertical profiles of *PAI* were measured in 2008 during IOP2 of the EGER experiment. The maximum vegetation density is concentrated in the canopy level at a 14 m height, with the canopy top at 25 m above ground. See Foken et al. (2011) for vertical *PAI* profiles. Combining horizontal and vertical *PAI* information leads to the following conclusions with regards to air movement relative to the canopy: preferred low resistance flow paths for horizontal movement are above the canopy, as well as below the canopy in the trunk-space with a few decimeters vertical displacement due to understorey vegetation as well as in-canopy gaps for vertical movement. There is a positive correlation between canopy gaps and understorey vegetation, i.e. the north-eastern section of the study area with generally lower *PAI* (Fig. 6) has more young understorey trees (Fig. 1), thus restricting in-canopy flow in the trunk-space compared to the litter dominated high *PAI* areas in the south-western section.

Footprints, shown for stable stratification in Fig. 6, have their maximum extent oriented in the upslope direction. This demonstrates the presence of downslope flow, being the preferred flow direction during stable stratification. Although footprint calculations were done for all classes of atmospheric stratification, Fig. 6 shows the stable case only, which has the largest and most variable footprints. For less stable stratification footprints are smaller (about 50 %) and more circular.



(a)



(b)

Fig. 7. Mean daily cycle of local CO_2 concentration perturbations with a 30-minute time resolution for a sample location with a low representative *PAI*, M13 (a) and one with a high representative *PAI*, M5 (b). Circles show the mean, dashes the standard deviation for 30-minute intervals. Number of values: 1181 from 11th of June to 13th of July 2008.

3.4. Sub-canopy CO_2 concentration versus Plant Area Index

To investigate the link between sub-canopy CO_2 concentration, which was used for the computation of horizontal advection (Fig. 3), and *PAI*, Fig. 7 displays the mean daily cycle of local concentration perturbations at a sample location with low *PAI* (Fig. 7a) and one with high *PAI* (7b). The location with low *PAI* clearly shows negative local concentration perturbations most of the time, the scatter being smallest during the day. In contrast, the high *PAI* location has positive perturbations during the day and partly at night. Those two locations correspond to extrem local perturbations in Fig. 4, with Fig. 7a corresponding to the second point from the left in Fig. 4b, and Fig. 7b corresponding to the fourth point from the left in Fig. 4b.

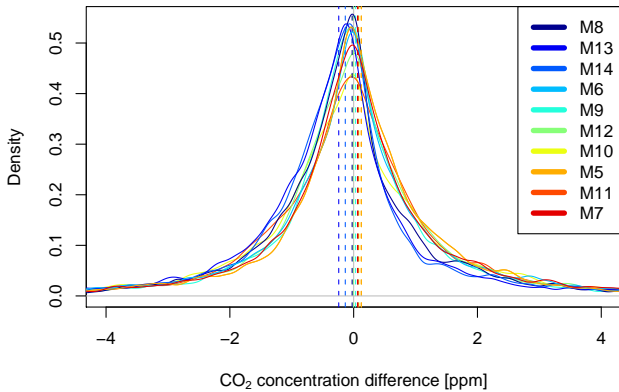
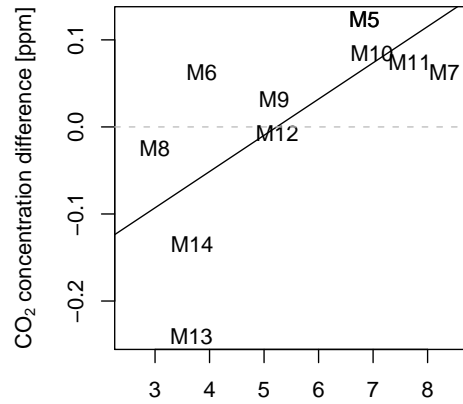


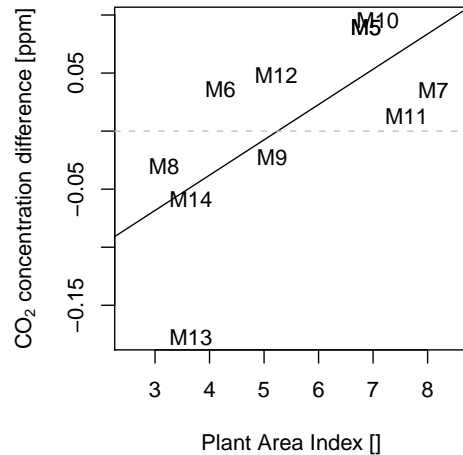
Fig. 8. Density distributions (solid line) of local CO_2 concentration perturbations and the mean of the distribution (dashed line) for all sample positions separately. The most numbers in the legend and the associated colors are sorted according to increasing PAI at the sample location, from blue (low PAI) to red (high PAI). Unstable stratification only. Note the grouping of colors in the graph.

The difference in mean local perturbations between the two sample points is largest for unstable stratification and decreases towards stable conditions (Fig. 4b). Combining PAI and stability effect leads to the hypothesis that sample points with low representative PAI are more frequently subject to low concentration air, either from the photosynthetically active canopy top or from aloft, which penetrate into the trunk-space through canopy gaps under unstable and neutral and less frequent even under stable conditions. Moreover, locations with high PAI have a lower chance to release CO_2 , which has accumulated close to the ground, due to the transport barrier of a dense canopy. This is supported by the density distributions of local CO_2 concentration perturbations of all sample points, given in Fig. 8 for unstable stratification. Sample locations with low PAI (blue colors) frequently show lower concentrations at both sides of the distribution compared to locations with high PAI (red colors), with both PAI groups clearly clumping together. This results in a positive correlation of the mean of each distribution with PAI (compare color sequence of dashed lines (distribution mean) in Fig. 8). However, the mode of all distributions of local perturbations, remains close to zero, thus ruling out concentration offsets between instruments.

Correlation of mean local CO_2 concentration perturbations with PAI is presented in Fig. 9 for unstable and neutral stratification. The slope of a linear regression is consistently positive for all classes of atmospheric stratification. Correlation is strongest for unstable and neutral stratification with Spearman's correlation coefficient (and p-value) $\rho = 0.71$ ($p = 0.14$) and 0.90 ($p = 0.08$) for the across slope and along slope transect, respectively, (unstable), $\rho = 0.66$ ($p = 0.18$) and 0.60 ($p = 0.35$) (neutral) and $\rho = 0.09$ ($p = 0.92$) and 0.10 ($p = 0.95$) (stable, not shown). The lower correlation during stable cases can be attributed on the one hand to reduced importance of the mixing effect described above due to the limited vertical coupling (Sec. 3.6) and



(a)



(b)

Fig. 9. Mean local perturbations of CO_2 concentration versus Plant Area Index PAI for unstable stratification (a) and neutral stratification (b) for all sample locations (with M number for mast identification according to Fig. 1). Linear regression shown as solid line.

on the other hand to the fact that footprint estimates for higher stability might be less representative. Even though they might approximate the footprint attributed to the Reynolds flux reasonably well, they might not be representative for the true footprint, the latter being affected by canopy gaps further away from the measurement location acting as passages for entrainment of CO_2 -depleted air from levels above. Moreover, correlation might be generally obscured and lower during stable stratification because the estimate of a representative PAI is generated from a projection of plant material well above the measurement height and not at the sub-canopy level, whereas the horizontal component of air flow in the trunk-space, particularly during stable stratification, is more pronounced than the vertical component, leading to advection of air from the surroundings with possibly a different PAI .

Whereas the mean of perturbation distributions is positively correlated with PAI (Fig. 9), the second statistical

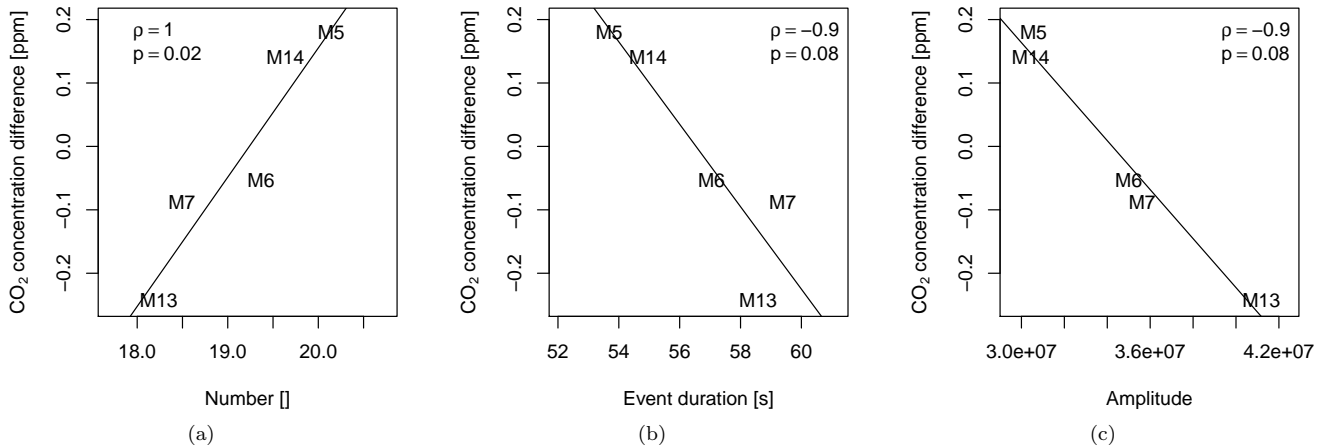


Fig. 10. Mean local perturbations of CO₂ concentration, downslope transect (with M number for mast identification according to Fig. 1), versus number of coherent structures per 30-minute interval (a), event duration (b) and amplitude of wavelet variance of coherent structures (c), stable stratification. Linear regression shown as solid line. Number of values: 307 from 11th of June to 13th of July, 2008.

moment, skewness, is negatively correlated with *PAI* (not shown). In the case of positive skewness, the right tail is longer (right-skewed). The distribution has relatively few high concentration values, whereas for negative skewness, the left tail of the distribution is longer (left-skewed). It has relatively few low concentration values. This supports the above-mentioned hypothesis through the same mechanism described for the mean. The third moment, kurtosis, is also negatively correlated with *PAI* (not shown), meaning that perturbation distributions of low *PAI* locations show high kurtosis, which can be interpreted as a result of low *PAI* locations frequently sampling above-canopy concentrations, which are relatively constant compared to close to the ground conditions. The latter are more frequently sampled by high *PAI* locations, leading to wider tails in the distribution and consequently a lower kurtosis.

3.5. Sub-canopy CO₂ concentration versus coherent structures

Coherent structures have been proposed as a mechanism relating the sub-canopy CO₂ concentration field to vegetation structure in Sec. 1. Thus the dependence of local CO₂ concentration characteristics on coherent structure statistics is presented in Fig. 10 and shows strong correlation. During mixed conditions (neutral and unstable stratification), CO₂ concentration perturbations do not depend on coherent structure statistics (not shown). This can be interpreted as follows: no matter whether coherent structures are large or small, short or long in duration, they transport air with relatively similar CO₂ concentration. However, during stable stratification coherent structures affect the local concentration because they originate from different heights in a highly stratified vertical profile with strong vertical CO₂ concentration gradients. This might be an explanation for the strong correlation of horizontal local concentration perturbations with coherent structure statistics

during stable stratification in contrast to low correlation during neutral and unstable conditions. Regarding the correlation of concentration perturbations with individual statistical properties of coherent structures for cases of stable stratification, positive perturbations are correlated with high numbers of coherent structures per 30-minute interval (Fig. 10a), short duration (Fig. 10b) and low amplitude (Fig. 10c), whereas negative perturbations go along with few but longer-lived structures with high amplitude. Due to spatial restrictions in areas with high canopy density, coherent motion breaks up into many small structures, assuming interdependence of event duration (Fig. 10b) and size of coherent structures. However, sub-canopy sample points with low canopy density in the footprint have a higher chance of being affected by coherent structures which originate from other heights in the vertical profile and therefore carry lower CO₂ concentration. Space permitting, those structures are larger and longer lived but observed less frequently, which is to be expected in the light of stable stratification. This finding supports the hypothesis of a dependence of the local sub-canopy concentration on canopy structure.

Entrainment of air from heights above the sub-canopy measurement level with relatively low CO₂ concentration is demonstrated in Fig. 11 for the low *PAI* location M13 under stable stratification at the beginning of the night. Coherent structures show negative deviations from the general concentration evolution by as much as 20 $\mu\text{mol mol}^{-1}$, reaching down to above-canopy concentration levels. Equivalent data of negative concentration deviations has been published by Heinesch et al. (2007, Fig. 4, p. 467), but has only been discussed as a source of measurement uncertainty with respect to mean values. The current study suggests that low *PAI* favours low concentration air entrainment by coherent structures, which contribute to the true signal observed in the trunk-space.

There is a higher correlation between CO₂ concentration perturbations and coherent structure statistics (Sec. 3.5)

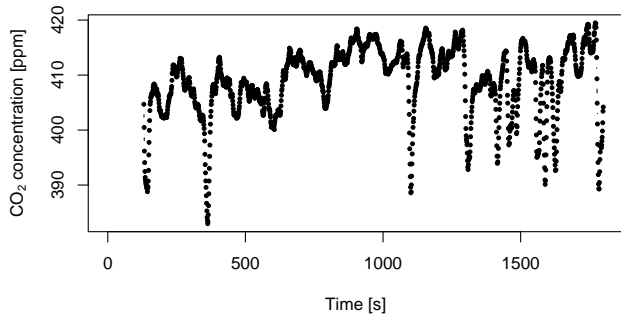


Fig. 11. CO₂ concentration at M13 over a 30-minute period, starting at 22.06.2008, 20:07.

compared to the correlation of perturbations with Plant Area Index (Sec. 3.4). Whereas coherent structure statistics can be taken as relatively accurate in the sense that they are computed from the true wind and concentration signal observed at a measurement point, the representative *PAI* for each sample position was estimated by weighing *PAI* distribution with a footprint estimate. However, due to limitations of the footprint model, which is based on the Reynolds flux and does not fully account for flux generated by coherent structures, the resulting representative *PAI* might be biased, e.g. a gap in the canopy (low *PAI* area) at the fringe of the footprint will have relatively little weight in the computation of the representative *PAI* for a particular location, but coherent structures might pass through this canopy gap and affect the CO₂ concentration measurement of the sub-canopy sampling point. The uncertainty in the footprint and thus in the *PAI* estimate is assumed to be largest during stable stratification when footprints are large. This might be another reason for best correlation of concentration perturbations with *PAI* occurring during unstable and neutral stratification when footprint extent is moderate, and low correlation occurring during stable stratification in the case of *PAI*, whereas correlation of concentration perturbations and coherent structure statistics greatly increase with stability.

3.6. Sub-canopy CO₂ concentration versus exchange regimes

Having investigated possible links between local characteristics of sub-canopy CO₂ concentration and vegetation structure and vertical exchange, this section presents the distribution of exchange regimes and their characteristics with respect to CO₂ transport, identifies individual coherent structures typical for a given regime and analyzes their fingerprints found in concentration time series measured in the trunk-space.

Table 2 summarizes the relative importance of different exchange regimes as defined in Table 1. The regime *Ds*, i.e. decoupled sub-canopy, is the most frequent one, followed by well coupled regimes *Cs* and *C*. Wave motion *Wa* is almost as frequent as fully coupled conditions *C*, with the decoupled canopy regime *Dc* of minor importance. The un-

Table 2

Occurrence of exchange regimes: number of 30 min intervals with a particular exchange regime (see table 1 for definition) for the entire data set (03.06.2008, 12:00 to 14.07., 12:00) and for “Golden days” (29.06.2008, 00:00 to 02.07., 24:00), representing a fair weather period. NA means that classification is not available.

Period	Exchange regime					NA
	<i>Wa</i>	<i>Dc</i>	<i>Ds</i>	<i>Cs</i>	<i>C</i>	
Entire data set	181	37	729	307	252	457
“Golden days”	17	3	85	37	16	34

even distribution of exchange regimes might be a reason for the bimodal concentration density distribution presented above (Fig. 5).

In the following Fig. 13, 14, 15, 16 and 17, one case will be presented for each exchange regime, covering a typical daily cycle of vertical coupling on the 29th of June, 2008, the first of the “golden days” of the measurement campaign. Cases are presented in chronological order as conditions evolve during the course of the day rather than sticking to Table 1. Subfigures (a) show the wind- and CO₂ concentration field in height versus time sections for selected 30-minute intervals, together with selected time series of local concentration perturbations, with associated CO₂ concentration perturbation time series displayed in Subfig. (c) to (e) for three sample locations: M8, corresponding to the 2 m level of the vertical profile in wind- and concentration field plots, M13, a sample location with low *PAI* and M5, a location with high *PAI*. The presentation of vertical CO₂ exchange is complemented by vertical profiles of temperature (Fig. 12a) and CO₂ concentration (Fig. 12b), with one for each selected exchange regime case.

Fig. 13a, an example of exchange regime *Cs*: “Coupled sub-canopy by sweeps”, demonstrates moderate vertical exchange even in the middle of the night (01:00–01:30 CET). The vertical temperature profile above 3 m height is near neutral (Fig. 12a, 01:00 CET), allowing for vertical mixing. There is a clearly confined cold air layer below 3 m. Examples of ejections with positive vertical wind velocities, extending from the trunk-space to the top level above the canopy at 36 m, are found starting at minutes 3 and 23, among others. Sweeps, characterized by a pronounced increase in above-canopy wind speed and correspondingly low CO₂ concentration in the trunk-space, including the 2 m level, are found starting at minutes 2, 11 and 28, among others. In between sweeps, there is accumulation of high CO₂ concentrations close to the ground, affecting the 2 m concentration measurement level, visible e.g. at minutes 7 to 9. Low concentration, associated with sweeps and high concentration in between, can be clearly seen in the corresponding CO₂ concentration perturbation time series of M8 (Fig. 13c). Comparing the concentration time series of locations M13, M5 and M8 (not shown), there is very little cross correlation, meaning each sample location has its own local condition, which is interpreted as vertical exchange dominating the concentration signal, given relatively minor horizontal coupling of sub-canopy sample points.

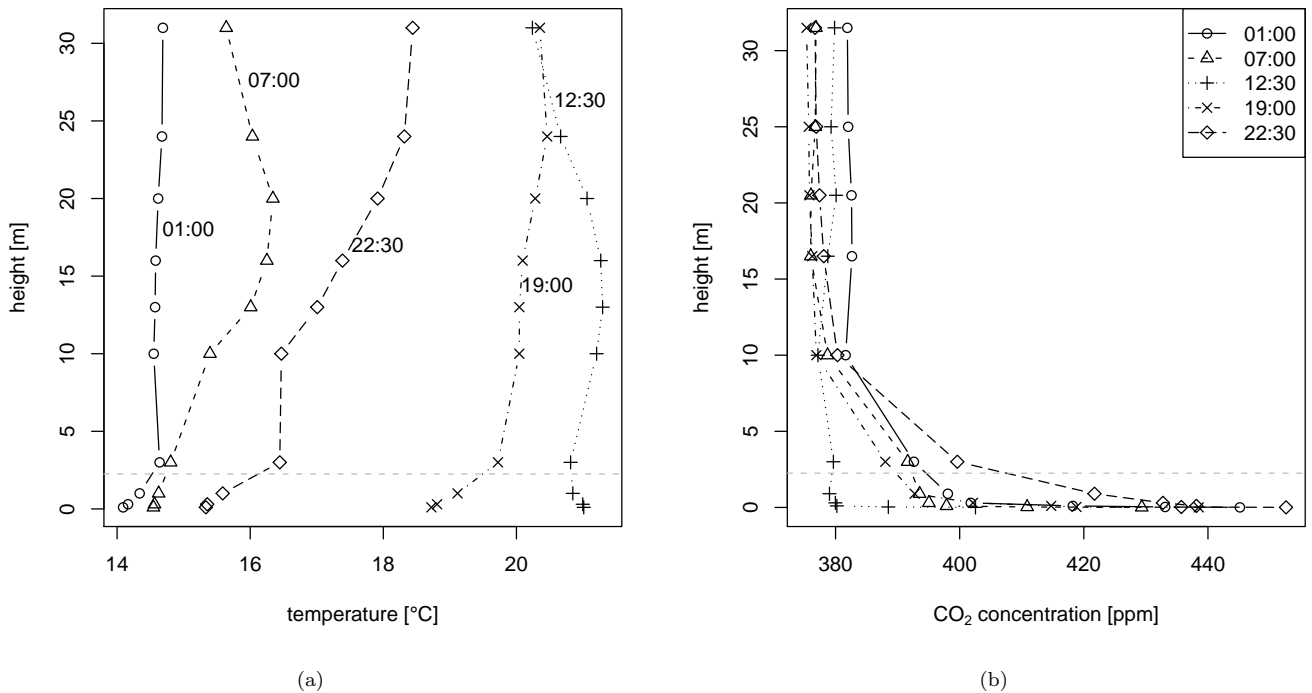


Fig. 12. Vertical profiles of temperature (a) and CO₂ concentration (b) on 29.06.2008 at the main tower for five selected 30-minute intervals, corresponding to exchange regimes *C_s* (01:00 CET), *D_s* (07:00 CET), *C* (12:30 CET), *D_c* (19:00 CET), *W_a* (22:30 CET). Times indicate beginning of 30-minute intervals. Dashed lines mark height of horizontal sub-canopy CO₂ concentration measurements.

The following case, an example of exchange regime *D_s*: “Decoupled sub-canopy”, marks the transition between night time and day time conditions with regard to trunk-space CO₂ concentration (Fig. 14). During this transition at around 06:00–07:00 CET, high trunk-space CO₂ concentrations, which have gradually accumulated over night, are released during intermittent events. Despite the exchange classification *D_s* (“decoupled sub-canopy”), indicating moderate vertical exchange only, which is controlled by a temperature inversion at the canopy level (Fig. 12a, 07:00 CET) due to increasing radiation energy input in the upper canopy, a highly dynamic wind and concentration field and distinct events of vertical exchange are observed (Fig. 14a). One major event of venting by vertical exchange starts at minute 5 with increasing wind speed above the canopy and initially negative vertical wind velocity, followed by a secondary wind maximum in the trunk-space at minutes 8 and 9 with low CO₂ concentration at the same time. Probably as a consequence of the wind maximum in the trunk-space, two consecutive plumes with high CO₂ concentration are lifted to the canopy level and subsequently vented to above-canopy layers by ejections, characterized by strong positive vertical wind velocities from minutes 11 to 13 and at minute 15. The mean trunk-space concentration from all sample locations at a 2 m height is effectively lowered by almost 20 $\mu\text{mol mol}^{-1}$ within the first 15 minutes of the 30-minute interval shown (Fig. 14b). The second 15 minutes of the interval are further dominated by interwoven sweeps (e.g. minutes 18 to 19) and ejections (minutes 20.5, 24

and 26) with even lower trunk-space CO₂ concentrations during sweeps and less dramatic ejections, due to the already diminished trunk-space CO₂ resource. Ejections and sweeps described for Fig. 14a can clearly be identified as positive and negative local perturbations at M8 in Fig. 14c. Comparing time series of local perturbations for three different locations (Fig. 14c, 14d, 14e), the relatively smooth second 15 minutes of M13’s local concentration perturbation (Fig. 14d) are interpreted as an effect of low *PAI* at the station, which is consequently one of the first locations to lose accumulated high time CO₂ and drop to a more constant background determined by above-canopy concentration. In contrast, the perturbations at sample position M5 with high *PAI* continue to show negative deviations from the mean throughout the whole 30-minute interval, which are interpreted as low concentration coherent structures, interrupting the otherwise still higher concentration level at the location, which remained due to reduced removal of accumulated night time CO₂ as a consequence of the sheltering effect of the relatively dense canopy.

The turbulent, fully coupled exchange regime *C*: “Fully coupled canopy” is presented in Fig. 15. While there is still a weak temperature inversion, which has moved to the lower canopy, the night time cold air layer below 3 m has vanished (Fig. 12a, 12:30 CET) and there is no accumulation of high CO₂ concentration in the trunk-space any more (Fig. 12b, 12:30 CET). A chain of highly fluctuating and relatively high wind velocities sweeps over the canopy top, driving major sweeps into the canopy (e.g. minutes 15 and

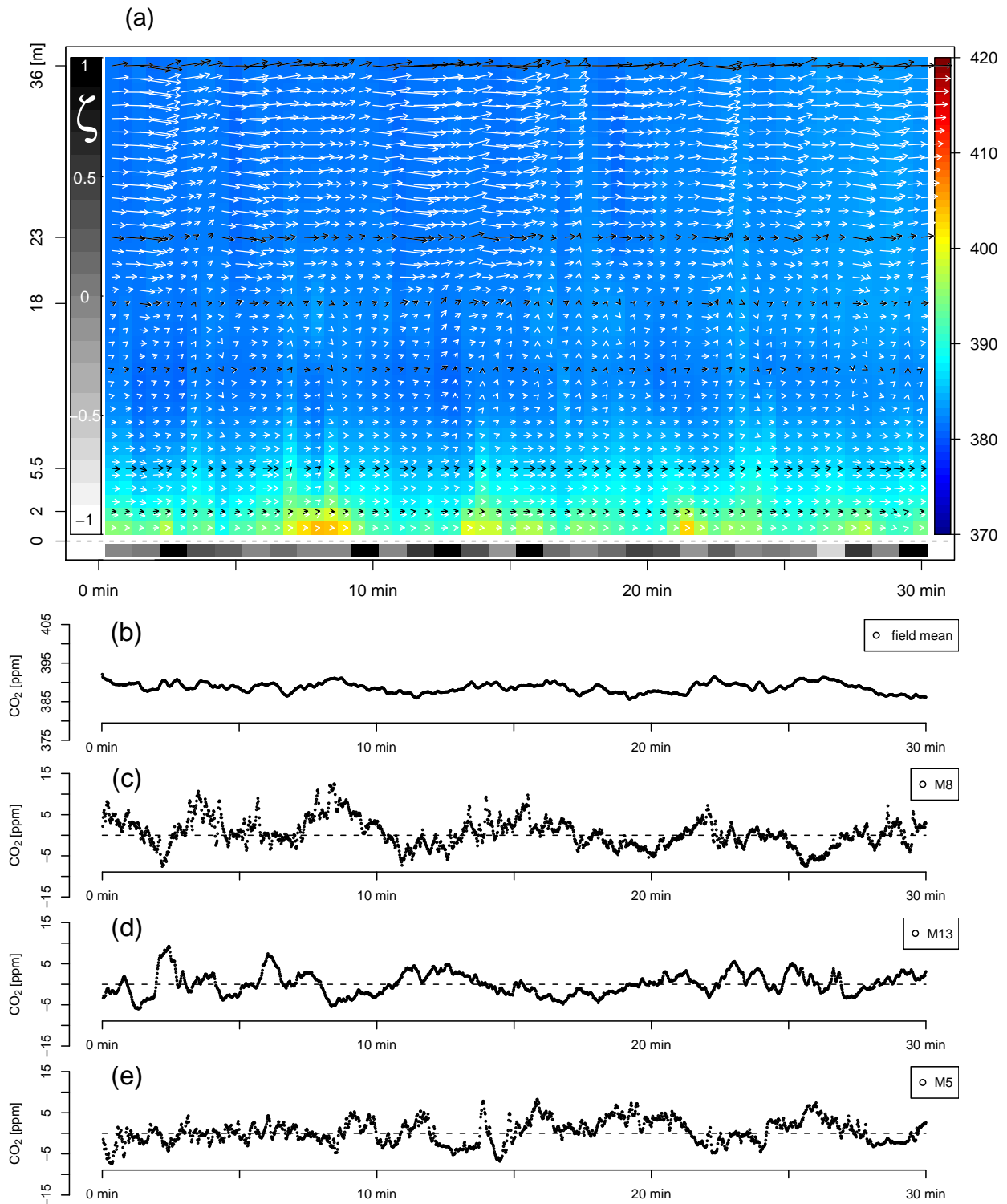


Fig. 13. Vertical profile of CO₂ concentration [$\mu\text{mol mol}^{-1}$] (colors) and wind velocity (arrows) versus time and stability parameter ζ (grayscale bar, bottom, legend: left). Y-axis: height above ground [m]. Wind vectors: resultant of absolute value of horizontal wind velocity and vertical wind velocity. Black arrows: measurements, white arrows: Akima interpolation (Akima, 1970). Measurement heights and interpolation equivalent for CO₂, (a). CO₂ concentration: field mean (b), local perturbation at M8 (c), (collocated with the measurement at the 2 m level in Subfig. a), at M13 with low *PAI* (d) and at M5 with high *PAI* (e). Exchange regime *Cs*. 29.06.2008 01:00–01:30 CET.

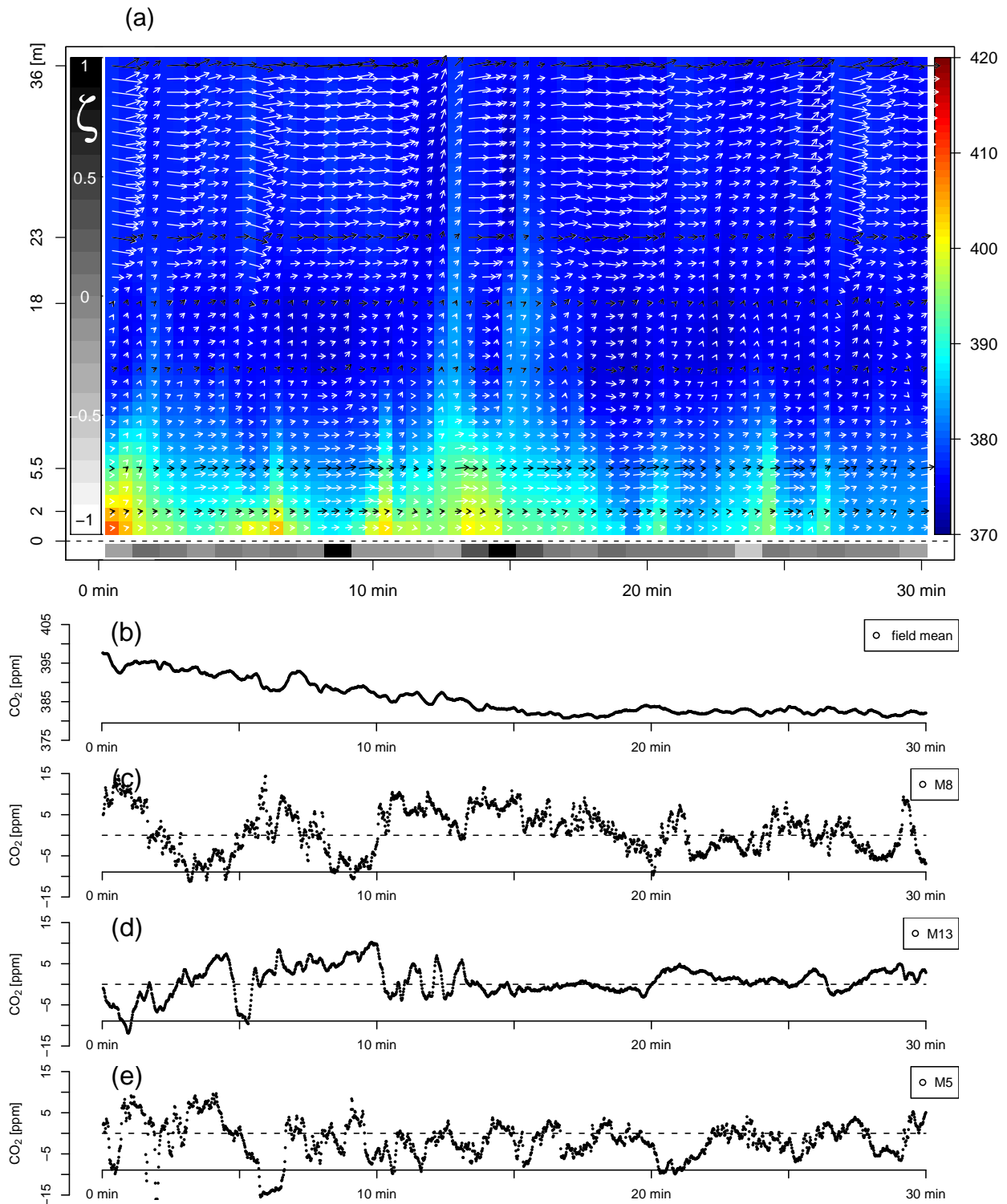


Fig. 14. Vertical profile of CO_2 concentration [$\mu\text{mol mol}^{-1}$] (colors) and wind velocity (arrows) versus time and stability parameter ζ (grayscale bar, bottom, legend: left). Y-axis: height above ground [m]. Wind vectors: resultant of absolute value of horizontal wind velocity and vertical wind velocity. Black arrows: measurements, white arrows: Akima interpolation (Akima, 1970). Measurement heights and interpolation equivalent for CO_2 , (a). CO_2 concentration: field mean (b), local perturbation at M8 (c), (collocated with the measurement at the 2m level in Subfig. a), at M13 with low PAI (d) and at M5 with high PAI (e). Exchange regime D_s . 29.06.2008 07:00–07:30 CET.

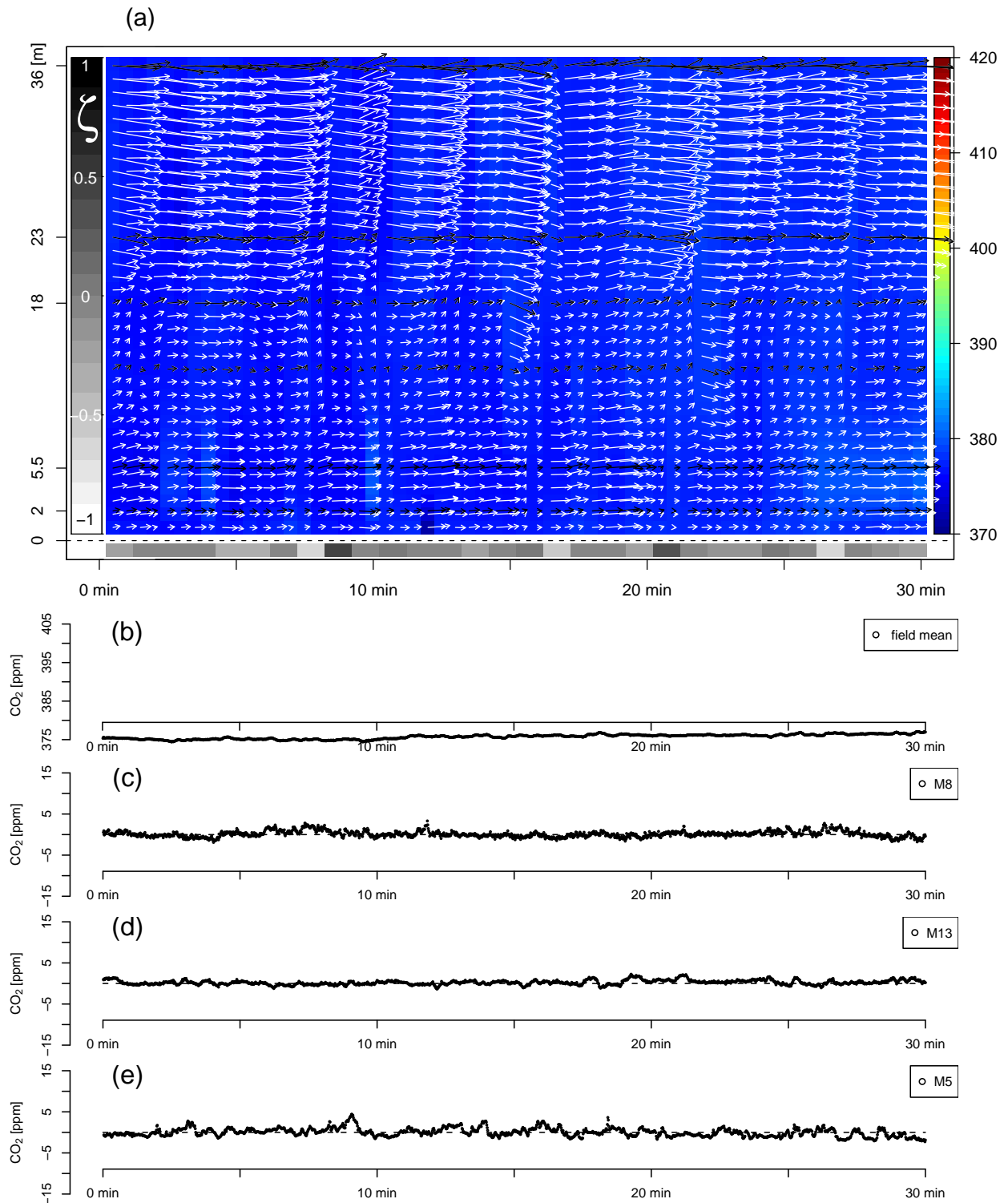


Fig. 15. Vertical profile of CO_2 concentration [$\mu\text{mol mol}^{-1}$] (colors) and wind velocity (arrows) versus time and stability parameter ζ (grayscale bar, bottom, legend: left). Y-axis: height above ground [m]. Wind vectors: resultant of absolute value of horizontal wind velocity and vertical wind velocity. Black arrows: measurements, white arrows: Akima interpolation (Akima, 1970). Measurement heights and interpolation equivalent for CO_2 , (a). CO_2 concentration: field mean (b), local perturbation at M8 (c), (collocated with the measurement at the 2 m level in Subfig. a), at M13 with low PAI (d) and at M5 with high PAI (e). Exchange regime C. 29.06.2008 12:30–13:00 CET.

22). During sweeps, divergence of vertical wind velocities is frequently observed at the 23 m and 36 m measurement levels (e.g. minutes 16 and 21). Similarly, trunk-space wind velocities are large and fluctuating, an indication of well developed turbulence. Ejections (e.g. minutes 8, 10 and 12) and sweeps do not carry major CO₂ concentration differences, given the turbulent conditions, which effectively remove any accumulation, leaving the most notable concentration perturbations in the relatively sheltered canopy. Local trunk-space CO₂ perturbations are small with little variation (Fig. 15c, 15d, 15e). However, as in the previous cases, there are differences in concentration perturbations between low and high *PAI* locations, i.e. close to zero perturbations with little variance for the low *PAI* location M13 (Fig. 15d) with some low amplitude coherent structures (e.g. minutes 18, 19 and 21), M13 being closely tied to a relatively constant above-canopy concentration due to its sparse canopy versus higher variance and single positive structures in concentration perturbation at M5. The latter is interpreted as the sheltering effect of the canopy and the chance of accumulation of higher concentrations due to soil and canopy respiration.

The following example of exchange regime *Dc*: “Decoupled canopy” at 19:00 CET (Fig. 16) marks the transition between day time and night time conditions with a cooling canopy layer due to longwave radiation losses and cold air accumulation below 3 m (Fig. 12a, 19:00 CET), as well as accumulation of CO₂ in the trunk-space (Fig. 12b, 19:00 CET). The transition period is characterized by an increase in mean trunk-space CO₂ concentration (Fig. 16b), since canopy respiration overcompensates assimilation, with turbulent CO₂ fluxes above the canopy at 36 m height being positive (not shown). Occasional sweeps still counteract trunk-space CO₂ accumulation (e.g. minutes 13 and 22), at the same time leading to negative concentration perturbations at the 2 m level (Fig. 16c). While the first 10 minutes of the interval shown mark the end of day time conditions, during the second 10 minute interval, it is shown that, in analogy to the transition from night to day described above (07:00 CET case), the open canopy sample location M13 is the first one to witness the increase in CO₂ concentration (Fig. 16d), whereas more sheltered locations such as M5 still have relatively low concentrations i.e. negative local perturbations (Fig. 16e), before all locations enter a regime typical for night time conditions in the third 10 minute interval of Fig. 16b to 16e with large amplitude fluctuations with respect to local CO₂ concentrations perturbations.

The final example describes exchange regime *Wa*: “Wave motion”, shown in Fig. 17, a classical case of a hydrodynamically driven katabatic drainage flow, which has been described before as a main driver for night time CO₂ advection in sloping terrain (Aubinet et al., 2003) and is accepted as one reason for the night flux problem of eddy covariance measurements (Aubinet, 2008). The wind field from 22:30 to 23:00 CET is characterized by relatively constant velocities both above and below the canopy (Fig. 17a). The presence of a drainage sublayer can be deduced from a strong

temperature inversion at a 3 m height (Fig. 12a, 22:30 CET), the secondary wind maximum in the trunk-space with a horizontal wind velocity of 0.6 ms⁻¹ at the 2 m level and constant wind direction of 43° oriented perfectly downslope, flowing from north-east to south-west, which is a 180° turn relative to daytime wind direction with abrupt transitions (not shown). Given stable conditions for the whole 30-minute interval shown (see grayscale bar at the bottom of Fig. 17a), there are no signs of turbulence, but quasi laminar flow conditions can be assumed, considering the following additional characteristics: friction velocity $u_* = 0.01 \text{ ms}^{-1}$ (the value corresponding to 7% of the day time value), variance of horizontal wind velocity $\text{var}(u) = 0.007 \text{ ms}^{-1}$ (1% of day time value) and variance of vertical wind velocity $\text{var}(w) = 0.001 \text{ ms}^{-1}$ (3% of day time value). Regarding the CO₂ concentration field, all heights from the 5 m measurement level and upwards show constant concentration over time (Fig. 17a). At the 2 m level, high CO₂ concentration is observed during the first 12 minutes of the 30-minute interval shown (see red colors at 2 m level in Fig. 17a) with a mean CO₂ concentration for all horizontal sub-canopy measurements above 400 μmol mol⁻¹ (Fig. 17b a). With regards to classical advection measurements based on sequential sampling of horizontal transects with a time resolution on the order of minutes, the first 10 minute interval shown might serve as a case, yielding meaningful gradients, comparing e.g. M8 (Fig. 17c) and M5 (Fig. 17e). Excluding high frequency fluctuations, M8 has a constantly negative local concentration deviation, whereas M5 is more positive, with a long wave component in the signal. In contrast, the concentration at the low *PAI* location M13 (Fig. 17e) increases over the first 10 minute interval with the increase being frequently disrupted by individual structures with low concentration. This might be an effect of low concentration air entrainment from higher levels. Around minute 10 there is a sudden change in local perturbations of all locations shown (Fig. 17c, 17d, 17e), with concentration drops as large as 25 μmol mol⁻¹ at M13 (Fig. 17d). Explanations for an abrupt concentration change are the sheet-like characteristics of the katabatic drainage flow layer, with changes in thickness, meandering flow paths or CO₂ concentration, inherited from upslope sources. Individual sample locations will be affected to varying extents by such changes. For the remaining 20 minutes of the 30-minute interval shown, the imprint of coherent structures is visible in all of the perturbation time series. Another characteristic of local perturbations shown is high frequency fluctuations with periods on the order of a few seconds and amplitudes of up to several μmol mol⁻¹. See the first 10 minute interval of M5 (Fig. 17e) for an example, but also M8 (Fig. 17c), with M13 (Fig. 17e) being different, probably due to a somewhat lower response time of the analyzer with a nominal value of 2 s as compared to 1 s for the other two. High frequency fluctuations might be a consequence of the high vertical CO₂ concentration gradient in the lower 2 m above ground (Fig. 12b, 22:30 CET), combined with laminar flow over a rough surface, generating small wave structures, which might trans-

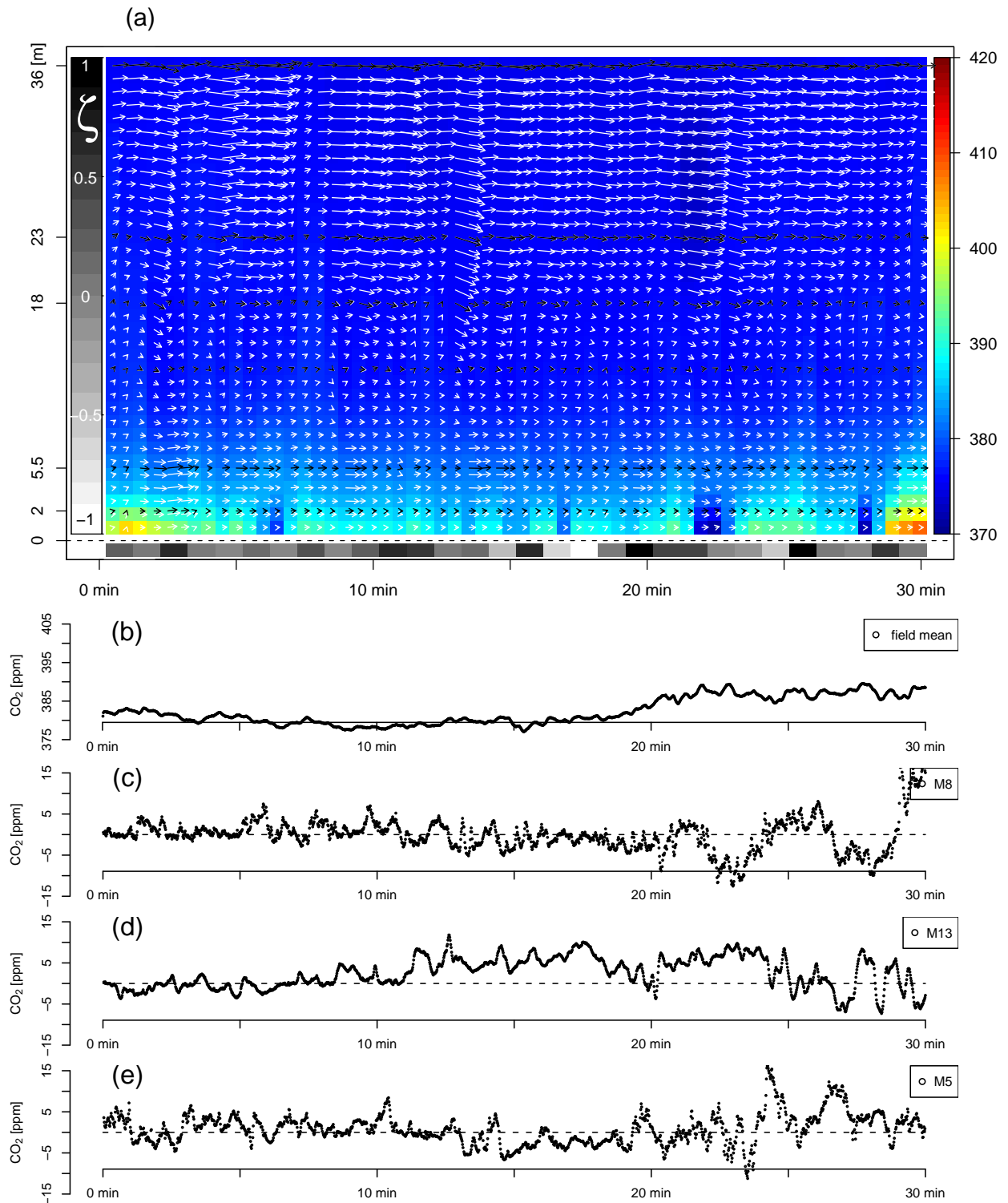


Fig. 16. Vertical profile of CO_2 concentration [$\mu\text{mol mol}^{-1}$] (colors) and wind velocity (arrows) versus time and stability parameter ζ (grayscale bar, bottom, legend: left). Y-axis: height above ground [m]. Wind vectors: resultant of absolute value of horizontal wind velocity and vertical wind velocity. Black arrows: measurements, white arrows: Akima interpolation (Akima, 1970). Measurement heights and interpolation equivalent for CO_2 , (a). CO_2 concentration: field mean (b), local perturbation at M8 (c), (collocated with the measurement at the 2 m level in Subfig. a), at M13 with low PAI (d) and at M5 with high PAI (e). Exchange regime D_c . 29.06.2008 19:00–19:30 CET.

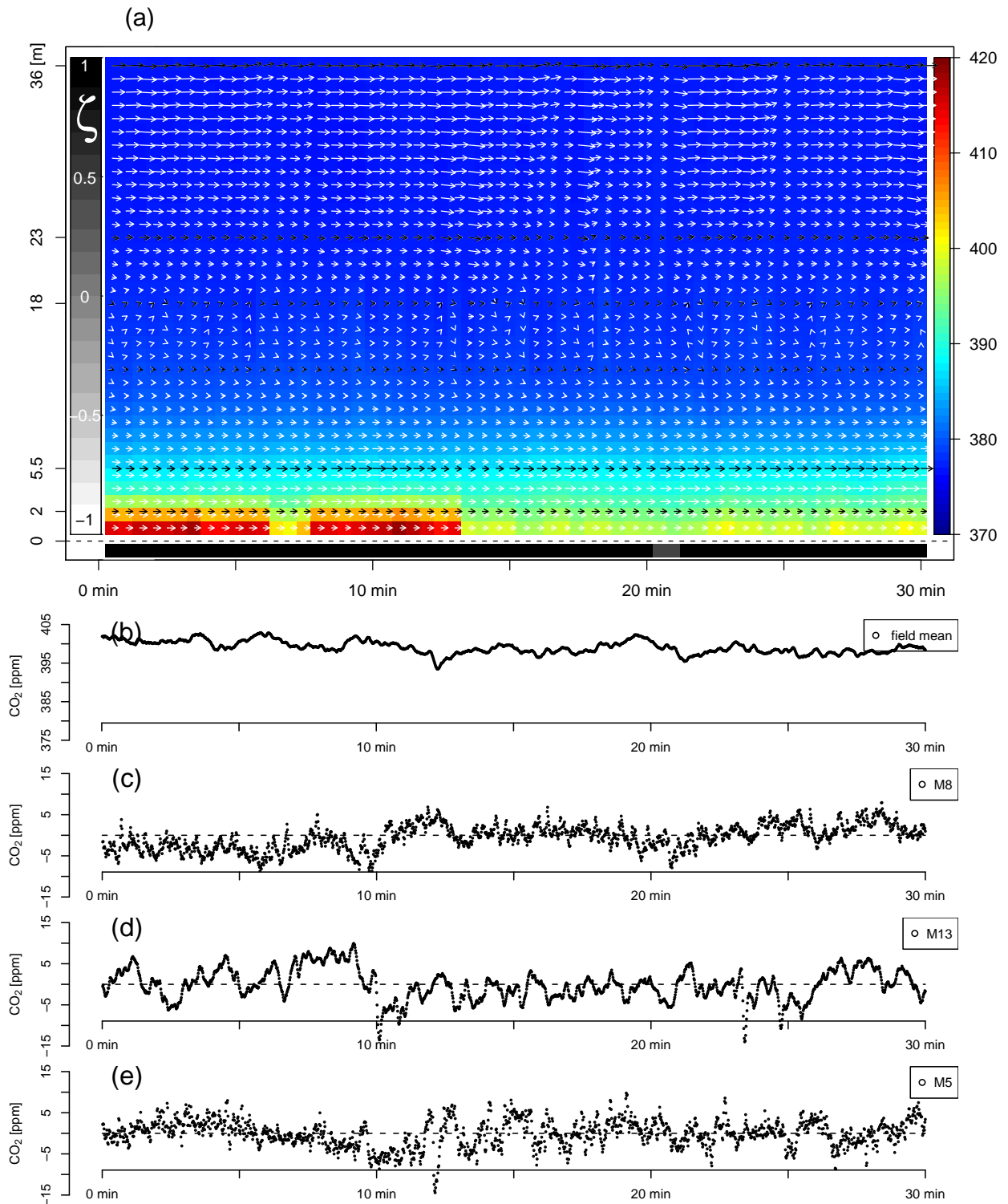


Fig. 17. Vertical profile of CO_2 concentration [$\mu\text{mol mol}^{-1}$] (colors) and wind velocity (arrows) versus time and stability parameter ζ (grayscale bar, bottom, legend: left). Y-axis: height above ground [m]. Wind vectors: resultant of absolute value of horizontal wind velocity and vertical wind velocity. Black arrows: measurements, white arrows: Akima interpolation (Akima, 1970). Measurement heights and interpolation equivalent for CO_2 , (a). CO_2 concentration: field mean (b), local perturbation at M8 (c), (collocated with the measurement at the 2 m level in Subfig. a), at M13 with low PAI (d) and at M5 with high PAI (e). Exchange regime Wa . 29.06.2008 22:30–23:00 CET.

late to an oscillation of the concentration signal at a 2 m fixed height. Instrument noise can be ruled out as the cause of this phenomenon, since those fluctuations are characteristic of night time measurements only when there is CO₂ accumulation at a 2 m height and not observed during the day (compare Fig. 15e), when trunk-space CO₂ concentration is well mixed with layers above (Fig. 12b, 12:30 CET).

4. Conclusions

Despite the fact that the motivation for a major part of CO₂ advection research is the attempt to accompany single point above-canopy eddy covariance flux measurements with in-canopy advection measurements to improve estimates of *NEE*, the current study does not compare eddy covariance fluxes with advection measurements, but rather concentrates on the mechanisms generating horizontal sub-canopy CO₂ concentration gradients. An attempt was made to evaluate the spatial consistency and representativeness of horizontal gradients under various conditions of atmospheric stratification and vertical exchange. Conclusions are, firstly, that vegetation structure influences the sub-canopy CO₂ concentration field locally, and secondly, that gradients are spatially inconsistent. It was shown that part of the variance in gradients can be explained by the effect of vegetation structure. It was further demonstrated that coherent structures can act as a mechanism relating vegetation structure and local CO₂ concentration characteristics with varying effect under different conditions of atmospheric stratification and associated vertical exchange regimes. In that sense, vegetation structure can be seen as a time-variant distribution of sources and sinks of transported CO₂. The classical advection situation was observed at the site, driven by katabatic drainage flows in the sub-canopy, which has previously been described by Aubinet et al. (2003) and others for other locations. However, the distribution of exchange regimes indicates, that the frequency of occurrence of the associated regime is minor compared to regimes, which allow for enhanced vertical exchange. The latter are not limited to daytime conditions, when they are most common, but there can be significant vertical exchange even during the night. Therefore, conclusions drawn with regards to the effect of canopy structure on gradients, i.e. the very local origin of concentration perturbations and the limited representativity of gradients, are not limited to daytime conditions. Given the limited spatial representativity of horizontal CO₂ concentration gradients, which depend on stratification and conditions of vertical exchange, with the latter varying over time, current measurement designs – featuring a time invariant setup with a spatially and temporally limited number of sampling points – tend to fail to produce reliable gradients for a given control volume. This is a main reason for the limited success of attempts to use advection measurements for the correction of eddy covariance flux measurements and is the cause of additional scatter being in-

troduced. The results obtained regarding the spatial representativity of horizontal CO₂ concentration gradients and the mechanisms controlling them, particularly through the use of high frequency gradient measurements, aid to design future measurement setup, which are better suited to the measurement of advective fluxes and more representative for the control volume for which the budget is intended to be closed.

5. Acknowledgments

The authors wish to acknowledge the help and technical support performed by the staff of the Bayreuth Center for Ecology and Environmental Research (BayCEER) of the University of Bayreuth. The 2008 experiment was funded by the German Science Foundation (FO 226/16-1, ME2100/4-1, ZE 792/4-1). We would like to thank E. Falge, who provided the raw data of *PAI* and carried out the measurements in the frame of the EGER project with the help of the EGER team. We would also like to thank T. Behrendt for providing the map of understorey vegetation (Fig. 1); we appreciate the effort of the extensive small scale sampling work. We further acknowledge the team from the Max Plank Institute, Mainz, for providing the data of vertical profiles of wind, temperature and CO₂ at the main tower.

References

- Akima, H., 1970. A new method of interpolation and smooth curve fitting based on local procedures. *J. Assc. Comp. Mach.* 17, 589–602.
- Antonia, R. A., 1981. Conditional sampling in turbulence measurements. *Ann. Rev. Fluid Mech.* 13, 131–156.
- Aubinet, M., 2008. Eddy covariance CO₂ flux measurements in nocturnal conditions: an analysis of the problem. *Ecological Applications* 18, 1368–1378.
- Aubinet, M., Berbigier, P., Bernhofer, C., Cescatti, A., Feigenwinter, C., Graniers, A., Grunwald, T., Havrankova, K., Heinesch, B., Longdoz, B., Marcolla, B., Montagnani, L., Sedlak, P., 2005. Comparing CO₂ storage and advection conditions at night at different CARBOEUROFLUX sites. *Boundary-Layer Meteorol.* 116, 63–94.
- Aubinet, M., Feigenwinter, C., Heinesch, B., Bernhofer, C., Canepa, E., Lindroth, A., Montagnani, L., Rebmann, C., Sedlak, P., Gorsel, E. V., 2010. Direct advection measurements do not help to solve the night-time CO₂ closure problem: Evidence from three different forests. *Agric. For. Meteorol.* 150, 655–664.
- Aubinet, M., Heinesch, B., Yernaux, M., 2003. Horizontal and vertical CO₂ advection in a sloping forest. *Boundary-Layer Meteorol.* 108, 397–417.
- Behrendt, T., 2010. A small-scale geostatistical analysis of the variability of soil properties. An example from the Weidenbrunnen (Fichtelgebirge) research area. Master's thesis, University of Mainz.
- Bergström, H., Högström, U., 1989. Turbulent exchange above a pine forest. II. organized structures. *Boundary-Layer Meteorol.* 49, 231–263.
- Brunet, Y., Irvine, M. R., 2000. The control of coherent eddies in vegetation canopies: streamwise structure spacing, canopy shear scale and atmospheric stability. *Boundary-Layer Meteorol.* 94, 139–163.
- Burns, S. P., Delany, A. C., Sun, J., Stephens, B. B., Oncley, S. P., Maclean, G. D., Semmer, S. R., Schröter, J., Ruppert, J., 2009. A programmable portable trace-gas measuring system and an evaluation of calibration techniques for in-situ carbon dioxide measurements. *Journal of Atmospheric and Oceanic Technology* 26, 291–316.
- Collineau, S., Brunet, Y., 1993. Detection of turbulent coherent motions in a forest canopy. Part I: Wavelet analysis. *Boundary-Layer Meteorol.* 65, 357–379.
- de Araujo, A. C., Kruijt, B., Nobre, A. D., Dolman, A. J., Waterloo, M. J., Moors, E. J., de Souza, J. S., 2008. Nocturnal accumulation of CO₂ underneath a tropical forest canopy along a topographical gradient. *Ecological Applications* 18, 1406–1419.
- Etzold, S., Buchmann, N., Eugster, W., 2010. Contribution of advection to the carbon budget measured by eddy covariance at a steep mountain slope forest in Switzerland. *Biogeosciences* 7, 2461–2475.
- Feigenwinter, C., Bernhofer, C., Eichelmann, U., Heinesch, B., Hertel, M., Janous, D., Kolle, O., Lagergren, F., Lindroth, A., Minerbi, S., Moderow, U., Molder, M., Montagnani, L., Queck, R., Rebmann, C., Vestin, P., Yernaux, M., Zeri, M., Ziegler, W., Aubinet, M., 2008. Comparison of horizontal and vertical advective CO₂ fluxes at three forest sites. *Agric. For. Meteorol.* 148, 12–24.
- Finnigan, J., 2000. Turbulence in plant canopies. *Ann. Rev. Fluid Mech.* 32, 519–571.
- Finnigan, J., 2008. An introduction to flux measurements in difficult conditions. *Ecological Applications* 18, 1340–1350.
- Finnigan, J. J., 1979a. Turbulence in waving wheat. I. Mean statistics and Honami. *Boundary-Layer Meteorol.* 16, 181–211.
- Finnigan, J. J., 1979b. Turbulence in waving wheat. II. Structure of momentum transfer. *Boundary-Layer Meteorol.* 16, 213–236.
- Foken, T., Meixner, F. X., Falge, E., Zetzsch, C., Serafimovich, A., Bargsten, A., Behrendt, T., Biermann, T., Breuninger, C., Gerken, T., Hunner, M., Lehmann-Pape, L., Hens, K., Jocher, G., Kesselmeier, J., Lüers, J., Mayer, J.-C., Moravek, A., Plake, D., Riederer, M., Rütz, F., Schier, S., Siebicke, L., Sörgel, M., Staudt, K., Trebs, I., Tsokankunku, A., Wolff, V., Zhu, Z., 2011. Atmospheric transport and chemistry in forest ecosystems – overview of the EGER-project. *Agric. For. Meteorol.* (to be submitted).
- Foken, T., Skeib, G., Richter, S. H., 1991. Dependence of the integral turbulence characteristics on the stability of stratification and their use for doppler-sodar measurements. *Z. Meteorol.* 41, 311–315.
- Furrer, R., Nychka, D., Sain, S., 2008. fields: Tools for spatial data. R package version 4.3.
URL <http://www.image.ucar.edu/Software/fields>
- Gao, W., Shaw, R. H., PawU, K. T., 1989. Observation of organized structure in turbulent flow within and above a forest canopy. *Boundary-Layer Meteorol.* 47, 349–377.
- Garratt, J., 1978. Flux profile relations above tall vegetation. *Q. J. R. Meteorol. Soc.* 104, 199–211.
- Gerstberger, P., Foken, T., Kalbitz, K., 2004. The Lehstenbach and Steinkreuz Catchments in NE Bavaria, Germany. In: Matzner, E. (Ed.), *Biogeochemistry of Forested Catchments in a Changing Environment: A German Case Study*. Vol. 172. Springer, Heidelberg, pp. 15–41.
- Göckede, M., Markkanen, T., Hasager, C. B., Foken, T., 2006. Update of a footprint-based approach for the characterisation of complex measurement sites. *Boundary-Layer Meteorol.* 118, 635–655.
- Heinesch, B., Yernaux, M., Aubinet, M., 2007. Some methodological questions concerning advection measurements: a case study. *Boundary-Layer Meteorol.* 122, 457–478.
- Holmes, P., Lumley, J. L., Berkooz, G., 1996. *Turbulence, coherent structures, dynamical systems and symmetry*. Cambridge University Press, Cambridge, 420 pp.
- Katul, G., Kuhn, G., Schieldge, J., Hsieh, C.-I., 1997. The ejection-sweep character of scalar fluxes in the unstable

- surface layer. *Boundary-Layer Meteorol.* 83, 1–26.
- Kutsch, W. L., Kolle, O., Rebmann, C., Knohl, A., Ziegler, W., Schulze, E.-D., 2008. Advection and resulting CO₂ exchange uncertainty in a tall forest in central Germany. *Ecological Applications* 18, 1391–1405.
- Leuning, R., Zegelin, S. J., Jones, K., Keith, H., Hughes, D., 2008. Measurement of horizontal and vertical advection of CO₂ within a forest canopy. *Agric. For. Meteorol.* 148, 1777–1797.
- Paw U, K. T., Brunet, Y., Collineau, S., Shaw, R. H., Maitani, T., Qiu, J., Hipps, L., 1992. Evidence of turbulent coherent structures in and above agricultural plant canopies. *Agric. For. Meteorol.* 61, 55–68.
- Plake, D., 2009. Vertikale Konzentrationsprofile und Flüsse von reaktiven und nicht reaktiven Spurengasen im Fichtelgebirge. Master's thesis, Max-Planck-Institut für Chemie, Mainz, Germany, 144 p.
- R Development Core Team, 2009. R: A Language and Environment for Statistical Computing. R Foundation for Statistical Computing, Vienna, Austria, ISBN 3-900051-07-0.
URL <http://www.R-project.org>
- Rannik, Ü., Markkanen, T., Raittila, J., Hari, P., Vesala, T., 2003. Turbulence statistics inside and over forest: Influence on footprint prediction. *Boundary-Layer Meteorol.* 109, 163–189.
- Raupach, M. R., 1979. Anomalies in flux-gradient relationships over a forest. *Boundary-Layer Meteorol.* 16, 467–486.
- Raupach, M. R., Finnigan, J. J., Brunet, Y., 1989. Coherent eddies in vegetation canopies. In: 4th Australasian Conference on Heat and Mass Transfer. Christchurch, NZ, pp. 75–90.
- Raupach, M. R., Finnigan, J. J., Brunet, Y., 1996. Coherent eddies and turbulence in vegetation canopies: the mixing-layer analogy. *Boundary-Layer Meteorol.* 78, 351–382.
- Raupach, M. R., Thom, A. S., 1981. Turbulence in and above plant canopies. *Ann. Rev. Fluid Mech.* 13, 97–129.
- Schmid, H. P., 2002. Footprint modeling for vegetation atmosphere exchange studies: a review and perspective. *Agric. For. Meteorol.* 113, 159–183.
- Serafimovich, A., Siebicke, L., Staudt, K., Lüers, J., Hunner, M., Gerken, T., Schier, S., Biermann, T., Rütz, F., von Buttler, J., Riederer, M., Falge, E., Mayer, J.-C., Foken, T., 2008. Exchange processes in mountainous regions (EGER) - documentation of the intensive observation period (IOP2) June, 1st to July, 15th 2008. *Arbeitsergebnisse*, 37, University of Bayreuth, Department of Micrometeorology, ISSN 1614-8916, 180 pp.
- Serafimovich, A., Thomas, C., Foken, T., 2010. Vertical and horizontal transport of energy and matter by coherent motions in a tall spruce canopy. *Boundary-Layer Meteorol.* (submitted).
- Shaw, R. H., Paw U, K. T., Gao, W., 1989. Detection of temperature ramps and flow structures at a deciduous forest site. *Agric. For. Meteorol.* 47, 123–138.
- Shaw, R. H., Tavangar, J., Ward, D. P., 1983. Structure of the Reynolds stress in a canopy layer. *J. Clim. Appl. Meteorol.* 22, 1922–1931.
- Siebicke, L., Steinfeld, G., Foken, T., 2010. CO₂-gradient measurements using a parallel multi-analyzer setup. *Atmospheric Measurement Techniques Discussions* 3, 4383–4421.
- Staebler, R., Fitzjarrald, D., 2004. Observing subcanopy CO₂ advection. *Agric. For. Meteorol.* 122, 139–156.
- Staudt, K., Foken, T., 2007. Documentation of reference data for the experimental areas of the Bayreuth Centre for Ecology and Environmental Research (BayCEER) at the Waldstein site. *Arbeitsergebnisse* 35, University of Bayreuth, Department of Micrometeorology, ISSN 1614-8916, 37 pp.
- Thomas, C., Foken, T., 2005. Detection of long-term coherent exchange over spruce forest using wavelet analysis. *Theor. Appl. Climatol.* 80, 91–104.
- Thomas, C., Foken, T., 2007a. Flux contribution of coherent structures and its implications for the exchange of energy and matter in a tall spruce canopy. *Boundary-Layer Meteorol.* 123, 317–337.
- Thomas, C., Foken, T., 2007b. Organised motion in a tall spruce canopy: temporal scales, structure spacing and terrain effects. *Boundary-Layer Meteorol.* 122, 123–147.
- Thomson, D. J., 1987. Criteria for the selection of stochastic models of particle trajectories in turbulent flows. *Journal of Fluid Mechanics* 189, 529–552.
- Tóta, J., Fitzjarrald, D. R., Staebler, R. M., Sakai, R. K., Moraes, O. M. M., Acevedo, O. C., Wofsy, S. C., Manzi, A. O., 2008. Amazon rain forest subcanopy flow and the carbon budget: Santarém LBA-ECO site. *J. Geophys. Res.* 113.
- Vickers, D., Mahrt, L., 1997. Quality control and flux sampling problems for tower and aircraft data. *Journal of Atmospheric and Oceanic Technology* 14 (3), 512–526.
- Wilczak, J. M., Oncley, S., Stage, S. A., 2001. Sonic anemometer tilt correction algorithms. *Boundary-Layer Meteorol.* 99, 127–150.
- Wilson, J. D., Sawford, B. L., 1996. Review of Lagrangian stochastic models for trajectories in the turbulent atmosphere. *Boundary-Layer Meteorol.* 78, 191–210.
- Yi, C., Anderson, D. E., Turnipseed, A. A., Burns, S. P., Sparks, J. P., Stannard, D. I., Monson, R. K., 2008. The contribution of advective fluxes to net ecosystem exchange in a high-elevation, subalpine forest. *Ecological Applications* 18, 1379–1390.

D Siebicke et al. (2010a)

Siebicke, L., Hunner, M., Foken, T., 2010. Some aspects of CO₂-advection measurements in discussion. Theoretical and Applied Climatology (submitted).

Theoretical and Applied Climatology manuscript No.
(will be inserted by the editor)

Some aspects of CO₂-advection measurements in discussion

Lukas Siebicke¹ · Martina Hunner^{1,2} · Thomas Foken¹

Received: date / Accepted: date

Abstract Vegetation-atmosphere exchange of carbon dioxide (CO₂) has previously been intensively studied to address climate change related issues and quantify carbon sources and sinks. The widely used eddy-covariance (EC) technique has its limitations under difficult conditions such as nighttime measurements and heterogeneous terrain. Therefore, research is being performed to include measurements of advective flux components into the Net Ecosystem Exchange (*NEE*) budget. However, advection measurements are experimentally challenging and do not always help to solve the night flux problem of the EC technique.

This study investigates alternative methods for the observation of horizontal advection, in particular horizontal concentration gradients, as well as different approaches to coordinate rotation and vertical advection. Continuous high frequency measurements of the horizontal CO₂ concentration field are employed and compared to the often used discontinuous sequential sampling. Significant differences were found in the case of 30-minute mean concentration values between the conventional discontinuous sampling approach and the complete observation of the time series by continuous sampling.

Estimates of vertical advection rely on accurate estimates of vertical wind velocity (w). Therefore, different approaches to the planar fit coordinate rotation have been investigated. Sector-wise rotation was able to eliminate directional dependencies of mean w . Furthermore, the effect of the data set

length used for rotation (window length) was investigated and was found to have significant impact on estimates of vertical advection, with larger window lengths yielding about 50% larger vertical advection. A sequential planar fit with controlled window length is proposed to give reproducible results.

The different approaches to the measurement and calculation of horizontal and vertical advection presented are applied to data obtained during the EGER experiment at the FLUXNET site Waldstein-Weidenbrunnen (DE-Bay). Estimates of *NEE* including advection are compared to *NEE* from turbulent and storage flux alone without advection. *NEE* including vertical advection with sector-wise planar fit rotation and controlled window length and including horizontal advection from continuous gradient measurements, which were comprehensively bias corrected by a new approach, did compare well with the expected night flux error, with meteorological drivers of the fluxes and with soil chamber measurements. Unrealistically large and noisy values of horizontal advection from the conventional discontinuous sampling approach, which lead to unrealistic values of *NEE*, could be eliminated by the alternative approaches presented. We therefore suggest the further testing of those approaches at other sites in order to improve the accuracy of advection measurements and, subsequently, estimates of *NEE*.

Keywords Advection · CO₂-flux · carbon budget · coordinate rotation

L. Siebicke

(1) Dep. of Micrometeorology, University of Bayreuth, Universitätsstr. 30, 95440 Bayreuth, Germany

E-mail: lukas.siebicke@uni-bayreuth.de

Present address: INRA, BP 709, 97387 Cedex Kourou, France

E-mail: lukas.siebicke@ecofog.gf

M. Hunner

(2) now: Wind Cert Services, TÜV SÜD Industrie Service GmbH, Ludwig-Eckert-Str. 10, 93049 Regensburg, Germany

1 Introduction

Increasing awareness of climate change has stimulated the study of ecosystem processes. In particular, vegetation-atmosphere exchange of carbon dioxide (CO₂), which is one of the major greenhouse gases, has been intensively studied to

determine the source and sink potential of different ecosystems. Measurements of the turbulent flux of CO_2 are commonly obtained by the eddy-covariance (EC) technique (Moncrieff et al, 1997; Aubinet et al, 2000; Baldocchi et al, 2001; Baldocchi, 2003) and are applied in a worldwide system of flux measurement stations, the FLUXNET (Baldocchi et al, 2001). Despite its widespread application there are conditions where the EC technique fails to give reliable results. These are night-time conditions when turbulence intensity is low, which typically leads to an underestimation of the flux measured by the EC technique (Goulden et al, 1996; Lee, 1998; Acevedo et al, 2007; Gorsel, van et al, 2007; Aubinet, 2008; Finnigan, 2008). Furthermore, the application of the EC technique in heterogeneous terrain, which has become common, is challenging because prerequisites of the EC technique are not necessarily fulfilled (Foken and Wichura, 1996; Massman and Lee, 2002; Finnigan, 2004; Katul et al, 2006; Beyrich et al, 2006; Oncley et al, 2007; Sun et al, 2007; Belcher et al, 2008; Aubinet, 2008; Rebmann et al, 2010, and many others). Therefore, measurements of Net Ecosystem Exchange (NEE) of CO_2 during conditions of low turbulence are often replaced by modelled values using the u_* -filter approach (Goulden et al, 1996; Falge et al, 2001).

It has been common practice, and still is at the majority of FLUXNET sites, to describe NEE as the sum of turbulent flux and storage flux. In order to address the night flux problem of the EC technique, attempts were made to include advective flux terms in the NEE budget equation. Lee (1998); Finnigan (1999); Lee (1999) and later Baldocchi et al (2000); Paw U et al (2000); Lee and Hu (2002) suggested the inclusion of a vertical advection term in the NEE equation. See Paw U et al (2000) for a comparison of the two approaches to the mean vertical flux by Lee (1998), addressing term IIIa of Eq. 2, and by Webb et al (1980), addressing term IIIb of Eq. 2. The approach by Lee (1998), which assumed incompressible flow and included only a vertical component of advection was criticized by Finnigan (1999) and Paw U et al (2000) as neglecting the horizontal component of advection as well as horizontal derivatives of turbulent fluxes, thus oversimplifying the budget calculation to one dimension. Based on a simple model study which showed that horizontal and vertical advection could be of similar magnitude but with opposing sign, Finnigan (1999) also pointed to the risk of degrading the quality of the budget by including vertical advection alone. To address the 3-dimensional nature of the flux, it was proposed that not only vertical advection but also horizontal advection be included in the NEE equation (Finnigan, 1999; Paw U et al, 2000; Baldocchi et al, 2000; Aubinet et al, 2003; Staebler and Fitzjarrald, 2004). Many studies have attempted to measure the full NEE budget including advection (Baldocchi et al, 2000; Aubinet et al, 2003; Staebler and Fitzjarrald,

2004; Feigenwinter et al, 2004; Paw U et al, 2004; Aubinet et al, 2005; Wang et al, 2005; Marcolla et al, 2005; Sun et al, 2007; Zeri, 2007; Heinesch et al, 2007, 2008; Mammarella et al, 2007; Leuning et al, 2008; Kutsch et al, 2008; Yi et al, 2008; de Araujo et al, 2008; Oncley et al, 2008; Tóta et al, 2008; Feigenwinter et al, 2010a,b; Zeri et al, 2010; Etzold et al, 2010) including the ADVEX campaign (Feigenwinter et al, 2008; Montagnani et al, 2010), which intended to apply a uniform methodology at sites in Italy (Renon), Germany (Wetzstein) and Sweden (Norunda).

While observed advection did account for the missing flux at night at some sites and could be related to meaningful physical drivers such as katabatic drainage, the advective contribution to NEE is site dependent and often affected by large scatter and uncertainty. Aubinet et al (2003); Sun et al (2007); Yi et al (2008) and others found that advective flux terms can be of considerable magnitude at night, although vertical and horizontal advection partly cancelled each other. Sun et al (2007); Rebmann et al (2010) and others reported large uncertainty which they related to the above mentioned partial cancellation of vertical and horizontal advection. Aubinet et al (2010) concluded from the ADVEX campaign that direct advection measurements do not help to solve the night-time CO_2 closure problem. One reason for the inability of advection measurements to close the NEE balance is the mismatch of the spatial representativeness of different terms of the NEE equation. The footprint (Schmid, 2002; Vesala et al, 2008) of the turbulent flux measurements above the canopy, particularly in heterogeneous terrain (Leclerc et al, 2003; Göckede et al, 2004; Foken and Leclerc, 2004; Sogachev et al, 2005; Klaassen and Sogachev, 2006), need not match the footprint of advective flux measurements inside the canopy, the latter often being influenced by sub-canopy drainage flows (Mahrt et al, 2001; Soler et al, 2002; Komatsu et al, 2003; Yi et al, 2005; Froelich and Schmid, 2006; Goulden et al, 2006; Pypker et al, 2007) which are observed even for small slope angles. Another reason for the inability of advection measurements to close the NEE balance is the uncertainty of advection estimates. The biggest challenges for accurate advection measurements are the measurement of horizontal concentration gradients which are often small relative to the instrument accuracy and the measurement of vertical wind velocity w (Heinesch et al, 2007). Due to the commonly applied sequential sampling of several measurement points, the synchronous observation of horizontal gradients is not possible. Therefore averaging is needed which results in a low temporal resolution of horizontal gradient measurements. Furthermore, owing to the limited spatial resolution of observations, the 3-dimensional wind and concentration field is generally undersampled (Aubinet et al, 2010). Heinesch et al (2007) investigated the influence of the sampling resolution on a CO_2 concentration time series recorded at a single point and estimated

related uncertainties concerning the calculation of storage change and advection. Their results confirm that increasing the temporal resolution of concentration sampling reduces the uncertainty. However, the ability to increase the number of samples per half hour is limited in a sequential system by the tradeoff between temporal resolution and spatial resolution (number of sample locations). Leuning et al (2008) addressed the issue of spatial resolution by line integrated concentration measurements using perforated tubing at several levels as opposed to the more common point measurement setup. Spatially representative measurements of horizontal wind velocity as well as accurate vertical velocity measurements remained challenging.

Accurate measurements of vertical wind velocity are not only limited by the instruments' specifications but also by the ability to define a suitable coordinate reference. It is common practice to perform a coordinate rotation to minimize flow distortion effects and to align the sonic coordinate system with the mean stream lines (McMillen, 1988; Wilczak et al, 2001; Paw U et al, 2000; Geissbühler et al, 2000; Finnigan et al, 2003; Finnigan, 2004; Froelich et al, 2005; Vickers and Mahrt, 2006; Sun, 2007; Dellwik et al, 2010). The rotation is performed in order to obtain a zero mean vertical wind velocity $\bar{w} = 0$ either on a short term basis (McMillen, 1988), for the averaging interval of the flux, e.g. 30-min interval (e.g. Lee et al, 2004, and others) or for a longer period which is the case for the planar fit technique (Wilczak et al, 2001). Whereas the choice of coordinate rotation procedure or sonic orientation (see e.g. Geissbühler et al (2000) for surface normal versus vertical orientation) is comparatively less critical for turbulent flux measurements, they can have a large impact on the estimate of vertical advection at night when vertical concentration gradients are large. For a given tilt correction approach the choice of time scale for averaging the wind components is critical (Finnigan et al, 2003; Vickers and Mahrt, 2006). Furthermore, regardless of the coordinate rotation chosen, a single above-canopy point measurement can only determine the local vector basis at that point but not the streamlines for the complete surface of the volume under consideration (Lee et al, 2004; Sun, 2007; Mahrt, 2010). However, by choosing a suitable coordinate rotation the information from a point measurement can be optimized in terms of its representativity for the surface of the control volume (Finnigan, 2004).

As most sites and long-term measurements rely on incomplete observations of the 3-dimensional flow field, the current study aims at optimizing information about w obtained from single tower measurements. Both spatial and temporal effects of coordinate rotation will be addressed. Furthermore, this study presents improvements in the temporal resolution of horizontal concentration gradients. Thus, two of the main issues concerning the accuracy of advection estimates which have evolved during previous studies are

considered in the current paper with the aim of improving estimates of NEE .

The main objectives of the present study are:

- to investigate the differences between continuous high frequency measurements of horizontal concentration gradients designed for improved horizontal advection estimates and the common discontinuous sampling approach,
- to investigate different approaches to how to apply the planar fit coordinate rotation aiming at an optimized representativity of vertical wind velocity at the control volume scale in order to improve vertical advection estimates (and turbulent flux estimates) given one above-canopy point measurement of 3D wind velocity and quantify the impact on vertical advection,
- to present the regime of CO_2 advection and NEE at the FLUXNET site Waldstein-Weidenbrunnen (DE-Bay),
- to evaluate the effect of the above mentioned alternative approaches to advection observation on the Net Ecosystem Exchange budget.

2 Material and Methods

Having introduced the scientific background of this work and related it to previously published studies, this section will focus purely on those details of the introduced topic which are specific to the current study.

2.1 Site

Measurements were carried out at the FLUXNET site Waldstein-Weidenbrunnen (DE-Bay), $50^\circ 08' 31''$ N, $11^\circ 52' 01''$ E, a hill site in the Fichtelgebirge Mountains in Southern Germany. The forest site is on the upper section of a hill, 775 m ASL, with a 3° slope facing south-west (Fig. 1). The 25 m high Norway spruce (*Picea abies*) stand is about 55 years old. The trunkspace reaches a height of 9.2 m. The maximum vegetation density is concentrated in the canopy level at a 14 m height (see Foken et al (2010) for vertical profiles of vegetation density, i.e. Plant Area Index). The site is described in detail in Gerstberger et al (2004) and a summary of background data can be found in Staudt and Foken (2007).

2.2 Data sets

The CO_2 advection data set presented in the current study was collected during the EGER ("ExchanGE processes in mountainous Regions") experiment (Foken et al, 2010), which comprised two intensive observation periods (IOP). The first intensive observation period was conducted from 06th of September to 7th of October 2007 (IOP1) and the

4

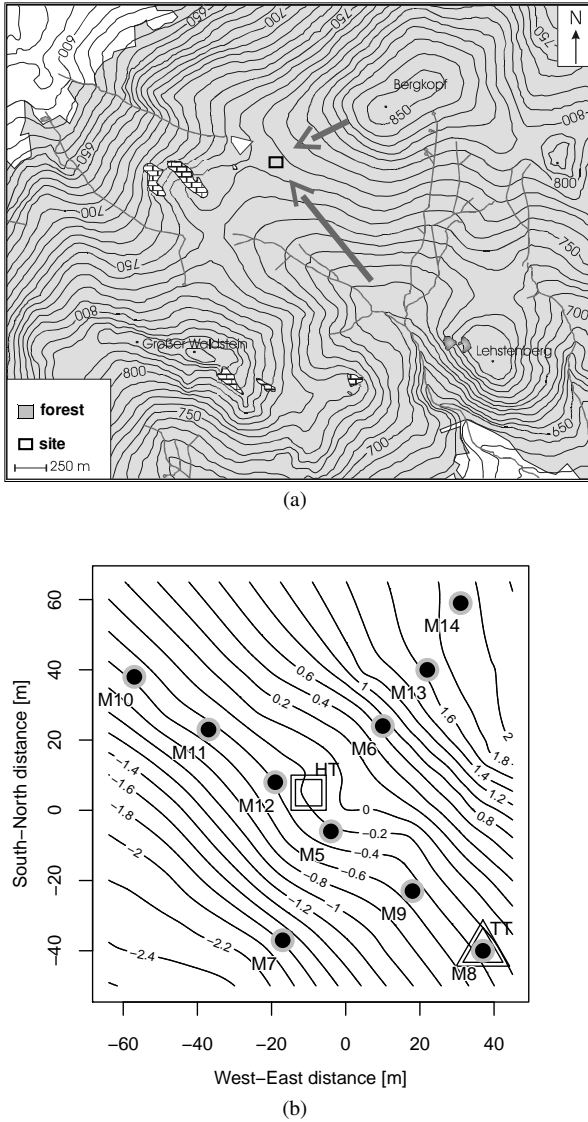


Fig. 1 (a) Measuring site Waldstein-Weidenbrunnen location. Arrows indicate downhill drainage flow (NE-SW) and upslope wind from the valley (SE-NW). Topography is shown by contour lines with an interval of 10m. Black square marks location of closeup (b). (b) Sampling locations M5, M6, ..., M14 for sub-canopy CO₂ concentration at a 2.25m height. Tall towers with vertical profiles: “main tower” (MT) and “turbulence tower” (TT). M-numbers are used for reference in the text. Topography is shown by isolines with an equidistance of 0.2m relative to 750m ASL

second intensive observation period from 1st of June to 15th of July 2008 (IOP2). Regarding the IOP1 data set a total of 8.2 available days was used for the analysis, i.e. 394 half hourly values taken from a window of 14.0 days. Regarding the IOP2 data set 24.6 days worth of data were used for the analysis, i.e. 1181 half hourly values taken from a window of 32.0 days (11th to 13th of June). Data meeting the fol-

lowing criteria were excluded: instruments powered off or malfunctioning.

A third, long-term data set from the same site was used for the analysis of vertical wind velocity and coordinate rotation (“long-term data set”). The vertical wind velocity data set originates from 3D sonic wind velocity measurements at a 32m height at the FLUXNET tower Waldstein-Weidenbrunnen (DE-Bay). From a given 10-year data set (1999 to 2008), a subset of 3.2 years (1181 days) was selected which was free of changes with respect to instrument type and instrument orientation. The selected data cover the period from 21st of May, 2003, 00:00, to 14th of August, 2006, 00:00.

Atmospheric stratification, expressed in terms of the stability parameter ζ , measured at a 36m height, was used to select data subsets during the analysis. ζ is defined as $\zeta = (z - d)L^{-1}$ with measurement height z , displacement height d and Obukhov-length L . Results were distinguished with respect to different classes of atmospheric stratification, using the criteria given in Eq. 1 according to Foken et al (1991):

$$\zeta = \begin{cases} \text{free convection} & \text{for } \zeta < -1 \\ \text{unstable} & \text{for } -1 < \zeta < -0.0625 \\ \text{neutral} & \text{for } -0.0625 < \zeta < 0.125 \\ \text{stable} & \text{for } 0.125 < \zeta < 1 \\ \text{extremely stable} & \text{for } \zeta > 1 \end{cases} \quad (1)$$

2.3 Instrumental setup

table

The measurement design relies on the assumption that the CO₂ budget of a cartesian control volume, with horizontal dimensions of approx. 100m × 100m in the x - and y -direction respectively and a vertical extension of 36m from the forest floor to an above-canopy measurement in the z -direction, can be approximated by measuring the vertical and horizontal fluxes at selected transects within the control volume. The general features of the measurement design which was used in the current study to quantify individual terms of the CO₂ Net Ecosystem Exchange budget equation included the following:

- an eddy-covariance system above the canopy to measure the turbulent flux, this technique being a standard at FLUXNET sites (Aubinet et al, 2000),
- a vertical profile of CO₂ concentration measurements reaching from the forest floor to the above-canopy top measurement level, where vertical wind velocity was recorded, to quantify vertical advection,
- a horizontal array of CO₂ concentration and horizontal wind velocity measurements in the sub-canopy at a height where horizontal advection has been observed to

Table 1 Instrumental setup during Intensive Observation Period 1 (IOP1) and Intensive Observation Period 2 (IOP2)

Description	height above ground (m)	tower	instrument type
IOP1			
eddy-covariance	36	TT	USA-1 (Metek GmbH) + LI-7500 (LI-COR, Inc.)
vert. profile wind	2.25, 5.5, 13, 18, 23, 36	TT	CSAT3 (Campbell Scientific, Inc.), R2 (Gill Instruments Ltd.), CSAT3 (Campbell Scientific, Inc.), R2 (Gill Instruments Ltd.), CSAT3 (Campbell Scientific, Inc.), USA-1 (Metek GmbH)
vert. profile CO ₂	0.05, 0.3, 1, 2, 5, 10, 16, 24.3, 31	MT	LI-7000 (LI-COR, Inc.) + LI-820 (LI-COR, Inc.) multiplexer system
horiz. array wind	2.25	M5, M6, M7, M8	3x USA-1 (Metek GmbH) + 1x CSAT3 (Campbell Scientific, Inc.)
horiz. array CO ₂	1, 2.25	M5, M6, M7, M8 M5, M6, M7, M8, M9	Climatronics F460 cup anemometer LI-820 (LI-COR, Inc.) multiplexer system
IOP2			
eddy-covariance	36	TT	USA-1 (Metek GmbH) + LI-7500 (LI-COR, Inc.)
vert. profile wind	0.03, 0.3, 1, 2, 16, 25, 32	MT	4x Wind Sensor WS425 (Vaisala), 2x Solent R2 (Gill Instruments Ltd.), 1x USA-1 (Metek GmbH)
vert. profile CO ₂	0.005, 0.03, 0.1, 0.3, 0.9, 3, 10, 16.5, 20.5, 25, 31.5	MT	LI-7000 (LI-COR, Inc.) + LI-820 (LI-COR, Inc.) multiplexer system
horiz. array wind	2.25	M5, M6, M7, M9, M10, M8	5x USA-1 (Metek GmbH) + 1x CSAT3 (Campbell Scientific, Inc.)
horiz. array CO ₂	1, 2.25	M5, M6, M7, M8 M5, M6, M7, M8, M10, M13, M9, M11, M12, M14	Climatronics F460 cup anemometer 5x LI-6262 (LI-COR, Inc.), 4x BINOS (Leybold Heraeus GmbH), 1x LI-6251 (LI-COR Biosciences Inc.)

be most pronounced, in order to quantify horizontal advection, and a vertical profile of horizontal wind velocity measurements to integrate horizontal advection over the height of the control volume.

The location of horizontal and vertical profiles, their relative position and their orientation with respect to the terrain are illustrated in Fig. 1. Vertical profiles were installed at a 32 m high tower, hereafter referred to as “main tower”, MT, as well as on a 36 m high tower, hereafter referred to as “turbulence tower”, TT (Fig. 1b). The horizontal sub-canopy measurement array is indicated by mast numbers M5 to M14 in Fig. 1(b).

The x -axis of the experimental coordinate system was defined parallel to the up-slope direction running from south-west (218.71°) to north-east (38.71°). The y -axis was defined perpendicular to the slope running from north-west (308.71°) to south-east (128.71°), which corresponds to the line of sight between M10 and M8 (Fig. 1b). The z -axis was defined in the vertical starting at the forest floor with a positive sign upwards. Details about the setup and instruments used, some of which were specific to the observation period, are described in the following. A summary is presented in Table 1.

2.3.1 Intensive Observation Period 1 (IOP1)

Vertical and horizontal CO₂ profile measurements were based on closed-path infrared gas analyzers in combination with switching valve systems. For the investigation of vertical advection, CO₂ concentration was sampled along a vertical profile using a combination of a LI-7000 (LI-COR, Inc.) and a LI-820 (LI-COR, Inc.) gas analyzer at measurement heights of 0.05, 0.3, 1, 2, 5, 10, 16, 24.3 and 31 m installed at the main tower (Fig. 1b). The tube length was 55 m for each height with a flow rate of 1 L min^{-1} . Vertical wind velocity was recorded above the canopy at a 36 m height (1.4 times canopy height) using a USA-1 (Metek GmbH) 3D sonic anemometer installed at the turbulence tower (Fig. 1b).

For the investigation of horizontal advection, CO₂ concentration was measured along horizontal transects with a switching valve system based on a LI-820 (LI-COR, Inc.) analyzer (Ruppert, 2005). Measurements were taken at a 2.25 m height at locations M5, M6, M7, M8 and M9 according to Fig. 1(b), defining a transect along the terrain slope direction (M7, M5, M6) and a transect across the slope direction (M5, M9, M8), with M5 being a common point in both transects. The tube length was 55 m for each sample point. The system was automatically calibrated every 24 hours using high precision reference gases ($0.1 \mu\text{mol mol}^{-1}$ accuracy). Horizontal wind velocity was observed in the sub-

canopy space at a 2.25 m height using USA-1 3D sonic anemometers at M5, M6, M7 and a CSAT3 (Campbell Scientific, Inc.) 3D sonic anemometer at M8. Additional measurements of horizontal wind velocity were made at a 1 m height at M5, M6, M7 and M8 using Climatronics F460 cup anemometers. Vertical integration of horizontal advection is based on measurements of horizontal wind velocity recorded along a vertical profile installed at the turbulence tower using 3D sonic anemometers at heights of 2.25, 5.5, 13, 18, 23 and 36 m as well as on above mentioned vertical profile of CO₂ concentration.

The above-canopy turbulent flux of CO₂ was measured by the eddy-covariance technique using a USA-1 sonic anemometer and a LI-7500 (LI-COR, Inc.) open-path infrared gas analyzer installed at the turbulence tower. More detail and additional instrumentation during IOP1 is given in Serafimovich et al (2008a).

2.3.2 Intensive Observation Period 2 (IOP2)

The setup and instrumentation during IOP2 was generally similar to the one during IOP1. However, considerable improvements were made with respect to the temporal and spatial measurement resolution of the horizontal concentration and wind field in the sub-canopy as will be detailed below.

In order to measure vertical advection, a vertical profile of CO₂ concentration was installed at the main tower using a combination of two closed-path infrared gas analyzers (LI-7000 and LI-820), sequentially sampling 11 inlets at heights of 0.005, 0.03, 0.1, 0.3, 0.9, 3, 10, 16.5, 20.5, 25 and 31.5 m (Plake, 2009) and one closed-path infrared gas analyzers (LI-7000), continuously sampling at a 32 m height. Vertical wind velocity was measured at 36 m at the top of the turbulence tower using a USA-1 sonic anemometer.

For the quantification of horizontal advection, the CO₂ concentration and wind field was measured in the sub-canopy at a 2.25 m height (Fig. 1b). Ten CO₂ concentration sample points were distributed between an along-slope transect from south-west to north-east (M7, M5, M6, M13, M14) and an across-slope transect from north-west to south-east (M10, M11, M12, M5, M9, M8), including one common point (M5). Each point was sampled by an individual closed-path infrared gas analyzer. Tube length was 75 m each with a flow rate of 2 L min⁻¹. Instruments used were 5 LI-6262, 1 LI-6251 and 4 BINOS. All CO₂ closed-path gas analyzers shared a common housing in a central position, with controlled conditions resulting in a constant common temperature and common pressure regime as well as radiation protection. Moreover, all analyzers shared a common tailor-made automatic calibration system, using high precision reference gases (accuracy 0.1 μmol mol⁻¹). The calibration routine included an automatic calibration every 4 hours using two reference concentrations. In addition to factory calibra-

tion, each instrument's polynomial calibration function was established on site using multiple standards. The polynomial was checked before and during the experiment. CO₂ concentration measurements were recorded with a 1 Hz frequency at each sample point. A detailed description of the multi-analyzer system, calibration and data processing can be found in Siebicke et al (2010). In addition to CO₂ concentration measurements at a 2.25 m height, sample locations M5, M6, M7, M8, M9, M10 were equipped with sonic anemometers (USA-1) to measure wind velocity and direction. Sonic data were recorded with a 20 Hz frequency. Vertical integration of horizontal advection is based on wind velocity and direction measurements from sonic anemometers installed at the main tower at heights of 0.03 m, 0.3 m, 1 m, 2 m (Wind Sensor WS425), 16 m, 25 m (Solent R2) and 32 m (USA-1) as well as on above mentioned vertical profiles of CO₂ concentration.

The above-canopy turbulent flux of CO₂ was measured by the eddy-covariance technique using a USA-1 sonic anemometer and a LI-7500 gas analyzer installed at the turbulence tower at a 36 m height. More detail and additional instrumentation during IOP2 is given in Serafimovich et al (2008b).

2.3.3 Long-term measurements

The long-term study of vertical wind velocity and coordinate rotation is based on measurements recorded at the main tower at a 32 m height using a Solent R3 (Gill Instruments Ltd.) 3D sonic anemometer. This data set was recorded as part of the continuous FLUXNET measuring program.

2.4 Net Ecosystem Exchange

The exchange of CO₂ between the ecosystem (control volume) and the atmosphere, the Net Ecosystem Exchange (*NEE*), which is controlled by the net effect of assimilation and respiration, was calculated according to the following formula (Aubinet et al, 2003; Feigenwinter et al, 2004, and others):

$$\begin{aligned}
 NEE = & \frac{1}{V_m} \int_0^h \left(\frac{\partial \bar{c}}{\partial t} \right) dz + \frac{1}{V_m} (\overline{w'c'})_h \\
 & + \frac{1}{V_m} \int_0^h \left(\overline{w(z)} \frac{\partial \bar{c}}{\partial z} + \bar{c}(z) \frac{\partial \overline{w}}{\partial z} \right) dz \\
 & + \frac{1}{V_m} \int_0^h \left(\overline{u(z)} \frac{\partial \bar{c}}{\partial x} + \overline{v(z)} \frac{\partial \bar{c}}{\partial y} \right) dz
 \end{aligned} \quad (2)$$

with the molar volume of dry air V_m , CO₂ concentration c , time t , horizontal distances x and y , vertical distance above ground z , height of the control volume $h = 32$ m, horizontal

wind velocity u along the x -direction, horizontal wind velocity v along the y -direction and vertical wind velocity w along the z -direction. See Sec. 2.3 for the definition of the x -, y -, and z -direction in the experimental coordinate system. Overbars denote temporal means and primes denote the temporal fluctuations relative to the temporal mean. All flux terms of equation (2) were calculated with a 30-min resolution. The terms on the right hand side of Eq. 2 are the change of storage (term I), the vertical turbulent flux (term II), vertical advection (term IIIa), vertical mass flow from the surface e.g. due to evaporation (term IIIb) according to Webb et al (1980), and horizontal advection (term IV). The form of NEE presented in Eq. 2 excludes the horizontal variation of the vertical turbulent flux and the horizontal variation of vertical advection. Eq. 2 further neglects the flux divergence term: $\frac{1}{V_m} \int_0^h \left(\frac{\partial(u'c')}{\partial x} + \frac{\partial(v'c')}{\partial y} \right) dz$.

The change of storage of CO_2 in the control volume (term I of Eq. 2) was calculated using concentration measurements from the top of the main tower following an approach by Hollinger et al (1994), which assumes the same mean CO_2 density $\bar{\rho}_c$ for the entire air column below measurement height h . The storage flux $F_{S(i)}$ is then written:

$$F_{S(i)} = \frac{\bar{\rho}_{c(i+1)} - \bar{\rho}_{c(i-1)}}{t(i+1) - t(i-1)} h \quad (3)$$

with time t and measurement interval i . The storage flux was calculated using the software TK2 (Mauder and Foken, 2004). It could be shown by Ruppert et al (2006) with measurements made in 2003 (Thomas et al, 2004) and previous work at the site under study that storage estimates from a one point approach, which are said to underestimate the storage term under certain conditions (Finnigan, 2006), are comparable to estimates computed from multi-level profile measurements below the top measurement level at height h under most conditions at the Waldstein-Weidenbrunnen site. Furthermore, storage was found to be relatively small at the site, contributing only a minor fraction to the NEE budget.

The vertical turbulent flux (term II of Eq. 2) was calculated according to standard methodology using the TK2 software (Mauder and Foken, 2004). The computation involved filters, conversions and flux corrections including spike detection (Vickers and Mahrt, 1997), determination of the time delay between sonic anemometer and gas analyzer using cross-correlation analysis, cross-wind correction of sonic temperature (Liu et al, 2001), planar fit coordinate transformation (Wilczak et al, 2001), high frequency spectral correction (Moore, 1986), conversion of sonic temperature fluctuations into actual temperature fluctuations (Schoanus et al, 1983), density correction for scalar fluxes of H_2O and CO_2 and correction for mean vertical mass flow (Webb et al, 1980) as well as quality control according to

Foken and Wichura (1996) in a scheme with nine quality classes (Foken et al, 2004).

Vertical advection (term IIIa of Eq. 2) was calculated according to Eq. 4:

$$\frac{1}{V_m} \int_0^h \bar{w}(z) \frac{\partial \bar{c}}{\partial z} dz = \frac{1}{V_m} \bar{w}_h (\bar{c}_h - \langle \bar{c} \rangle) \quad (4)$$

with the temporal and spatial mean CO_2 concentration $\langle \bar{c} \rangle$ given as

$$\langle \bar{c} \rangle = \frac{1}{h} \int_0^h \bar{c}(z) dz, \quad (5)$$

following Lee (1998), who assumed a linear increase of vertical wind velocity with height.

Horizontal advection F_{HA} (term IV of Eq. 2) was estimated based on CO_2 concentration and wind velocity measurements as observed with the sub-canopy measurement array described in Sec. 2.3. Vertical integration of horizontal advection followed an approach published by Aubinet et al (2003) and Staebler and Fitzjarrald (2004), which is based on the assumption of similarity between horizontal gradients and the vertical profile, assuming that a single vertical profile of CO_2 concentration and wind speed, measured at a central location, translates with spatial similarity to all sub-canopy sampling points ("similarity approach"). Staebler and Fitzjarrald (2004) substitute absolute CO_2 concentration c by a concentration $c^* = c - c_0$ relative to a baseline level c_0 , the latter having no effect on budget calculations, chosen to be $c_0 = c(h)$, i.e. equal to above-canopy concentration. Using the above-stated similarity assumptions, vertical integration of horizontal advection was performed according to Eq. 6:

$$F_{HA} = \frac{1}{V_m} \left(u(x, z_1) \frac{\partial c^*(x, z_1)}{\partial x} + v(y, z_1) \frac{\partial c^*(y, z_1)}{\partial y} \right) \int_0^h f(z) g(z) dz \quad (6)$$

with $f(z)$ and $g(z)$ being profile functions of the vertical profile of CO_2 concentration c^* and the vertical profile of the horizontal wind velocity component respectively, normalized by their value at $z_1 = 2.25m$. To obtain $\int_0^h f(z) g(z) dz$, measurements of CO_2 concentration (closed-path infrared gas analyzer system) and wind speed (sonic anemometers) along a vertical profile at the main tower, discrete measurement heights detailed in Section 2.3 were used to fit continuous Akima interpolation functions (Akima, 1970), which were then numerically integrated.

2.5 Horizontal concentration gradients

In order to evaluate the effect of temporal measurement resolution of the CO₂ concentration measurements on 30-minute mean CO₂ concentrations at the individual sample locations in the sub-canopy, a comparison between two alternative approaches with different measurement strategies was made. The most common approach for horizontal gradient measurements published in the literature is characterized by measurements at several sample locations where the individual locations are sampled discontinuously by a switching valve system with one analyzer, sampling one point after the other. Although the analyzer measurement frequency might be high, continuous measurements at more than one point as well as measurements at more than one point at a time are not possible due to the system's design. The return rate to the same sample location has a low frequency. Therefore truly synchronous measurements of a concentration gradient are impossible with a single-analyzer switching valve system. In the following this will be called the “discontinuous” approach. Concentration gradients have to be computed by averaging measurements over a longer period, typically over 30 minutes. Inter-instrument bias was corrected by a simple time-constant offset in analogy to Fig. 10 in Aubinet et al (2003).

An alternative approach is the synchronous continuous measurement at several sample locations with a high sampling frequency using one individual analyzer for every sample location. Such a system and the method for obtaining inter-instrument accuracy by comprehensive bias correction is presented in Siebicke et al (2010) and was applied by the author to study the spatio-temporal variability of the sub-canopy CO₂ concentration field. In the following this will be called the “continuous” approach.

2.5.1 Discontinuous versus continuous sampling

With continuous high frequency measurements available at all sample locations in the sub-canopy, a comparison between the discontinuous and the continuous approach was made by simulating discontinuous sampling of the continuous individual real 1 Hz time series by a virtual representation of a typical switching valve single-analyzer system such as the “Hydra” (Burns et al, 2009). The following parameters were chosen for the simulation: sampling frequency of the analyzer = 1 Hz, measurement duration at one sample location $\Delta t_{meas} = 45$ s, duration of flushing of tubes before switching to the next sample location $\Delta t_{flush} = 15$ s, number of sample locations $n = 10$. This gives a return period to the same sample location of 10 min and 3 sample data blocks per sample location per 30-min average. The order in which the individual locations were sampled during the simulation was a repetitive sequence of mast locations M5, M6,

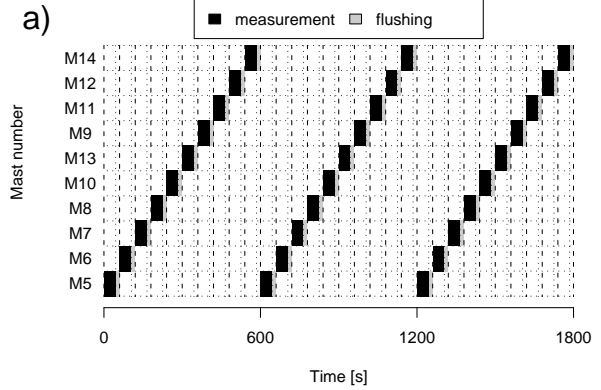


Fig. 2 Discontinuous sampling scheme of the simulated switching valve single-analyzer system. Periods marked with ‘measurement’ are used for calculating concentration averages, periods marked with ‘flushing’ indicate transition times between switching from one mast location, i.e. one sample tube, to the next one and are not available to calculate concentration averages

M7, M8, M10, M13, M9, M11, M12, M14 (Fig. 1b). The sampling procedure for one 30-min interval is illustrated in Fig. 2 for the discontinuous sampling approach of the simulated switching valve system. Only the periods of the time series which are marked black in the figure represent measurements whereas in the case of the continuous sampling approach of the multi-analyzer system, the complete time series are measured.

To obtain the 30-min mean concentration at the individual sample locations, all measurements of the corresponding time series within the corresponding 30-min interval were averaged using the mean as the averaging operator, i.e. three blocks of 45 s duration each, to give a total of 135 s. The thus obtained 30-min averages, which are based on discontinuous measurements, were compared to 30-min averages from continuous measurements, i.e. the mean of 1800 s of measured data in each 30-min interval. One important difference between the discontinuous and the continuous approach is the fraction of the total duration of the time series where actual measurements are available. Disregarding data gaps caused by instrument malfunction or similar causes, this observed fraction of the time series can be calculated as

$$\frac{\text{observed}}{\text{total}} = \frac{\Delta t_{meas}}{(\Delta t_{meas} + \Delta t_{flush}) * n}. \quad (7)$$

With the given simulation settings the observed fraction of the time series is 100% for the continuous approach and a mere 7.5% for the discontinuous approach.

The differences between 30-min averages generated by the two approaches will be presented in Sec. 3. Other than for this comparison, all results regarding IOP2 are based on 30-min averages calculated from continuous measurements, since a continuous observation is obviously a more realistic representation of the true mean of the complete time series

than an incomplete observation. It can be further assumed that a 1 Hz measurement resolution is sufficient for finding a precise 30-min mean concentration and that processes with a frequency higher than 1 Hz don't affect the 30-min mean significantly.

Some results are presented in terms of local concentration deviations at a point i from the instantaneous average field concentration, which are calculated as the difference of the local concentration $c_i(t)$ at time t from the median field concentration $\bar{c}(t)$ according to $c_i(t) - \bar{c}(t)$ with ten sampling locations M5, M6, ..., M14 with CO₂ concentrations $c_1(t), c_2(t), \dots, c_n(t)$.

2.6 Coordinate rotation

Measurements of vertical wind velocity w were transformed by coordinate rotation in order to align the coordinate system of the sonic anemometer along the direction of the mean flow, resulting in a zero mean vertical velocity. The rotation was based on the planar fit rotation technique (Wilczak et al, 2001), to which several modifications were applied (see below). The planar fit rotation is shown by matrix notation:

$$\vec{u}_p = P(\vec{u}_m - \vec{c}) \quad (8)$$

where \vec{u}_m is the measured wind vector, \vec{u}_p is the wind vector in a mean streamline coordinate system (not yet rotated into the mean wind direction), P is a partial rotation matrix that places the z -axis perpendicular to the plane of the mean streamlines, and \vec{c} is the mean offset error in the measured winds due to instrument error. The equations for the mean wind components are:

$$\bar{u}_p = p_{11}(\bar{u}_m - c_1) + p_{12}(\bar{v}_m - c_2) + p_{13}(\bar{w}_m - c_3) \quad (9)$$

$$\bar{v}_p = p_{21}(\bar{u}_m - c_1) + p_{22}(\bar{v}_m - c_2) + p_{23}(\bar{w}_m - c_3) \quad (10)$$

$$\bar{w}_p = p_{31}(\bar{u}_m - c_1) + p_{32}(\bar{v}_m - c_2) + p_{33}(\bar{w}_m - c_3) \quad (11)$$

The mean streamline coordinate system is defined so that $\bar{w}_p = 0$. The tilt angle was then determined by two-dimensional linear regression:

$$\bar{w}_m = c_3 - \frac{p_{31}}{p_{33}}\bar{u}_m - \frac{p_{32}}{p_{33}}\bar{v}_m = b_0 + b_1\bar{u}_m + b_2\bar{v}_m. \quad (12)$$

The overbar denotes averaging over the turbulent 30-min record. From the coefficients it is possible to determine the rotation angles around the u - and v -axis, where $p_{31} = \sin \alpha$, $p_{32} = \cos \alpha \sin \beta$ and $p_{33} = \cos \alpha \cos \beta$. Finally a rotation of each averaging interval about the z -axis was performed:

$$\gamma = \arctan\left(\frac{\bar{v}_p}{\bar{u}_p}\right). \quad (13)$$

The original planar fit rotation as outlined above defines a rotation plane using measured data from a relatively long period (much longer than 30 minutes, e.g. weeks to months,

typically the length of the experiment), including all wind directions present in the long period's data set. In the following, modifications are described which were tested in addition to the original planar fit approach in order to reduce the effect of flow distortion from instruments, mounting structures and the tower on the rotation plane as well as the effect of local features of the terrain, and thus determine rotation coefficients which are more representative of the mean streamlines at the top boundary of the control volume. The effect of different modifications of the coordinate rotation on vertical advection and subsequently on NEE was evaluated.

One modification used filtered input data to first determine the rotation angles and then rotate the total data set by the angles found ("input filter test"). One filter test used data during neutral stratification (see Eq. 1) only (Finnigan, 1999; Paw U et al, 2000; Aubinet et al, 2003). In a second test data were filtered according to a friction velocity (u_*) quality flag (Foken et al, 2004). The quality flag implies a steady state test of $\overline{u'w'}$ and $\overline{v'w'}$ and tests of the integral turbulence characteristics (ITC) $\sigma_u u_*^{-1}$, $\sigma_v u_*^{-1}$ and $\sigma_w u_*^{-1}$. Only high quality data (flag 1-3) were used to determine the rotation coefficients. The u_* -quality flag is an output from the TK2 software.

A second modification applied a sector-wise planar fit rotation ("sector-wise test") to reduce direction specific flow distortion effects and allow for non-planar mean streamlines (Paw U et al, 2000; Mammarella et al, 2007). The procedure for the sector-wise test included the following steps: first rotation of raw w data including all data from all directions, manual identification of sector limits to coincide with local maxima or minima in a plot of w (after first rotation) versus wind direction, second rotation of raw w data separately for each sector with the sector limits found after first rotation. If not otherwise specified, the displayed results in Sec. 3 use w data from a sector-wise rotation with the u_* -filter.

A third modification was designed to study the effect of the length of the data set used for the planar fit rotation on the rotation angles ("window length test"). This was stimulated by the observation of a large impact of the length of the data set used for coordinate rotation on vertical advection during IOP1, when comparing the IOP1 w measurements rotated with planar fit coefficients obtained from a planar fit based on a half year data set as compared to coefficients obtained from a planar fit based on the IOP1 data set (shorter). A coordinate rotation such as the planar fit acts as a high-pass filter (Finnigan et al, 2003; Moncrieff et al, 2004), excluding information which is contained in the low frequency part of the spectrum of w with periods longer than the length of the input data for the planar fit rotation. In order to determine the contribution of different frequencies to the signal of w , a long-term data set (3.2 years) was analyzed. Planar fit was sequentially applied to adjacent subsets of the

data set with equal length (“window length”), resulting in rotation coefficients β_0 , β_1 and β_2 for each window and a sequence of coefficients for the complete data set. In the following this technique will be called “sequential planar fit”. Different window lengths were chosen, corresponding to periods which are characterized by low energy in the spectrum of w , thus separating periods with high energy. The following window lengths were analyzed: 1181, 400, 57, 15 and 2.3 days. To evaluate the effect of different estimates of w generated by different planar fit window lengths on vertical advection F_{VA} , the mean daily cycle (30-minute resolution) of F_{VA} was computed from a mean daily cycle of w and a mean daily cycle of the vertical CO₂ concentration distribution. Although vertical profile measurements of CO₂ were not available to cover the complete time of w measurements, this exercise does quantify the potential impact of planar fit window length on vertical advection.

3 Results and Discussion

This section presents a comparison between continuous high frequency measurements of horizontal concentration gradients and the discontinuous sampling approach in Subsec. 3.1, shows the effect of different approaches to planar fit coordinate rotation on vertical wind velocity and vertical advection in Subsec. 3.2, presents horizontal advection estimates from discontinuous and continuous gradient measurements in Subsec. 3.3 and finally displays the combined advective flux in Subsec. 3.4 and its impact on NEE in Subsec. 3.5.

3.1 Gradient sampling

The comparison of the discontinuous and the continuous sampling approach is presented in Fig. 3(a) by regression of instantaneous local concentration perturbation values, i.e. $c_i(t) - \bar{c}(t)$, calculated as the local concentration $c_i(t)$ at location i minus the instantaneous median field concentration $\bar{c}(t)$, from both approaches. Although the slope m of a linear regression of discontinuously versus continuously sampled data is close to unity ($m = 0.99$, and $m = 0.82$ for the reverse regression), there is considerable scatter in the data, yielding a low coefficient of determination $R^2 = 0.81$ (all days) and $R^2 = 0.78$ (“golden days”: DOY 181 to 184). A typical deviation of $5 \mu\text{mol mol}^{-1}$, as estimated from the cross sectional width of the point cloud in Fig. 3(a), is a relatively small fraction of the absolute concentration of typically $378 \mu\text{mol mol}^{-1}$, but it is a large fraction of the relative concentrations, i.e. $c_i(t) - \bar{c}(t)$. The range of the latter is indicated by the axis range in the figure. Because differences between the two approaches are large at small absolute values, their relative proportion can be far from unity and even

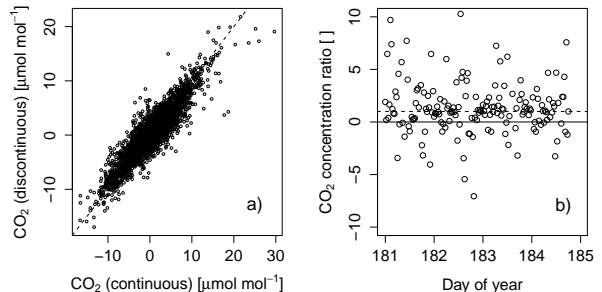


Fig. 3 a) Regression of 30-minute mean CO₂ concentration differences during IOP2 from the discontinuous sampling approach versus CO₂ concentration differences from the continuous sampling approach. Concentration differences $c_i(t) - \bar{c}(t)$ for $i \in (1, 10)$ are calculated as the local concentration minus the instantaneous median field concentration (see Sec. 2.5.1). b) Ratio of 30-minute mean CO₂ concentration differences from the discontinuous sampling approach to values from the continuous sampling approach for a selected four day period (“golden days”: DOY 181 to 184, 2008). Dashed line marks a ratio equal to one

change sign as shown in Fig. 3(b) for a selected four day period. The consequence for gradient measurements is that the 30-min gradient estimates from the two approaches are very different in magnitude and possibly in sign. Even though the average impact is small as shown by the regression slope, the scatter on a 30-min basis introduces scatter in horizontal advection estimates using discontinuously sampled gradients.

3.2 Coordinate rotation and vertical advection

The effect of different coordinate rotation approaches on vertical wind velocity w is presented in Fig. 4, which plots w versus wind direction. Results are shown for the “long-term” data set only but are essentially similar for the IOP1 and IOP2 data set. Unrotated w (Fig. 4a) is strongly dependent on wind direction, approximating a sinusoidal function, which results from the relative tilt between sensor plane and flow field tangent plane due to the terrain slope. After a standard planar fit rotation the mean w is closer to zero but directional dependencies remain (Fig. 4b). They can be caused by local flow field perturbation due to instrument structures, mounting structures, trees or terrain. Applying a sector-wise rotation essentially removes directional dependencies and yields a mean w close to zero (Fig. 4c to 4f). As there is no significant improvement obtained by applying additional filters (Fig. 4d to 4f), or even larger deviations of w from zero occur when using the neutral stratification filter (Fig. 4d and 4f), the sector-wise rotation of the unfiltered (Fig. 4c) or possibly u_* filtered w (Fig. 4e) is recommended.

Having presented directional dependencies of w , Fig. 5 and 6 show temporal characteristics of w and the effect of planar fit window length on w and on vertical advection F_{VA} .

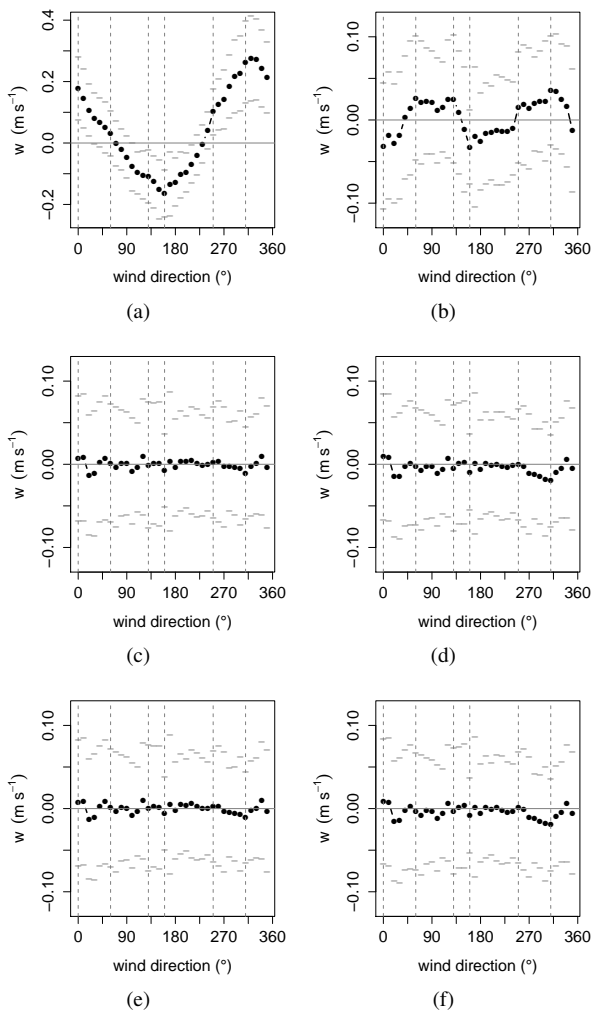


Fig. 4 Vertical wind velocity w versus wind direction (long-term data set): a) before coordinate rotation (note different y-scale in a), b) after standard planar fit rotation, c) sector-wise planar fit rotation, d) sector-wise planar fit rotation with neutral stratification filter, e) sector-wise planar fit rotation with u_* quality flag filter, f) sector-wise planar fit rotation with neutral stratification filter and u_* quality flag filter. Sector limits are indicated by dashed vertical lines in all subfigures, although only applied in c), d), e) and f). Data are averaged in 10° wind direction bins. Grey dashes indicate $w \pm$ standard deviation. Planar fit window length: 3.2 years

Fig. 5 displays F_{VA} calculated with w from the different filter approaches described above for two different planar fit window lengths: if w is rotated by rotation coefficients obtained from a half-year data set, F_{VA} (black line) is much larger than F_{VA} obtained by rotating w with rotation coefficients obtained from the IOP1 period only, i.e. 8 days (grey line). This result serves as one example and a warning of how large the impact of the length of the data set used to determine rotation coefficients on F_{VA} can be (in this case up to $7 \mu\text{mol m}^{-2} \text{s}^{-1}$). The effect of data set length is even larger

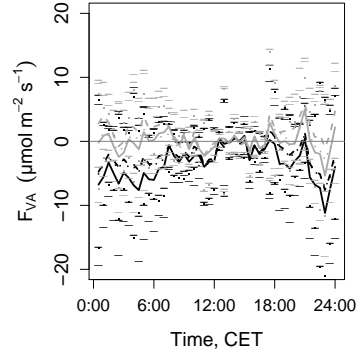


Fig. 5 Mean daily cycle of vertical advection (lines) \pm standard deviation (dashes) during IOP1 with a 30-min resolution, comparing the effect of different planar fit rotations (see Sec. 2.6). Black lines: half year planar fit, grey lines: IOP1 planar fit, solid lines: no filter, dashed lines: neutral stratification filter (sector-wise rotation), dotted lines: friction velocity flag filter (sector-wise rotation)

than the effect of any of the filter approaches applied. Assuming a stable instrument orientation over the course of the experiment, the presented differences in F_{VA} coming from differences in w are an expression of low frequency components of the w signal.

The results of a systematic analysis of the energy distribution over the spectrum of w are given in Fig. 6. Fig. 6a) shows w after sequential planar fit (Sec. 2.6) for planar fit window lengths from 2.3 to 400 days. Since planar fit acts as a high-pass filter tuned by the window length, the difference between w from a 2.3 days window length and w from a 400 days window length is due to the energy contained in the low frequency part (periods between 2.3 and 400 days) of the spectrum of w . This difference is significant on the basis of the mean daily cycle of w , particularly at night when w from a 400 days window length is about 200% of w from a 2.3 days window length (Fig. 6a). The impact of sequential planar fit window length on F_{VA} is estimated by calculating the mean daily cycle of F_{VA} (Fig. 6c) from w (Fig. 6a) and the vertical CO_2 concentration distribution (Fig. 6b). Differences in w transfer to differences in F_{VA} , as can be deduced from Eq. 4, again with the largest differences at night (Fig. 6c) when advection itself is largest due to large vertical concentration gradients at night (Fig. 6b). The average impact of sequential planar fit window length of 400 days versus 2.3 days on F_{VA} is expressed in Fig. 6d). The slope of a linear regression shows that F_{VA} from a sequential planar fit with a window length of 400 days is about 50% larger than F_{VA} from a 2.3 day window length. Essentially the same results are obtained using data from IOP2 (not shown).

While the previous figures have shown the effect of different measurement or calculation approaches, Fig. 7 to 11 present the regime of advective and turbulent flux components and their drivers for IOP1 and IOP2. To recall, the

12

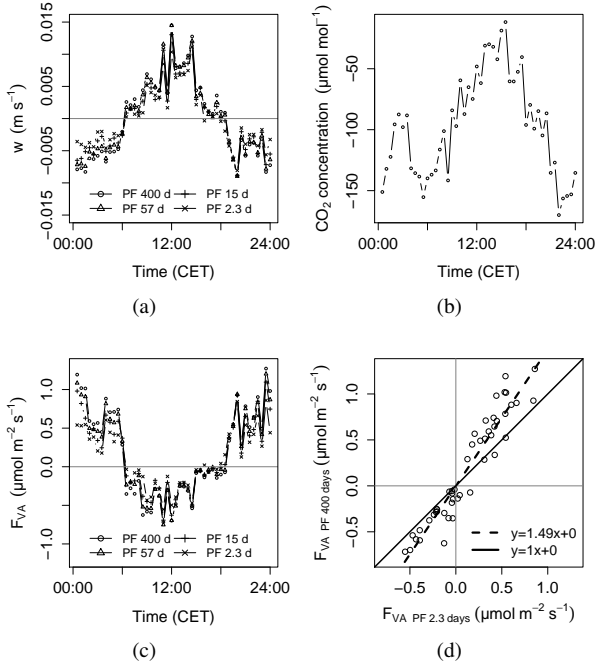


Fig. 6 a) Mean daily cycle (30-min resolution) of vertical wind velocity on top of the main tower (long-term data set, see Sec. 2.2) for planar fit window lengths from 2.3 to 400 days (see Sec. 2.6), b) mean daily cycle (30-min resolution) of vertical CO₂ concentration distribution $\bar{c}_h - \langle \bar{c} \rangle$ (see Eq. 4 and 5) during IOP1, c) hypothetical mean daily cycle of vertical advection, computed as a product of data in a) and b), for planar fit window lengths from 2.3 to 400 days, d) regression of vertical advection (as in Subfig. c) with a planar fit window length of 400 days versus vertical advection with a planar fit window length of 2.3 days and linear model fit (dashed line)

only methodological difference between the two IOPs is the way that horizontal gradients were measured, i.e. discontinuously and with simple bias correction during IOP1 versus continuously, with comprehensive bias correction and different analyzer models during IOP2.

Atmospheric stratification, expressed by the stability parameter ζ (Fig. 7) is a main driver for advection. A similar mean daily cycle of ζ was observed during IOP1 (Fig. 7a) and IOP2 (Fig. 7b) with stable stratification at night and unstable stratification during the day. However, the daytime period with negative values of ζ is longer during IOP2 due to longer days and higher energy input in summer as opposed to fall (IOP1).

The mean daily cycle of vertical advection F_{VA} during IOP1 (Fig. 8a) and IOP2 (Fig. 8b) shows positive fluxes during the night with a maximum of 4.4 μmol mol⁻¹ (IOP1) and 4.3 μmol mol⁻¹ (IOP2) and often negative F_{VA} during the day. This pattern is somewhat obscured during IOP1 by the scatter between 30-min mean values, which is also affected by the shorter data set of IOP1. The highest positive F_{VA} , i.e. emission of CO₂ from the control volume, was observed

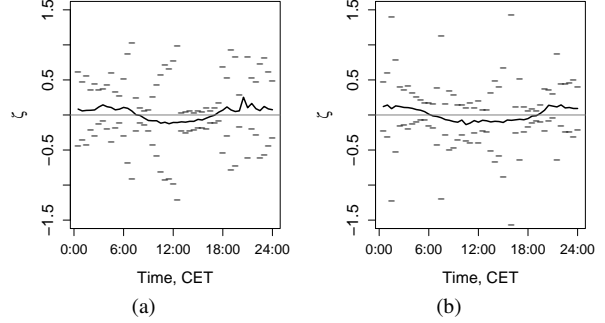


Fig. 7 Median daily cycle of stability parameter ζ (line) \pm standard deviation (dashes) with a 30-min resolution for IOP1 a), and IOP2 b). Values of $\zeta \pm$ standard deviation not covered by the plotting region are: 2.4 at 13:20, -1.9 at 20:30 in (a) and 6.9 at 15:30, -7.1 at 16:00 in (b)

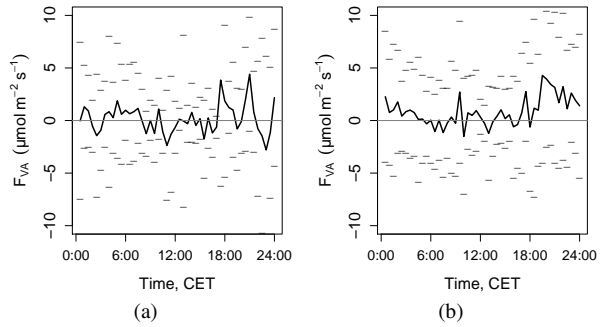


Fig. 8 Mean daily cycle of vertical advection F_{VA} (lines) \pm standard deviation (dashes) with a 30-min resolution for IOP1 a), and IOP2 b)

during the early evening, which is consistent with a negative vertical concentration profile after the onset of the stable stratification regime, the lack of assimilation after sunset and still relatively high soil temperatures (not shown), which favor respiration. During IOP1, this positive peak in F_{VA} starts earlier (shorter days in fall) but does not continue as long during the night as during IOP2, consistent with lower temperatures and higher soil water content and therefore potentially lower soil respiration during the nights of IOP1. Mean nocturnal (6:00 pm to 6:00 am) soil temperature was 9.6°C (IOP1) and 12.6°C (IOP2) at a 0.02 m depth. Mean nocturnal soil water content was 31.1 % (IOP1) and 27.3 % (IOP2) at a 0.01 m depth.

3.3 Horizontal gradients and horizontal advection

Horizontal concentration gradients are shown in Fig. 9(a) for IOP1 and in Fig. 9(b) for IOP2. The along-slope and across-slope gradients partly cancel each other, particularly during IOP1, with the along-slope gradient being dominant. Maximum gradients coincide with decreasing air temperature and stable stratification after sunset and a second maximum with

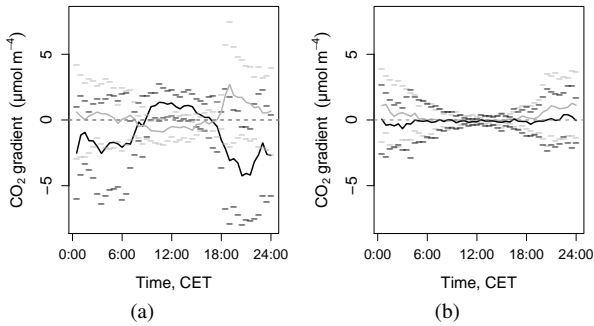


Fig. 9 Mean daily cycle of horizontal CO_2 concentration gradient (lines) \pm standard deviation (dashes) with a 30-min resolution for IOP1 a), and IOP2 b). Gradient along the slope (black) and perpendicular to the slope (grey)

stable stratification and low air temperature due to radiative cooling at the end of the night. Despite the generally similar sign of the gradients during both IOPs, there are major differences in magnitude of the mean gradients and also in the scatter of the data which is indicated by the standard deviation (dashes). Smaller gradients and less scatter during IOP2 are in line with the different gradient sampling approaches. The higher number of sample points in time and space during IOP2 results in a better averaging over the control volume and time and reduces the impact of temporally and spatially local effects (e.g. heterogeneous vegetation structure) on the 30-min average. Furthermore, with the IOP2 setup the risk of unrealistically large gradients caused by contamination of real gradients by measurement errors is reduced by comprehensive correction of inter-instrument bias.

Horizontal advection F_{HA} during IOP1 (Fig. 10a, black line) is dominated by the along-slope component (light grey line) during the first half of the night and by the across-slope component for the remaining night. Large values of F_{HA} were observed during stable stratification with katabatic drainage (not shown). Mean F_{HA} during IOP1 is positive most of the time, indicating a loss of CO_2 from the control volume. Values and standard deviation during the afternoon are small. F_{HA} during IOP2 (Fig. 10b) rapidly increases to positive values in the evening before sunset, coinciding with the onset of stable stratification and is negative later at night. A similar peak of F_{HA} at 18:00 to 19:00 has been reported by Kutsch et al (2008) who found that the peaks of horizontal advection correlated with changes (decrease) in temperature. Mahrt et al (2001) also describe a similar pattern of drainage flows, distinguishing the following phases: “early evening very stable period” with katabatic drainage due to rapid cooling in a thin layer close to the surface, “middle-of-the-night mixing” with reduced or ceased katabatic drainage due to entrainment of warmer air and momentum from aloft which is mixed into the canopy by low-level jet induced shear and shear-generated turbulence, and finally an “early

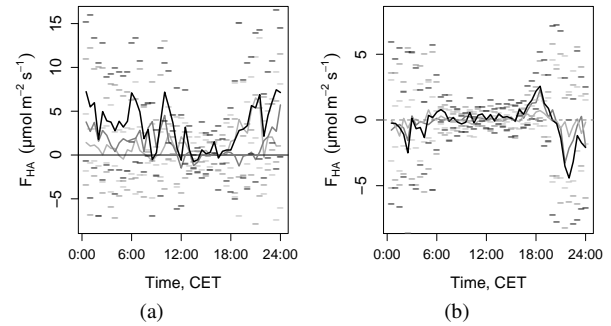


Fig. 10 Mean daily cycle of total horizontal advection F_{HA} (black line), F_{HA} in slope direction (light grey line) and perpendicular to the slope (grey line) \pm standard deviation (dashes) with a 30-min resolution for IOP1 a), and IOP2 b). Note different y-scale

morning more stable period” after the weakening of the low-level jet above the surface inversion layer with decreasing turbulence, decreasing temperature and a re-formulation of katabatic drainage close to the surface. Also Sun et al (2007) report significant horizontal CO_2 advection during transition periods in the early evening and early morning when turbulence intensity is low. Those findings cited are similar to observations of horizontal advection presented in the current study. The large range of $F_{HA} \pm$ standard deviation (sd) at night correlates with periods of stable stratification. F_{HA} and $F_{HA} \pm sd$ are small during the day when gradients are small due to the presence of turbulence. Scatter of F_{HA} between mean 30-min values and the magnitude of the latter are considerably reduced during IOP2 as compared to IOP1.

3.4 Total advection

Adding vertical and horizontal advection yields total advection $F_A = F_{VA} + F_{HA}$, as shown in Fig. 11(a) for IOP1 and in Fig. 11(b) for IOP2. Common characteristics of the mean daily cycle of total advection during both IOP1 and IOP2 are a minimum of F_A at noon and in the early afternoon, a maximum in the evening and a considerable contribution during the remaining night. Specific to F_A observed during IOP1 is its predominantly positive sign with the exception of the period at noon and in the early afternoon with small values and changing sign. The maximum of the mean daily cycle of F_A during IOP1 is $12 \mu\text{mol m}^{-2} \text{s}^{-1}$. In contrast, the mean daily cycle of F_A during IOP2 is more balanced around zero with changing sign and a maximum of $4 \mu\text{mol m}^{-2} \text{s}^{-1}$. As shown above for F_{VA} and for F_{HA} , the absolute value of F_A agrees with the notion that stable conditions favor large advective fluxes due to large concentration gradients during stable stratification (compare Fig. 7, 6b and 9), whereas neutral and unstable stratification generally cause smaller advective fluxes because concentration gradients are reduced

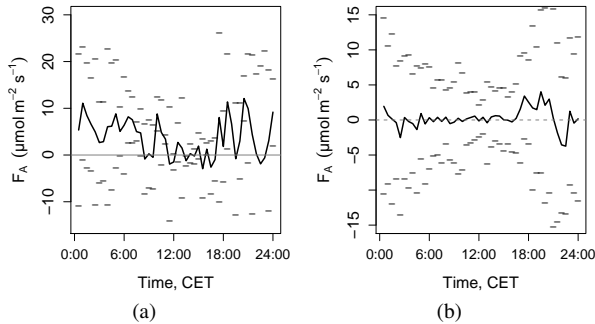


Fig. 11 Mean daily cycle of total advection F_A (line) \pm standard deviation (dashes) with a 30-min resolution for IOP1 a), and IOP2 b). Note different y-scale

by turbulent mixing. However, exceptions have to be made from this finding for the mean daily cycle of F_A during IOP1, where its absolute value cannot be explained by atmospheric stratification: this is the case around 10:00 am with relatively large values of F_A but no corresponding stable stratification. Furthermore, the scatter between individual 30-min mean values of F_A shown in Fig. 11(a) cannot be explained by atmospheric stratification. As the data presented provide no other obvious reason, the scatter could be attributed to differences in the sampling scheme which were presented in this study, i.e. mainly to discontinuous sampling and fewer sample locations during IOP1 and the lack of comprehensive bias correction of concentration gradients during IOP1 which could be applied to the IOP2 data set due to the use of the continuous sampling approach.

3.5 Net Ecosystem Exchange

Fig. 12 presents the mean daily cycle of Net Ecosystem Exchange (NEE) for IOP1 (a) and IOP2 (b) as well as individual flux components contributing to NEE . As mentioned above, fluxes shown are based on the sector-wise coordinate rotation with the u_* -filter. The storage flux is small during both IOPs with small negative values during the morning and otherwise small positive values. The turbulent flux shows a typical daily cycle with maximum negative fluxes (assimilation) being similar between IOP1 ($-17.9 \mu\text{mol m}^{-2} \text{s}^{-1}$) and IOP2 ($-18.7 \mu\text{mol m}^{-2} \text{s}^{-1}$). Differences in maximum assimilation are small despite the different season because maximum assimilation is limited by a relatively constant assimilation potential of the spruce forest. The length of the daytime assimilation period, however, is larger in the summer season during IOP2 due to radiative forcing, and the peak is observed about four hours earlier in the day during IOP2 than in IOP1. Likewise, the negative storage flux peak is observed earlier in the day in summer. Observations concerning maximum and duration of daytime

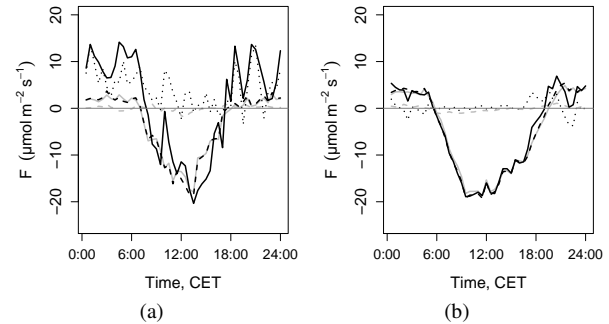


Fig. 12 Median daily cycle of NEE with a 30-min resolution for IOP1 a), and IOP2 b), without advection (black dashed line), calculated as the sum of turbulent flux (grey solid line) and storage flux (grey dashed line) in comparison with NEE including advection (black solid line), calculated as the sum of turbulent flux, storage flux and the sum of vertical and horizontal advection (black dotted line)

turbulent flux are similarly true for NEE . The maximum of the mean nocturnal turbulent flux (respiration) as presented in Fig. 12 is larger for the summer measurements during IOP2 ($4.9 \mu\text{mol m}^{-2} \text{s}^{-1}$) compared to measurements in fall during IOP1 ($3.1 \mu\text{mol m}^{-2} \text{s}^{-1}$), which is interpreted as an effect of higher air and soil temperatures, lower soil moisture and the more frequent coupling of the sub-canopy with the above-canopy eddy-covariance measurement level during nights of IOP2, which allows for a larger portion of the respiratory flux to be observed by the above-canopy sensor. The temperature dependence of respiration has been previously published by Wofsy et al (1993); Lloyd and Taylor (1994); Goulden et al (1996) for soil temperature and Lindroth et al (1998) for air temperature. Concerning nocturnal NEE with advection included (black solid line), large maximum values are observed during IOP1 ($14.1 \mu\text{mol m}^{-2} \text{s}^{-1}$) as compared to IOP2 ($6.9 \mu\text{mol m}^{-2} \text{s}^{-1}$). There are no obvious natural reasons why nocturnal respiration should be much larger during fall. Those differences in nocturnal NEE result in different mean values of the daily cycle presented which are $0.9 \mu\text{mol m}^{-2} \text{s}^{-1}$ for IOP1 and $-5.0 \mu\text{mol m}^{-2} \text{s}^{-1}$ for IOP2. The advective contribution to NEE is relatively large during IOP1 and considerably adds variability to NEE , whereas the advective contribution to NEE is relatively small during IOP2.

A different representation of cumulative NEE is given in Fig. 13 for IOP1 (a) and IOP2 (b) as daily sums of NEE with and without advection. Adding advection F_A to the sum of turbulent and storage flux $F_T + F_S$ for the IOP1 data set changes the carbon budget from a sink to a source with a mean daily sum of $F_T + F_S = -6.0 \text{ g C m}^{-2} \text{ d}^{-1}$ and a mean daily sum of $F_T + F_S + F_A = 1.3 \text{ g C m}^{-2} \text{ d}^{-1}$. In contrast, including advection in the calculation of NEE during IOP2 reduces the sink but does not cause a change in the sign with a mean daily sum of $F_T + F_S = -5.0 \text{ g C m}^{-2} \text{ d}^{-1}$ and a mean

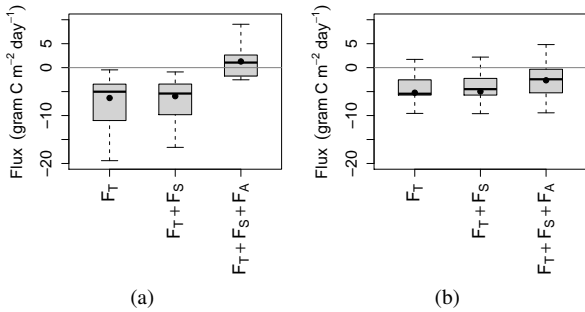


Fig. 13 Statistics of daily sums of NEE , computed as the turbulent flux (F_T), as the sum of turbulent flux and storage flux ($F_T + F_S$) and as the sum of turbulent flux, storage flux and total advective flux ($F_T + F_S + F_A$) for IOP1 a), and IOP2 b). Displayed statistics are the range of the data (whisker), the quartiles (box), the median (line) and the mean (point)

Table 2 Comparison of mean nocturnal CO_2 fluxes from soil chamber measurements (“chamber”), the sum of turbulent flux and storage flux (“ $F_T + F_S$ ”) and the sum of turbulent flux, storage flux and advection (“ $F_T + F_S + F_A$ ”) for the “golden days” period of IOP1 (DOY 264 to 267, 2007) and the “golden days” period of IOP2 (DOY 181 to 184, 2008). Night-time was defined as 18:00 to 6:00. Figures are given in units of $\mu mol m^{-2} s^{-1}$. Soil chamber measurements during IOP1 (Hens, 2009) and IOP2 (Riederer, 2009) follow methods described in Ammann (1998)

	IOP1	IOP2
Chamber	3.2	2.0
$F_T + F_S$	2.5	3.5
$F_T + F_S + F_A$	10.8	3.2

daily sum of $F_T + F_S + F_A = -2.6 g C m^{-2} d^{-1}$. A reduction of cumulative NEE calculated as $F_T + F_S + F_A$ instead of $F_T + F_S$ is consistent with assuming the presence of a night flux error caused by inefficiencies of the eddy-covariance method under conditions of low or absent turbulence. Our interpretation is that CO_2 originating from nocturnal respiration is removed from the control volume by advection. The night flux error explains the more negative daily sums of NEE without advection ($F_T + F_S$) compared to NEE including advection ($F_T + F_S + F_A$) shown in Fig. 13(b).

As advection has significant impact on NEE , particularly at night, but affects NEE to a different extent during the two observation periods, nocturnal micrometeorological CO_2 fluxes are compared to nocturnal soil chamber flux measurements in Table 2. In a horizontally homogeneous system at night the sum of soil respiration (measured by chambers) and the respiration from above ground biomass should equal NEE including advection ($F_T + F_S + F_A$). However, observations during IOP1 (Table 2) show a difference between NEE and chamber measurements of $10.8 - 3.2 = 7.6 \mu mol m^{-2} s^{-1}$. Assuming for the moment that the chamber measurements were correct and spatially representative

within the footprint of the micrometeorological measurements, this would leave $7.6 \mu mol m^{-2} s^{-1}$ to be explained by the sum of above ground respiration and the error associated with the micrometeorological NEE estimate. Above ground respiration can be assumed not to exceed soil respiration significantly if it is not much smaller (see e.g. Kutsch et al (2008) who report for another German site in a similar climate and season that soil respiration accounted for 63% of total ecosystem respiration, foliage respiration for 27% at night and above-ground woody parts for 10%). Similarly, Rebmann (2004) reported foliage respiration accounting for 30% of total respiration at night at the site of the current study with a total respiration of $3 \mu mol m^{-2} s^{-1}$, based on micrometeorological methods, trunk and needle respiration measurements by Mirschkorsch (1996) and soil chamber measurements (Subke, 2002). With a hypothetical maximum above ground respiration equal to soil respiration, the remaining error of NEE including advection would be $7.6 - 3.2 = 4.4 \mu mol m^{-2} s^{-1}$, which is large relative to NEE without advection ($2.5 \mu mol m^{-2} s^{-1}$). Doing the same comparison for observations during IOP2 (Table 2) yields a significantly different result. The difference between NEE and chamber measurements is $3.2 - 2.0 = 1.2 \mu mol m^{-2} s^{-1}$. This would leave $1.2 \mu mol m^{-2} s^{-1}$ to be explained by the sum of above ground respiration and the error associated with the micrometeorological NEE estimate. Using a hypothetical maximum above ground respiration estimate equal to soil respiration as was done in the previous case, the remaining error of NEE including advection would be $1.2 - 2.0 = -0.8 \mu mol m^{-2} s^{-1}$, which is small relative to NEE without advection ($3.5 \mu mol m^{-2} s^{-1}$). When using an above-ground respiration of $1.17 \mu mol m^{-2} s^{-1}$, which would result from using the percentages cited from Kutsch et al, 2008, and which is also even more realistic in relation to measured soil respiration than above used value, the remaining error of NEE including advection vanishes almost completely ($1.2 - 1.17 = 0.03 \mu mol m^{-2} s^{-1}$). Regarding the relative magnitude of the presented soil chamber measurements in consideration of soil temperatures (lower during IOP1, higher during IOP2, see above) and soil moisture (higher during IOP1, lower during IOP2, see above), if any, a relative adjustment towards lower soil respiration during IOP1 and higher soil respiration during IOP2 would be justified. This in turn would possibly increase the error stated for IOP1 and/or decrease the error during IOP2 further if there was a remaining error.

To summarize, based on the chamber measurements as presented in Table 2 (which we are aware are subject to their own specific uncertainty), the relative error of NEE during IOP1 is $4.4/2.5 = 176\%$ whereas during IOP2 it is $(0 \text{ to } -0.8)/3.5 = 0 \text{ to } 23\%$. These numbers are intended to be taken as a first estimate only. Among the explanations for the different values of the error during the two obser-

vation periods are the uncertainty of the chamber measurements, particularly due to spatial heterogeneity of soil respiration and non-matching footprints of micrometeorological and chamber flux measurements, as well as uncertainties in the turbulent flux, storage flux and advective flux. There was no major systematic difference between any of the factors listed during the two observation periods other than the methods for sampling horizontal concentration gradients (discontinuously with LI-820 versus continuously with LI-6262, LI6251 and BINOS) and correcting them (constant bias correction versus comprehensive time variant bias correction approach) prior to the calculation of advection.

4 Conclusions

This study has for the first time presented Net Ecosystem Exchange including horizontal and vertical advection at the FLUXNET station Waldstein-Weidenbrunnen (DE-Bay). As the experimental observation of advective fluxes has proven to be challenging and a generally successful method has not yet emerged, this study has focused on different methodological approaches. Temporally continuous observations of horizontal concentration gradients have been shown to yield significantly different results compared to the standard sequential sampling approach. As the complete observation of a time series by continuous sampling is physically more correct, this approach should be preferred whenever possible. The application of comprehensive bias correction could deal with the side effects of continuous measurements, i.e. inter-instrument bias. In contrast to the sequential approach, horizontal advection estimates from the continuous sampling approach with bias correction showed smaller absolute values, reduced scatter and could be explained by meteorological drivers. Furthermore they produced estimates of nocturnal *NEE* which agreed with flux measurements from soil and plant chambers, which was not the case for *NEE* with advection from the sequential approach.

Different approaches to coordinate rotation were tested. Sector-wise rotation successfully eliminated directional dependencies of vertical wind velocity. Additional data filters had no significant effect. Therefore, in order to achieve $\bar{w} = 0$, the sector-wise application of the planar fit rotation is recommended. The window length of the coordinate rotation has a large impact on estimates of vertical advection (approx. 50 % of F_{VA}) because a considerable portion of energy is contained in the long wave component of the spectrum of w . We therefore recommend making an intentional choice of the coordinate rotation window length and applying a sequence of rotation windows if necessary rather than letting the window length be determined by an arbitrary length of the data set. A sequential coordinate rotation with adjustable window length as well as sector-wise coordinate rotation according to individually selectable sector borders should be

made available as a user selectable option of major flux processing software packages.

We conclude that the total advective contribution to *NEE* was minor during most of the day relative to the turbulent flux but was considerable during the night and during transition periods in the early evening. Including advection in the *NEE* budget caused a reduction of the mean daily sum of *NEE* from -5.0 to $-2.6 \text{ gC m}^{-2} \text{ d}^{-1}$ during the days of IOP2, i.e. an almost 50 % reduction of the estimated potential of the forest as a carbon sink. The measurement of advection thus remains an important issue for accurate *NEE* estimates.

Applying different methods to measure and calculate vertical and horizontal advection has been shown to give significantly different values for the flux, with the method-specific differences even exceeding the magnitude of the fluxes themselves. The alternative methods presented in this study yielded plausible advective fluxes when compared to other terms in the *NEE* budget as well as to supplementary meteorological data and to chamber measurements. Considering that it is still an open question as to how to best address the advective flux components in the measurement of *NEE* budgets, we suggest the testing and further validation of the above presented approaches at other sites, as many of our findings should not be restricted to the given site but be generally applicable.

Acknowledgements The authors wish to acknowledge the help and technical support performed by the staff of the Bayreuth Center for Ecology and Environmental Research (BayCEER) of the University of Bayreuth. The 2007 and 2008 experiment was funded by the German Science Foundation (FO 226/16-1, ME2100/4-1, ZE 792/4-1).

References

- Acevedo O, Moraes O, Fitzjarrald D, Sakai R, Mahrt L (2007) Turbulent carbon exchange in very stable conditions. *Boundary-Layer Meteorol* 125:49–61
- Akima H (1970) A new method of interpolation and smooth curve fitting based on local procedures. *J Assc Comp Mach* 17:589–602
- Ammann C (1998) On the applicability of relaxed eddy accumulation and common methods for measuring trace gas fluxes. PhD thesis, Swiss Federal Institute of Technology (ETH), Zuerich, Switzerland
- de Araujo AC, Kruijt B, Nobre AD, Dolman AJ, Waterloo MJ, Moors EJ, de Souza JS (2008) Nocturnal accumulation of CO₂ underneath a tropical forest canopy along a topographical gradient. *Ecological Applications* 18:1406–1419
- Aubinet M (2008) Eddy covariance CO₂ flux measurements in nocturnal conditions: an analysis of the problem. *Ecological Applications* 18:1368–1378

- Aubinet M, Grelle A, Ibrom A, Rannik Ü, Moncrieff JB, Foken T, Kowalski AS, Martin P, Berbigier P, Bernhofer C, Clement R, Elbers JA, Granier A, Grünwald T, Morgenstern K, Pilegaard K, Rebmann C, Snijders W, Valentini R, Vesala T (2000) Estimates of the annual net carbon and water exchange of European forests: the EUROFLUX methodology. *Advances in Ecological Research* 30:113–175
- Aubinet M, Heinesch B, Yernaux M (2003) Horizontal and vertical CO₂ advection in a sloping forest. *Boundary-Layer Meteorol* 108:397–417
- Aubinet M, Berbigier P, Bernhofer C, Cescatti A, Feigenwinter C, Graniers A, Grünwald T, Havrankova K, Heinesch B, Longdoz B, Marcolla B, Montagnani L, Sedlak P (2005) Comparing CO₂ storage and advection conditions at night at different CARBOEUROFLUX sites. *Boundary-Layer Meteorol* 116:63–94
- Aubinet M, Feigenwinter C, Heinesch B, Bernhofer C, Canepa E, Lindroth A, Montagnani L, Rebmann C, Sedlak P, Gorsel EV (2010) Direct advection measurements do not help to solve the night-time CO₂ closure problem: Evidence from three different forests. *Agric For Meteorol* 150:655–664
- Baldocchi D, Finnigan JJ, Wilson K, Paw U KT, Falge E (2000) On measuring net ecosystem carbon exchange over tall vegetation on complex terrain. *Boundary-Layer Meteorol* 96:257–291
- Baldocchi DD (2003) Assessing the eddy covariance technique for evaluating carbon dioxide exchange rates of ecosystems: past, present and future. *Global Change Biology* 9(4):479–492
- Baldocchi DD, Falge E, Gu L, Olson R, Hollinger D, Running S, Anthoni P, Bernhofer C, Davis K, Evans R, Fuentes J, Goldstein A, Katul G, Law B, Lee X, Malhi Y, Meyers T, Munger W, Oechel W, Paw KT, Pilegaard K, Schmid HP, Valentini R, Verma S, Vesala T, Wilson K, Wofsy S (2001) Fluxnet: A new tool to study the temporal and spatial variability of ecosystem-scale carbon dioxide, water vapor, and energy flux densities. *Bulletin of the American Meteorological Society* 82(11):2415–2434
- Belcher SE, Finnigan JJ, Harman IN (2008) Flows through forest canopies in complex terrain. *Ecological Applications* 18:1436–1453
- Beyrich F, Leps JP, Mauder M, Bange J, Foken T, Huneke S, Lohse H, Lüdi A, Meijninger W, Mironov D, Weisense U, Zittel P (2006) Area-averaged surface fluxes over the Litfass region based on eddy-covariance measurements. *Boundary-Layer Meteorol* 121:33–65
- Burns SP, Delany AC, Sun J, Stephens BB, Oncley SP, Maclean GD, Semmer SR, Schröter J, Ruppert J (2009) A programmable portable trace-gas measuring system and an evaluation of calibration techniques for in-situ carbon dioxide measurements. *Journal of Atmospheric and Oceanic Technology* 26:291–316
- Dellwik E, Mann J, Larsen KS (2010) Flow tilt angles near forest edges – Part 1: Sonic anemometry. *Biogeosciences* 7:1745–1757
- Etzold S, Buchmann N, Eugster W (2010) Contribution of advection to the carbon budget measured by eddy covariance at a steep mountain slope forest in Switzerland. *Biogeosciences* 7:2461–2475
- Falge E, Baldocchi D, Olson R, Anthoni P, Aubinet M, Bernhofer C, Burba G, Ceulemans R, Clement R, Dolman H, Granier A, Gross P, Grünwald T, Hollinger D, Jensen NO, Katul G, Keronen P, Kowalski A, Laim CT, Lawc BE, Meyers T, Moncrieff J, Moors E, Munger JW, Pilegaard K, Rannik Ü, Rebmann C, Suyker A, Tenhunen J, Tu K, Verma S, Vesala T, Wilson K, Wofsy S (2001) Gap filling strategies for defensible annual sums of net ecosystem exchange. *Agric For Meteorol* 107:43–69
- Feigenwinter C, Bernhofer C, Vogt R (2004) The influence of advection on the short term CO₂-budget in and above a forest canopy. *Boundary-Layer Meteorol* 113:201–224
- Feigenwinter C, Bernhofer C, Eichelmann U, Heinesch B, Hertel M, Janous D, Kolle O, Lagergren F, Lindroth A, Minerbi S, Moderow U, Molder M, Montagnani L, Queck R, Rebmann C, Vestin P, Yernaux M, Zeri M, Ziegler W, Aubinet M (2008) Comparison of horizontal and vertical advective CO₂ fluxes at three forest sites. *Agric For Meteorol* 148:12–24
- Feigenwinter C, Montagnani L, Aubinet M (2010a) Plot-scale vertical and horizontal transport of CO₂ modified by a persistent slope wind system in and above an alpine forest. *Agric For Meteorol* 150(5):665 – 673
- Feigenwinter C, Mölder M, Lindroth A, Aubinet M (2010b) Spatiotemporal evolution of CO₂ concentration, temperature, and wind field during stable nights at the Norunda forest site. *Agric For Meteorol* 150(5):692 – 701
- Finnigan J (1999) A comment on the paper by Lee (1998): "on micrometeorological observations of surface-air surface exchange over tall vegetation". *Agric For Meteorol* 97:55–67
- Finnigan J (2006) The storage term in eddy flux calculations. *Agric For Meteorol* 136(3-4):108 – 113
- Finnigan J (2008) An introduction to flux measurements in difficult conditions. *Ecological Applications* 18:1340–1350
- Finnigan JJ (2004) A Re-Evaluation of Long-Term Flux Measurement Techniques Part II: Coordinate Systems. *Boundary-Layer Meteorol* 113:1–41
- Finnigan JJ, Clement R, Malhi Y, Leuning R, Cleugh H (2003) A Re-Evaluation of Long-Term Flux Measurement Techniques Part I: Averaging and Coordinate Rotation. *Boundary-Layer Meteorol* 107:1–48
- Foken T, Leclerc MY (2004) Methods and limitations in validation of footprint models. *Agric For Meteorol* 127:223–

- 234
- Foken T, Wichura B (1996) Tools for quality assessment of surface-based flux measurements. *Agric For Meteorol* 78:83–105
- Foken T, Skeib G, Richter SH (1991) Dependence of the integral turbulence characteristics on the stability of stratification and their use for doppler-sodar measurements. *Z Meteorol* 41:311–315
- Foken T, Göckede M, Mauder M, Mahrt L, Amiro BD, Munger JW (2004) Post-field data quality control. In: *Handbook of Micrometeorology: A Guide for Surface Flux Measurements*, Kluwer Academic Publishers, Dordrecht, pp 181–208
- Foken T, Meixner FX, Falge E, Zetzsch C, Serafimovich A, Balzer N, Bargsten A, Behrendt T, Biermann T, Breuninger C, Gerken T, Hunner M, Lehmann-Pape L, Hens K, Jocher G, Kesselmeier J, Lüers J, Mayer JC, Moravek A, Plake D, Riederer M, Rütz F, Scheibe M, Schier S, Siebicke L, Sörgel M, Staudt K, Trebs I, Tsokankunku A, Welling M, Wolff V, Zhu Z (2010) Atmospheric transport and chemistry in forest ecosystems – overview of the EGER-project. *Agric For Meteorol* (in preparation)
- Froelich NJ, Schmid HP (2006) Flow divergence and density flows above and below a deciduous forest Part II. Below-canopy thermotopographic flows. *Agric For Meteorol* 138:29–43
- Froelich NJ, Schmid HP, Grimmond CSB, Su HB, Oliphant AJ (2005) Flow divergence and density flows above and below a deciduous forest: Part I. Non-zero mean vertical wind above canopy. *Agric For Meteorol* 133(1-4):140 – 152
- Geissbühler P, Siegwolf R, Eugster W (2000) Eddy covariance measurements on mountain slopes: the advantage of surface-normal sensor orientation over a vertical set-up. *Boundary-Layer Meteorol* 96:371–392
- Gerstberger P, Foken T, Kalbitz K (2004) The Lehstenbach and Steinkreuz Catchments in NE Bavaria, Germany. In: Matzner E (ed) *Biogeochemistry of Forested Catchments in a Changing Environment: A German Case Study*, vol 172, Springer, Heidelberg, pp 15–41
- Gorsel, van E, Ev A, Leuning R, Cleugh HA, Keith H, Suni T (2007) Nocturnal carbon efflux: reconciliation of eddy covariance and chamber measurements using an alternative to the u_* -threshold filtering technique. *Tellus B* 59:397–403
- Goulden ML, Munger JW, Fan SM, Daube BC, Wofsy SC (1996) Measurements of carbon sequestration by long-term eddy covariance: methods and a critical evaluation of accuracy. *Global Change Biology* 2(3):169–182
- Goulden ML, Miller SD, Humberto, da Rocha R (2006) Nocturnal cold air drainage and pooling in a tropical forest. *Journal of Geophysical Research* 111:D08S04, DOI 10.1029/2005JD006037
- Göckede M, Rebmann C, Foken T (2004) A combination of quality assessment tools for eddy covariance measurements with footprint modelling for the characterisation of complex sites. *Agric For Meteorol* 127:175–188
- Heinesch B, Yernaux M, Aubinet M (2007) Some methodological questions concerning advection measurements: a case study. *Boundary-Layer Meteorol* 122:457–478
- Heinesch B, Yernaux M, , Aubinet M (2008) Dependence of CO₂ advection patterns on wind direction on a gentle forested slope. *Biogeosciences* 5:657–668
- Hens K (2009) Der bodennahe, vertikale, turbulente Transport von ²²²Rn, ²²⁰Rn und anderen Spurengasen im Stammraum eines Fichtenbestandes. Master's thesis, Institut for Physics, Johannes Gutenberg–University, Mainz, Germany, 93 p.
- Hollinger DY, Kelliher FM, Byers JN, Hunt JE, McSeveny TM, Weir PL (1994) Carbon dioxide exchange between an undisturbed old-growth temperate forest and the atmosphere. *Ecology* 75:134–150
- Katul G, Finnigan J, Poggi D, Leuning R, Belcher S (2006) The influence of hilly terrain on canopy-atmosphere carbon dioxide exchange. *Boundary-Layer Meteorol* 118:189–216
- Klaassen W, Sogachev A (2006) Flux footprint simulation downwind of a forest edge. *Boundary-Layer Meteorol* 121:459–473
- Komatsu H, Yoshida N, Takizawa H, Kosaka I, Tantasirin C, Suzuki M (2003) Seasonal trend in the occurrence of nocturnal drainage flow on a forested slope under a tropical monsoon climate. *Boundary-Layer Meteorol* 106:573–592
- Kutsch WL, Kolle O, Rebmann C, Knohl A, Ziegler W, Schulze ED (2008) Advection and resulting CO₂ exchange uncertainty in a tall forest in central Germany. *Ecological Applications* 18:1391–1405
- Leclerc MY, Karipot A, Prabha T, Allwine G, Lamb B, Gholz HL (2003) Impact of non-local advection on flux footprints over a tall forest canopy: a tracer flux experiment. *Agric For Meteorol* 115(1-2):19 – 30
- Lee X (1998) On micrometeorological observations of surface–air surface exchange over tall vegetation. *Agric For Meteorol* 91:39–49
- Lee X (1999) Reply to comment by Finnigan on “On micrometeorological observations of surface-air exchange over tall vegetation”. *Agric For Meteorol* 97(1):65 – 67
- Lee X, Hu X (2002) Forest-air fluxes of carbon, water and energy over non-flat terrain. *Boundary-Layer Meteorol* 103:277–301
- Lee X, Finnigan J, Paw U K (2004) *Handbook of Micrometeorology—A Guide for Surface Flux Measurement and Analysis*, Kluwer Academic Publishers, chap Coordinate systems and flux bias error, p 33–54

- Leuning R, Zegelin SJ, Jones K, Keith H, Hughes D (2008) Measurement of horizontal and vertical advection of CO₂ within a forest canopy. *Agric For Meteorol* 148:1777–1797
- Lindroth A, Grelle A, Moren AS (1998) Long-term measurements of boreal forest carbon balance reveal large temperature sensitivity. *Global Change Biology* 4:443–450
- Liu H, Peters G, Foken T (2001) New equations for sonic temperature variance and buoyancy heat flux with an omnidirectional sonic anemometer. *Boundary-Layer Meteorol* 100:459–468
- Lloyd J, Taylor JA (1994) On the temperature dependence of soil respiration. *Functional Ecology* 8:315–323
- Mahrt L (2010) Computing turbulent fluxes near the surface: Needed improvements. *Agric For Meteorol* 150(4):501–509
- Mahrt L, Vickers D, Nakamura R, Soler MR, Sun J, Burns S, Lenchow D (2001) Shallow drainage flows. *Boundary-Layer Meteorol* 101:243–260
- Mammarella I, Kolar P, Rinne J, Keronen P, Pumpanen J, Vesala T (2007) Determining the contribution of vertical advection to the net ecosystem exchange at Hyytiälä forest, Finland. *Tellus* 59B:900–909
- Marcolla B, Cescatti A, Montagnani L, Manca G, Kerschbaumer G, Minerbi S (2005) Importance of advection in the atmospheric CO₂ exchanges of an alpine forest. *Agric For Meteorol* 130:193–206
- Massman WJ, Lee X (2002) Eddy covariance flux corrections and uncertainties in long-term studies of carbon and energy exchanges. *Agric For Meteorol* 113(1–4):121–144
- Mauder M, Foken T (2004) Documentation and instruction manual of the eddy covariance software package TK2. *Arbeitsergebnisse* 26, University of Bayreuth, Department of Micrometeorology, ISSN 1614-8916, 45 pp.
- McMillen RT (1988) An eddy correlation technique with extended applicability to non-simple terrain. *Boundary-Layer Meteorol* 43:231–245
- Mirschorsch M (1996) Die Stamm- und Zweigrespiration eines jungen Fichtenbestandes [*Picea abies* (L.) Karst.] und die Bedeutung für den CO₂-Netto-Austausch. Master's thesis, University of Bayreuth, Germany
- Moncrieff J, Clement R, Finnigan J, Meyers T (2004) *Handbook of Micrometeorology—A Guide for Surface Flux Measurement and Analysis*, Kluwer Academic Publishers, chap Averaging, detrending, and filtering of eddy covariance time series, pp 7–31
- Moncrieff JB, Massheder JM, de Bruin H, Elbers J, Friborg T, Heusinkveld B, Kabat P, Scott S, Soegaard H, Verhoef A (1997) A system to measure surface fluxes of momentum, sensible heat, water vapour and carbon dioxide. *Journal of Hydrology* 188–189:589–611
- Montagnani L, Manca G, Canepa E, Georgieva E (2010) Assessing the method-specific differences in quantification of CO₂ advection at three forest sites during the ADVEX campaign. *Agric For Meteorol* 150:702–711
- Moore CJ (1986) Frequency response corrections for eddy correlation systems. *Boundary-Layer Meteorol* 37:17–35
- Oncley S, Foken T, Vogt R, Kohsiek W, DeBruin H, Bernhofer C, Christen A, Gorsel E, Grantz D, Feigenwinter C, Lehner I, Liebethal C, Liu H, Mauder M, Pitacco A, Ribeiro L, Weidinger T (2007) The Energy Balance Experiment EBEX-2000. Part I: overview and energy balance. *Boundary-Layer Meteorol* 123:1–28
- Oncley SP, Schwenz K, Sun J, Burns SP, Monson RK (2008) Measuring in-canopy advection of carbon dioxide using a new transect measurement system (TRAM). In: 28th Conference on Agricultural and Forest Meteorology, American Meteorological Society, 28 April–2 May 2008.
- Paw U KT, Baldocchi DD, Meyers TP, Wilson KB (2000) Correction of eddy-covariance measurements incorporating both advective effects and density fluxes. *Boundary-Layer Meteorol* 97:487–511
- Paw U KT, Falk M, Suchanek TH, Ustin SL, Chen J, Park YS, Winner WE, Thomas SC, Hsiao TC, Shaw RH, King TS, Pyles RD, Schroeder M, Matista AA (2004) Carbon dioxide exchange between an old-growth forest and the atmosphere. *Ecosystems* 7:513–524
- Plake D (2009) Vertikale Konzentrationsprofile und Flüsse von reaktiven und nicht reaktiven Spurengasen im Fichtelgebirge. Master's thesis, Max-Planck-Institut für Chemie, Mainz, Germany, 144 pp.
- Pypker T, Unsworth M, Lamb B, Allwine E, Edburg S, Sulzmann E, Mix A, Bond B (2007) Cold air drainage in a forested valley: Investigating the feasibility of monitoring ecosystem metabolism. *Agric For Meteorol* 145(3–4):149–166
- Rebmann C (2004) Kohlendioxid-, Wasserdampf- und Energieaustausch eines Fichtenwaldes in Mittelgebirgslage in Nordostbayern. *Bayreuther Forum Ökologie* 106, Bayreuther Institut für Terrestrische Ökosystemforschung (BITÖK), Bayreuth, Germany, 140 pp.
- Rebmann C, Zeri M, Lasslop G, Mund M, Kolle O, Schulze ED, Feigenwinter C (2010) Treatment and assessment of the CO₂-exchange at a complex forest site in Thuringia, Germany. *Agric For Meteorol* 150:684–691
- Riederer M (2009) Fluxes of reactive and non-reactive trace gases near the forest floor. Master's thesis, University of Bayreuth, Germany, 79 pp.
- Ruppert J (2005) ATEM software for atmospheric turbulent exchange measurements using eddy covariance and relaxed eddy accumulation systems and Bayreuth whole-air REA system setup. *Arbeitsergebnisse*, 28, University of Bayreuth, Department of Micrometeorology, ISSN 1614-8916, 29 pp.

- Ruppert J, Mauder M, Thomas C, Lüers J (2006) Innovative gap-filling strategy for annual sums of CO₂ net ecosystem exchange. *Agric For Meteorol* 138:5–18
- Schmid HP (2002) Footprint modeling for vegetation atmosphere exchange studies: a review and perspective. *Agric For Meteorol* 113:159–183
- Schotanus P, Nieuwstadt FTM, Bruin HARD (1983) Temperature measurement with a sonic anemometer and its application to heat and moisture fluxes. *Boundary-Layer Meteorol* 26(1):81–93
- Serafimovich A, Siebicke L, Staudt K, Lüers J, Biermann T, Schier S, Mayer JC, Foken T (2008a) Exchange processes in mountainous regions (EGER) - documentation of the intensive observation period (IOP1) September, 6th to October, 7th 2007. *Arbeitsergebnisse*, 36, University of Bayreuth, Department of Micrometeorology, ISSN 1614-8916, 147 pp.
- Serafimovich A, Siebicke L, Staudt K, Lüers J, Hunner M, Gerken T, Schier S, Biermann T, Rütz F, von Buttler J, Riederer M, Falge E, Mayer JC, Foken T (2008b) Exchange processes in mountainous regions (EGER) - documentation of the intensive observation period (IOP2) June, 1st to July, 15th 2008. *Arbeitsergebnisse*, 37, University of Bayreuth, Department of Micrometeorology, ISSN 1614-8916, 180 pp.
- Siebicke L, Steinfeld G, Foken T (2010) CO₂-gradient measurements using a parallel multi-analyzer setup. *Atmospheric Measurement Techniques Discussions* 3:4383–4421
- Sogachev A, Panferov O, Gravenhorst G, Vesala T (2005) Numerical analysis for flux footprints for different landscapes. *Theoretical and Applied Climatology* 80:169–185
- Soler M, Infante C, Buenestado P, Mahrt L (2002) Observations of nocturnal drainage flow in a shallow gully. *Boundary-Layer Meteorol* 105:253–273
- Staebler R, Fitzjarrald D (2004) Observing subcanopy CO₂ advection. *Agric For Meteorol* 122:139–156
- Staudt K, Foken T (2007) Documentation of reference data for the experimental areas of the Bayreuth Centre for Ecology and Environmental Research (BayCEER) at the Waldstein site. *Arbeitsergebnisse* 35, University of Bayreuth, Department of Micrometeorology, ISSN 1614-8916, 37 pp.
- Subke JA (2002) Forest floor CO₂ flux in temperate forest ecosystems. *Bayreuther Forum Ökologie* 96, University of Bayreuth, Germany, 131 pp.
- Sun J (2007) Tilt corrections over complex terrain and their implication for CO₂ transport. *Boundary-Layer Meteorol* 124:143–159
- Sun J, Burns SP, Delany AC, Oncley SP, Turnipseed AA, Stephens BB, Lenschow DH, LeMone MA, Monson RK, Anderson DE (2007) CO₂ transport over complex terrain. *Agric For Meteorol* 145(1-2):1 – 21
- Thomas C, Ruppert J, Lueers J, Schröter J, Mayer JC, Bertolini T (2004) Documentation of the Waldatem-2003 Experiment. *Arbeitsergebnisse*, 24, Abteilung Mikrometeorologie, Universität Bayreuth, ISSN 1614-8916, 59 pp.
- Tóta J, Fitzjarrald DR, Staebler RM, Sakai RK, Moraes OMM, Acevedo OC, Wofsy SC, Manzi AO (2008) Amazon rain forest subcanopy flow and the carbon budget: Santarém LBA-ECO site. *J Geophys Res* 113
- Vesala T, Kljun N, Rannik Ü, Rinne J, Sogachev A, Markkanen T, Sabelfeld K, Foken T, Leclerc M (2008) Flux and concentration footprint modelling: State of the art. *Environmental Pollution* 152(3):653 – 666
- Vickers D, Mahrt L (1997) Quality control and flux sampling problems for tower and aircraft data. *J Atmos Oceanic Tech* 14:512–526
- Vickers D, Mahrt L (2006) Contrasting mean vertical motion from tilt correction methods and mass continuity. *Agric For Meteorol* 138(1-4):93 – 103
- Wang W, Davis KJ, Cook BD, Bakwin PS, Yi C, Butler MP, Ricciuto DM (2005) Surface layer CO₂ budget and advective contributions to measurements of net ecosystem-atmosphere exchange of CO₂. *Agric For Meteorol* 135(1-4):202 – 214
- Webb EK, Pearman GI, Leuning R (1980) Correction of the flux measurements for density effects due to heat and water vapour transfer. *Q J R Meteorol Soc* 106:85–100
- Wilczak JM, Oncley SP, Stage SA (2001) Sonic anemometer tilt correction algorithms. *Boundary-Layer Meteorol* 99:127–150
- Wofsy SC, Goulden ML, Munger JW, Fan SM, Bakwin PS, Daube BC, Bassow SL, Bazzaz FA (1993) Net Exchange of CO₂ in a Mid-Latitude Forest. *Science* 260:1314–1317
- Yi C, Monson RK, Zhai Z, Anderson DE, Lamb B, Allwine G, Turnipseed AA, Burns SP (2005) Modeling and measuring the nocturnal drainage flow in a high-elevation, subalpine forest with complex terrain. *Journal of Geophysical Research* 110:D22,303
- Yi C, Anderson DE, Turnipseed AA, Burns SP, Sparks JP, Stannard DI, Monson RK (2008) The contribution of advective fluxes to net ecosystem exchange in a high-elevation, subalpine forest. *Ecological Applications* 18:1379–1390
- Zeri M (2007) Investigation of high nighttime CO₂-fluxes at the Wetzstein spruce forest site in Thuringia, Germany. PhD thesis, University of Bayreuth, Germany, 102 pp.
- Zeri M, Rebmann C, Feigenwinter C, Sedlak P (2010) Analysis of periods with strong and coherent CO₂ advection over a forested hill. *Agric For Meteorol* 150(5):674 – 683

Erklärung

Hiermit erkläre ich, dass ich die Arbeit selbstständig verfasst und keine anderen als die angegebenen Hilfsmittel verwendet habe.

Ferner erkläre ich, dass ich nicht anderweitig mit oder ohne Erfolg versucht habe, eine Dissertation einzureichen oder mich einer Doktorprüfung zu unterziehen.

Bayreuth, den

(Unterschrift)